Signals and metabolic consequences during the interaction of Brassicaceae and *Verticillium longisporum*

Dissertation

zur Erlangung des Doktorgrades

der Mathematisch-Naturwissenschaftlichen Fakultäten

der Georg-August-Universität zu Göttingen

vorgelegt von

Mareike Possienke

aus

Frankfurt

Göttingen 2012

Referent:	Prof. Dr. Ivo Feußner
Korreferent:	Prof. Dr. Andrea Polle
Tag der mündlichen Prüfung:	29. 02. 2012

Index

Abbreviations

1D-SOM	One-dimensional self-organizing-map
1MI3G	1-methoxy-indole-3-ylmethyl glucosinolate
4MI3G	4-methoxy-indole-3-ylmethyl glucosinolate
ABA	abscisic acid
A. thaliana	*Arabidopsis thaliana*
AWF	apoplastic wash fluid
B. napus	*Brassica napus*
°C	Celsius
CDM	Czapek-Dox-Medium
CE	collision energy
CID	collision-induced dissociation
Col-0	Columbia-0
cps	counts per second
C. sativa	*Camelina sativa*
CSV	Comma Separated Values
$CuCl_2$	copper (II) chloride
CHCl3	chloroform
Da	Dalton
DAD	diode-array-detector
DCA	3,5-dichloroanthranilic acid
DHBA	dihydroxybenzoic acid
DHBAG	dihydroxybenzoic acid glucoside
DP	declustering potential
dpi	days past infection
e.g.	example given
EIC	extracted ion chromatogram
EP	entrance potential
ESI	electrospray ionization
eV	electron volt
FA	formic acid
Fig.	figure
FW	fresh weight
g	gram
GC	gas chromatography
GC-MS	gas chromatography-mass spectrometry
Glc	glucose
GSH	glutathione
h	hour
HPLC	high performance liquid chromatography
HSS	high strength silica column
Hz	Hertz
I3G	indole-3-ylmethyl glucosinolate = glucobrassicin
inf.	infected
JA	jasmonic acid
kV	kilovolt
M	Molar
Mal	malonyl
Mal-Glc	malonyl glucose
mDa	millidalton

mg	milligram
MICA	2-mercapto-indole-3-carboxylic acid
min	minute
mL	milliliter
mM	millimolar
MS	mass spectrometry
MS medium	Murashige and Skoog medium
MTBE	*tert*-methylbutylether
m/z	mass to charge ratio
µl	microliter
NAE	*N*-acylethanolamine
nanoESI	nanoelectrospray
nm	nanometre
NMR	nuclear magnetic resonance
PCA	principal component analysis
PDA	photodiode array
PDB	potato dextrose broth
p-value	probability value
QQQ	triple quadrupole mass spectrometer
RA	raphanusamic acid
rpm	revolutions per minute
RP	reversed phase
RT	retention time
s	second
SA	salicylic acid
SAG	salicylic acid glucoside
SAR	system acquired resistance
SD	standard deviation
sp.	species
SXM	simulated xylem sap medium
Tab.	Table
TIC	total ion chromatogram
TOF	time-of-flight
™	trademark
TriHOE	9,12,13-trihydroxy-10-octadecenoic acid
TriHOD	9,12,13-trihydroxy-10,15-octadecadienoic acid
UPLC	ultra-performance liquid chromatography
UPLC-TOF-MS	UPLC-time-of-flight mass spectrometry
v	volume
V	Volt
V. longisporum	*Verticillium longisporum*
VL 43	*Verticillium longisporum* strain 43
V. dahliae	*Verticillium dahliae*
vs.	versus

1 Introduction

Plant-pathogen interactions have always been a major topic in plant related research due to the important impact of plant diseases on energy supply and human nutrition. In Ireland for example the potato blight (caused by the fungus *Phytophthora infestans)* led to the Great Famine in the nineteenth century (Haas et al. 2009). More than a fifth of the population died or left the island. Therefore many investigations in crop science were in search of resistant phenotypes or genetic predispositions in order to improve the plant breeding success (Eynck et al. 2009, Kliebenstein et al. 2002). For a better understanding of the direct interaction on molecular level also the metabolites involved in the plant-pathogen interactions came more and more into focus. Two examples of pathogen derived substances might illustrate the complexity that has evolved in the metabolite-based manipulations. The bacterial pathogen *Pseudomonas syringae* was shown to produce the phytotoxin coronatine. This mimics the phytohormone jasmonoyl-isoleucine and influences the host plant to open its stomata as pathogen entry sites (Melotto et al. 2006). Oxalic acid in contrast secreted by the fungus *Sclerotinia sclerotiorum* was identified to manipulate the redox-status of the host plants (Williams et al. 2011). In general, the plants answer pathogen attacks with an arsenal of defence reactions that can either be specific or a general non-host resistance. Another example of pathogen-induced metabolite changes in the interaction with the host plant was described by Djamei and coworkers (2011) in maize. The enzyme chorismate mutase (cmu1) is thereby secreted by the smut fungus *Ustilago maydis* and taken up by the plant cells. This was shown to lead to a change in the metabolic status through metabolic priming in the maize plants. In every case the plant-pathogen interaction leads to a change on the metabolic level that offers a lot of information of involved processes like plant hormone networks or accumulation of defence substances. These reactions can be accessed by identification of the involved substances. The metabolite pattern caused in different host plant species by the pathogenic fungus *Magnaporthe grisea* for example led to a common metabolite signature upon infection including the accumulation of substances from the primary metabolism like amino acids (Parker et al. 2009).

This work focuses on the identification of metabolite changes in Brassicaceae species that occur after the infection with the pathogenic fungus *Verticillium longisporum*. Different crucifer species as oilseed rape (*Brassica napus*), camelina *(Camelina sativa)* and the model plant *Arabidopsis thaliana* were analysed by metabolite fingerprinting analysis to find similarities and differences in response to the fungal invasion. It was searched for putative fungal substances involved in the plant-pathogen interaction as well as for plant defence related metabolites.

1.1 The importance of the Brassicaceae species

The plant family of Brassicaceae (also named crucifers) includes many economically important plant species like *Brassica oleraceae* (cabagge, cauliflower and broccoli), *Brassica nigra* (black mustard) and *Raphanus sativus* (radish). Oilseed rape (*Brassica napus*) is an important crop plant and one of the most cultivated regenerative oil sources. In Germany in 2009 more than 1.4 million hectare were used for *B. napus* cultivation resulting in a harvested amount of more than 6 million tons (source: www.bmelv-statistik.de). Germany is the fourth largest producer of oilseed rape worldwide (source: www.fao.org).

Oilseed rape is the second biggest player on the international oilseed market apart from soybean (*Glycine max*) and mature seeds of *B. napus* contain 45-50 vol. % oil (Wittkop et al. 2009). The composition differs from predominantly cultivated so called LEAR (low erucic acid rapeseed; 0 % erucic acid (C22:1) and low glucosinolate amounts) to HEAR quality (high erucic acid rapeseed). Canola seeds include about 60 % oleic acid (C18:1), about 20 % linoleic acid (C18:2) and 10 % linolenic acid (C18:3) (Wittkop et al. 2009). The oil is used for the food industry or can be converted by transesterification into biofuel (RME rapeseed methyl ester). The seeds provide furthermore a protein-rich meal after oil extraction that can be used for animal feeding. *B. napus* is reported to originate from a spontaneous hybridisation of *Brassica oleracea* and *Brassica rapa* and is therefore an amphiploid species. The origin is described by the "triangle of U" (Fig. 1) and leads to the genome AACC for *B. napus* (Nagaharu 1935).

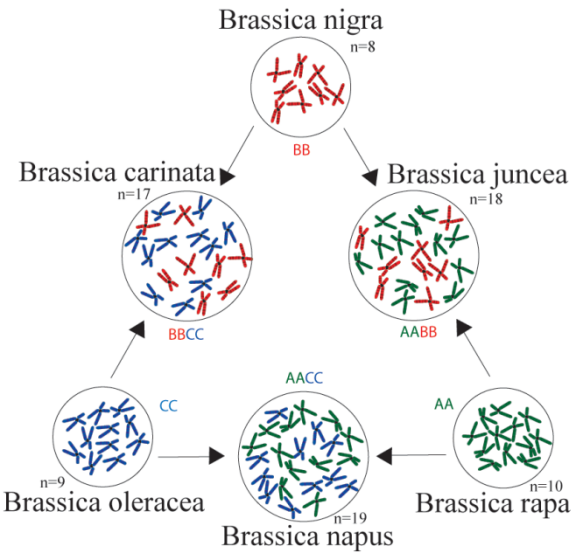

Fig. 1: Triangle of U
The relationship of the different *Brassica* spp. according to their genome can be arranged in a triangle. The amphiploid species are located on the arms whereas the original species are depicted at the angles. n indicates the number of chromosomes in the haploid stage. (from www.wikipedia.org)

A second crucifer species analysed in this work is Camelina *(Camelina sativa)* also called gold of pleasure or false flax. It is an ancient crop plant that has been cultivated in Europe for nearly 4000 years (Dalby 2003). *C. sativa* is appreciated for its low requirements for water and nutrition. Its importance as a crop plant decreased during the last century but the need for enhanced amounts of regenerative oil sources will most likely lead to a renaissance in cultivation (Zubr 1997). It can be used as food oil or for biodiesel production. The oil contains a high level of unsaturated fatty acids (about 90 %) of which 50 % are

the polyunsaturated linoleic and α-linolenic acid (Zubr 1997). Additionally, the pressed seeds offer an oil cake rich in valuable proteins that can especially be used for poultry feeding (Zubr 1997, Hrastar et al. 2009). Genetically *C. sativa* seems to be the closest crop plant relative to the model plant *Arabidopsis thaliana*. They resemble each other in metabolic pathways like the production of the phytoalexin camalexin (Flannery et al. 2006).

A. thaliana was included as a third plant species in the analyses of this work. It is a cruciferous plant species and could therefore be used as a host plant for *V. longisporum* (Johansson et al. 2006) Additionally, it is a well-characterized model plant. For more than 60 years *A. thaliana* has been studied and its genome was sequenced already in 2000 by the Arabidopsis Genome Initiative (2000). For *A. thaliana* many metabolite pathways were investigated thoroughly and the according mutants are available. Comprehensive genetic and molecular data are collected and publicly available at the Arabidopsis information resource (TAIR, www.arabidopsis.org).

In this work metabolic fingerprinting is performed in these three Brassicaceae species with a main focus on *B. napus*. It was aimed to find similarities and differences in the metabolic pathways involved in defence responses. In *A. thaliana* the analysis of mutant strains is the classical approach to investigate metabolite pathways. This was performed e.g. by Chapple et al. 1992 for the phenylpropanoid pathway in *A. thaliana*. There is a well-established toolbox for genetic manipulations available. In contrast, *B. napus* mutant strains are difficult to develop due to many gene duplications in the genome caused by the hybridisation**.** This makes it difficult to introduce a specific mutation. Therefore alternative methods have to be used for metabolite pathway elucidation. This work shows that metabolite fingerprinting combined with structural elucidation of metabolites can be a valuable tool for elucidation of metabolic pathways.

1.2 The vascular pathogens *Verticillium* spp.

The genus *Verticillium* belongs to the phylum of the Ascomycota and includes various hemi-biotrophic pathogenic species like *V. dahliae*, *V. albo-atrum* and *V. longisporum*. Since no sexual stage in the lifecycle was detected they are classified as Deuteromycota (fungi imperfecti). They are soil-borne pathogens that can infect a large range of more than 200 dicotlyledonous host plants, of which many are economically important. *V. dahliae* for example has been described to cause wilting symptoms on crop plants like cotton or tomato and can lead to nearly complete yield losses (Fradin and Thomma, 2006).

V. longisporum has focused on the plant family of Brassicaceae as host plants and preferably infects *B. napus*. Long-spored *Verticillium* isolates were already detected in the 1960s (Stark 1961) but it

lasted more than 35 years before *V. longisporum* was regarded as a distinct species (Karapapa et al. 1997). It is still under discussion whether *V. longisporum* can be clearly distinguished from *V. dahliae* on a taxonomic level. *V. longisporum* has been described to be a stable near-diploid hybrid that has its origin in at least three independent hybridisation events. One of the parental species seems to be *V. dahliae* whereas it is still unclear if *V. albo-atrum* represents the other parental lineage (Inderbitzin et al. 2011).

The lifecycle of *Verticillium* spp. is depicted in Fig. 2. Its successive steps are also valid for *V. longisporum*. The germination of microsclerotia, the dormant structures of *Verticillium* spp., can be induced by the root exudates of the host plants. This has been demonstrated for *V. dahliae* (Mol and van Riessen 1995). The fungal hyphae grow towards the root tips and penetrate them. Subsequently the host plant is colonized via the root cortex and the fungus enters the xylem vessels where it spreads within the vessels. Within the xylem the fungus propagates by forming conidiospores. These are transported in the vascular tissue via the transpiration stream. Chlorosis, necrosis and for many *Verticillium* spp. wilting symptoms are characteristic disease symptoms. The fact that not all vessels are colonized might explain why no wilting symptoms are visible in *V. longisporum* infected host plants (Eynck et al. 2007). In the saprophytic stage of the fungal lifecycle the whole plant tissue is colonized. The microsclerotia which are formed on the senescing tissue can survive for more than ten years in the soil and are the source for further infection cycles (Heale and Karapapa 1999). In contrast to *V. longisporum, V. dahliae* is not able to colonize *B. napus* plants successfully (Eynck et al. 2007).

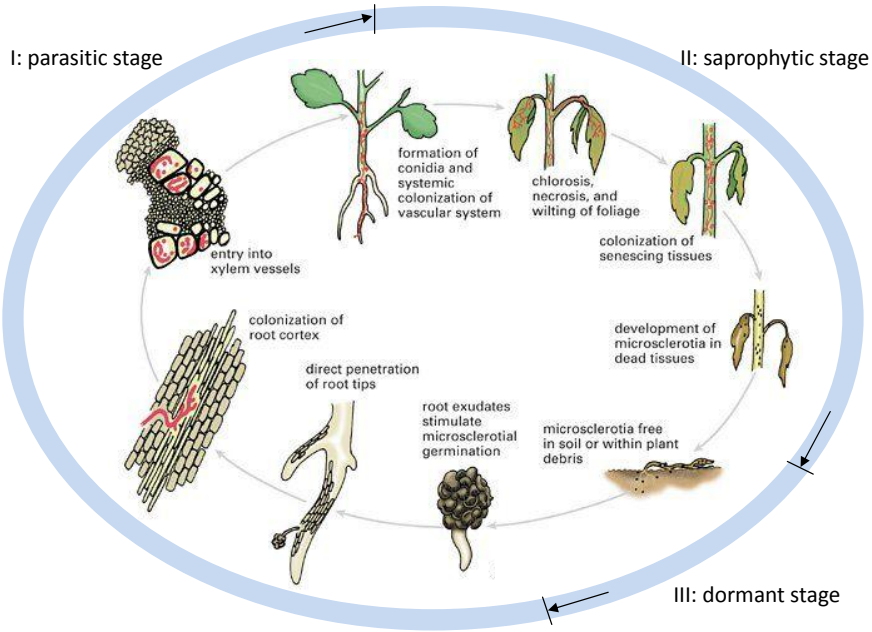

Fig. 2: Life cycle of *Verticillium* spp.
Figure adapted from a drawing of Vickie Brewster, coloured by Jesse Ewing (from Berlanger and Powelson 2000). The life cycle of *Verticillium* spp. consists of three stages: I: parasitic stage, II: saprophytic stage, III: dormant stage.

Detectable disease symptoms in *B. napus* are stunting, axillary branching, the induction of early flowering as well as the formation of black leaf veins and chlorosis, which can in the end lead to necrotic tissue (Zhou et al. 2006; Eynck et al. 2007). In the field the symptoms are less severe than in greenhouse experiments but *V. longisporum* infection nevertheless leads to significant yield losses. The symptoms in the field are difficult to distinguish from senescence or other diseases so that a diagnosis is often only possible in late infection stages. Until now no fungicides against *Verticillium* spp. are available once the host plants are infected (Dunker et al. 2008).

A pathogenic strain of *V. longisporum* has been isolated from *B. napus* (VL 43; Zeise and Tiedemann 2002). Over the last years this strain has been investigated thoroughly. Successful procedures for infection of *B. napus* and *A. thaliana* were established and by various methodical approaches the host-pathogen interaction has been analysed. Physiological observations of *V. longisporum* infection by Eynck et al. (2007) and Zhou et al. (2006) have led to a proper understanding of the timeline of the infection process in *B. napus*. Studies of the disease development in field and greenhouse experiments evaluated the impact of the fungal infection on yield and found more and less susceptible genotypes (Dunker et al. 2008, Eynck et al. 2009, Eynck et al. 2009b). In *A. thaliana* different quantitative trait loci (QTL) could be identified. It was shown that resistance to systemic spread and stunting resistance were controlled by different QTLs (Häffner et al. 2010). Transcriptome profiles of the fungus were analysed by cDNA-amplified fragment length polymorphism (AFLP) and a genetic fingerprint of *V. longisporum* was generated (Weiberg et al. 2009). The mutation of *V. longisporum* by RNA-mediated silencing has led to the generation of a mutant with reduced expression of the chorismate synthase, a key enzyme in the aromatic amino acid biosynthesis (Singh et al. 2009). This strain infects *B. napus* less effectively. The mutant showed an increased expression of the gene cross pathway control A (cpcA) indicating an active amino acid cross pathway control. This control mechanism is supposed to be turned on by an imbalanced amino acid supply in the xylem. In the leaf apoplast of *B. napus* 12 proteins were found to be up regulated after *V. longisporum* VL 43 infection (Floerl et al. 2008). Some of them could be identified as pathogen defence enzymes e.g. a *ß*-1,3-glucanase and a peroxidase. This suggested a systemic signalling induced by the fungus because at that time point, the fungus was not detectable in upper plant tissue. The analysis of the fluids from the apoplastic space in *B. napus* and *A. thaliana* indicated that neither the nutrient uptake of the fungus from the xylem sap nor the clogging of the vessels could be responsible for the disease symptoms of stunting and chlorosis (Floerl et al. 2008, Floerl et al. 2010). These findings led to the hypothesis that a fungal substance is spread within the plant. This compound is supposed to cause disease symptoms in the upper plant organs by toxic or signalling function before fungal hyphae have colonized the tissue. A first investigation on metabolic level was

performed by Ratzinger et al. (2009), who identified salicylic acid (SA) and its glucoside (SAG) as accumulating substances in xylem sap and surrounding tissue of *B. napus* upon fungal infection. Apart from this study, information on metabolic changes in Brassicaceae infected with *V. longisporum* is scarce and more information about the metabolic consequences of the host-pathogen interaction is needed. One additional question is, if the analysis of the "artificial" host plant *A. thaliana* is suited to study the infection process as a model for the natural host *B. napus*. The infection of *C. sativa* with *V. longisporum* has not been investigated before although a more extensive cultivation of this crop plant might be threatened by *V. longisporum*. In this work it was therefore investigated if *C. sativa* can be infected by *V. longisporum* and how the metabolic reaction resembles the induced changes in *B. napus* and *A. thaliana*.

1.3 Defence responses in the plant-pathogen interaction

In the plant-pathogen interaction a broad spectrum of defence mechanisms has evolved. The recognition of highly conserved microbe associated molecular pattern (MAMP) by plant receptors leads to an activation of multiple defence responses. This can include programmed cell death, the production of reactive oxygen species, callose deposition or the synthesis of antimicrobial substances as phytoanticipins and phytoalexins (Clay et al. 2009).

Glucosinolates are phytoanticipins in crucifers (Pedras and Hossain 2011) which means that are present in the healthy plant prior to infection (VanEtten et al. 1994). This distinguishes them from phytoalexins are a class of secondary plant metabolites that are synthesized *de novo* in reaction to biotic (e.g. fungal infection) and abiotic stress (e.g. UV radiation). The process of phytoalexin biosynthesis induction is known as elicitation. Within a certain plant family common building blocks are used for the biosynthesis of different phytoalexins (Pedras and Yaya 2010). In Brassicaceae these are indole alkaloids that contain a sulphur atom and are synthesized from the amino acid tryptophan as precursor (Pedras et al. 2011). The rate and blend of their biosynthesis depends on the elicitor and the plant species (Pedras et al. 2008). The first phytoalexin described in Brassicaceae has been brassinin (Takasugi et al. 1986) but until now 44 phytoalexins from crucifers have been identified. Based on structural features they can be divided into six groups as it was recently reviewed by Pedras et al. (2011). All so far known phytoalexins are illustrated in Fig. 3.

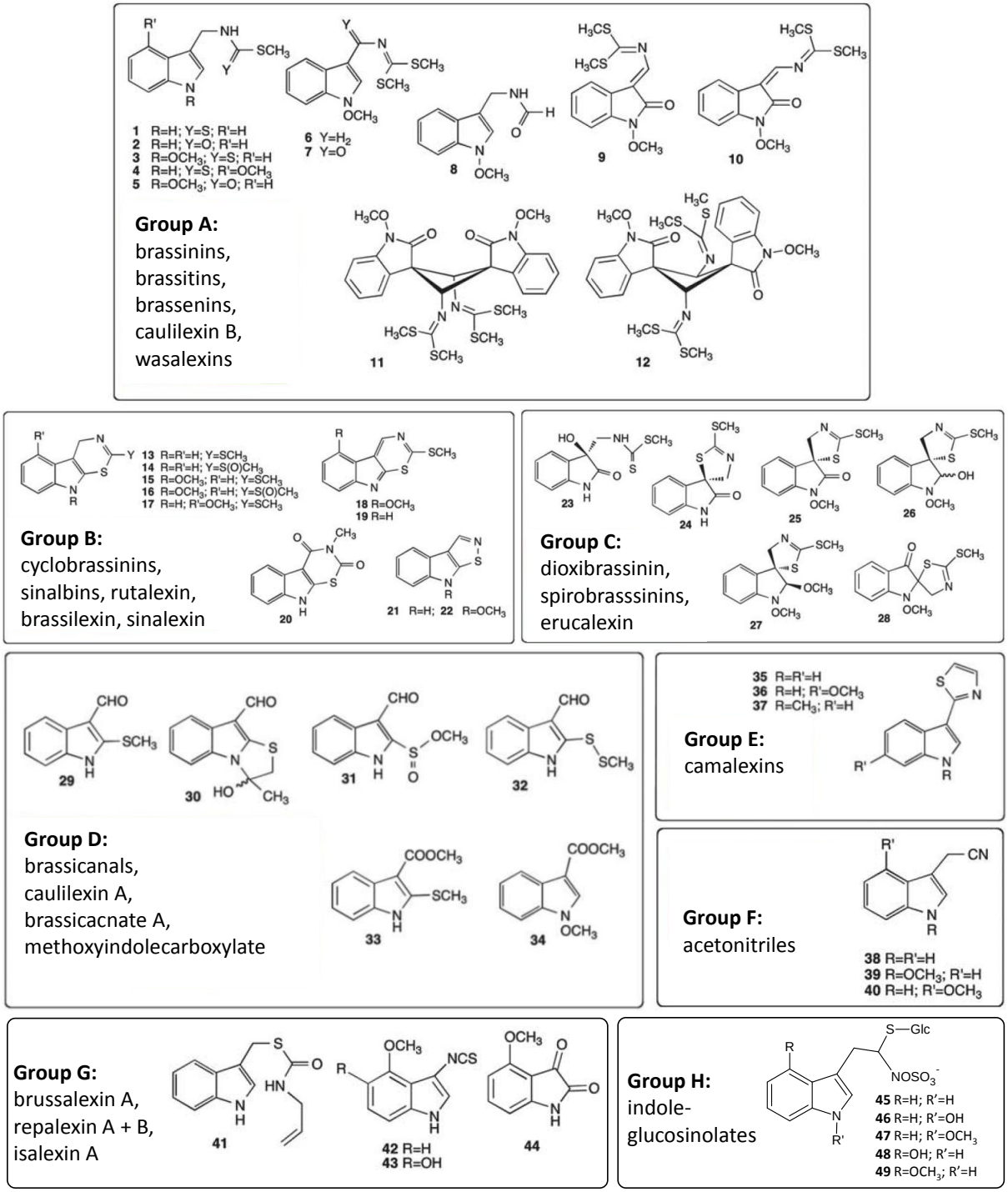

Fig. 3: Phytoalexins and phytoanticipins from Brassicaceae (modified from Pedras et al. 2011)
1 brassinin, 2 brassitin, 3 1-methoxybrassinin, 4 4-methoxybrassinin, 5 1-methoxybrassitin, 6 1-methoxy-brassenin A, 7 1-methoxybrassenin B, 8 caulilexin B, 9 wasalexin A, 10 wasalexin B, 11 biswasalexin A1, 12 biswasalexin A2, 13 cyclobrassinin, 14 cyclobrassinin sulfoxide, 15 sinalbin B, 16 sinalbin A, 17 4-methoxycyclobrassinin, 18 4-methoxydehydrocyclobrassinin, 19 dehydrocyclobrassinin, 20 rutalexin, 21 brassilexin, 22 sinalexin, 23 dioxibrassinin, 24 (S)-spirobrassinin, 25 (R)-1-methoxyspirobrassinin, 26 1-methoxyspirobrassinol, 27 (2R,3R)-1-methoxyspirobrassinol methyl ether, 28 erucalexin, 29 brassicanal A, 30 brassicanal B, 31 brassicanal C, 32 caulilexin A, 33 brassicanate A, 34 methyl-1-methoxyindole-3-carboxylate, 35 camalexin, 36 6-methoxycamalexin, 37 1-methylcamalexin, 38 indolyl-3-acetonitrile, 39 caulilexin C, 40 arvelexin, 41 brussalexin A, 42 rapalexin A, 43 rapalexin B, 44 isalexin, 45 indol-3-yl-methyl glucosinolate, 46 1-hydroxy-indol-3-yl-methyl glucosinolate, 47 1-methoxy-indol-3-yl-methyl glucosinolate, 48 4-hydroxy-indol-3-yl-methyl glucosinolate, 49 4-methoxy-indol-3-yl-methyl glucosinolate

Phytoalexins are defined as substances with antimicrobial activities. They are only locally distributed. Therefore their occurrence indicates a stress response within the analysed tissue. Phytoalexins are discussed to possess additionally anti-proliferating effects and can therefore be valuable tools in cancer prevention. They are components of our daily diet but are only produced in low amounts in the plant (about 1-5 mg/kg fresh weight). Many of them can be synthesized chemically (Kutschy and Mezencev 2008). In *B. napus* the phytoalexins brassinin, 1-methoxybrassinin, cyclobrassinin, dehydrocyclobrassinin, 4-methoxydehydrocyclobrassinin, cyclobrassinin sulfoxide, spirobrassinin, brassicanal A, brassicanate A, brassilexin, isalexin, rutalexin and indole-3-acetonitrile have been found after biotic or abiotic elicitation (Pedras and Yaya 2010). This includes representatives of group A to D and F (Fig. 3). In contrast to *B. napus,* camalexin (Fig. 3 group E) is the major phytoalexin of *A. thaliana* and *C. sativa*. Its biosynthesis including all enzymes has been investigated thoroughly in *A. thaliana*. A currently published model for the camalexin biosynthesis is depicted in Fig. 4 (Geu-Flores et al. 2011). Tryptophan is converted by CYP79B2/B3 and CYP71A13 via indole-3-acetaldoxime (IAOx) into indole-3-acetonitrile (IAN). The sulphur donating molecule was identified to be glutathione (GSH) (Su et al. 2011) which is attached to IAN. This leads to the formation of a GSH conjugate intermediate (GSH-IAN). In the following enzymatic steps glutamate and glycine are supposed to be cleaved of by a γ-glutamyl-peptidase and a carboxypeptidase. The subsequent cyclisation of the IAN cysteine conjugate (Cys-IAN) and the oxidative decarboxylation of the intermediate dihydrocamalexic acid were described already a few years ago (Schuhegger et al. 2006, Böttcher et al. 2009).

In order to counteract the antimicrobial activity of the phytoalexins some pathogens are able to metabolize and thereby detoxify them. Glycosylation, oxidative degradation or hydrolysis reactions performed by fungal enzymes have been shown to reduce the antimicrobial activity (Sexton et al. 2010, Pedras et al. 2011b). These transformations lead to a complex mixture of substances which were originally synthesized by plants but are enzymatically modified by fungi.

This biosynthesis model (Fig. 4) includes also a second group of defence related metabolites in Brassicaceae, the glucosinolates. These are sulphur and nitrogen containing compounds as well. Glucosinolates share a common core structure which includes a glucose bound to the aglycone via a sulphur atom and a sulphate group bound via nitrogen to the central carbon atom. They differ in their variable side chains that derive from the amino acid precursor tryptophan, phenylalanine or methionine (Grubb and Abel 2006, Yan and Chen 2007). According to Pfalz et al. (2011) they can be divided into the groups of aliphatic, aromatic and indole glucosinolates. The indole glucosinolates are displayed in Fig. 3 (group H). It was shown that *A. thaliana* is able to synthesize more than 30 different glucosinolates (Kliebenstein et al. 2001). In the biosynthesis of the tryptophan derived indole glucosinolates they share a first step in biosynthesis with the phytoalexins (Fig. 4).

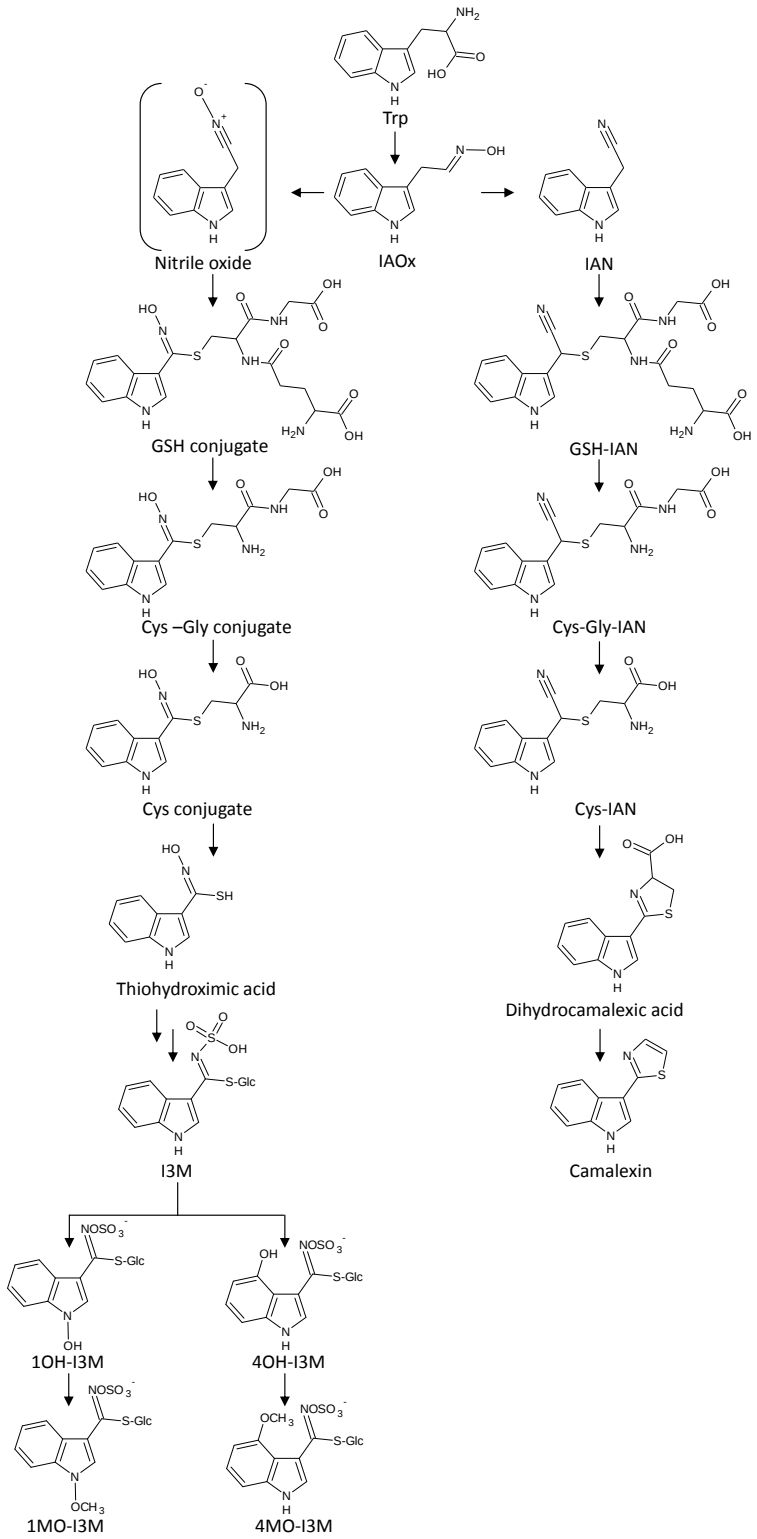

Fig. 4: Model for the proposed biosynthesis of tryptophan-derived glucosinolates and camalexin in *A. thaliana* (modified from Geu-Flores et al. 2011 and Pfalz et al. 2011)

The left branch represents the proposed indole glucosinolate biosynthesis whereas the right branch described the putative pathway leading to the phytoalexin camalexin. IAOx = indole-3-acetaldoxime, IAN = indole-3-acetonitrile, GSH = red. Glutathione, I3M = indol-3-yl-methyl glucosinolate, 1OH-I3M = 1-hydroxy-indol-3-yl-methyl glucosinolate, 1MO-I3M = 1-methoxy-indol-3-yl-methyl glucosinolate, 4OH-I3M = 4-hydroxy-indol-3-yl-methyl glucosinolate, 4MO-I3M = 4-methoxy-indol-3-yl-methyl glucosinolate

Subsequent steps seem to be comparable to the phytoalexin biosynthesis like the synthesis of a glutathione conjugate as intermediate. These precursors were found to accumulate in an *A. thaliana* γ-glutamyl peptidase mutant due to a blockage in the biosynthesis which prevents the following enzymatic reaction steps (Geu-Flores et al. 2011). The subsequent cleavage of glutamate and glycine (similar to phytoalexin biosynthesis) results in the formation of thiohydroximic acid, the precursor for glucosinolate formation. The following indole glucosinolate modifications like hydroxylation and the addition of methoxy groups have been described by Pfalz et al. (2011).

The breakdown of glucosinolates in disrupted tissue (mustard oil bomb) can lead to the formation of isothiocyanates. This substance class is volatile and lipophilic and has been demonstrated to be toxic for many plant pathogenic organisms (Fahey et al. 2001). The degradation of glucosinolates in intact tissue was reported to result in different end products like amines and raphanusamic acid (Bednarek et al. 2009).

Often the deglycosylation of metabolites results in toxic products as for example in the glucosinolate degradation by myrosinases (*ß*-thioglucoside glucohydrolases). In contrast the glycosylation of compounds as mentioned above for the phytoalexins can help to decrease their toxic potential. With the glycosylation of SA to the corresponding glucoside (SAG) the plant prevents itself to high levels of the plant hormone and enables an easier transport and storage (Yalpani et al. 1992). Therefore the addition of glucose to a metabolite or its cleavage can be regarded as an important regulation step in the defence processes between plants and their pathogens.

1.4 Metabolite fingerprinting

The metabolome is defined as the complete set of metabolites of an organism (Dettmer et al. 2006). The analysis of the metabolome can be based on different strategies. Until now no analytical platform is able to analyse all kind of metabolites of a biological sample in one step due to their huge variation in physical and chemical properties. Additionally, huge differences in the concentrations of the substances must be covered (magnitude of 4 to 5 powers of ten). Metabolite profiling focuses on a certain group of metabolites. The measurements of this targeted analysis should be optimized to the certain substance or substance class e.g. oxylipins (Göbel and Feussner 2009). In most cases quantification is included. In contrast, a non-targeted approach called metabolite fingerprinting, can be performed. The aim of a metabolite fingerprinting analysis is to detect metabolite pattern that change in response to an altered condition. This can include biotic stresses like diseases or abiotic stresses as toxin treatments. It can also be used to find metabolic differences of genetic variations e.g. wild type vs. mutant (Dettmer et al. 2007, Fiehn 2002). All results from metabolite fingerprinting

are obtained from the comparison to a control condition. Therefore this differential approach only provides relative data which include metabolites with a different amount in control and changed condition. To create datasets that allow a statistical analysis, a sufficient number of technical replicates is needed. Therefore a high-throughput technique is needed to enable a rapid analysis of the samples. Metabolite fingerprinting can be performed in aqueous samples like blood plasma, culture media or apoplastic fluids from plants or in tissues like fungal mycelium, human cells or plant tissue (Lucio et al 2010, Catchpole et al. 2005, Mintz-Oron et al. 2008). The metabolite fingerprinting workflow used here consists of three major steps that can be described as metabolite extraction, detection and data analysis (Vinayavekhin et al. 2010). These steps will be described in more detail in the following paragraphs. A more detailed workflow for the metabolite fingerprinting is depicted in Fig. 5.

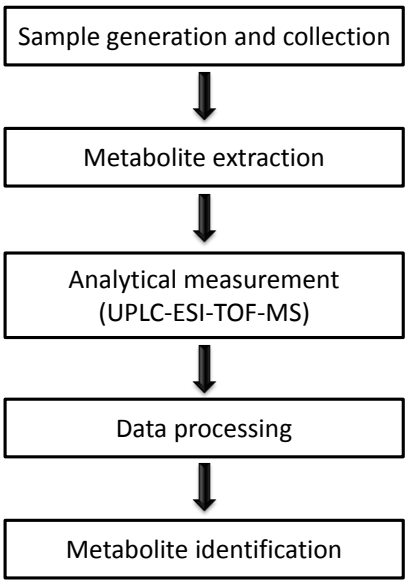

Fig. 5: Scheme of the metabolite fingerprinting workflow used in this work

1.4.1 Extraction of metabolites

Metabolite fingerprinting starts with the sample collection. This is a step that must be performed quickly since the metabolic reactions must be quenched immediately. Some treatments like cold shock can nevertheless lead to a metabolite leaching from the cells (Wittmann et al. 2004). For sample extraction various methods have been described (Fiehn et al. 2000, Matyash et al. 2008, Sellick et al. 2010) but it must be stated that no general method can be found since the sample properties can be different e.g. aqueous vs. solid sample. Therefore a method must be validated and optimized before being transferred to a new field of application. In most cases an extraction of metabolites is necessary because high protein levels in the sample can lead to a decrease in instrument performance and an increasing backpressure when directly injected (Pham-Tuan et al.

2003). Additionally, extraction enables the release of non-polar metabolites from tissue structures of the biological matrix and allows removing of the remaining matrix components (Dettmer et al. 2007).

1.4.2 Separation and detection of metabolites

The analysis of metabolites can be performed on various platforms. Gas chromatography (GC) coupled to a mass spectrometer (MS) was the first method used for metabolite fingerprinting. GC analysis is described as robust and reproducible (Allwood and Goodacre 2009). On the other hand it has its disadvantage of being suitable only for volatile compounds. Only the addition of the volatile trimethylsilyl group (TMS) by a derivatisation step allows including more polar metabolites (Fiehn et al. 2000). Liquid chromatography (LC) coupled to MS is becoming more and more important for metabolite fingerprinting as no derivatisation is needed and almost any metabolite that dissolves in liquid can be accessed (Allwood and Goodacre 2009, de Vos et al. 2007). ^{1}H-NMR (nuclear magnetic resonance) is only suited for metabolite fingerprinting for highly abundant substances and can therefore easily miss metabolites in low concentrations with an important influence like hormones. It nevertheless is superior to mass spectrometry in providing structural information and in quantitation and is furthermore non-destructive (Schripsema et al. 2009). The analysis of complex samples with MS offers advantages like a high sensitivity and the minimal sample volume which is needed for the analysis. This allows the rapid measurement of hundreds of metabolites and is suitable for the determination up to trace level of medium- and high-polarity metabolites (Capiello et al. 2008). Despite the advantages of MS in metabolic fingerprinting, the method also does have some limitations. Unfortunately, so called matrix effects often prevent a stabile quantification. During ionization of different metabolites at the same time a phenomenon named ion suppression can occur. This can lead to a false estimation of the substance amount of a particular analyte (Annesley 2003, Capiello et al. 2008). In order to reduce ion suppression a chromatographic separation of a sample can precede the MS measurement. This separates the substances on a time scale and thereby reduces coelution of metabolites. Hence better ionisation efficiency for the single substances can be achieved.

LC is a technique for separation of molecules carried by a solvent (mobile phase) through a matrix (stationary phase). For the LC stationary phase (column) a reverse-phased (RP) chromatography is now often used. Reversed-phase columns are mostly based on silica-C18 particles because of their good pH stability, low column bleed and efficient retention of hydrophobic compounds (information from www.waters.com). Alternatively, a normal-phase column that uses the hydrophilic interactions for separation (HILIC) can be used. To reduce the analytical run time and to minimize the usage of solvents without losing resolution special LC systems have been developed. Short columns with very small particles (diameter of <2 µm) can achieve this advantages. This however results in a high

backpressure up to 1000 bar. Only ultra-performance LC (UPLC) instruments are able to cope with such a high pressure. Special column materials have been developed that withstand the high pressure and guarantee a reproducible chromatographic separation (Allwood and Goodacre 2010). Therefore UPLC instruments are especially suitable for the high-throughput measurements with short run-times needed for metabolite fingerprinting. A continuously changing mixture of the liquid phase that includes a polar solvent e.g. water and a non-polar solvent e.g. acetonitrile leads to successive elution of metabolites from the stationary phase.

After the chromatographic separation the solvent flow carries the metabolites to a coupled detector. This can be in a first step a non-destructive absorbance method. Thereby the UV or visible light absorbance is recorded by a photodiode array (PDA). Obtaining UV-Vis spectra can be useful to assign the detected compounds to a certain substance class (Allwood and Goodacre 2009). Subsequently or instead of PDA detection, MS detection can be performed. For LC-MS based metabolomics two ionisation techniques for MS measurements are used: electrospray ionisation (ESI) and atmospheric pressure chemical ionisation (APCI). The setup in both ionisation sources is similar but differs by the corona pin in APCI sources. This forms a reagent gas plasma by which the sample molecules are ionized. APCI is more appropriate for non-polar metabolite ionisation while ESI has the disadvantage to ionize non-polar substances less effective. On the other hand has ESI proven to be a softer ionization method and to causes less in-source fragmentation (Allwood and Goodacre 2010). ESI is therefore the most commonly used technique for metabolite fingerprinting. The high voltage (about 4000 V) applied at the needle leads to the formation of ions from the sample molecules (Fig. 6).

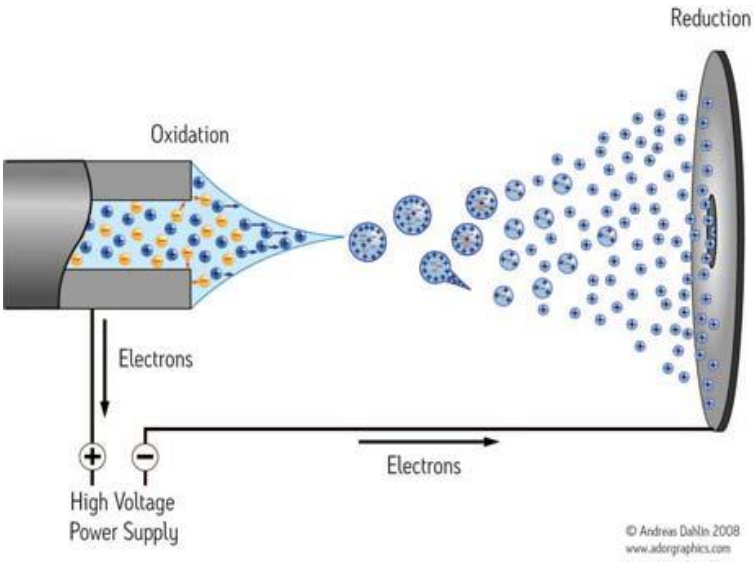

Fig. 6: Schematic diagram of electrospray ionisation (ESI) (from www.adorgraphics.com by A. Dahlin)

Displayed is a schematic process of electrospray ionisation of metabolites. The high voltage indicates the electric field which is applied to the needle and a counter plate. The figure shows the positive ionisation mode.

After nebulisation with nitrogen gas the solvent is evaporated until a critical threshold (Rayleigh limit) is reached. Then the ions repel each other and in a so-called Coulombic explosion a spray of

ions is formed. Subsequently the ions enter the mass analyser. During this process not only singly charged ions can be formed but also multiple charging of a single molecule can occur (Gaskell 1997). While the ionisation is performed under atmospheric pressure the mass analysis and detection must happen under high vacuum.

After the complex process of ionisation, a separation of the generated ions according to their m/z is carried out using one of several existing types of mass analysers such as quadrupoles, ion traps, ion cyclotron resonance (ICR) or time of flight (TOF). The mass analyser uses electrical and/or magnetic fields to focus and transfer the ion stream to the detector. For metabolite fingerprinting it is necessary to achieve a high mass accuracy during measurement. Therefore quadrupole and ion trap mass analyser are not suitable since they are only able to acquire nominal masses. In contrast ICR- and TOF-MS can perform mass measurements that are sufficient to generate molecular formulas from the recorded masses. ICR-MS instruments display the highest resolution and detection efficiency. On the other hand it is difficult to couple their high vacuum needed for detection to the high pressure of the ion sources (Lemiére 2001). Additionally, considerable financial resources for purchase and maintenance of an ICR-MS instrument are necessary. Time of flight (TOF) mass detection is characterized by a high scan rate (up to 20.000 scans/s), a high resolution and a high sensitivity. The technique is based on the principle, that the mass of an ion is related to its flight velocity. Therefore it allows calculating its mass-to-charge ratio. In a reflectron TOF with W optics the flight distance is extended resulting in an enhanced mass spectral resolution (Allwood and Goodacre 2009). TOF-MS has become popular in the last decades due to the rapidly developing data recording velocity. Moreover computing facilities are now able to cope with the fast and extensive generation of mass data information in a TOF-MS (Guilhaus 1997).

The final step of a mass spectrometric analysis is the detection of the analysed ions. The detectors for TOF-MS analysers are mostly so called micro-channel plates (MCPs). They record the passing ions by a current that is produced or by an induced charge. These signals were counted, amplified and summed into time bins across the mass spectral scan (Allwood and Goodacre 2010). When all scans of an analytical run are combined and all measured ions are summed up, it results in a total ion chromatogram (TIC, Fig. 7 A). From this TIC a certain mass can be extracted ending up in a so called extracted ion chromatogram (EIC). Thereby the specific mass is extracted from each single mass spectrum. In each mass spectrum a defined number of scans has been summed up. When the mass of protonated tryptophan is extracted from the TIC in Fig. 7 A, it results in the EIC displayed in Fig. 7 B. The single mass spectrum recorded at the retention time of tryptophan (2.48 min) includes the protonated tryptophan as well as putative adducts and other ions eluting at the same retention time (Fig. 7 C).

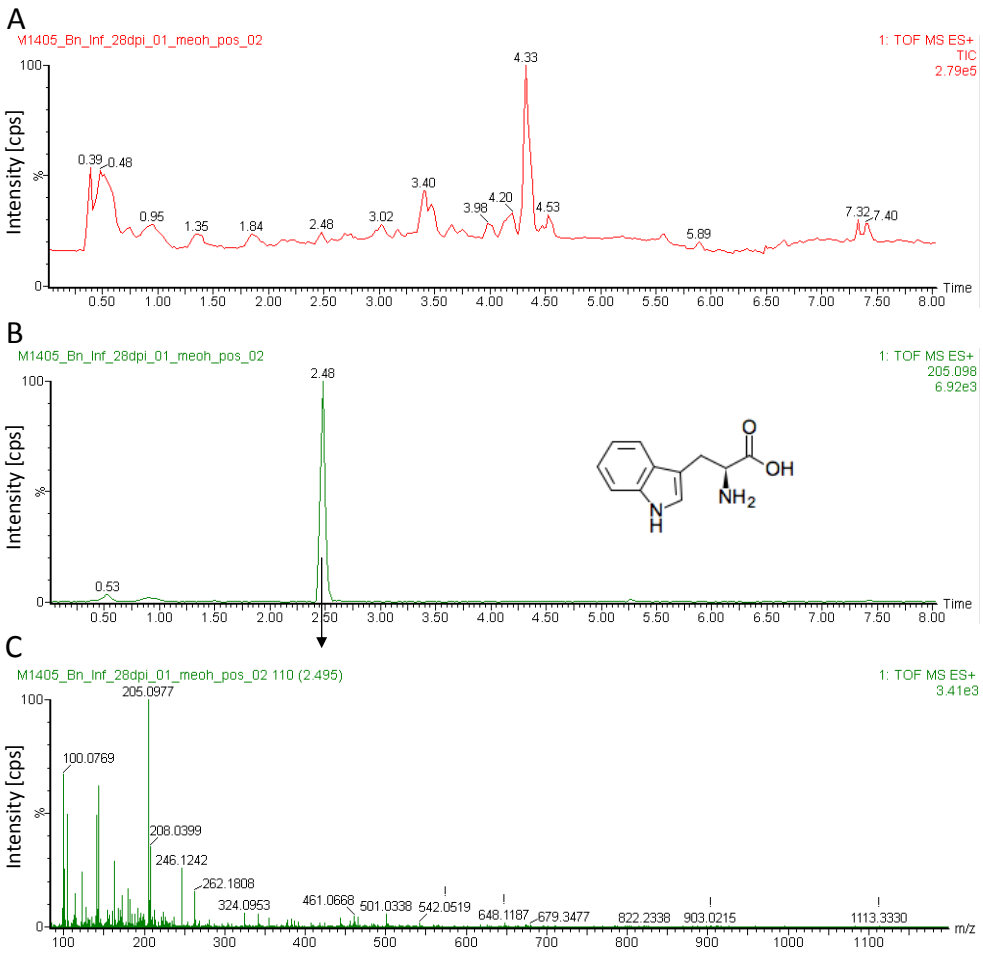

Fig. 7: Recorded data from an LC-TOF-MS analysis
(A) Total ion chromatogram (TIC) of a *B. napus* sample analysed with UPLC-ESI-TOF-MS (B) Extracted ion chromatogram (EIC) of m/z 205.098 (corresponding to protonated mass of tryptophan) (C) Mass spectrum recorded at the retention time 2.49 min. It displays the protonated mass of tryptophan.

In this work an LC-MS based approach was chosen. The chromatographic separation for metabolite fingerprinting was achieved by an UPLC operated with two different C18 reversed-phase columns. One was used primarily for polar the other for non-polar metabolites. A PDA detector recorded the UV-Vis spectra subsequent to the separation. For ionisation an ESI source was used before the exact mass detection was performed with a TOF-MS.

1.4.3 Data processing

The obtained data from high-throughput analytical measurements must be converted in a next step in user-friendly and clearly structured form. In a first step data pre-processing includes deconvolution of data, peak integration and alignment of all raw data files, which should be incorporated in one data matrix. This can be done by freeware programs as MZmine (Katajamaa et al. 2006) or by software provided from the analytical instrument supplier as Mass Hunter Workstation by Agilent Technologies (Böblingen, Germany). For metabolite fingerprinting of this work MarkerLynx^{TM} by Waters Corporation (Milford, MA, USA) was used for data pre-processing. MarkerLynx was

furthermore able to remove additional masses from the naturally occurring ^{13}C isotope (isotopomers) and deisotope the resulting datasets. This pre-processing results in the creation of a multidimensional data matrix that can be processed further for statistical analysis and data mining. The matrix contains a number of markers. Thereby a marker is defined by a retention time (RT) recorded after chromatographic separation, a certain m/z obtained from the TOF-MS measurement and the corresponding intensity. In the matrix, data from at least two conditions is included. These conditions are for example control and infected plants. Each condition includes multiple measurements from biological and/or technical replicates. The pre-processing additionally includes a differential analysis. This means that the data matrix includes only markers that differ in their intensity within the measured samples. By this metabolites with unchanged levels are discarded from the matrix even if they are highly abundant.

In order to get an overview of the quality of the recorded data e.g. reproducibility within technical or biological replicates a principal component analysis (PCA) can be used. This is a sample-based clustering that can illustrate differences of the various conditions. It is able to reduce the dimensions of a dataset into its major components (Jolliffe 2002) but it cannot assign ranks or a priority to a certain characteristic trait (Baumgartner et al. 2011).

In order to identify substances that accumulate or are depleted in samples from a certain conditions a metabolite-based clustering can be performed. For that the data matrix obtained from pre-processing tools is processed further. The data mining for metabolite fingerprinting in this work was carried out with the MarVis (Marker Visualisation) software toolbox that was designed for the analysis of data from metabolomic experiments (Kaever et al. 2009, Meinecke et al. 2008). After import of the data matrices, the intensities of the different measurements per condition are aggregated and the resulting intensity vectors are normalized. To order to improve the quality of the data the MarVis toolbox has been expanded to a filtering tool that is able to rank the imported markers based on statistical analysis and allows discarding of low quality markers (high p-values in ANOVA or Kruskal-Wallis test) prior to the clustering process (Kaever et al. submitted). Markers can be excluded from further processing by this filtering if they are not reliably detected or oscillate considerably in their intensity in the measurements.

The remaining high-quality markers are then clustered in a metabolite-based way and subsequently visualized according to their intensity profile. The visualisation is a colour-coded matrix that gives a quick and comprehensive overview on the metabolite pattern of all conditions. This one-dimensional self-organizing map (1D-SOM) is based on a variable number of clusters (prototypes) which are sorted according to their similarity. Each prototype contains a variable number of markers with a similar intensity profile. A screen shot of the MarVis Cluster tool is depicted in Fig. 8 and it displays

the colour-coded 1D-SOM in the upper figure as well as the number of markers in the associated clusters in the lower figure.

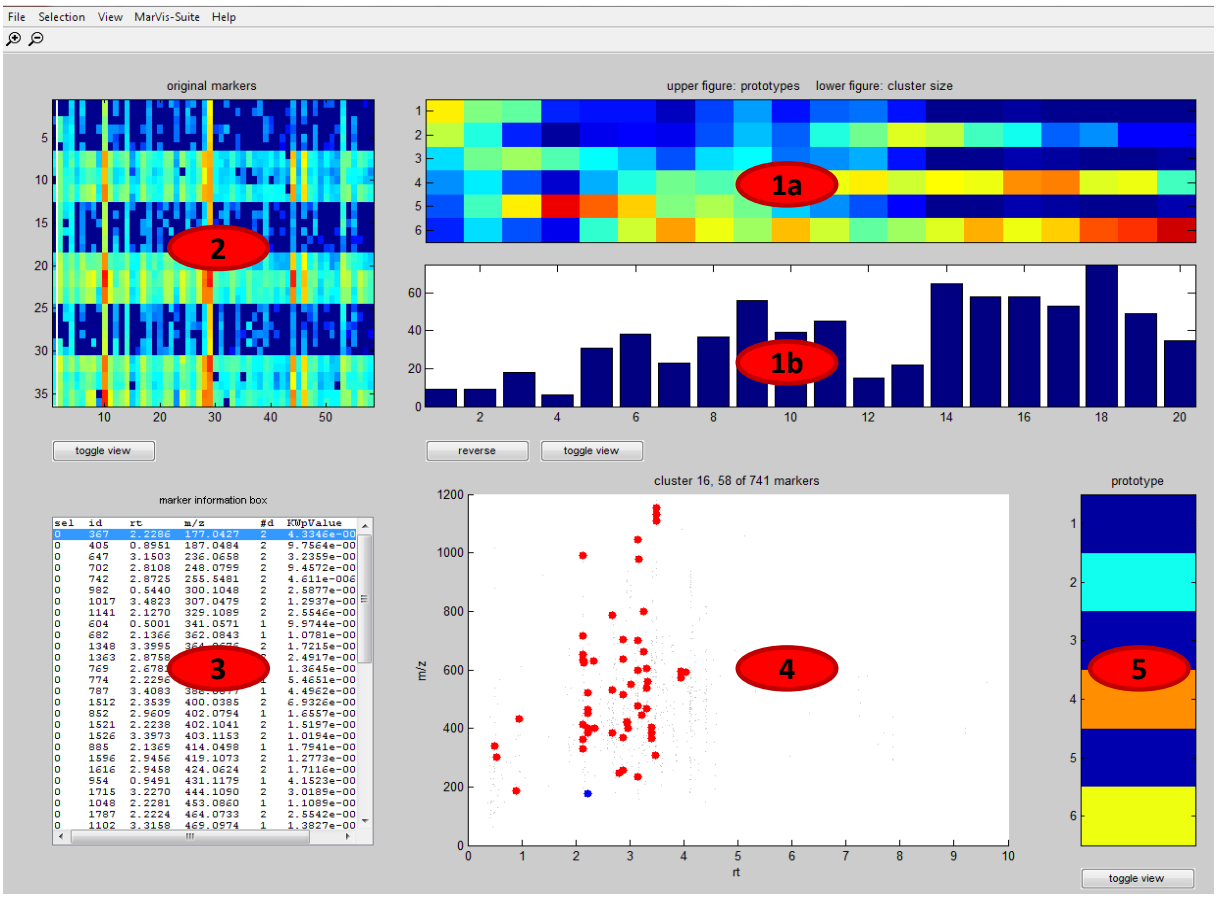

Fig. 8: MarVis Cluster main window (modified from Kaever et al. 2009)
The main window is divided into several regions, which display different information: The colour-coded 1D-SOM (1a), the number of markers in the associated clusters (1b), the cluster plot displaying the intensity profiles of markers in the currently activated cluster (2), the marker information box showing detailed information like m/z or retention time (3), the marker scatter plot displaying the retention time vs. m/z of all markers in the currently activated cluster (4), the active-prototype/marker plot displaying the magnified prototype profile of the activated cluster (5).

Additionally, a cluster plot (titled original markers) is included in the MarVis main window. It illustrates the original intensity profiles of the markers in the currently activated cluster. The marker information box displays detailed information like m/z, retention time or p-value of the single markers. A marker scatter plot (RT / m/z plane) gives an overview of the markers in the currently activated cluster. The prototype plot shows the magnified prototype profile but can be switched to a magnified single marker profile.

After the clustering process, MarVis allows a selection of prototypes that include markers of interest for the experimental setup (e. g. markers accumulated or only detected in samples of infected plants). By selection of these prototypes the contained markers can be exported to various spreadsheet formats or imported into another tool included into the MarVis toolbox. This add-on is able to query various publicly available metabolite databases. The database search can compare the

masses measured in the metabolite fingerprinting with the exact masses stored in databases. In case of a database hit within a certain mass window the identity of the marker can be tentatively assigned. Databases that can be queried by MarVis include for example KEGG (Kanehisa et al. 2009), AraCyc (Zhang et al. 2005) or LIPID MAPS (Sud et al. 2007). In some databases the substances are grouped to metabolic pathways (e.g. KEGG and AraCyc). By a pathway-based search with the MarVis pathway tool it is additionally possible to highlight certain pathways or groups of substances as affected. This can be noticed by an accumulation of database hits in e.g. a certain metabolic pathway for accumulating metabolites under the experimental condition. The MarVis pathway function thereby enables a quick screening for the involvement of already annotated metabolic pathways or substance classes. This was demonstrated successfully for sterigmatocystin biosynthesis in fungal development of *Aspergillus nidulans* (Nahlik et al. 2010).

One additional point that needs to be taken into account in data processing is the formation of adducts during LC-MS measurements. Solvent additives like formic acid are used to increase the ionization efficiency but they can be attached to a molecule so that the detected mass-to-charge ratio (m/z) is not consistent with the mass of the parental ion. Also other adducts can be formed in both ionization modes but the attached molecules or ions differ. In negative ionisation the addition of formic acid (FA) and sodium formate is most common whereas in positive ionisation mostly sodium or ammonium adducts are formed (Brown et al 2009). Due to their formation during ionisation they exhibit the same retention time as the charged mass without adducts. Based on this knowledge MarVis Filter enables an automated determination and correction of adducts in the data sets according to customer-defined rules (Kaever et al. submitted). It nevertheless must be kept in mind that the formation of adducts depends on various parameters as the used solvent additive, the concentration of the metabolite and its chemical properties. For this reasons an automated adduct correction of measured m/z values in the data processing must be used very carefully. A correction routine which includes too many putative adduct masses can lead to the calculation of false masses for the parental ions.

The features included in the MarVis toolbox (filtering, adduct correction and clustering) enable a drastic decrease in the number of markers by eliminating low quality markers, adducts and uninteresting intensity profiles for the biological question. This drastically increases the probability to find relevant metabolite markers within the large background of “noisy” high-throughput LC-MS data (Kaever et al. submitted). The database and pathway search enable a fast tentative annotation of the relevant markers.

1.4.4 Metabolite identification

Although a large number of metabolites can be rapidly annotated by a database search the bottleneck of metabolite fingerprinting remains the unequivocal identification of metabolites. Various databases contain information about exact mass, fragmentation pattern or UV/Vis spectra. When an authentic standard of a substance proposed by a database hit is available, a comparison of retention time by coelution, a comparison of the MS/MS pattern or UV/Vis spectrum allows its identification. But for most markers the substances indicated by the database search are not commercially available. Highly abundant compounds might be identified by NMR. Metabolites of low concentrations however can only be assigned by mass spectral elucidation from the sample material (Brown et al. 2009). The high mass accuracy obtained in metabolite fingerprinting often allows generating a molecular formula that can be helpful in the identification of a substance. For structural elucidation of metabolites a fragmentation analysis can be performed. Thereby more information of a metabolite than its exact mass is needed. It is necessary to break the substance into fragments. The obtained pattern is specific for a substance but it is depending on the used mass analyser and the applied energy. As mass analysers tandem instruments are used. Since two mass spectrometric steps are performed this is called tandem-MS (MS/MS or MS^2). One part of the mass analyser usually is a quadrupole (Q). It works like a filter that allows only the passing of ions within a certain mass range to reach the detector. The quadrupole can be combined with a collision cell in which the parental ion can be fragmented by collision-induced decomposition (CID). Another quadrupole cell is then able to detect the created daughter ions (Allwood and Goodacre 2009). This mass analyser combination is called triple quadrupole (QQQ). Alternatively a quadrupole ion trap (Q-TRAP) can be used whereby one cell is acting as an ion trap instead of a quadrupole. The ion trap concept is based on the separation of the ions in time instead of separation in space. Low abundant metabolites are trapped by electric fields and are collected until MS/MS or MS^n measurements can be performed (Allwood and Goodacre 2009). QQQ and Q-TRAP MS instruments are only able to obtain nominal masses for the generated fragments. Another mass analyser system used for MS/MS is the Q-TOF. In a Q-TOF a quadrupole filters the ions followed by a fragmentation and subsequently a TOF-MS is used to detect the created daughter ions. In contrast to the QQQ and Q-TRAP MS, a Q-TOF instrument has a much higher mass resolution which is able to acquire exact masses for the fragments. An additional advantage is its enhanced sensitivity enabling the fragmentation of low abundant metabolites (Steen et al. 2001).

For structural elucidation of metabolites in this work, fragmentation analyses of various compounds were performed on a Q-TOF and a Q-TRAP. Furthermore, an additionally method of identification was used. Chemical syntheses have been performed resulting in the authentic standards for unequivocal identification of several metabolites.

1.5 Aim of this work

In this work it was aimed to identify metabolites that are involved in the metabolic interaction of three host plants from the plant family of Brassicaceae and the invading soil-borne fungus *V. longisporum*. This should be achieved by a metabolite fingerprinting approach based on LC-MS measurements.

For an optimal usage of the provided analytical platform the metabolite fingerprinting method had to be optimized for efficient sample extraction of liquid samples. For the instrumental analytics, the LC performance as well as the TOF-MS sensitivity had to be validated and improved. A first step focused on the identification of extracellular metabolites from *V. longisporum* in *in vitro* experiments that might act as signals *in planta*. A second step included the differential analysis of apoplastic fluids (xylem sap and apoplastic wash fluid from leaves) and defined plant tissues of *V. longisporum* infected plants in comparison to healthy controls. This should lead to a better understanding of spatial occurrence and local differences upon fungal infection within the plant organs. In *B. napus* the metabolic changes should be observed at different time points after infection (from 5 to 35 days past infection) to obtain an overview of the kinetics of infection related compounds. Infection markers resulting from the metabolite fingerprinting analysis should be unequivocally identified by comparison with authentic standards (purchased or chemically synthesized) or by fragmentation analysis. It should be analysed if certain metabolic pathways were affected. Therefore pathway databases should be queried in order to find an accumulation of database hits for infection markers in plant-pathogen related pathways. Alternatively, the elucidation of new metabolic pathways from infection related metabolites was intended. Identified substances should be tested on their effects on fungal growth (toxicity assay) and on their ability to induce expression of *V. longisporum* responsive genes. Furthermore is should be tested whether plant derived infection markers possess signalling functions. In order to distinguish species specific infection markers from general infection markers in Brassicaceae analyses from *C. sativa* and *A. thaliana* should be included in the comprehensive approach. From the results a hypothesis for the host plant reaction of *B. napus* to the biotic stress of fungal infection should be created. This should be tested against an applied abiotic stress. In this comparison it should be differentiated between the *V. longisporum* specific metabolite changes and a general stress response. Additionally, the question if *A. thaliana* is an adequate model for *V. longisporum* infection of oilseed rape, its natural host plant, should be addressed.

2 Material and methods

2.1 Material

2.1.1 Chemicals

Firefly luciferin for luciferase assays was provided by Biosynth (Staad, Switzerland). All oxylipin standards were purchased from Larodan Fine Chemicals AB (Malmö, Sweden). The authentic standard of SAG was provided by Prof. Karlovsky (Department of Crop Sciences, Georg-August-University, Göttingen, Germany). Cyclobrassinin was provided by Prof. Kutschy (Department of Organic Chemistry, P.J. Safárik University, Kosice, Slovak Republic). All other chemicals and authentic standards were obtained from Sigma-Aldrich (Deisenheim, Germany) or Merck (Darmstadt, Germany) unless stated otherwise. Solvents for LC-MS analyses were used as follows: water, acetonitrile and methanol in LC-grade quality from Fisher Scientific (Schwerte, Germany). Camalexin was synthesized in the workgroup previously according to (Ayer et al. 1992).

2.1.2 Media

MS

Murashige and Skoog (MS) medium including vitamins was purchased from Duchefa (Haarlem, Netherlands). The medium was prepared with half of the suggested amount leading to ½ MS. For agar plates 1 % micro agar also provided by Duchefa (Haarlem, Netherlands) was added.

PDB (PDA)

Potato-dextrose-broth (PDB) was purchased from Sigma-Aldrich (Deisenheim, Germany) and prepared according to labelling. Potato-dextrose-agar (PDA) was delivered by Roth (Karlsruhe, Germany).

SXM

Preparation of simulated xylem sap medium (SXM) was adapted from Neumann and Dobinson (2003) according to Tab. 1. Pectins from citrus fruits and casein hydrolysate were purchased from Sigma-Aldrich (Deisenheim, Germany.)

CDM

Czapek-Dox-Medium (CDM) (adapted from Smith, 1960) was prepared according to Tab. 1.

Tab. 1: Composition of the simulated xylem sap medium (SXM) including the 1000x Trace elements solution and Czapek-Dox-medium (CDM) used for fungal cultures and plant cultivation, respectively.

Simulated xylem sap medium (SXM)	
Pectin from citrus fruits	2 g/L
Casein hydrolysate	4 g/L
$NaNO_3$	70 mM
KCl	7 mM
KH_2PO_4	11 mM
$MgSO_4$	2 mM
1000x Trace elements	1 mL/L

1000x Trace elements	
$ZnSO_4.7\ H_2O$	22 g/L
H_3BO_4	11 g/L
$MnCl_2.4\ H_2O$	5 g/L
$FeSO_4.7\ H_2O$	5 g/L
$CoCl_2.6\ H_2O$	1.7 g/L
$CuSO_4.5\ H_2O$	1.6 g/L
$Na_2MoO_4.2\ H_2O$	1.5 g/L
Na_2-EDTA	50 g/L

Czapek-Dox medium (CDM)	
Saccharose	30 g/L
$NaNO_3$	70 mM
KCl	7 mM
KH_2PO_4	11 mM
$MgSO_4$	2 mM
$FeSO_4.7\ H_2O$	10 mg/L

2.1.3 Plant and fungal material

Plant material

Rapid-cycling rape (*Brassica napus* var. *napus*, ACaacc) was obtained originally from Prof. Williams (Department of Plant Pathology, University of Wisconsin, Madison, WI, USA). *A. thaliana* ecotype Columbia-0 seeds were supplied by Imara Perera (North Carolina State University, Raleigh, NC, USA). *A. thaliana* mutant PIP2.2::LUC was provided by Prof. Christiane Gatz (Department of Molecular Biology and Plant Physiology, Georg-August-University, Göttingen, Germany) whereas the mutant CYP79B2/B3::LUC was obtained from Prof. Wolfgang Dröge-Laser (Department of Pharmaceutical Biology, Julius-Maximilians-University, Würzburg, Germany). *Camelina sativa* seeds ecotype Ligena were obtained from Deutsche Saatgutveredelung AG (DSV, Lippstadt, Germany).

Fungal material

The fungal isolate of *Verticillium longisporum* VL 43 was supplied by Prof. Andreas von Tiedemann (Department of Crop Sciences, Division of Plant Pathology and Crop Protection, Georg-August-University, Göttingen, Germany). The strain was isolated as described in Zeise and von Tiedemann (2001). The isolates of *Verticillium longisporum* VL Bob (Bob-70 isolated from *B. oleracea* var. *botrytis* in the USA), *Verticillium dahliae* VD (Vd-73 isolated from *Linum usitatissimum* in Mecklenburg, Germany) and *Verticillium albo-atrum* VA (Va-1 isolated from *Solanum tuberosum* in Wiconsin, USA) were supplied by Prof. Gerhard Braus (Department of Molecular Microbiology and Genetics, Georg-August-University, Göttingen, Germany). The *V. longisporum* VL 43 mutant strains CS-6 and CS-12 were also provided by Prof. Gerhard Braus. They were RNAi knock-down mutants of chorismate synthase (Singh et al. 2009). Fungal spores were stored at -80°C in 25 % glycerol.

2.2 Methods

2.2.1 Transfer experiment

2.2.1.1 Transfer procedure

About 4,5 x 10^5 *Verticillium* spores were inoculated in 40 mL PDB or SXM supplemented with 10 µL streptomycin (1 mg/mL) and cultivated in the dark at 20 °C on horizontal shaker at 100 rpm. After 4 d the supernatant was removed under sterile conditions and 40 mL of fresh medium (PDB or SXM) was added including 20 µL streptomycin. The fungal cultures were kept for additional 4 d under the conditions already described. Subsequently the mycelium and the supernatant were separated and stored at -80 °C until extraction. Mycelium was weighed prior to freezing. All experiments were prepared in triplicates.

For transfer in xylem sap of healthy plants the procedure described above was downsized to 2,5 mL media per sample. For xylem sap collection *B. napus* plants grew for 6 weeks in the green house. The cultures were incubated in 50 mL falcon tubes. The xylem sap was sterile filtered (Vivaspin 15R MWCO 10 kDa, Sartorius, Göttingen, Germany) before added to the pre-cultivated mycelium. Three biological replicates were performed for VL 43, VD and the chorismate mutant strains VL 43 CS-6 and VL 43 CS-12.

2.2.1.2 Glucose inhibition experiment

Fungal cultures were cultivated as described above for the transfer procedure (2.2.1.1) with the difference, that SXM and PDB were supplemented with 40 g/L sterile-filtered glucose as described previously (Frases et al. 2007). The state of melanisation in the mycelium was documented by photos after 2, 4, 7-11 d. Inhibition of melanisation by glucose was analysed in two independent experiments.

2.2.2 Toxicity assay

Salicylic acid (SA), raphanusamic acid (RA) and the saturated dicarboxylic acids (C3, C4, C8-C13, C16) as well as pipecolic acid were tested on large agar plates (12 x 12 cm) including a concentration gradient from 0 up to 350 µM. 350 µM of camalexin was used as a positive control. The monoamide synthesis product and 2,5-DHBA were tested on small petri dishes of PDA (Ø 4 cm) with concentrations of 50, 100, 200 and 350 µM with three biological replicates each. 2,5 µL fungal spore solution (1 x 10^6 spores/mL) was directly added to the plates. The plates were cultivated in the dark at 20 °C for 9 d.

2.2.3 Infection procedure

2.2.3.1 Plant growth and cultivation

B. napus seeds were surface sterilized and sown on silica sand (Vitakraft, Bremen, Germany) as described by Ratzinger et al. (2009). *C. sativa* seed were treated likewise. The seeds were kept moist under a 16 h light / 8 h dark regime for 14 d. *A. thaliana* seeds were surface sterilized with 6 % $Na(OCl)_2$ solution including 0.02 % Triton X-100 for 15 min, then washed three times with sterilized water. The seeds were sown sterile on ½ MS-agar plates. After stratification for 1 d in the dark at 4 °C they were cultivated as described in Floerl et al. (2010).

2.2.3.2 Spore solution

Spores used for infection of Brassicaceae were generated as follows: 1 mL of a VL 43 spore stock solution (1 x 10^6 spores/mL) was diluted in 200 mL PDB spiked with 10 µL Streptomycin (20 mg/mL) and cultivated on a horizontal shaker for 7 d at 100 rpm at 20 °C. Subsequently the mycelium was harvested sterile, washed once with CDM and incubated for 4 d in 100 mL CDM and 10 µL Streptomycin on a shaker. The accumulated spores were harvested under sterile conditions by sieving mycelium from medium. The spores containing medium was centrifuged (15 min, 2500 g, 20 °C) and the supernatant discarded. The pellet was resuspended in sterilized water and the spore concentration adjusted to 5 x 10^7 spores/mL including 25 % glycerin. The spores were stored until infection at -20 °C and diluted 1:50 in tap water for infection (end concentration 1 x 10^6 spores/mL).

2.2.3.3 Infection process

A. thaliana plants were infected as described by Floerl et al. (2010). One or five plants were planted into water drenched soil (T25 Fruhstorfer Erde, Hawita Gruppe, Vechta, Germany) and 10 or 4 mL spore solution was cast directly to the roots, respectively. Control plants were treated equally with equivalent amounts of tap water.

B. napus and *C. sativa* plants were released carefully from silica substrate (see 2.2.3.1) and the roots washed with tap water. *C. sativa* roots were cut corresponding to *A. thaliana* roots. *B. napus* roots were not cut. The roots were incubated in spore solution or tap water (mock controls) for 10 - 20 min. Then the plants were transferred into a mixture of soil and sand (1:1, by weight) one plant per pot. The plants were watered with either 10 mL fungal spore solution or an equal amount of tap water (mock controls). 15 pots were collected on a tray.

2.2.3.4 Growth conditions

A. thaliana was grown under short day conditions as described previously (Floerl et al. 2010) in a climate chamber. *B. napus* and *C. sativa* were cultivated with 16 h /d light regime, at 60 %

humidity, a light intensity of 150 µmol m^{-2} sec^{-1} and 20 °C in climate chamber. *B. napus* and *C. sativa* plants were watered 3 times a week and fertilized after the second and third week after infection.

2.2.3.5 Documentation of infection symptoms

Leaf area

The reduction of the leaf area as an infection symptom was documented by photos of single plants as described by König (2011).

Stunting

The reduction of height in infected plants as an infection symptom of *B. napus* was measured once a weak with a folding rule from soil surface to the highest part of the plant. For *B. napus* metabolite fingerprinting analyses only infected plants with a height of less than 70 % of the control heights mean value were selected to ensure a successful infection process.

2.2.3.6 Sample collection

Collection of xylem sap

Xylem sap collection was performed for *A. thaliana* as described (Horie et al. 2006). Rosette leaves were removed by cutting the stem with a sharp blade and emerging drops were collected after washing the cut surface with distilled water and discarding the first drop. The same method was used successfully for *B. napus* and *C. sativa*. Here the stems were cut in height of the first true leaf. Xylem sap collection was most effective shortly after the lights turned on. The xylem sap was stored on ice during the collection procedure and then frozen at -80 °C until extraction. For *B. napus* three biological replicates with three technical replicates were obtained, for *C. sativa* one biological sample was extracted three times. For *A. thaliana* only xylem sap of healthy plants could be obtained (three technical replicates).

Apoplastic wash fluid (AWF)

The extracellular fluid of the leaves of *A. thaliana, B. napus* and *C. sativa* was collected according to Floerl et al. (2008). Slight modifications were made as follows: The infiltration solution contained 100 mM KCl and 0.003 % Triton-X 100. Big leaves of *B. napus* were cut into suitable pieces. For vacuum infiltration the atmospheric pressure was reduced to 100-150 mbar for 5 min. The centrifugation of the infiltrated leaves was performed with 950 g at 4 °C for 8 min. The solution was frozen in liquid nitrogen and stored at -80°C until extraction. Leaves of at least 5 plants were pooled for AWF collection. For *B. napus* and *A. thaliana* three biological replicates

with at least two technical replicates were obtained, for *C. sativa* three biological samples were extracted and measured three times.

Leaf, stem, hypocotyl and root tissue

Leaf material of *B. napus* plants was divided from stem and frozen separately in liquid nitrogen immediately after cutting. Hypocotyl and roots were harvested after xylem sap collection by releasing the roots carefully from the soil and washing it thoroughly with water. Then the chlorophyll-free root was detached from the hypocotyl region and both organs frozen separately in liquid nitrogen quickly and stored at -80 °C until homogenization and extraction. For *B. napus* and *C. sativa* three biological replicates with at least two technical replicates were obtained.

2.2.3.7 Priming procedure

To prime *B. napus* plants prior to infection they were treated according to Jung et al. (2009) adapted in the following way: 250 mM azelaic acid was dissolved in 5 mM MES buffer (pH 5.6) supplemented with 0.01 % Tween 20. A mix of 250 mM sebacic acid and 250 mM suberic acid was dissolved in the same way. Both solutions were used for priming *B. napus* two week old seedlings. Leaves were sprayed thoroughly and roots were dipped into the priming solution until infection. Control plants were treated equally with pure buffer solution. Priming took place 24 h prior to infection with *V. longisporum* VL 43. To compare the effects to normal infection procedure mock controls and infected plants were used additionally. Culture conditions and sample collection was performed as described above. Xylem sap, AWF, hypocotyl and leaves were harvested 28 dpi. All infected plants harvested were smaller than 70 % of the control heights mean value. At least 6 plants were pooled for a biological sample. For hypocotyl tissue three biological replicates with two technical replicates were obtained whereas for xylem sap and AWF one biological sample was extracted three times.

2.2.4 Extraction methods

2.2.4.1 MTBE extraction

The two-phase extraction of plant and fungal material was performed according to Matyash et al. (2008). The method was adapted as follows. For extraction methanol and water were used in LC-grade quality.

Aqueous media

200 µL of an aqueous sample (xylem sap, AWF or culture supernatant) was mixed with 150 µL methanol and 500 µL *tert*-methylbutylether (MTBE) was added. After shaking for 1 h in the dark additional 120 µL water induce a phase separation during 10 min of incubation and 15 min

centrifugation (1000 g, 20°C). The polar and non-polar phases were collected in a new vial together avoiding interphase and pellet. The combined phases were evaporated and resuspended in 50 µL acetonitrile / methanol / water (1:1:12, by vol.) for metabolite fingerprinting.

Plant and fungal tissue

Plant tissue and fungal mycelium was homogenized prior to the extraction with a ball mill (model MM200, Retsch, Haan, Germany). The tissue was kept frozen during the whole process by liquid nitrogen.

About 80 mg ground, frozen material was solved in 0.75 mL methanol. After adding 2.5 mL MTBE all was mixed thoroughly and shaken for 1 h in the dark. 600 µL of water were added and the mixture incubated for 10 min, then centrifuged (15 min, 1000 g, 20 °C). The non-polar phase was transferred to a new vial, the polar phase re-extracted with 1.3 mL MTBE and 0.7 mL methanol / water (6:5, by vol.). After a centrifugation the non-polar phase was combined with the previously collected non-polar phase and evaporated under a nitrogen stream. The sample was resolved in 250 µL chloroform / methanol / water (60:30:4.5, by vol.). The polar phase is as well evaporated and resolved in 140 µL acetonitrile / methanol / water (1:1:12, by vol.). After shaking 10 min and a short centrifugation step (30 sec, 10000 g, 20 °C) the clear supernatant was taken for metabolite fingerprinting.

2.2.4.2 Methanol/chloroform extraction

For fungal tissue extraction the chloroform extraction for plant material (Fiehn et al. 2000) was adapted. 30 mg of ground, frozen and lyophilized mycelium of *V. longisporum* VL 43 was suspended in 1 mL of methanol and shaken for 10 min at 70 °C. After a centrifugation step (10 min, 10000 g, 20 °C) the supernatant was transferred in a new vial and 1 mL water was added. The pellet was dried under nitrogen and resolved in 500 µL chloroform and extracted for 10 min at 37 °C shaking vigorously. The non-polar extract was filtered (2 µm PTFE, Whatman GmbH, Dassel, Germany) and combined with the supernatant selected before. After incubation and centrifugation (20 min, 1000 g, 20 °C) two phases can be separated. The upper polar phase was evaporated, resuspended in 200 µL methanol, evaporated and resolved in 200 µL acetonitrile / methanol / water (1:1:18, by vol.). After shaking 10 min and a short centrifugation step the clear supernatant was taken for metabolite fingerprinting. The non-polar phase was evaporated separately and resolved in acetonitrile / methanol / water (1:1:2.5, by vol.). After another centrifugation step the clear supernatant was taken for metabolite fingerprinting.

2.2.4.3 Ultrafiltration

For ultrafiltration centrifugal filters Nanosep 300K Omega were used (Pall Life Science Corporation, Port Washington, WI, USA). Filters were washed 10 times with water before use as described in Tiziani et al. (2008). 250 µL of the sample were centrifuged at 4 °C for 10 min and 10700 g. The filtrate was evaporated and resuspended by shaking for 10 min in 125 µL acetonitrile/methanol/water (1:1:12, by vol.). After another centrifugation step the clear supernatant was taken for metabolite fingerprinting. For non-polar metabolites the filter was washed three times after filtration of the sample with 0.5 mL methanol / water (3.2:1, by vol.). The three combined filtrates were added to 400 µL chloroform and 600 µL water. After vortexing, incubation for 10 min and centrifugation (10 min, 3100 g, 4 °C) the organic phase was collected and evaporated. The extract was resolved in 100 µL chloroform / methanol / water (60:30:4.5, by vol.). For method optimization 250 µL of fungal culture supernatant was extracted in three technical replicates and each sample measured three times.

2.2.4.4 Acetone extraction

1.2 mL of ice-cold acetone was added to 0.3 mL aqueous sample. It was mixed and incubated at -20 °C for 1 h. Subsequently centrifugation for 10 min at 13000 g was performed. 1.25 mL supernatant (corresponds to 5/6 of starting material) was evaporated under a stream of nitrogen and resolved shaking for 10 min in 125 µL acetonitrile/methanol/water (1:1:12, by vol.). After another centrifugation step the clear supernatant was taken for metabolite fingerprinting. For method optimization fungal culture supernatant was extracted in three technical replicates and each sample measured three times. Only a polar phase was available due to lacking a phase separation whereas MTBE extraction and ultrafiltration result in a polar and a non-polar phase.

2.2.5 Analytical parameters

2.2.5.1 Metabolite fingerprinting (UPLC-TOF-MS)

Metabolic fingerprinting analysis was performed by UPLC (ACQUITY UPLC System, Waters Corporation, Milford, MA, USA) coupled with an orthogonal TOF-MS(LCT Premier, Waters Corporation Milford, MA, USA). It was used for the non-targeted, differential analysis of culture supernatants from the transfer experiment (2.2.1) and samples collected in the infection experiments (2.2.3), abiotic elicitation (2.2.10) and flotation (2.2.11). Chromatographic separation was performed as described previously (Djamei et al. 2011). Metabolite separation was achieved with the a RP 18 column (ACQUITY UPLC BEH shield RP 18, 1.7 µm, 1 x 100 mm, Waters Corporation, Milford, MA, USA) for non-polar samples whereas for polar samples a HSS T3 column (ACQUITY UPLC HSS T3 column 1.7 µm, 1 x 100 mm, Waters Corporation, Milford, MA, USA) was used. All samples were measured in positive and negative ionisation mode. For

aqueous samples (e.g. extracted AWF) and the polar extraction phase of tissue samples the polar gradient and the HSS T3 column for chromatographic separation were used. The non-polar extraction phase of tissue samples was measured using the non-polar gradient and the RP 18 column. All retention times were noted as measured on the HSS T3 column by using the polar gradient unless stated otherwise. Mobile phases were water (A) and acetonitrile (B) with 0.1 % formic acid, respectively. The gradient program for the non-polar phase (RP 18 column) was set up as follows: 0-0.5 min 46 % B, 0.5-5.5 min increase of B up to 99.1 %, 5.5-10 min increase of B up to 100 %, 10-13 min 46 % B. For the polar phase (HSS T3 column) the gradient program was set up: 0-0.5 min 1 % B, 0.5-3 min increase of B up to 20 %, 3-8 min increase of B up to 95 %, 8-10 min isocratic run at 95 % B, 10-14 min equilibration with 1 % B. The UV-Vis data were recorded for the wavelength of 190 to 800 nm. Data were acquired by MassLynx^{TM} software (Waters Corporation, Milford, MA, USA).

2.2.5.2 Exact mass fragmentation analysis (UHPLC-Q-TOF-MS)

The exact mass fragmentation analysis based on UHPLC-Q-TOF-MS measurement was used for identification of substances via their MS/MS pattern and for pseudo MS/MS/MS for fragmentation analysis by which previously unknown structures could be elucidated. Chromatographic separation was performed on an Agilent 1290 Infinity series UHPLC system (Agilent Technologies, Böblingen, Germany), which was equipped with a binary pump, thermostatically controlled column, PDA-detector and autoplate sampler (Agilent Technologies, Böblingen, Germany). Metabolite separation was achieved on a C18 column (ZORBAX RRHT Eclipse Plus, 1.8 µm, 2.1 x 150 mm, Agilent Technologies, Böblingen, Germany) operated at 40 °C. Mass detection was performed on an Agilent 6540 UHD Accurate-Mass Q-TOF mass spectrometer (Agilent Technologies, Böblingen, Germany). Mobile phases (A) and (B) were used as described for metabolite fingerprinting analysis. The gradient for polar samples was set up as follows: 0-8 min increase of B from 8 % up to 40 %, 8-11 min increase of B up to 70 %, 11-13 min increase to 100 % B, 13-15 min isocratic run at 100 % B, 15-15.5 min decrease to 8 % B and subsequent equilibration with 8 % B from 15.5-17 min. For non-polar samples gradient program was set up: 0-8 min increase of B from 40 to 100 %, 8-10 min isocratic run at 100 % B, returned to 40 % B for equilibration for 2 min. The flow rate was set to 0.4 mL/min. The mass spectrometer was operated using an ESI source with Agilent Jet Stream Technology (Agilent Technologies, Böblingen, Germany) in positive and negative mode. The ionization parameters were: gas temperature 300 °C, gas flow 8 L/min, nebulizer pressure 35 psi, sheath gas temperature 350 °C, sheath gas flow 11 L/min, VCap voltage 3.5 kV, nozzle voltage 100 V. The fragmentor voltage was varied depending on the substance from 80-150 V for MS and from 120-250 V for MS/MS measurements. A quadrupole was used for isolation of precursor ions within a mass window of ±

1.3 Da in MS/MS mode, a linear hexapole collision cell with N_2 as collision gas and collision energies of 5, 20 and 40 eV unless stated otherwise. The scan frequency was set to 4 GHz. The m/z was acquired in the range from 50 to 1000 Da with scan rates of 1 Hz for MS and 8 Hz for MS/MS experiments. Mass accuracy was monitored by using purine ($[M+H]^+$ 121.05087), trifluoroacetic acid ($[M-H]^-$ 112.98559) and HP-921 = hexakis-(1H,1H,3H-tetrafluoro-pentoxy)phosphazene ($[M+H]^+$ 922.00978, $[M+HCO_2]^-$ 966.00073) as reference compounds. Data were acquired by Mass Hunter Workstation Acquisition software, version B.03.01 with Service Pack 3 (Agilent Technologies, Böblingen, Germany). Mass Hunter Qualitative Analysis B.03.01 with Service Pack 3 was used for data analysis (Agilent Technologies, Böblingen, Germany).

2.2.5.3 Nominal mass fragmentation analysis (UPLC-Q-TRAP-MS)

The nominal mass fragmentation analysis based on UPLC-Q-TRAP-MS measurement was used for elucidation of the position of sulphur in the building blocks of cyclobrassinin related metabolites. Chromatographic separation was performed as described for metabolite fingerprinting analysis. Mass detection was performed on an Applied Biosystems 4000 hybrid triple quadrupole/linear ion trap mass spectrometer (AB-Sciex, Darmstadt, Germany). The mobile phases and the gradient were used as described (Djamei et al. 2011). Nanoelectrospray ionisation (nanoESI) analysis was achieved by using a chip ion source (TriVersa NanoMate, Advion BioSciences, Ithaka, NY, USA). Stable nanoESI was achieved by adding 0.1 mL/min of the make-up solvent isopropanol/acetonitrile/water (70:20:10, by vol.) via a mixing tee valve. A postcolumn splitter directed 460 nL/min to the nanoESI chip. Ionization voltage was set to 1.7 kV. Declustering potential was set to -130 V for negative and 30 V for positive ionization.

2.2.6 Data processing

2.2.6.1 Pre-processing

The data pre-processing was performed for all datasets that were acquired by high-throughput UPLC-TOF-MS analysis (metabolite fingerprinting). For data deconvolution, peak integration and sample alignment of the raw data the Application Manager software tool in MarkerLynx™ (Waters Corporation, Milford, MA, USA) was used. The parameters were set as follows: retention time from 0.3 to 10 min, mass range from 50 – 1200 Da, XIC window 0.03 Da, no relative retention time, peak width at 5 % height 12 sec, peak-to-peak baseline noise 200, no smoothing applied, intensity threshold 50 counts (negative ionization) and 100 counts (positive ionization), mass window 0.03, retention time window 0.2, noise elimination level 5. Isotopomers were removed. This resulted in the creation of a data matrix. The contained markers were defined by retention time, m/z and intensity profile. From the resulting mds-file markers were exported via a

csv-file. Sample-based principal component analysis (PCA) was performed in MarkerLynx^{TM} XS (Waters Corporation, Milford, MA, USA) using Pareto scaling.

2.2.6.2 MarVis

The obtained data matrices were imported into the software toolbox MarVis (http://marvis.gobics.de, Kaever et al. 2009) as csv-files and samples grouped by condition identifiers (condition specific names). In the tool MarVis Filter p-values were assigned by Kruskal-Wallis algorithm and cut at a specific p-value to ensure a high quality level in analysed markers (Kaever et al. submitted). With 6 conditions and at least 6 measurements per condition a p-value of $< 10^{-4}$ seemed to be appropriate. Adducts were automatically corrected in the filtered data sets according to the following rules: positive ionization: $[M+H]^+$, $[M+Na]^+$ and $[M+NH_4]^+$; negative ionization: $[M-H]^-$, $[M+CH_2O_2-H]^-$ and $[M+CH_2O_2+Na-2H]^-$. For corrected masses (neutral masses) the adduct rules had to be adjusted by adding or subtracting a proton to the according rule. More adduct rules (including e.g. $[2M+H]^+$ or $[M+K]^+$) lead to an enhanced number of false correction. Positive and negative datasets from one experiment were then combined.

For identification of infection markers the refined datasets were clustered and visualized in the tool MarVis Cluster by means of 1-dimensional self-organizing maps (1D-SOM). During normalization sample aggregation was performed on mean values and marker scaling was performed by the Euclidean norm (2-norm). Prototypes with intensity pattern indicating enhanced marker intensities after treatment were selected. The markers represented by the selected prototypes were used for pathway analysis or in-house database queries. Database hits were given within ± 5 mDa deviation.

Tab. 2: Queried databases for metabolite fingerprinting

Database	Link
Aracyc	http://www.plantcyc.org
MetaCyc	http://metacyc.org
RiceCyc	http://www.gramene.org/pathway
KEGG	http://www.genome.jp/kegg
Knapsack	http://kanaya.naist.jp/KNApSAcK
LIPIDMAPS	http://www.lipidmaps.org

Overlapping markers for the Venn-diagrams are calculated with MarVis. First adduct correction and dataset combination of positive and negative ionisation mode with the following adapted parameter settings was performed: retention time (RT) tolerance of 0.07 min, a m/z tolerance of 0.01 Da and a minimal cosine similarity of the intensity profile of 0.75. This technique reduced the number of infection markers by combining the known adducts and markers from both

ionisations modes to one marker. This resulted in a number of infection markers that could be regarded as an approximation of the number of metabolites involved in the analysed process.

2.2.7 Targeted analysis of free polyamines

The analysis of free polyamines was performed as described in Pommerrenig et al. (2011) in hypocotyl tissue from three independent infection experiments with *B. napus* with two technical replicates each.

2.2.8 Quantification of *V. longisporum* DNA

The quantification of *V. longisporum* DNA *in planta* was performed as described previously (Singh et al. 2011)

2.2.9 Contamination measurements

To determine if apoplastic fluids (xylem sap and AWF) were contaminated with cellular components malate dehydrogenase (MDH) activity was measured as described in Floerl et al. (2008). As control *B. napus* leaf extracts were tested. It was not possible to determine protein content in xylem sap and AWF with a Bradford protein assay as protein contents were below detection limits.

2.2.10 Abiotic elicitation of phytoalexins

Leaf assay

To elicit phytoalexins in *B. napus* by abiotic stress leaves of plants in the growth stage 2.3 to 2.4 according to Harper and Berkenkamp (1975) were sprayed with 10 mM $CuCl_2$ solution as described previously (Rouxel et al. 1990). After 48 h the leaves were washed in tap water to remove remaining $CuCl_2$ solution and immediately frozen in liquid nitrogen. The samples were stored at -80°C until homogenization and extraction. 6 leaves from two plants were for one sample and three independent samples were generated (6 plants control, 6 $CuCl_2$ treated plants).

Whole plant assay

For monitoring the effect of $CuCl_2$ on whole *B. napus* plants, the pre-cultivated plants (see 2.2.3.1) were transferred onto soil-sand mixture (1:1, by weight) in 9 cm pots and in growth stage 2.2 to 2.3 drenched with 100 mL of 10 mM $CuCl_2$ solution spiked with 5 mg/L Tween 80. The plants were kept as before in a 16 h light / 8 h dark light regime and were watered with tap water if necessary. Control plants were treated with tap water including Tween 80. The plants were harvested after 7 d by detaching the shoot and digging the roots carefully from the soil. Both plant parts were washed with tap water prior to freezing in liquid nitrogen. Two plants were

pooled for one sample and three independent samples were generated (6 plants control, 6 $CuCl_2$ treated plants).

2.2.11 Flotation assay

For the flotation assay *B. napus* seeds were sown on soil-sand mixture (1:1, by weight, one plant per pot) and grown under long day conditions (16 h light) for 10 d. Then they were pricked out and grown for another 10 d on soil-sand mixture.

According to Stenzel et al. (2003) substances were dissolved in deionised water within round Petri dishes (150 x 20 mm, Sarstedt, Nümbrecht, Germany). 100 mL deionized water was applied instead of 50 mL. Two independent experiments were conducted with 6 h and 24 h of flotation time. The concentrations of the applied substances for the flotation assay for 6 h were 250 µM substance and 250 mM NaCl. The concentration for the flotation assay for 24 h were 50 µM substance and 250 mM NaCl. Alternatively VL 43 or VL Bob spore solution ($2x10^6$ spores) was added for 24 h. Four secondary *B. napus* leaves were applied on each solution and floated for 6 h and 24 h, respectively. After the incubation time the leaves were washed in deionized water, frozen in liquid nitrogen and stored at – 80 °C for further analysis. Each experiment includes three biological replicates.

2.2.12 Chemical synthesis

2.2.12.1 *N*-acylethanolamines (NAEs)

NAE 7:0 and NAE 10:0 were chemically synthesized from ethanolamine and acylchloride as described in Devane et al. (1992). The identity of the end products was proven by mass spectrometry.

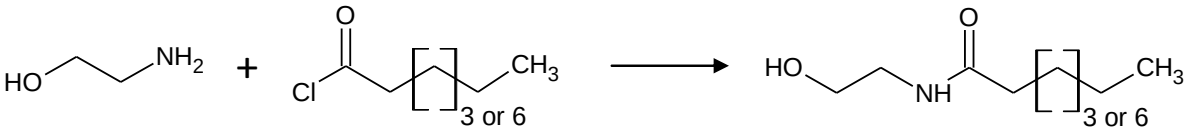

Fig. 9: Synthesis of NAEs

2.2.12.2 Dodecanediamide (Diamide)

Dodecanediamide was synthesized from dodecanedioic acid by activation of both carboxylic groups to carboxylic acid chlorides and subsequent formation of acid amides (Castillo et al. 2006). Only 10 mmol reactants were used and thionyl chloride was replaced by oxalyl chloride. The reaction was heated (80°C) for approx. 5 h and then stirred overnight by room temperature. In contrast to cited literature the intermediate product was resolved in tetrahydrofuran.

Concentrated aqueous ammonia was added instead of NH_3 gas. The successful chemical synthesis was proven by mass spectrometry.

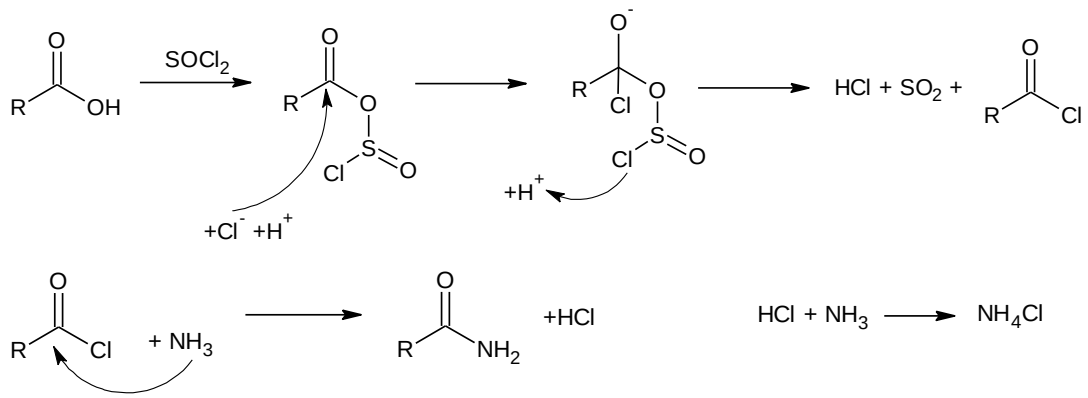

Fig. 10: Synthesis of an acid amide from a carboxylic acid

2.2.12.3 Azelaamic acid (Monoamide)

9-amino-9-oxo-nonanoic acid was synthesized as described (Bishop 1955) but using 10 mmol mono-methyl-azelaic acid as reactant solved in hexane. From the activated carboxylic acid resolved in tetrahydrofuran the corresponding acid amide was prepared by adding aqueous ammonia. After a completed reaction the solvent was evaporated. The intermediate product was washed with water, filtered and analysed by LC-MS. Hydrolysis of the methyl group was performed as described (Ravi et al. 2001). The end product was extracted with diethyl ether from the aqueous phase twice and dried. The successful chemical synthesis was proven by NMR and mass spectrometry.

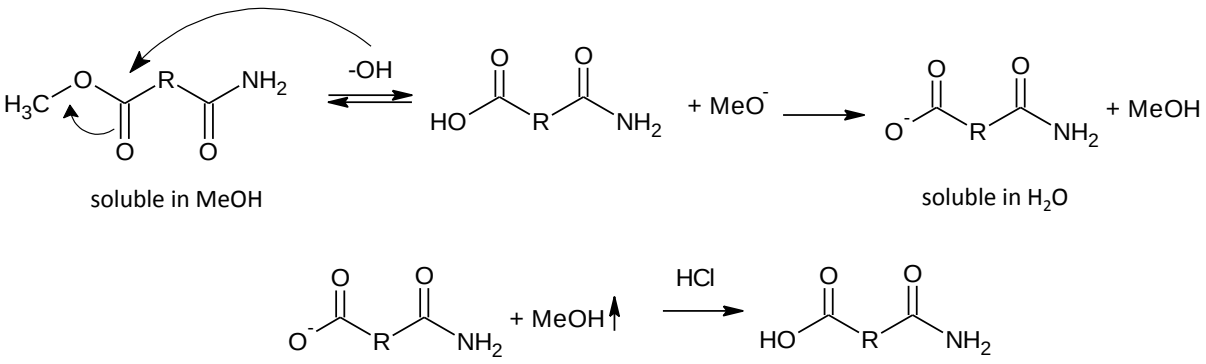

Fig. 11: Hydrolysis of the methyl group

2.2.13 Luciferase assay

A. thaliana seeds were surface sterilized as described above (2.2.3.1) and sown on ½ MS agar plates. After two weeks the roots were cut with a razor blade and about 5 x 10^5 VL 43 spores added to the injured roots under sterile conditions. Controls were supplied with autoclaved water. The plates were kept under short day conditions (8 h light/ 16 h dark). For monitoring the

condensed water was dried under the clean bench. Then 1 mM luciferin in 0,01 % Triton X100 was sprayed thoroughly on the plates and incubated for 30 min (Iven 2009). 500 µL sterile water was added to the plates to prevent dry stress of the plants. The fluorescence was measured with DIANA (raytest GmbH, Straubenhardt, Germany). The chlorophyll fluorescence was recorded during 3 min exposure time immediately after bringing the plates into the dark photo chamber. Then 3 min were spared to guarantee for a complete absence of remaining chlorophyll fluorescence. Subsequently 10 min exposure time recorded the luciferase generated signal. The AIDA software (raytest GmbH, Straubenhardt, Germany) was used to evaluate the pictures and convert them into TIFF of JPEG files.

For single leaf analyses leaves were detached from rosettes and non-sterile sprayed as described above. For the luciferase assay on soil the five rosettes per pot were sprayed and the photos were focused on the rosette layer.

3 Results

For the results of this work, the method optimization for metabolite fingerprinting analyses is described first. This is followed by results from *in vitro* experiments analysing extracellularly produced substances by *V. longisporum* in different media. Furthermore, markers for *V. longisporum* infection in three Brassicaceae were described. The chapter is completed by the results from several functional analyses.

3.1 Optimization of UPLC-TOF-MS-based method for metabolite fingerprinting

For metabolite fingerprinting many methods have been described recently (for examples see Allwood et al. 2010, Evans et al. 2009) but especially for complex matrices the conditions for extraction and analysis must be optimized every time to the analysed samples. Therefore it was an aim of this work to establish a comprehensive extraction method that can be used for small volumes of aqueous samples as well as for fungal mycelium and plant tissue. An optimized method would have high metabolite coverage preferably leading to high intensity levels for most masses as well as their optimal separation between polar and non-polar extraction phase. The analytic parameters for UPLC and MS analysis were also optimized with the objective to increase the separation performance of the LC as well as the sensitivity of the MS analysis.

3.1.1 Evaluation of two-phase extraction methods

To elucidate which sample preparation method was suitable for fungal mycelia, two commonly used two phase extraction methods were compared: the chloroform-based method described by Fiehn et al. (2000) and MTBE-based protocol by Matyash et al. (2008). In both methods the polar phase consisted of a methanol-water mixture while the properties of the non-polar phase differed. MTBE is even less polar than chloroform. Mycelium of *V. longisporum* VL 43 was analysed. The identity of the markers was not elucidated.

In a comparison of both methods MTBE-based extraction was found to cover more non-polar metabolites including high intensity markers than the chloroform-based method (Fig. 12 A). For the distribution in the polar phase both methods seemed to be comparable in their metabolite coverage of polar compounds. To test the distribution of metabolites in the polar and the non-polar extraction phases high quality markers of both ionization modes were combined and clustered by MarVis in two prototypes (Fig. 11 B). The diagram of the polar phase indicates that both extraction protocols result in a good coverage of polar substances. But the polar phase of the chloroform/methanol based extraction comprises of substances of the non-polar substances (Fig. 12 B circle) that were missing in the chloroform phase of this method. Non-polar metabolites are specified here as substances eluting from the column at 80 % or higher amount of organic solvent. This corresponded to an elution later

than 6.5 min in the polar gradient or later than about 3.2 min in the non-polar gradient. With MTBE based extraction the polar phase nearly exclusively consisted of polar metabolites. Non-polar substances were detected only in the corresponding phase, but additionally polar substances were detectable (mostly with retention times > 1 min).

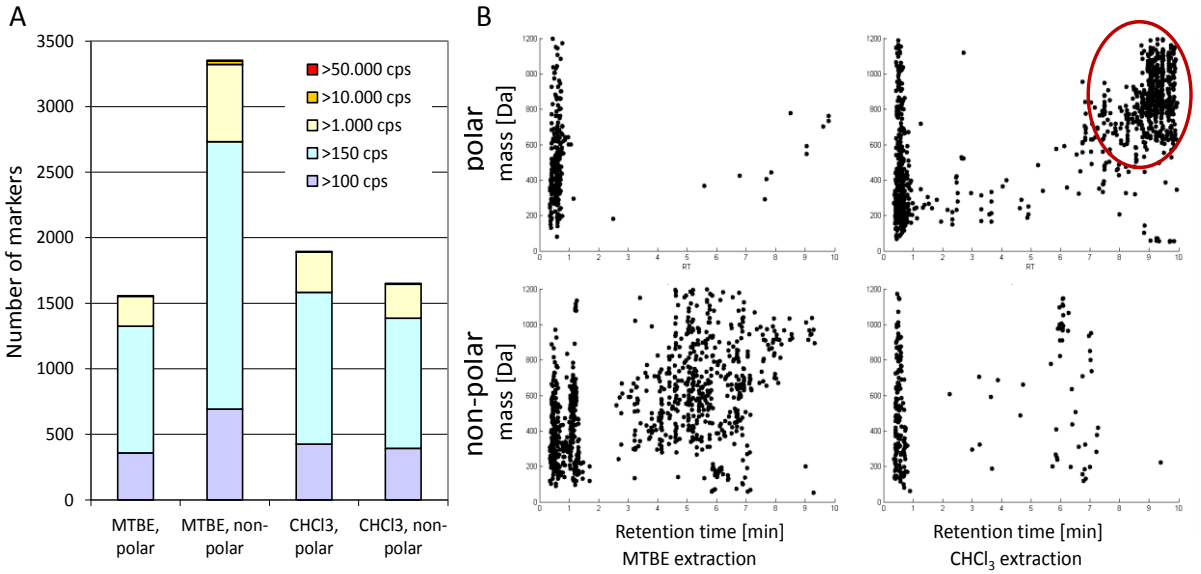

Fig. 12: Comparison of two-phase extraction methods for metabolite fingerprinting in fungal tissue
MTBE extraction was performed according to Matyash et al. (2008) whereas the $CHCl_3$ extraction was described by Fiehn et al. (2000). (A) Distribution of measured intensities in both extraction phases: Itemized by extraction method and solvent phase the number of markers is displayed colour-coded by their intensities. Markers are grouped in 5 intensity classes. (B) Comparison of phase separation: The marker scatter plots of two prototypes (retention time / m/z plane) show all markers from the polar and the non-polar extraction phase of both extraction methods with a p-value < 10^{-4} (Anova test). The red circle indicates a large amount of non-polar markers that were detected in the polar extraction phase of the $CHCl_3$-based extraction. Two extraction replicates each were analysed from mycelium of *V. longisporum* VL 43.

To determine metabolites extracted within both phases the following criteria were used: The mass difference should not be greater than 10 mDa and the pair should be eluted with the same ratio of solvents in the mobile phase e.g. 50 % water. The absolute amount of twice extracted substances in relation to masses that were found only once is shown in Fig. 13 A but when put into perspective the picture is becoming clearer: With the chloroform extraction the percentage of markers detected twice in both phases is much higher (Fig. 13 B). With the MTBE-based method substances were extracted more often in only one distinct phase. It can be concluded that not only the quantity and intensity (at least in the non-polar phase) were increased but also the phase separation was enhanced applying the MTBE extraction.

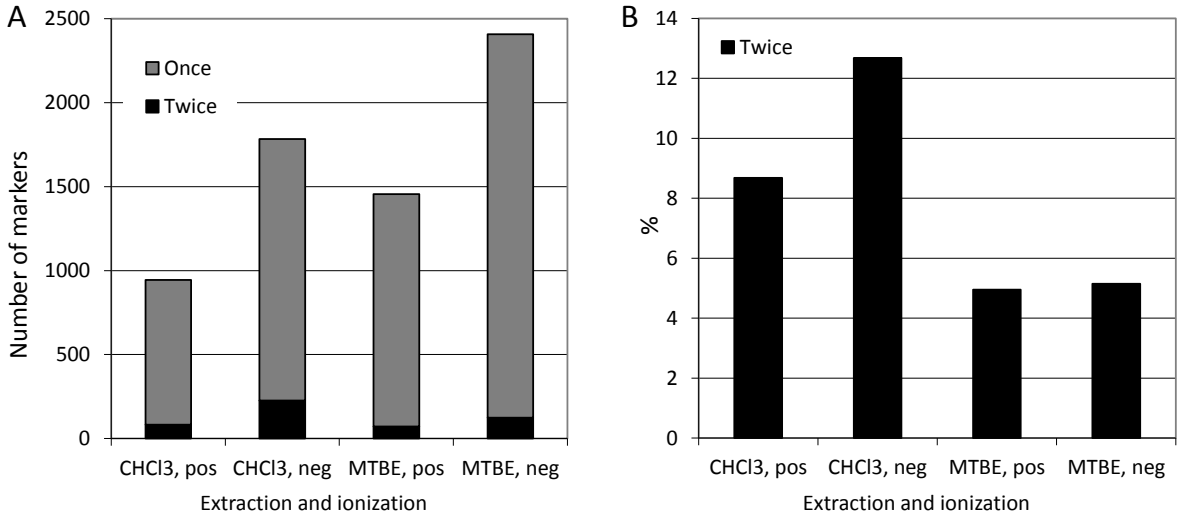

Fig. 13: Comparison of phase separation in a MTBE and a chloroform-based two phase extraction method
The MTBE extraction was performed according to Matyash et al. (2008) whereas the $CHCl_3$ extraction was described by Fiehn et al. (2000). (A) Absolute number of once/twice extracted markers in comparison of MTBE and chloroform-based extraction methods. A marker regarded as twice extracted elutes in polar and non-polar gradients at the same organic percentage and the exact mass differs in positive and negative measurement by maximal 10 mDa. (B) Percentage of markers extracted in both phases. Shown is the ratio of number of compound extracted in both phases to number of markers detected only in one phase. Markers are displayed by extraction method and ionization mode.

3.1.2 Evaluation of methods for optimal metabolite recovery from aqueous media

The MTBE extraction which was only described for tissue extraction before (Qiu et al. 2009, Matyash et al. 2008) was next tested for aqueous samples like culture filtrates or apoplastic fluids. The MTBE-based extraction protocol was compared to an ultrafiltration with centrifugal filters and an acetone-based protein precipitation. These two methods had been applied successfully for metabolite extraction of blood serum samples (Tiziani et al. 2008) with good results for reproducibility, metabolite recovery rates and in removing of protein background.

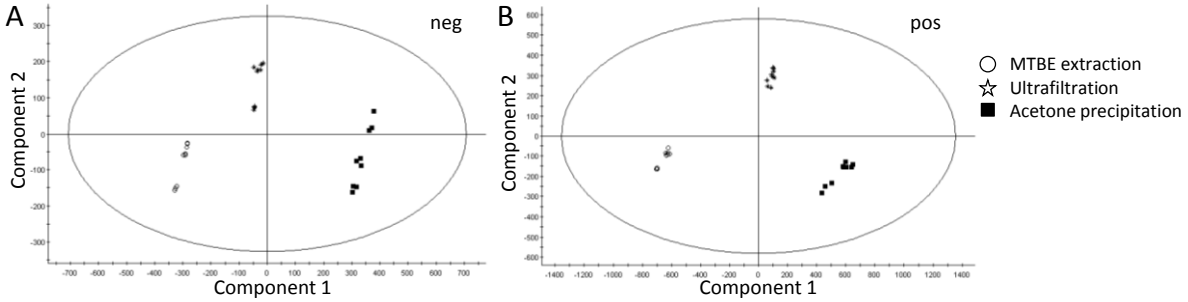

Fig. 14: PCA plot of samples from extraction method comparison
PCA plot proves reproducibility within a sample preparation method and highlights differences between the three analysed methods. (A) Polar phase measured in negative ionization mode (B) Polar phase measured in positive ionization mode; circle = MTBE extracted samples, star = ultrafiltrated samples, square = acetone precipitated samples. Each symbol stands for one analytical run.

The principal component analysis (PCA) plot showed that the reproducibility of all three tested methods was suitable for an aqueous sample (Fig. 14). But it was clearly visible that the methods differ a lot since they form clearly distinguishable groups in the PCA plot. In search of the most suitable extraction method, it was focused on the method which covered the highest number of substances. Especially those markers, which were not accessible by the other procedures (method specific markers) were of interest. Therefore, all polar and non-polar samples in both ionization modes were combined and visualized with the software tool MarVis. The specific markers for each technique were selected from a 1D-SOM. They were subsequently sorted by extraction phase (polar / non-polar) and ionization mode (positive / negative) (Tab. 3).

Tab. 3: Number of specific markers for tested sample preparation techniques

Specific for	Acetone precipitation	Ultrafiltration	MTBE extraction
Marker total	462	441	1270
polar, neg	195	0	26
polar, pos	267	1	36
non-polar, neg	-	100	434
non-polar, pos	-	340	774
Database hits (±4 mDa)	29 (6 %)	130 (29 %)	241 (19 %)

The MTBE extraction dominated with 1270 specific markers whereas the other methods showed only about 450 specific markers. With the simple acetone precipitation of proteins a large number of polar metabolites were measurable but a database search with MarVis only identified 6 % of them. This low value indicated an insufficient data quality and hinted to impurities and adduct formation. The ultrafiltration came up with only one specific polar substance but with 440 from non-polar washing from the filtering membrane. The database coverage was good with 29 %. For MTBE extraction 62 specific polar substances were detected and more than 1000 markers for the non-polar phase. The data quality seemed to be sufficient with 19 % coverage.

Conclusively it can be said that the MTBE extraction is more time consuming and cannot cover all metabolites but seems to educe more compounds also from aqueous samples even compared to the successfully tested methods. Since a lot of polar markers were detected in the non-polar phase the extraction was modified for metabolite fingerprinting of aqueous sample by uniting polar and non-polar phase prior to measurement followed by an extended recording time up to 10 min. This reduced the number of analytical runs to a half without losing information.

3.1.3 Optimization of the UPLC-TOF-MS analysis

3.1.3.1 Optimization of the chromatography

In plant tissue as well as in apoplastic fluids like xylem sap and AWF a huge amount of polar metabolites are expected, which should be detectable within the metabolome analysis. In order to improve the separation performances of polar metabolites during LC analysis, two UPLC columns were compared (ACQUITY shield RP 18 and the ACQUITY HSS T3). Both columns contain reversed-phase material, but the HSS T3 material was designed for especially for separation of polar organic molecules (information from www.waters.com). A mix of 13 polar test compounds was analysed on both columns. This mix included alanine, proline, valine, isoleucine, glutamate, histidine, arginine, sinigrin, kynurenine, citrate, shikimate, citrulline and zeatin. Each compound was provided in a concentration of 10 µg/mL. Due to the different binding properties of the column material the retention of the substances differed. For the better separation performance metabolites should elute over a wider range of retention times. By calculating the standard deviation (SD) of the retention times this increase of separation performance can be quantified. Results indicated that the HSS T3 performs slightly better in separation of polar metabolites (data not shown). This column was therefore used in the following for metabolite fingerprinting analysis of combined phases from aqueous media and for polar phase measurements from extracted tissue. The non-polar phase from extracted tissue was still analysed on the shield RP 18 column.

To enhance the separation performance on the HSS T3 column the solvent gradient was optimized. The aim was to find reasonable starting conditions of the LC that provide enough organic solvents required for high ionization efficiency on the MS on the one hand, but minimal amounts of organic solvent for retaining polar metabolites on the column on the other hand.

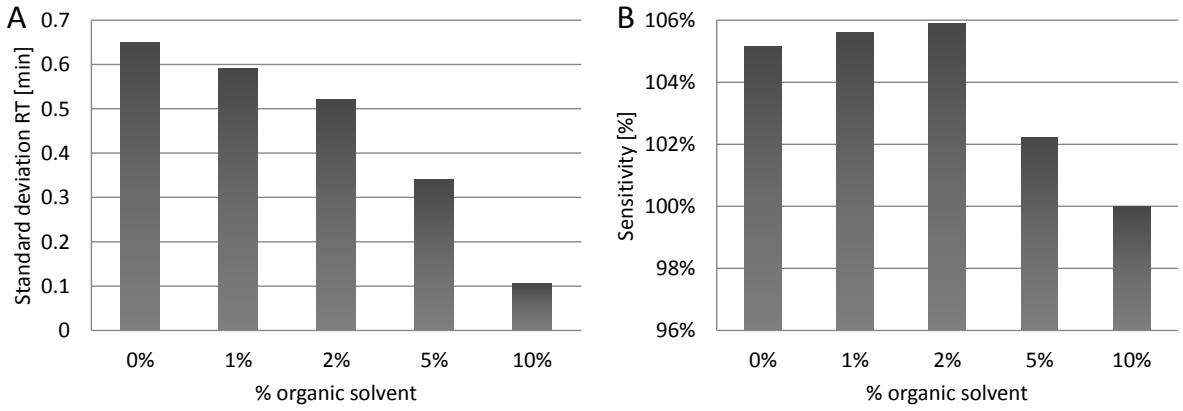

Fig. 15: Optimization of starting conditions for UPLC-MS measurements on HSS T3 column
Conditions tested with 12 polar substances with retention time < 0.6 min at 10 % organic solvent (1:1, by vol acetonitrile/methanol) (A) Changes of the separation performance by increasing amounts of organic solvent indicated by the standard deviation of the retention time (B) Changes of the sensitivity performance by increasing amounts of organic solvent indicated by mean value of all substances compared to 10 % organic solvent on a shield RP 18 column.

While LC separation was optimal with polar starting conditions (100 % water, Fig. 15 A), a rate of 2 % of organic solvent was required for high ionisation efficiency (Fig. 15 B). The results indicated that LC starting conditions of 99 % water and 1 % organic solvent fit best the demands of the LC separation and the MS sensitivity for analysing the metabolites of the polar extraction phase.

3.1.3.2 Optimization of the TOF-MS parameters

It is necessary for metabolite fingerprinting analysis to obtain high quality spectral data. But often mass signals derived from cluster formation of the solvents generate a distracting spectral background. This phenomenon can dramatically reduce the sensitivity of a MS analysis by ion suppression of the analyte ions. In our approach one intensive background mass was produced by an acetonitrile cluster ($[2M+H]^+$ 83.0620 Da). It was therefore opted for recording masses from 85 Da to 1200 Da in positive ionization mode. In negative mode no strong contaminants were found.

To increase the ionization efficiency of the MS analysis and to reduce adduct formation the desolvation temperature was optimized. A higher desolvation temperature should be coupled to an enhanced desolvation gas flow to guarantee a stable spray in the ion source. Therefore a dataset was generated, in which desolvation temperature and desolvation gas flow were varied as follows: 250 °C and 600 L/h or 350 °C and 800 L/h. The results of the analysis were visualized by MarVis Cluster (Fig. 16).

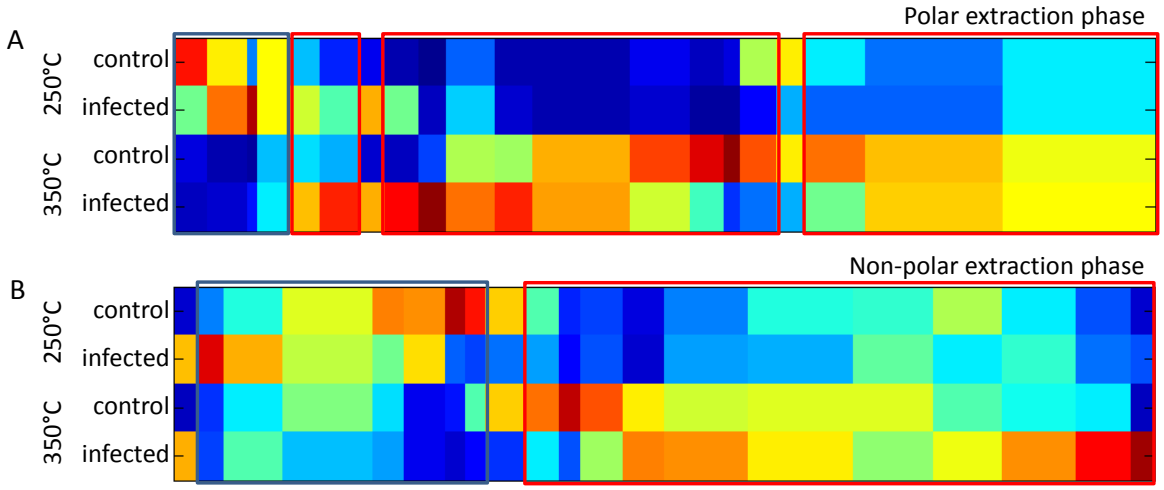

Fig. 16: Optimization of the analytical parameters desolvation temperature and desolvation gas flow
1D-SOM matrix after metabolite-based clustering of datasets recorded for the comparison of 350 °C in combination with 800 L/h to 250 °C in combination with 600 L/h gas flow. Prototypes that include markers with higher intensity levels with low desolvation temperature and gas flow are framed in blue whereas prototypes that include markers with a higher intensity levels with high desolvation temperature and gas flow are framed in red. Prototypes without a frame indicate similar intensity levels at both ionization conditions. Two conditions (control vs. infected) were analysed including three biological replicates, each replicate measured twice resulting in six measurements per condition. The intensity was normalized and colour-coded. The 20 prototypes were scaled to the number of markers contained. (A) Polar phase of leaf extracts of mock treated and infected *B. napus* plants at 35 dpi (B) Non-polar phase of hypocotyl extracts of mock treated and infected *B. napus* plants at 35 dpi.

Prototypes that include markers with a higher intensity levels with low desolvation temperature and desolvation gas flow are framed in blue. Framed in red are prototypes that contain markers with a higher intensity levels with high desolvation temperature and desolvation gas. Prototypes without a frame indicate similar intensity levels at both ionization conditions. The increase of desolvation temperature and an enhanced desolvation gas flow led to higher ionization efficiency and allowed detection of more markers in the polar as well as in the non-polar extraction phase (Fig. 16).

Since the number of markers does not indicate the quality of markers, the characteristics (retention time and m/z) of the enhanced markers were analysed. The markers were arranged by MarVis within a retention time / m/z plane to analyse their distribution compared to the distribution of all markers measured (Fig. 17). The composition of polar markers was not changed by the increase of desolvation temperature and gas flow, but sensitivity increases in general. In contrast, more non-polar markers in the mass range from 600-900 Da with a retention time of 5-8 min (Fig. 17 B, framed in red) were detected due to higher desolvation temperatures and an increased gas flow. It can therefore be assumed that the analysis of especially non-polar metabolites of higher molecular weight will be improved by an increased temperature and gas flow. Despite the improved ionization conditions it must be stated that the non-polar phase showed a higher degree of random noise than polar measurements. This might be due to an easier ionization by ESI for small, polar molecules but must be considered a problem when applying metabolite fingerprinting on hydrophobic substance classes.

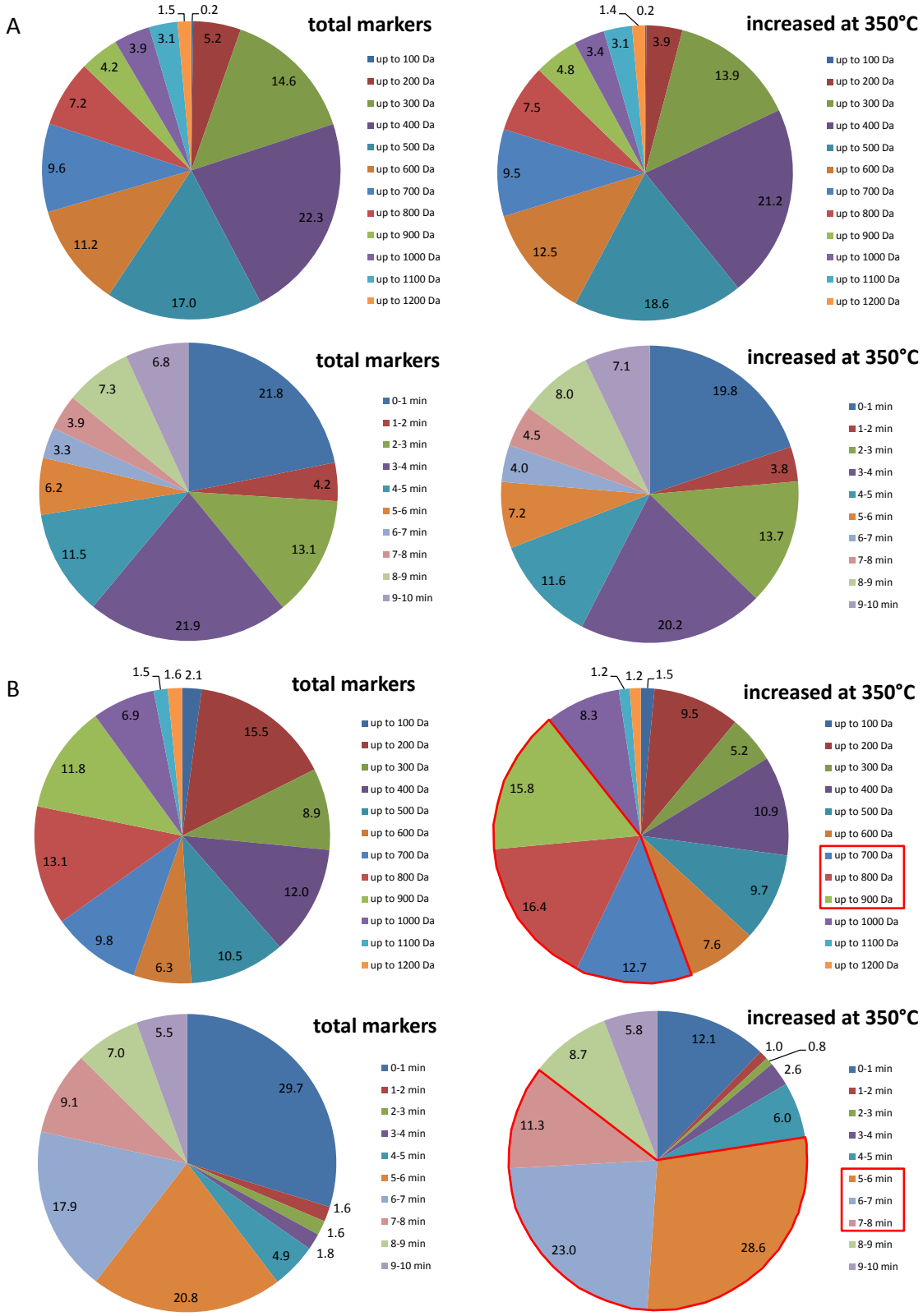

Fig. 17: Optimization of the desolvation temperature and desolvation gas flow for metabolic fingerprinting
Distribution of markers better detected with 350°C desolvation temperature and 800L/h gas flow compared to distribution of all markers measured in the comparison. (A) Distribution of polar markers sorted by either mass or retention time. (B) Distribution of non-polar markers sorted by either mass or retention time; > 2 % increased mass and retention time ranges at higher temperature are framed in red. Experimental conditions are given in Fig. 16.

3.1.4 Identification of markers

3.1.4.1 Combination of positive and negative ionization

In order to identify markers, it is necessary to distinguish between markers derived from protonated ($[M+H]^+$) and deprotonated ions ($[M-H]^-$) or from adducts and cluster ions. Such adducts ($[M+Na]^+$, $[M+NH_4]^+$ or ($[M+formate]^-$) and cluster ions ($[2M+H]^+$ or $[2M-H]^-$) were often formed during ESI mode.

The mass of a protonated or deprotonated ion can be corrected to its neutral mass by adding (negative ionization) or subtracting (positive ionization) the mass of a proton (1.0073 Da). Data sets which contain neutral masses can then be combined. No automated adduct correction is needed for this combination of the two data sets. Assuming a substance to ionize in both modes of ionization it will be detected with the same neutral mass twice after combination of datasets. This can give a hint to a true mass of a marker (substance mass), whereas adduct masses like the sodium adduct $[M+Na]^+$ are formed preferably in one mode of ionization. The correction of this adduct by subtracting the mass of a proton will lead to a false neutral mass (-1.0073 Da instead of -21.9898 Da) and will find no partner deriving from the negative ionization dataset (Fig. 18 A). The combination of both datasets can easily be performed by MarVis Filter. This method can deduce reliable markers and distinguish them from adducts but is of course limited to substances that ionize in both modes.

3.1.4.2 Adducts as helpful information

To overcome the restriction of positive and negative ionizable metabolites for finding reliable markers, the adduct formation can be used (Fig. 18 B). By an increased knowledge about occurring adducts and an automated adduct correction in MarVis Filter reasonable neutral masses of substances can be found. As an example the oxylipin 9,12,13-trihydroxy-10,15-octadecadienoic acid is provided. This substance ionizes as a singly charged ion only in negative ionization mode and would therefore not be detected in a mode combination based approach. Nevertheless it forms a lot of adducts that can be detected in positive or negative ionization mode (Fig. 18 C). The scheme contains only explicable adducts although numerous other adducts occurred during analysis. Noticeable is that the addition of one adduct can lead to the attachment of further adducts. This increases the overall complexity of adduct formation. But if at least some well-known adducts can be detected (positive: $[M+NH_4]^+$, $[M+Na]^+$; negative: $[M+CHO_2]^-$, $[M+CHO_2Na-H]^-$) MarVis Filter is able to assign them by their accurate mass difference to the substance mass. The heavier mass is only regarded as an adduct when the corresponding retention times lies within a small retention time window. The software tool can subsequently correct the adduct masses to the neutral substance mass. The automated adduct correction must nevertheless be used carefully. When too many adduct rules for

correction are used by MarVis Filter it can result in false positive recognition and overcompensation. With this a correction of an e.g. protonated substance that is by mistake recognized as an adduct can lead to a false calculation of the neutral substance mass. An automated adduct correction can therefore only be a first attempt to find the correct substance masses in a complex matrix and the results should be carefully verified. There is currently no automated routine available, which can detect all known adducts correctly, but the occurrence of several adducts can nevertheless point towards interesting metabolites (Fig. 18 C).

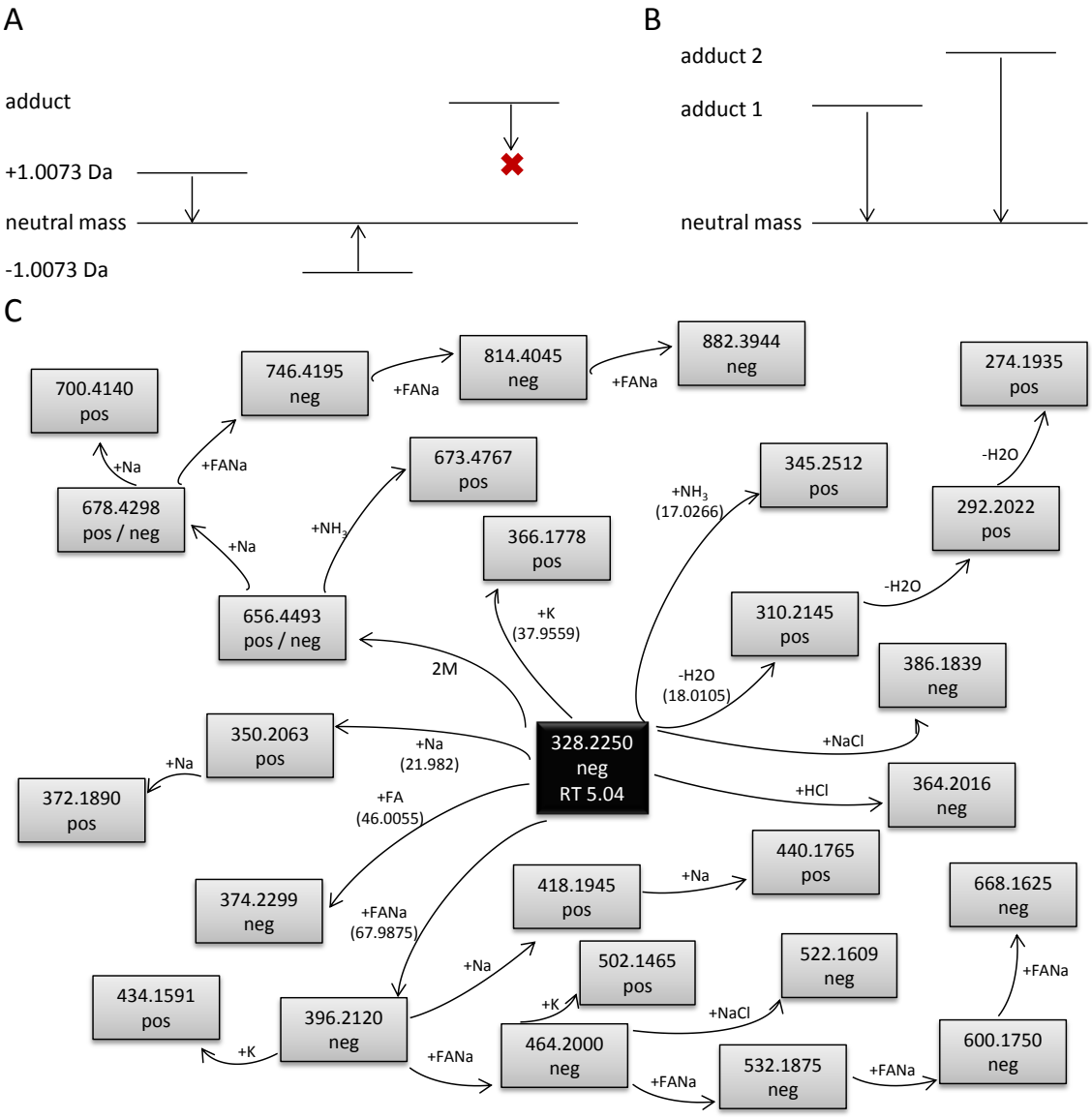

Fig. 18: Adduct recognition as an instrument to confirm the correct substance mass
Confirming the substance mass in complex datasets (A) by combining data of the positive and negative ionization mode. The correction of the adduct mass by the mass of a proton does not always lead to a reasonable neutral mass. (B) Therefore adducts have to be taken into account as additional source of information. (C) Adducts of 9,12,13-trihydroxy-10,15-octadecadienoic acid (black box) observed in the metabolite fingerprinting analysis. The masses were corrected to neutral masses by adding or subtracting 1.0073 Da for protonation or deprotonation depending on the ionization mode. The subtitle indicates if the adduct was detected in positive (pos) or negative (neg) ionization mode. Every mass difference specific for an adduct is indicated once. RT = retention time, FA = formic acid, FANa = sodium formate, 2M = $[2M+H]^+$.

In order to optimize the metabolite fingerprinting analysis for this work, all steps in the workflow have been tested and adapted. The extraction method was optimized for tissue and aqueous samples, as was the LC performance and the TOF-MS parameters. In the data processing the workflow was simplified by the combination of the data sets from negative and positive ionisation mode. An increased knowledge about occurring adduct formation improved the automated correction routine. When frequently occurring adducts as formed with formic acid are labelled as adducts within marker tables, they can be discarded from the further process of marker identification. This leads to a decreased number of markers, which have to be characterized. As a rough estimation, it can be assumed that less than 50 % of all detected markers represent a metabolite. It can be summarized, that by this new workflow the retrieval of information from the metabolome analysis was optimized.

3.2 Metabolite fingerprinting analysis of the secretome of *V. longisporum* grown in different media

3.2.1 Metabolite fingerprinting analysis of the secretome of *V. longisporum* grown in synthetic media

The extracellularly produced metabolites of *V. longisporum* grown in Simulated Xylem sap Medium (SXM) and potato dextrose broth (PDB) were analysed with the intention to identify metabolites, which might occur as fungal derived signals during the infection process *in planta*. Due to the reduced availability of xylem sap the synthetic xylem-like medium SXM was used. Neumann and Dobinson (2003) designed SXM to mimic the nutritional conditions within the apoplastic space. For the metabolite fingerprinting analysis the media SXM and PDB as well as the culture supernatants of *V. longisporum* grown in both media were compared. For that pre-cultivated mycelium (4 d) was transferred from PDB either to fresh PDB or to SXM and cultivated for another 4 d. The transfer from PDB to SXM should mimic the environmental change, when the fungus enters the apoplastic space of the plant during the infection. The transfer from in SXM pre-cultivated mycelium into fresh SXM was used as a control condition.

Metabolite fingerprinting analysis was performed for culture supernatants of *V. longisporum* in the different media. Data processing routines (see material and methods) led to a subset of 8129 high quality marker candidates from positive and negative ionization mode with a p-value < 10^{-4} (Kruskal-Wallis test). Clustering and visualization of this data set by training a 1D-SOM model allowed finding

of a group of 3621 markers, which specific accumulate in the SXM culture supernatant (Fig. 19 A). The exact mass information of these marker candidates was used for database search and pathway recognition. The obtained database hits indicated that the shikimate pathway was particularly affected. 25 metabolites of the tryptophan metabolism were tentatively assigned within the database search (Fig. 19 B). The raw data from the metabolite fingerprinting analyses for the *in vitro* experiments can be found in the supplemental datasets S 5.

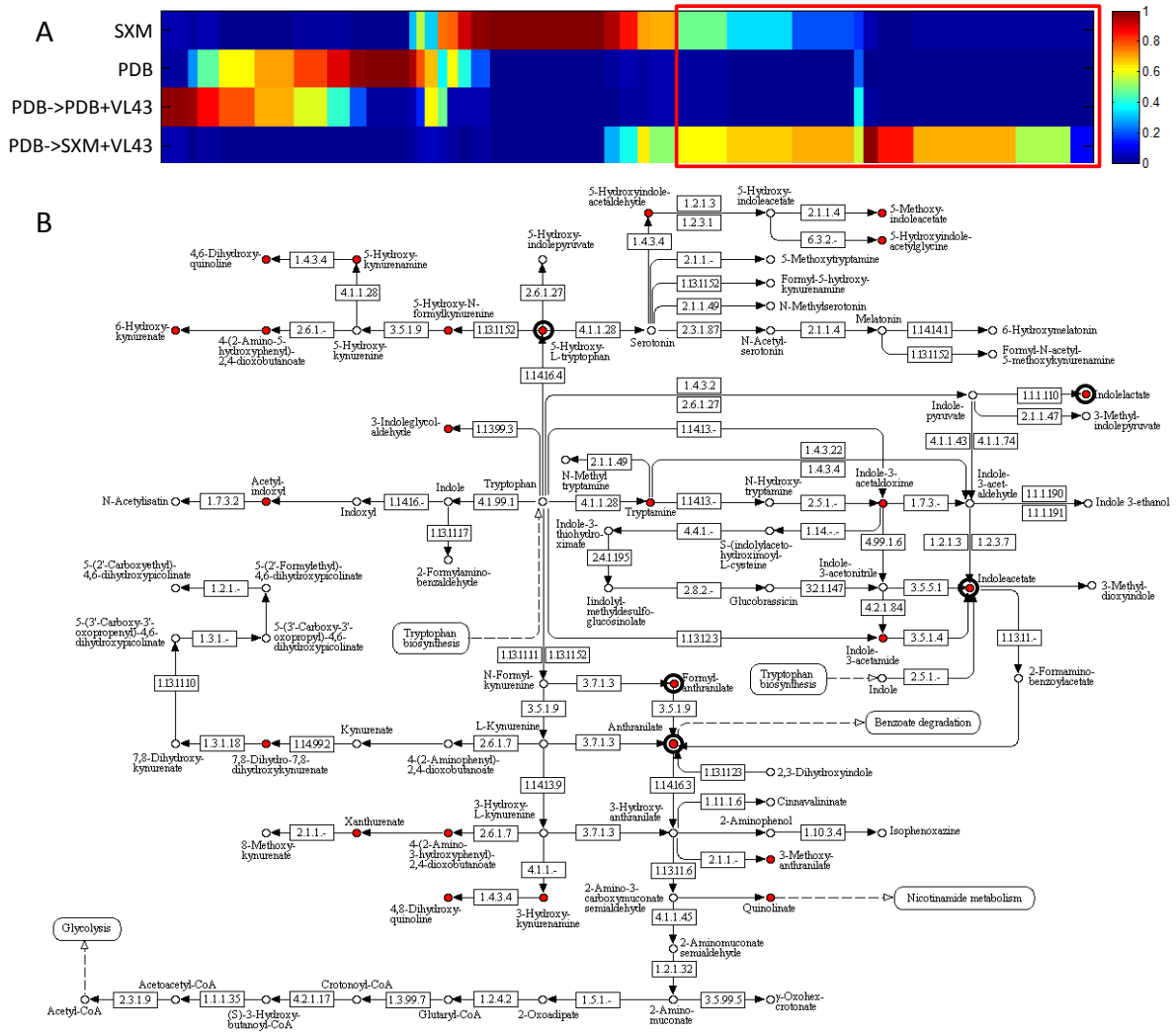

Fig. 19: Metabolite fingerprinting of the extracellular metabolome of *V. longisporum* grown in SXM or PDB medium

PDB and SXM as well as culture supernatants of *V. longisporum* pre-cultivated in PDB and grown for another 4 days in SXM or PDB were extracted by MTBE extraction. The samples were measured by UPLC-TOF-MS. The dataset includes representative results of three independent experiments including two technical replicates each. The displayed datasets include combined markers from positive and negative ionisation with a p-value < 10^{-4} (Kruskal-Wallis test). (A) 1D SOM matrix after metabolite-based clustering of 8129 markers. Prototypes that include markers specifically produced by the fungus grown in SXM are framed in red (3621 markers). The intensity was normalized and colour-coded by the attached key. The 20 prototypes were scaled to the number of markers contained. (B) The exact masses of 25 markers enriched in SXM culture filtrates are putatively assigned to metabolites of the tryptophan pathway (red dots). Unequivocally identified metabolites are marked by a black circle. Modified after http://www.genome.jp/kegg-bin/show_pathway?map00380

Three indolic compounds (indole-3-carboxylic acid, indole-3-acetic acid and indole-3-lactic acid), anthranilate and its derivatives (formylanthranilate and acetylanthranilate) and three modified aromatic amino acids (acetyltryptophan, acetylphenylalanine and hydroxytryptophan) were unequivocally identified as metabolites produced during *V. longisporum* growth in SXM. All accumulating substances are listed in Tab. 4.

Tab. 4: SXM specific secreted substances of *V. longisporum*
Metabolites enriched in the SXM culture supernatant of *V. longisporum* were unequivocally identified by coelution with authentic standards and comparison of the UV/Vis maxima (*). The retention time (RT) was measured on the ACQUITY UPLC HSS T3 column.

Exact mass [Da]	RT [min]	Molecular formula	Substance
137.0477	3.25	C7H7NO2	Anthranilate*
165.0426	3.75	C8H7NO3	Formylanthranilate*
179.0582	3.96	C9H9NO3	Acetylanthranilate
246.1004	3.94	C13H14N2O3	Acetyltryptophan
220.0848	1.71	C11H12N2O3	Hydroxytryptophan
207.0895	3.7	C11H13NO3	Acetylphenylalanine
175.0633	4.26	C10H9NO2	Indole-3-acetic acid*
205.0739	3.85	C11H11NO3	Indole-3-lactic acid
161.0477	3.97	C9H7NO2	Indole-3-carboxylic acid

The content of tryptophan, phenylalanine and other amino acids in contrast was reduced throughout cultivation (Fig. 20 B). Also some small organic acids were decreased.

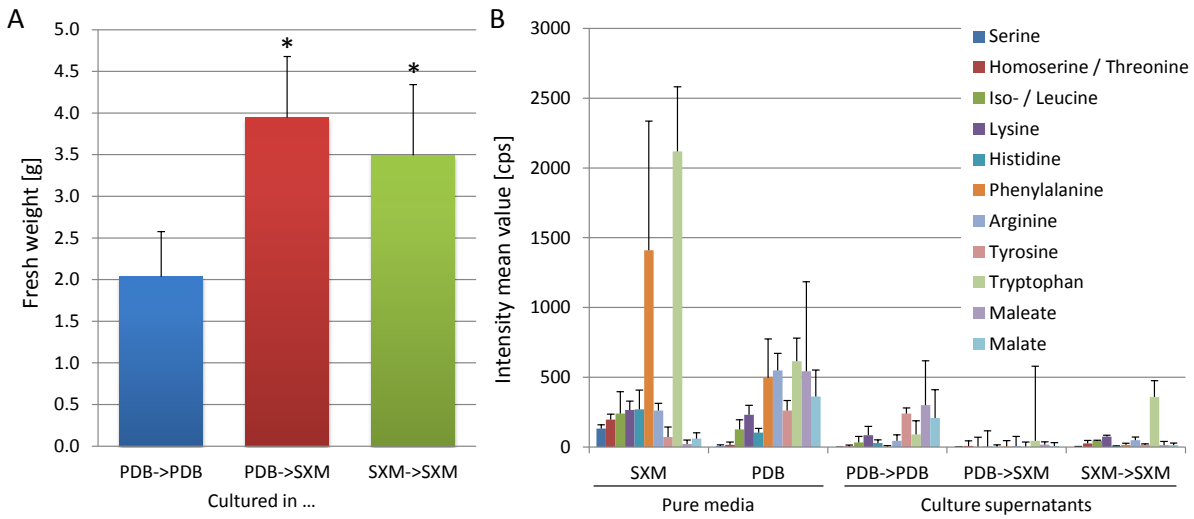

Fig. 20: Physiological and metabolic consequences of the transfer of VL 43 mycelium to different media
(A) Fresh weight of VL 43 mycelium when harvested after 8 d itemized by media conditions. The first medium indicates medium used for pre-cultivation for 4d, the second medium stands for the fresh medium supplied for the mycelium subsequently for another 4 d. The data include at least 9 biological replicates. Asterisks indicate fresh weight with a significant difference compared to PDB->PDB in an unpaired Students t-test (* = p-

value < 0.001). (B) Intensity distribution of selected amino acids and organic acids detected after 8 d fungal cultivation in indicated supernatant. Basic levels for PDB and SXM are indicated in the first two conditions. Error bars represent the standard deviation. PDB = Potato dextrose broth, SXM = Simulated xylem sap medium

The most intensive and reliable marker was formylanthranilate. It accumulated in high amounts in the medium SXM with *V. longisporum* but not in PDB with *V. longisporum* (Fig. 21). The variation in the detected amount seemed to depend on the fungal spore concentration which varied slightly in every experiment and can explain the high standard deviation.

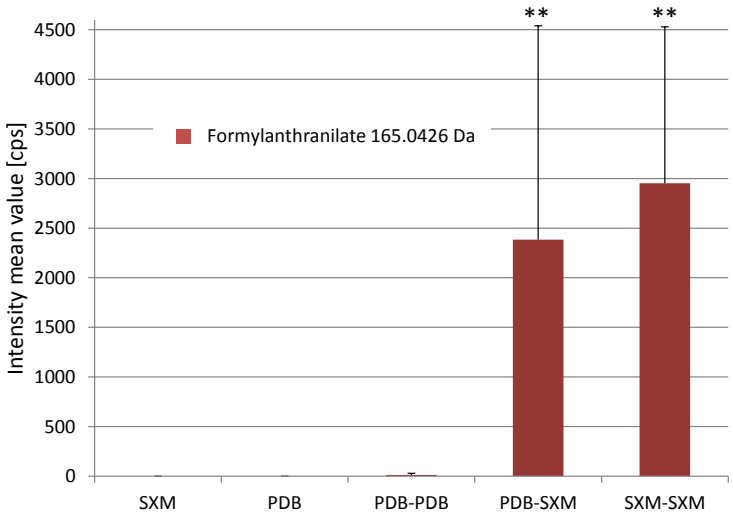

Fig. 21: Accumulation of formylanthranilate produced by *V. longisporum* during growth in different media
Accumulation of formylanthranilate in culture supernatants of *V. longisporum* pre-cultivated in PDB or SXM and grown for another 4 days in SXM (PDB-SXM, SXM-SXM). PDB-PDB describes the control for fungal cultivation in PDB medium. SXM and PDB represent the pure media without fungal cultivation. Shown are intensity mean values from three independent experiments including at least 18 measurements per condition. Error bars represent the standard deviation. Asterisks indicate intensity values with significant differences compared to SXM in an unpaired Students t-test (* = p-value < 0.05; ** = p-value < 0.001). Error bars represent the standard deviation.

As a physiological observation it can be stated that *V. longisporum* grows faster in SXM than in PDB as can be measured for the mycelium fresh weight after 8 days of cultivation (Fig. 20 A). Additionally, the fungus grown in SXM starts earlier to darken. The fungal substance responsible for this dark pigmentation is most likely melanin. These phenolic polymers protect the fungus from environmental stress. The identity of melanin as pigmenting substance of *V. longisporum* was confirmed by inhibition of the biosynthetic enzyme laccase (Bell and Wheeler 1986, Sjoblad and Bollag 1977) by adding glucose to the medium as described by Frases et al. (2007). The melanisation of the mycelium was delayed about three days in PDB and SXM.

3.2.2 Metabolite fingerprinting analysis of the secretome of *V. longisporum* grown in xylem sap of *B. napus*

In order to examine, if fungal growth in SXM can reflect the growth in the vascular tissue, the composition of SXM and xylem sap of *B. napus* and *A. thaliana* was compared. Additionally, the culture supernatants of *V. longisporum* grown in SXM and in xylem sap of *B. napus* were analysed.

Data mining by sample-based PCA analysis showed a clear group separation for SXM and the xylem sap of the two different Brassicaceae (Fig. 22 B). This indicated that all three samples differ significantly from each other. The metabolite-based clustering by 1D-SOM allows a more comprehensive view on the metabolite level. While there are some prototypes that include marker from *B. napus* and *A. thaliana*, rather no overlap to SXM was detectable. However the xylem sap of both plants resembled each other in a higher degree than the artificial SXM (Fig. 22 A).

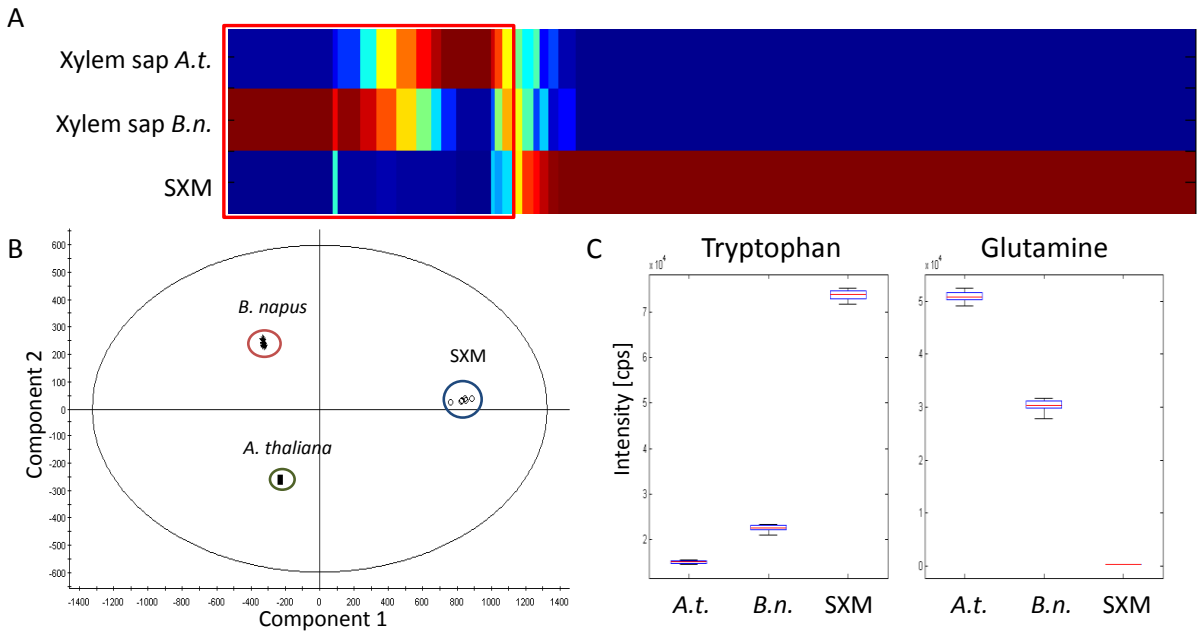

Fig. 22: Metabolite fingerprinting analysis of xylem sap collected from *B. napus* and *A. thaliana* and of Simulated Xylem sap Medium (SXM)

Xylem sap and SXM were extracted by MTBE extraction and measured by UPLC-TOF-MS. Three technical replicates were measured three (xylem sap) or two times (SXM). (A) 1D SOM matrix after metabolite-based clustering of 5017 marker candidates. The displayed datasets include combined markers from positive and negative ionisation with a p-value < 0.001 (Kruskal-Wallis test). Prototypes that include 1495 xylem sap specific markers are framed in red. The intensity was normalized and colour-coded. The 20 prototypes were scaled to the number of markers contained. A.t. = *Arabidopsis thaliana*, B.n. = *Brassica napus* (B) Sample-based PCA scatter plot of negatively ionized samples. (C) Box plots display intensities of the amino acids tryptophan and glutamine.

The strong differences in the metabolite composition between SXM and the xylem sap can be illustrated by the amino acid content. Tryptophan, phenylalanine, proline, arginine, lysine, histidin, valine and leucin / isoleucine display high levels in SXM in comparison to xylem sap (Fig. 22 C). In

contrast to that glutamine and asparagine as transport forms for nitrogen in the xylem (Pate et al. 1980) are detected in high amounts in the natural samples but are underrepresented in the SXM media. The results of this metabolite fingerprinting analysis revealed, that SXM is not adequate to mimic xylem sap. Since the metabolite composition of SXM does not resemble that of xylem sap collected from *B. napus* and *A. thaliana*, the cultivation of *V. longisporum* was also investigated in freshly harvested xylem sap of 28 d old *B. napus* plants (Fig. 23).

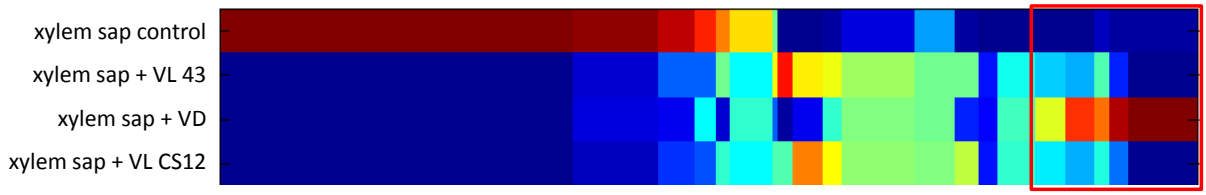

Fig. 23: Metabolite fingerprinting analysis of the extracellular metabolome of *Verticillium* sp. grown in xylem sap collected from *B. napus* plants
Xylem sap and culture supernatants were extracted by MTBE extraction and measured by UPLC-TOF-MS. Three biological replicates were measured three times. 1D SOM matrix after metabolite-based clustering of 1302 marker candidates. The displayed datasets include combined markers from positive and negative ionisation with a p-value < 0.001 (Kruskal-Wallis test). Prototypes that include 218 markers accumulated predominantly by *V. dahliae* are framed in red. The intensity was normalized and colour-coded. VL43 = *V. longisporum* wild type, VD = *V. dahliae*, VL CS12 = *V. longisporum* chorismate synthase mutant

The culture supernatant was analysed and comparable to the results of SXM supernatant a depletion of amino acids was detected. Tryptophan and ten other amino acids (tyrosine, phenylalanine, valine, glutamine, arginine, lysine, histidine, asparagine, aspartate and isoleucine / leucine) were identified as decreased markers. Additionally, some substances accumulated also in the provided xylem sap environment. Anthranilate and formylanthranilate were again the most intensive metabolites. About 90 % of the other markers differed completely from the ones in SXM. For many of the increased markers the database hits suggest plant derived substances so that they might be degradation products from more complex compounds in the provided xylem sap. The results of the metabolite fingerprinting analysis showed that the supernatants of *V. longisporum* grown in SXM and xylem sap differ strongly. Nevertheless it shares the involvement of aromatic amino acids pathways in *V. longisporum* noticeable by the extracellularly detected compounds related to tryptophan.

3.2.3 Metabolite fingerprinting analysis of *V. longisporum* vs. *V. dahliae* and *V. longisporum* mutant strains

From the results above aromatic amino acids and their derivatives were identified as most prominent markers. Therefore two strains of *V. longisporum* RNAi mutants with a reduced expression of chorismate synthase (Singh et al. 2009) were analysed in comparison to the wild type strain. The mutants were provided by the Prof. Braus (Department of Molecular Microbiology and Genetics, Georg-August-University, Göttingen, Germany). These mutants were already shown to be less

infective to *B. napus* (Singh et al. 2009). *V. dahliae* was included in the analysis for a more comprehensive overview. All four fungal strains were cultivated in freshly harvested xylem sap of 28 d old *B. napus* plants (Fig. 23). Metabolite fingerprinting of the extracted culture media indicated that the reduced expression of chorismate synthase had no effect on the marker pattern. All increased markers, like the anthranilate derivatives showed no significant differences in the intensity level between wild type and mutant strains. However, hydroxytryptophan, indole-3-acetic acid and indole-3-lactic acid were not detected in the supernatants in this experiment.

For *V. dahliae* a slightly different metabolite fingerprint was recorded (Fig. 23, red box). The accumulation of formylanthranilate as well as acetyltryptophan is significantly reduced in comparison to the *V. longisporum* wild type whereas enhanced levels of acetylphenylalanine were detected in the secretome of *V. dahliae*. When pathway analysis was performed the hits indicated a connection to different branches of the plant hormone metabolism of *V. dahliae* and *V. longisporum*. These connections still have to be verified by identification of the relevant metabolites from e.g. zeatin biosynthesis. Nevertheless a targeted analysis of phytohormones in the mycelium of *V. longisporum* was already performed by Dr. Cornelia Herrfurth. This has shown that *V. longisporum* is indeed able to produce abscisic acid (ABA) and indole-3-acetic acid (auxin).

3.2.4 Comparison of the secretome of *V. longisporum* grown in xylem sap with xylem sap of infected *B. napus* plants

The metabolic fingerprinting analysis of *V. longisporum* in SXM and xylem sap *in vitro* provided a list of metabolites that are enriched or reduced in a xylem-like environment by the fungus (Tab. 4 + Fig. 20 B) and could therefore be markers also *in planta*. To test this hypothesis the culture supernatant of *V. longisporum* incubated in xylem sap of healthy *B. napus* plants was compared to xylem sap obtained from *V. longisporum* infected oilseed rape plants. Unfortunately, the comparison showed no overlapping metabolite pattern between the two conditions. In addition no extracellular metabolite being specific for the fungus was detectable in the xylem sap of *V. longisporum* infected oilseed rape plants. This may indicate that the metabolic processes *in vitro* and *in vivo* differ significantly. Hence no candidates for fungal effector substances that might be spread in the infected plant within the xylem were found.

From the analysis of *V. longisporum* and related strains in different media it can be concluded that the established and optimized method for metabolite fingerprinting analysis in aqueous media works successful and reproducibly. On the other hand the fungus derived metabolic changes in a liquid culture and in infected plants do not resemble each other.

3.3 Identification of markers for *V. longisporum* infection in *B. napus* plants by metabolite fingerprinting analysis

3.3.1 Infection monitoring

In order to describe the metabolic consequences of the fungal invasion in *B. napus* plants, a successful and reproducible infection process must be guaranteed. It was often observed in *B. napus* and *A. thaliana* that plants infected with *V. longisporum* do not show any visible symptoms (Eynck et al. 2007). Therefore it cannot be ensured that pools of plants treated with VL 43 spores all contribute to an infection related pattern. For metabolic analysis only severely infected plants should be used. Therefore a reliable and straightforward criterion must be found that monitors the infection state of the plants prior to harvesting. Measurements of fungal DNA in infected plant material were therefore not applicable and could only be performed in retrospect.

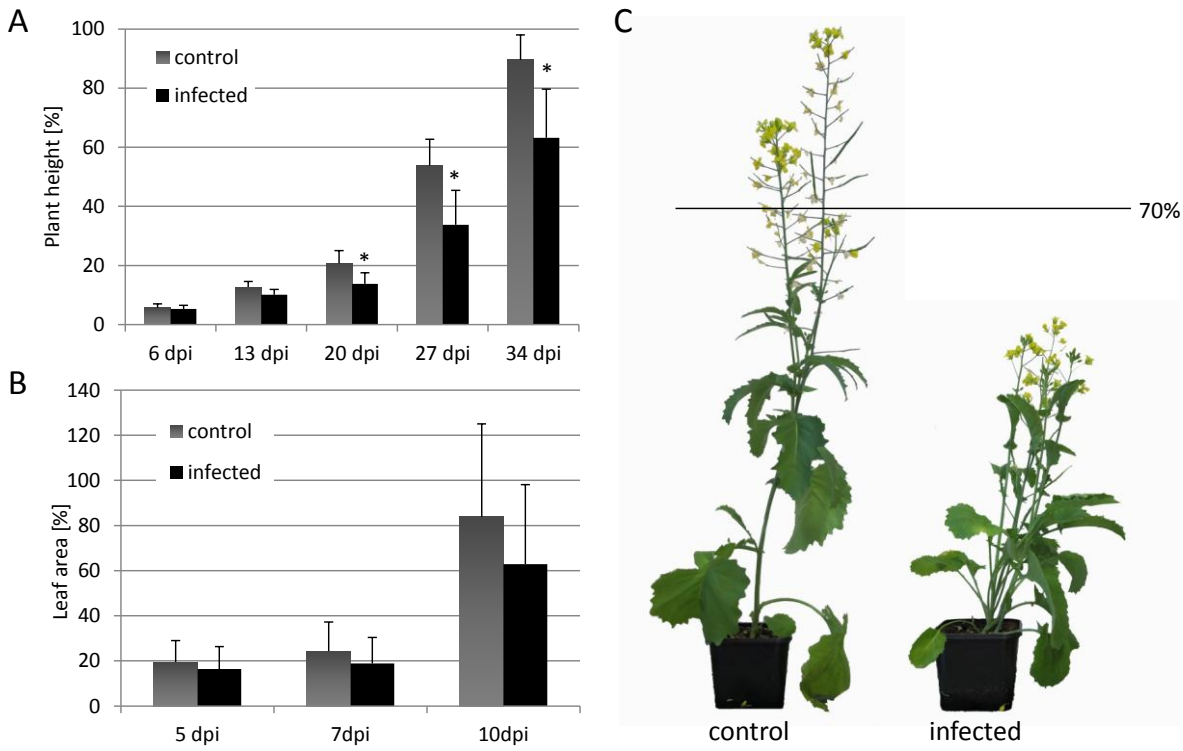

Fig. 24: Monitoring of the infection of *B. napus* with *V. longisporum*
(A) Height of control and infected plants during the infection time course up to 34 days past infection (dpi). Three independent experiments were normalized by percentage. The mean value of the height of the control plants was set to 100 %. Asterisks indicate intensity values with significant differences compared to the corresponding control in an unpaired Students t-test (* = p-value < 0.05). Error bars represent the standard deviation. (B) Leaf area of control and infected plants at early time points up to 10 dpi. Two independent experiments were normalized by percentage including 30 plants per condition. (C) Phenotype of a control plant and a strongly infected plant at 35 dpi.

Oilseed rape infected by *V. longisporum* shows specific symptoms like the reduced height so called stunting and strong axillary branching (Eynck et al. 2007). The stunting can easily be monitored by

determining the length of the intact plants. Ratzinger et al. (2009) documented the correlation of this reduction in shoot length and the amount of fungal DNA as a criterion for successful infection.

A significant reduction in shoot length was visible from 20 dpi on as shown in Fig. 24 A. Therefore it was decided to pool infected plants for the analysed time points 21, 28 and 35 dpi that do not exceed 70 % of the height of the control plant mean value. Plants taller than that were regarded as not successfully infected. The stunting was often not significant for infection monitoring of early time points. To overcome this problem the criterion of leaf area reduction, as used for infection monitoring in *A. thaliana,* was applied but the leaf area was only slightly, but not significantly reduced in infected plants (Fig. 24 B). Since no reliable criteria for infection of early time points (5, 7, 10 dpi) were found, all plants of this age treated with fungal spores were used for further analysis. The infection and analysis of early time points was performed together with Annette Weizbauer (Weizbauer 2011).

In order to verify the infection state of *V. longisporum* treated plants, the amount of fungal DNA was measured in collaboration with the workgroup of Prof. Braus (Department of Molecular Microbiology and Genetics, Georg-August-University, Göttingen, Germany).

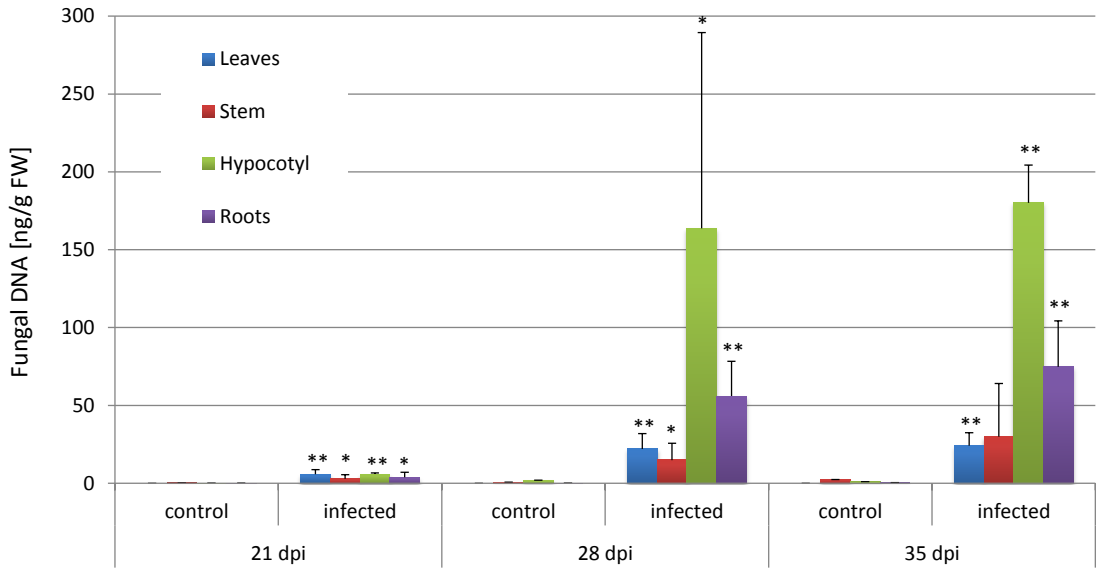

Fig. 25: Analysis of fungal DNA in leaves, stem, hypocotyl and roots of *B. napus*
Abundance of *V. longisporum* in control and infected plant tissue was analysed by real-time PCR with the *Verticillium spp*. specific primers OLG70 and OLG71. Plant material was harvested 21, 28 and 35 dpi. Leaf, stem, hypocotyl and root samples from three independent experiments were extracted and measured twice. Asterisks indicate intensity values with significant differences compared to the corresponding control in an unpaired Students t-test (* = p-value < 0.05; ** = p-value < 0.001). Error bars represent the standard deviation.

In the roots low but significant amounts of fungal biomass were already detectable from 5 dpi on (Fig. S 1). The amount of fungal DNA in the different plant tissues at late infection time points is

displayed in Fig. 25. From 21 dpi on fungal DNA was detectable in all analysed plant organs in low amounts. The highest concentrations were detected in the hypocotyl tissue at 28 and 35 dpi. Interestingly, it rises above the amount of the roots, where the pathogen starts its infection. In upper plant tissue (leaves and stem) only minor amounts of fungal DNA were measured. The results are in accordance with the infection process described by Eynck et al. (2007).

3.3.2 Overview of metabolic changes

The metabolite fingerprinting analysis was performed for early time points (5, 7 and 10 dpi) from infected and control *B. napus* plants to gain insight into metabolic changes shortly after the first contact of host and pathogen. The scarce material was only divided in shoot (aboveground) and root (belowground) samples. At the early infection time points no xylem sap could be obtained from the small plants. For the analysis of late time points of the *V. longisporum* infection in *B. napus* (21, 28 and 35 dpi) the plant material was divided into leaf, stem, hypocotyl and root samples to gain a comprehensive overview of the tissue specific distribution of infection markers in the different plant organs. Additionally, two different apoplastic fluids were collected. This includes xylem sap emerging from the stem and apoplastic wash fluid from leaves (AWF). For a comparison with the metabolic changes in *A. thaliana* the AWF of infected and control *Arabidopsis* plants was collected at 21 dpi but no xylem sap could be obtained from infected *A. thaliana* plants. The results from *A. thaliana* are included in the review of the identified infection markers if applicable. In a first step an overview of the metabolic changes in infected *B. napus* tissue in comparison to control plants was obtained. Therefore markers that were provided by metabolite fingerprinting analysis at early and late infection time points were analysed by MarVis. High quality markers obtained from positive and negative ionisation (p-value < 10^{-4}, Kruskal-Wallis test) from roots (early time points) and hypocotyl (late time points) were clustered according to their intensity profile. This results in the 1D-SOMs that are displayed in Fig. 26. The raw data from the metabolite fingerprinting analyses for the infection experiments can be found in the supplemental datasets S 1 (early time points), S 2 (late time points) and S 3 (*A. thaliana*).

Changes of the metabolic pattern in roots of infected plants were monitored already at early after infection (5 dpi). Markers with high normalized intensities indicated by orange or red colour are represented in 8 of the selected 10 prototypes in Fig. 26 A (red box) at 5 dpi. This indicated a fast metabolic response to fungal invasion in *B. napus* plants. Some markers kept or increased their intensity level when infection processes went on over 7 and 10 days (prototype 1-3) but many decreased after an early maximum. At later time points (from 21 dpi on) the infection markers tended to show a more stable or steadily increasing intensity level. As an example the 1D-SOM

matrix of a dataset generated from measurements of extracted hypocotyl tissue is displayed in Fig. 26 B. It is noticeable that more metabolites accumulate than decrease.

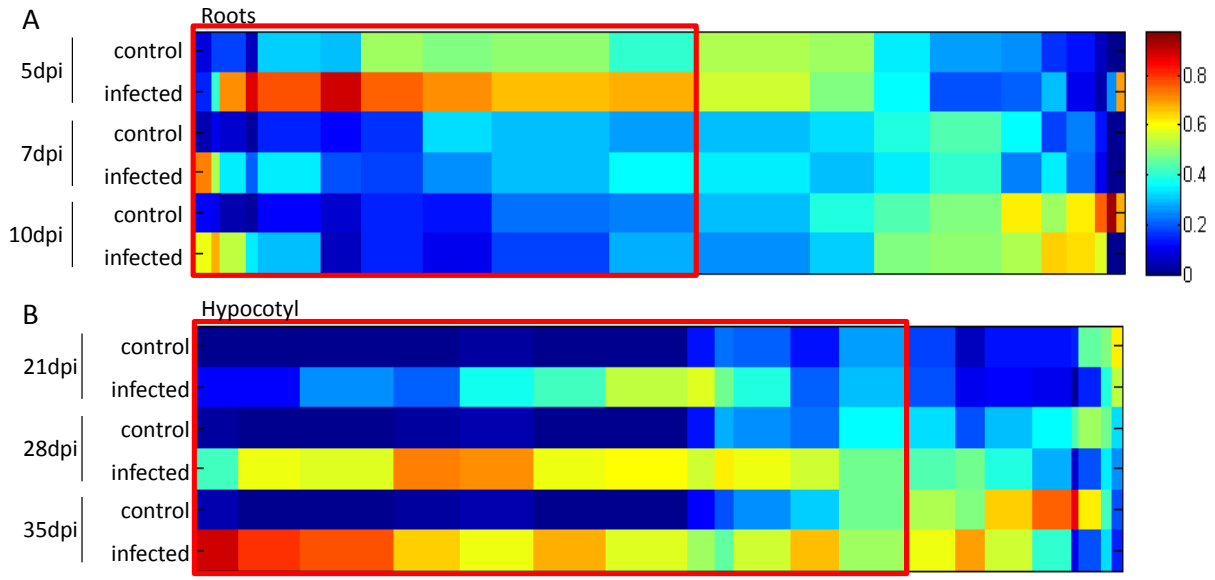

Fig. 26: Infection specific metabolite fingerprinting analysis in tissue of *B. napus* plants after infection with *V. longisporum*
Measurements of the MTBE extracted polar phase of different tissues from *B. napus* after fungal infection. 1D-SOM matrix after metabolite-based clustering of (A) 468 markers from root tissue at early time points after infection (5, 7, 10 dpi) and (B) 741 markers from hypocotyl tissue at late time points after infection (21, 28, 35 dpi). Prototypes that include accumulated markers after VL 43 infection are framed in red (252 markers for root, early time points and 570 markers for hypocotyl, late time points). The displayed datasets include combined markers from positive and negative ionisation with a p-value $< 10^{-4}$ (Kruskal-Wallis test). The intensity was normalized and colour-coded by the attached key. The 20 prototypes were scaled to the number of markers contained.

In order to find ubiquitously accumulated or decreased infection markers in *B. napus* plants, the different datasets from root, hypocotyl, stem and leaf tissue were analysed separately for each late infection time point. By this e.g. accumulating markers in roots at 28 dpi were selected. The resulting dataset was adduct corrected and data from negative and positive ionisation mode were combined. Subsequently this set of markers was compared with sets of accumulated markers from the other plant organs at the same time point. By applying certain retention times and mass windows as well as a similarity filter for the intensity pattern it was aimed to cover a metabolite occurring in the different tissues as one infection marker. Therefore the resulting number of markers from this calculation can be regarded as a realistic approximation of the real number of metabolites detected in metabolite fingerprinting. For Fig. 27 the datasets of 28 dpi from the four tissues were combined.

Of a total of 1256 accumulated markers, leaf tissue offered the highest number of specific accumulated infection markers (441) but stem, hypocotyl and root shared more infection markers

(54). Nevertheless 22 markers were increased in all four tissues and can therefore be regarded as markers, which ubiquitously occur in tissues of *V. longisporum* infected *B. napus* plants (Fig. 27 A).

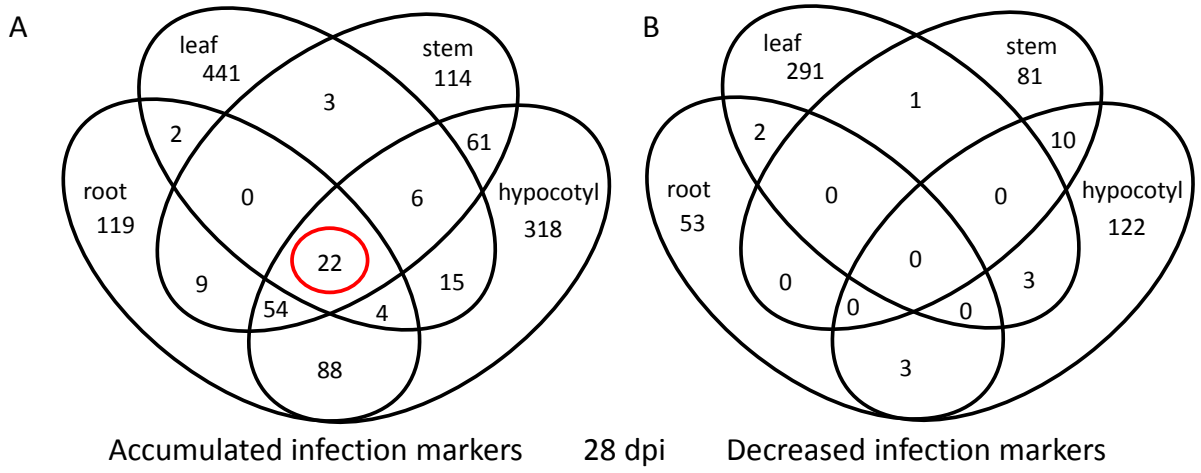

Fig. 27: Tissue specific and ubiquitous infection markers in *B. napus*
(A) Venn-Diagram of infection specific accumulated markers at 28 dpi in four different plant tissues. Overlap of markers was calculated with MarVis Filter as described under 2.2.6.2. The data sets include analysis of three independent experiments, two technical replicates each, two ionization modes and four plant organs. These resulted in total in 1256 accumulated markers. 22 markers (red circle) are ubiquitously accumulated infection markers. (B) Venn-Diagram of infection specific decreased markers at 28 dpi from the same datasets including 566 decreased markers in total.

For decreased markers this analysis led to only 566 markers in total and in an empty intersection for general metabolite changes (Fig. 27 B). The Venn-diagrams for 21 and 35 dpi are very similar to the situation at 28 dpi (Fig. S 2). There 1259 (21 dpi) and 1326 (35 dpi) accumulating markers in total were found including 19 or 21 ubiquitous infection marker, respectively. In contrast 362 (21 dpi) and 718 (35 dpi) marker were decreased with no ubiquitously detected marker.

It can be concluded that the successful infection of *B. napus* plants resulted in a fast and quickly declining metabolic response at early infection time points. Furthermore, a steady change in the metabolic pattern occurred. The determination of the identity of ubiquitously occurring infection markers is described in the following chapter.

3.3.3 Identification of infection markers in *B. napus* plants

3.3.3.1 New phytoalexin related infection markers identified by MS/MS experiments

Within the group of ubiquitously occurring infection markers a subgroup of 10 markers showed common characteristics, like a very similar intensity distribution within the plant organs, a preference for positive ionization and a retention time between 3.2 – 4.2 min. Characteristic was furthermore a pairwise grouping with a distinct mass difference of 86.0004 Da (equals a $C_3H_2O_3$ fragment). The isotopic pattern distribution and the high mass accuracy of less than 4 mDa allowed the generation

of putative molecular formulas for all ten marker. All markers of the subgroup contain two sulphur atoms as a further common feature. Since no conclusive database hit was obtained for any of the substances, fragmentation analysis by MS/MS and pseudo-MS/MS/MS was performed for structural elucidation.

By UPLC-Q-TRAP and UHPLC-Q-TOF analysis of the ten infection markers it was shown that they consist of three or four building blocks, respectively. In total seven fragments were found to be combined differently. The markers could be sorted according to their fragments as depicted in Fig. 28 A. The unambiguous assignment of the sulphur atom to certain fragments was achieved by MS/MS analysis of the molecular ion peak containing one ^{34}S isotope and one ^{32}S instead of two ^{32}S atoms. For this analysis the 1 x ^{34}S isotopomer of the most intensive marker was used ($[M+H]^+$ $C_{24}H_{29}N_4O_{11}{}^{34}S^{32}S$). The fragment information (for experimental data see supplemental section) suggests the incorporation of one sulphur atom in the fragment represented by the blue coloured block ($[C_9H_8NS]^+$ 162.0377 Da) as well as a sulphur-free fragment ($[C_9H_{13}O_8]^+$ 249.0610 Da) corresponding to the brown-green highlighted building block. The second sulphur was assigned to the moiety coloured in purple ($[C_6H_{10}N_3O_3S]^+$ 204.0443 Da). Following the same fragmentation scheme the molecular formulas for the other building blocks were determined as follows: pink ($[C_4H_7N_2O_2S]^+$ 147.0228 Da), wine red ($[C_3H_8NO_2S]^+$ 122.0276 Da), red ($[C_9H_6NOS]^+$ 176.0170 Da) and by neutral loss: brown ($C_6H_{10}O_5$, 162.0528 Da).

In a further step the fragments were analysed by pseudo-MS/MS/MS. In this technique a high voltage during ionization fragments the molecules before they are analysed by MS/MS. Thereby exact masses could be obtained for fragments of the building blocks. Information from this procedure allowed assigning structural formulas to the building blocks. These are depicted in Fig. 28 B and are numbered from (a) to (g). These abbreviations will be used in the following paragraphs. Pseudo-MS/MS/MS fragmentation of the blue highlighted moiety (a) revealed a cleavage of sulphur and a characteristic indole fragment leading to the structure of 3-methylene-1,3-dihydro-2*H*-indol-2-thione. The building block coloured in red (b) differs from (a) by oxidation (+O, -2H). Due to an observed CO and sulphur cleavage in fragmentation the structure of (2-thioxo-1,2-dihydro-3*H*-indole-3ylidene)-methanone was assigned. These fragments were shown to form in the MS/MS fragmentation of tricyclic compounds as known for the phytoalexins cyclobrassinin and cyclobrassinon (Takasugi et al. 1986, Gross et al. 1994). In the fragmentation of the tricyclic compounds, (a) and (b) were associated with the occurrence of methyl cyanates. This led in combination with the obtained fragmentation data of (c) and (d) (e.g. indicating cleavage of a carboxyl group) to the assumption that both fragment consist of thiocyanate building blocks (cyano-cysteinylglycinate (c) and cyano-cysteine (d), respectively). These building blocks might be derived

from the tripeptide glutathione. Although the fragment highlighted in wine red (e) could not be elucidated by pseudo-MS/MS/MS experiments the exact mass and the close relation to (c) and (d) led to the assumption that this third structure was a cysteine moiety.

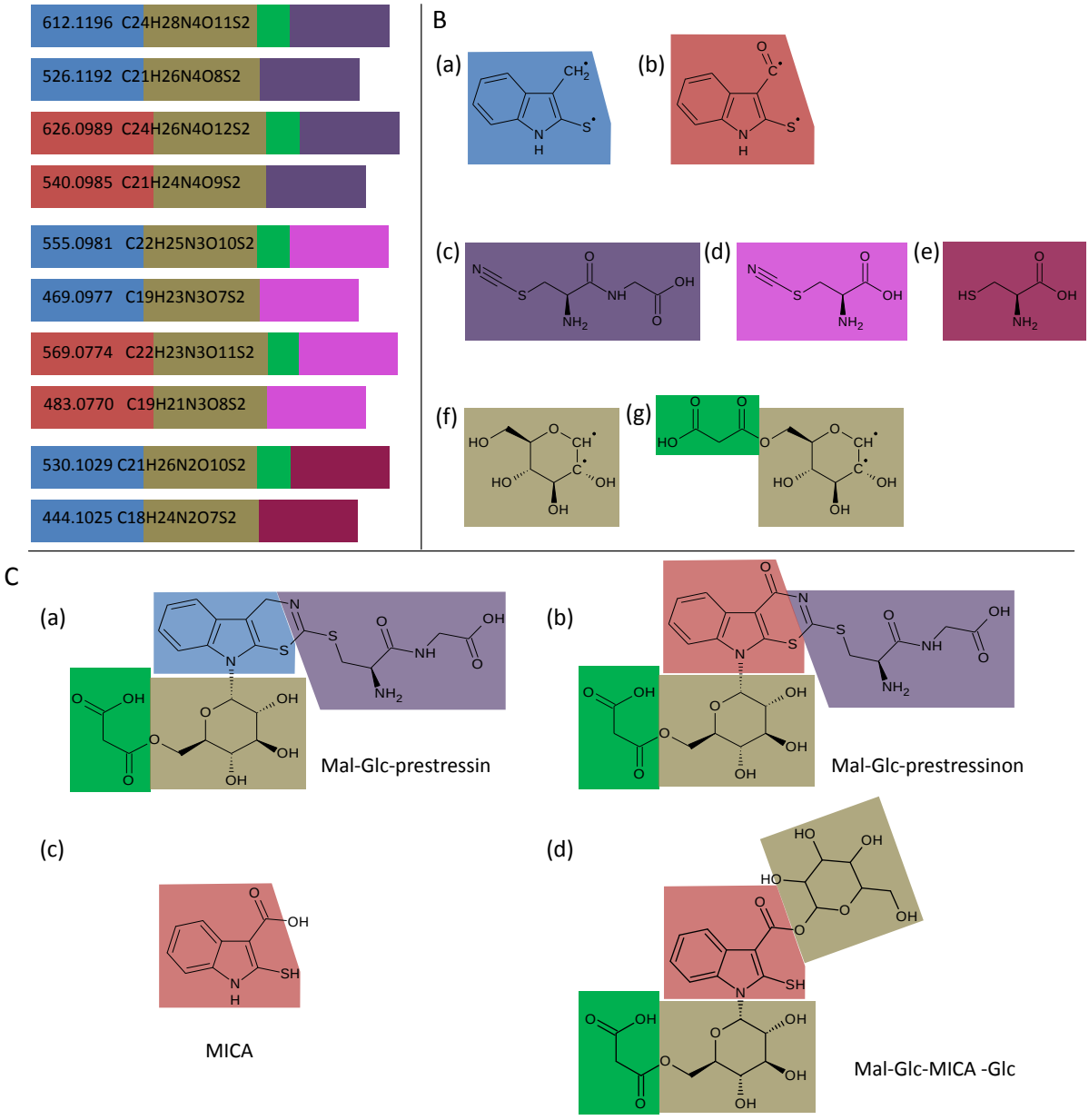

Fig. 28: Structural elucidation of new phytoalexin related infection markers of *B. napus* plants
(A) Combination of building blocks elucidated for a subgroup of ubiquitously accumulating infection markers including the assigned molecular formula and the calculated exact mass. Each coloured rectangle represents a building block. (B) Elucidated structural formulas from pseudo-MS/MS/MS experiments for the building blocks defined in A. (C) Putative structural formulas of (a) [9-(6-O-Malonyl-ß-D-glucopyranosyl)-4,9-dihydro[1,3]thiazino[6,5-b]indol-2-yl]-cysteinylglycine named as Mal-Glc-prestressin, (b) [9-(6-O-Malonyl-ß-D-glucopyranosyl)-4,9-dihydro[1,3]thiazino[6,5-b]indol-2-yl]cysteine named as Mal-Glc-prestressinon, (c) 2-mercapto-1-H-indole-3-carboxylic acid abbreviated as MICA and (d) ß-D-Glucopyranose 1-(6-O-Malonyl-ß-D-glucopyranosyl)-2-mercapto-1H-indole-3-carboxylate named as Mal-Glc-MICA-Glc.

For fragment (f) only the neutral loss was observed but since a corresponding structural element is known to be nearly undetectable in MS analyses this fragment was assigned to be a hexose moiety (-H_2O). The difference of fragment (f) and (g) was determined to correspond to the observed characteristic mass difference of 86.0004 Da. This led to the assumption that malonic acid is attached to the hexose by the loss of a water molecule. The experimental data obtained from fragment (g) supported this hypothesis. Since malonyl moieties are only described to be attached to glucose as a hexose (e.g. Böttcher et al. 2009, Bednarek et al. 2009) it can be assumed that the observed neutral loss derived from a glucose moiety (f) and that the brown-green highlighted building block correspond to malonyl glucose (-H_2O) (g).

From the structural elucidation of the single fragments, useful information about the orientation within the complex molecule was obtained like the fact that the indole core structure (a and b) is likely to form a tricyclic compound with the thiocyanates (c and d). Additionally, a treatment with *ß*-glucosidase did not release the glucose moiety from the molecule suggesting *N*-glycosylation of the indole core. Glycosylation of this position was already described for detoxification of brassinin by *Sclerotinia sclerotinorum* (Sexton et al. 2009). This leads to putative structural formulas for the ten infection markers assembled from the according building blocks. The most complex marker is displayed in Fig. 28 C (a) as well as its oxidized derivative in Fig. 28 C (b). The structural elucidation of fragments and infection markers was significantly supported by Dr. Farina Schill (Department of Plant Biochemistry, Georg-August-University Göttingen, Germany).

In the datasets of the metabolite fingerprinting analysis the non-glycosylated forms were found additionally as infection markers in low abundances. The marker consisting of the core fragment (a) and the pink highlighted fragment (d) was christened stressin due to its accumulation upon biotic stress by fungal infection. The combination of fragment (a) and (c) is supposed to be the stressin precursor in biosynthesis (for details see discussion, Fig. 54) and was therefore named prestressin. Therefore the syllable “pre” represents the glycinyl moiety. The infection marker that includes fragment (a) and (e) was named stressin related (SR) as the fragments indicate a close connection to stressin and prestressin. The glycosylated forms were named analogously with the addition of Glc- (glycosylated derivative) or Mal-Glc (malonylglycosylated derivative) leading to e.g. Mal-Glc-prestressin (Fig. 28 C a). For the oxidized core fragment marked in red (b) only a combination to the fragments (c) and (d) was detected but not an assembly to the cysteine fragment (e). The resulting compounds were named stressinon (b+c) and prestressinon (b+d) but they were only detectable as glycosylated or malonylglycosylated compounds e.g. Mal-Glc-prestressinon (Fig. 28 C b).

This structural elucidation results in a group of 13 infection markers that can be referred to as stressins. The trivial names as well as their chemical names are listed in Tab. 5. All elucidated

structures are depicted in the supplemental data (chapter 7.2). The structural formulas of prestressin, stressin and stressin related are depicted in the supplemental data on page 152.

Tab. 5: Stressins, a group of new markers related to *V. longisporum* infection in *B. napus* plants
The chemical names of the putative structures were assigned additional to the trivial names. The retention time (RT) was determined on the ACQUITY UPLC HSS T3 column.

Exact mass [Da]	RT [min]	Molecular formula	Trivial name	Chemical name
612.1197	3.40	C24H28N4O11S2	Mal-Glc-Prestressin	[9-(6-O-Malonyl-ß-D-glucopyranosyl)-4,9-dihydro[1,3]thiazino[6,5-b]indol-2-yl]-cysteinylglycine
526.1194	3.22	C21H26N4O8S2	Glc-Prestressin	[9-(ß-D-Glucopyranosyl)-4,9-dihydro[1,3]thiazino[6,5-b]indol-2-yl]cysteinylglycine
364.0664	3.40	C15H16N4O3S2	Prestressin	[4,9-dihydro[1,3]thiazino[6,5-b]indol-2-yl]cysteinylglycine
626.0976	4.20	C24H26N4O12S2	Mal-Glc-Prestressinon	[9-(6-O-Malonyl-ß-D-glucopyranosyl)-4-oxo-4,9-dihydro[1,3]thiazino[6,5-b]indol-2-yl]cysteinylglycine
540.0985	4.14	C21H24N4O9S2	Glc-Prestressinon	[9-(ß-D-Glucopyranosyl)-4-oxo-4,9-dihydro[1,3]thiazino[6,5-b]indol-2-yl]cysteinylglycine
555.0983	3.45	C22H25N3O10S2	Mal-Glc-Stressin	[9-(6-O-Malonyl-ß-D-glucopyranosyl)-4,9-dihydro[1,3]thiazino[6,5-b]indol-2-yl]cysteine
469.0979	3.28	C19H23N3O7S2	Glc-Stressin	[9-(ß-D-Glucopyranosyl)-4,9-dihydro[1,3]thiazino[6,5-b]indol-2-yl]cysteine
307.0449	3.48	C13H13N3O2S2	Stressin	[4,9-dihydro[1,3]thiazino[6,5-b]indol-2-yl]cysteine
569.0774	4.04	C22H23N3O11S2	Mal-Glc-Stressinon	[9-(6-O-Malonyl-ß-D-glucopyranosyl)-4-oxo-4,9-dihydro[1,3]thiazino[6,5-b]indol-2-yl]cysteine
483.0772	3.99	C19H21N3O8S2	Glc-Stressinon	[9-(ß-D-Glucopyranosyl)-4-oxo-4,9-dihydro[1,3]thiazino[6,5-b]indol-2-yl]cysteine
530.1030	3.60	C21H26N2O10S2	Mal-Glc-Stressin related	3-{[1-(6-O-Malonyl-ß-D-glucopyranosyl)-3-methyl-1H-indol-2-yl]dithio}alanine or S-{[1-(6-O-Malonyl-ß-D-glucopyranosyl)-2-mercapto-1H-indol-3-yl]methyl}cysteine
444.1026	3.20	C18H24N2O7S2	Glc-Stressin related	3-{[1-(ß-D-Glucopyranosyl)-3-methyl-1H-indol-2-yl]dithio}alanine or S-{[1-(ß-D-glucopyranosyl)-2-mercapto-1H-indol-3-yl]methyl}cysteine
282.0497	3.75	C12H14N2O2S2	Stressin related	3-methyl-1H-indol-2-yl]dithio}alanine or 2-mercapto-1H-indol-3-yl]methyl}cysteine

Among the 13 compounds the malonylglycosylated forms are the most intensive derivatives. As an example the intensity distribution of Mal-Glc-prestressin during the infection time course in several tissues and the apoplastic fluids is displayed in Fig. 22. Mal-Glc-prestressin is already significantly accumulated at 5 dpi in roots and shoots. At later time points (from 21 dpi on) Mal-Glc-prestressin is ubiquitously distributed in the whole plant including the apoplastic space. The highest intensities can be detected in the hypocotyl. This corresponds with the levels of fungal DNA being highest in this organ (Fig. 18) and underlines a local correlation of fungal infestation and high levels of stressins. In control samples very low basal levels of stressins (< 200 cps) were detected.

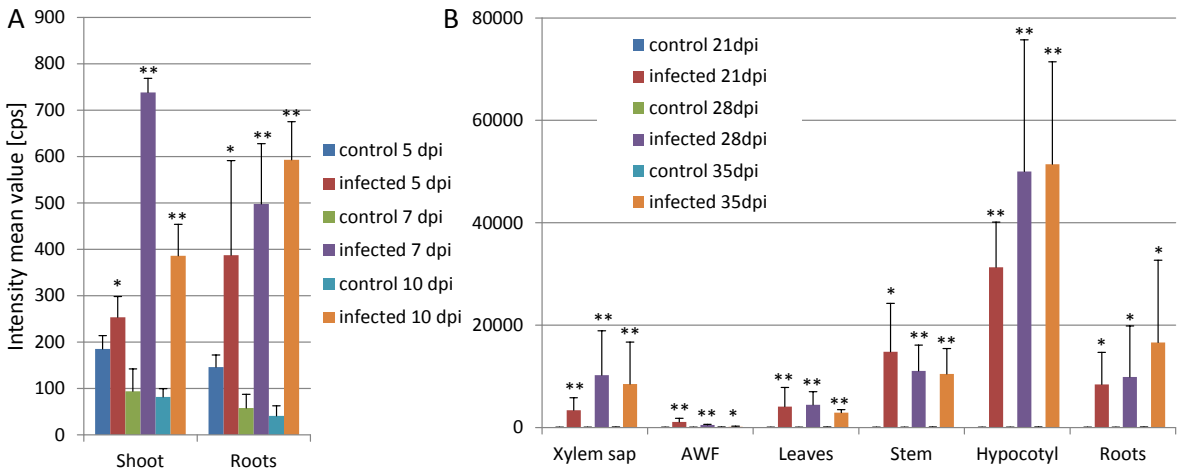

Fig. 29: Time course and tissue specific distribution of Mal-Glc-Prestressin in *B. napus* plants
Accumulation of Mal-Glc-Prestressin in (A) roots and shoots at early time points of infection and (B) apoplastic fluids and plant tissues at late infection time points. Data were determined from two technical replicates of two (early time points) or three (late time points) biological replicates. Asterisks indicate intensity values with significant differences compared to the corresponding control in an unpaired Students t-test (* = p-value < 0.05; ** = p-value < 0.001). Error bars represent the standard deviation.

The intensities for the oxidized derivatives Mal-Glc-stressinon and Mal-Glc-prestressinon are displayed in Fig. 30. The stressins accumulate very reproducibly in infected plants and give a good indication about the strength and progress of the infection process.

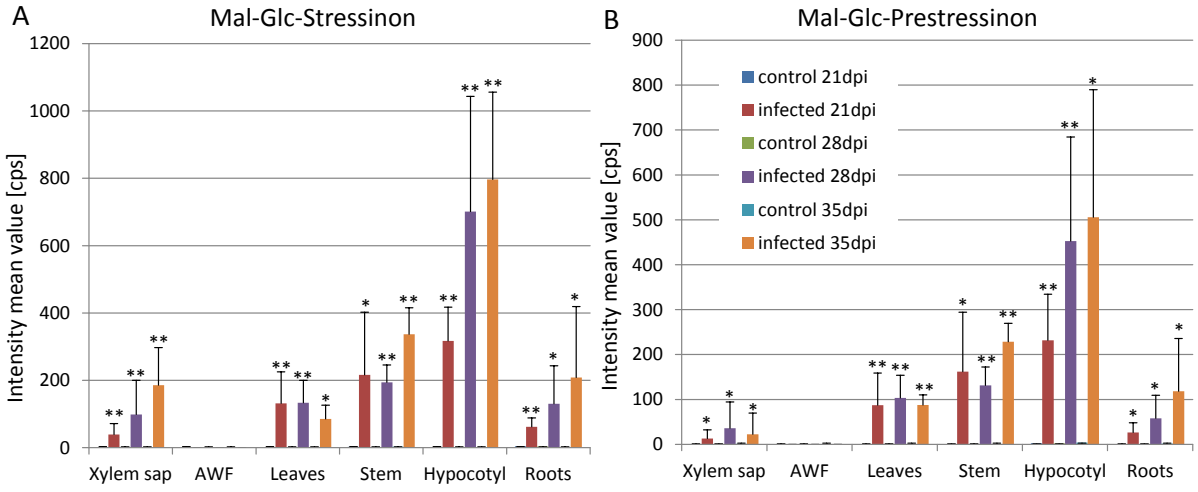

Fig. 30: Time course and tissue specific distribution of Mal-Glc-stressinon and Mal-Glc-prestressinon in *B. napus* plants
Accumulation of (A) Mal-Glc-stressinon and (B) Mal-Glc-prestressinon in apoplastic fluids and plant tissues at late infection time points. Data were determined from two technical replicates of three biological replicates. Asterisks indicate intensity values with significant differences compared to the corresponding control in an unpaired Students t-test (* = p-value < 0.05; ** = p-value < 0.001). Error bars represent the standard deviation.

A second group of seven infection markers was detected, that is strongly related to the stressins. They eluted at a retention time from 3.41 to 4.41 min and ionize better or exclusively in negative

ionisation mode. They contain two to four building blocks. In four of the markers the red highlighted core fragment (b, Fig. 28 B) was detected in MS/MS experiments. Since this oxidized core structure was found in combination with the cleavage of a carboxyl group the common motive was identified as 2-mercapto-indole-3-carboxylic acid (MICA, Fig. 28 C c). Therefore this second group of infection markers was named MICAs. The occurrence of glycosylated and malonylglycosylated derivatives is analogue to the stressins. The non-glycosylated forms are MICA and its decarboxylated derivative (decarboxy-MICA) which were detectable in low amounts comparable to the non-glycosylated stressins. Additionally, Glc-MICA-Glc and Mal-Glc-MICA-Glc (Fig. 28 C d) include a second glycosylation which is probably attached via an *O*-glycosidic bond to the carboxyl group since it was cleaved of by *ß*-glucosidase treatment. Combination of the obtained information from structural elucidation led to the assignment of putative structural formulas for the seven infection markers. All detected MICAs are summarized in Tab. 6 whereas the assigned structures are depicted in the supplemental data (chapter 7.2). The putative relation between stressins, MICAs and phytoalexins is described in the discussion.

Tab. 6: MICAs, a group of new markers related to *V. longisporum* infection in *B. napus* plants
The chemical names of the putative structures were assigned additional to the trivial names. The retention time (RT) was determined on the ACQUITY UPLC HSS T3 column.

Exact mass [Da]	RT [min]	Molecular formula	Trivial name	Chemical name
441.0730	4.10	C18H19NO10S	Mal-Glc-MICA	1-(6-O-Malonyl-ß-D-glucopyranosyl)-2-mercapto-1H-indole-3-carboxylic acid
355.0741	3.75	C16H13N5O3S	Glc-MICA	1-(ß-D-Glucopyranosyl)-2-mercapto-1H-indole-3-carboxylic acid
193.0198	4.12	C9H7NO2S	MICA	2-mercapto-1H-indole-3-carboxylic acid
603.1250	3.41	C24H29NO15S	Mal-Glc-MICA-Glc	ß-D-Glucopyranose 1-(6-O-Malonyl-ß-D-glucopyranosyl)-2-mercapto-1H-indole-3-carboxylate
517.1254	3.11	C21H27NO12S	Glc-MICA-Glc	ß-D-Glucopyranose 1-(ß-D-glucopyranosyl)-2-mercapto-1H-indole-3-carboxylate
397.0732	4.41	C17H19NO8S	Decarboxy-Mal-Glc-MICA	Decarboxylated 1-(6-O-Malonyl-ß-D-glucopyranosyl)-2-mercapto-1H-indole-3-carboxylic acid
149.0299	4.41	C8H7NS	Decarboxy-MICA	1H-indole-2-thiol

The distribution of the MICAs differs slightly from that of the stressins. They were not detected in roots and shoots of *B. napus* in significant amounts at early time points after infection with *V. longisporum*. The highest intensities at later time points (21, 28 and 35 dpi) were found in root tissue. The intensities for Mal-Glc-MICA and Mal-Glc-MICA-Glc are displayed in Fig. 31. In above ground tissue the amount of MICAs was less pronounced. These results indicate that the group of MICAs may accumulate in a later stage of infection than the stressins.

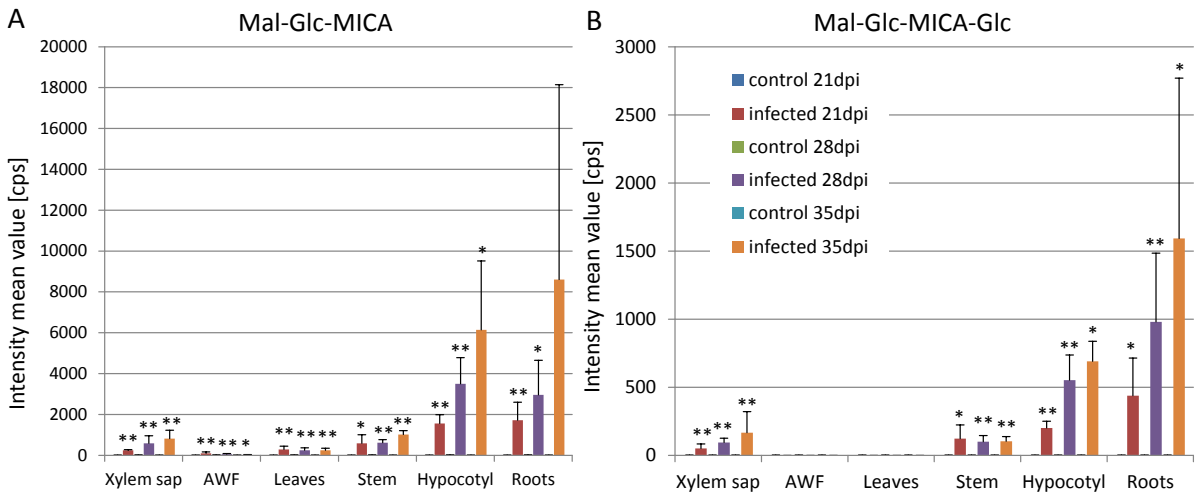

Fig. 31: Time course and tissue specific distribution of two representative 2-mercapto-indole-3-carboxylic acid derivatives (MICAs) in *B. napus* plants
Accumulation of (A) Mal-Glc-MICA and (B) Mal-Glc-MICA-Glc in apoplastic fluids and plant tissues at late infection time points. Data were determined from two technical replicates of three biological replicates. Asterisks indicate intensity values with significant differences compared to the corresponding control in an unpaired Students t-test (* = p-value < 0.05; ** = p-value < 0.001). Error bars represent the standard deviation.

It can be concluded that 20 compounds were structurally elucidated by fragmentation analysis that have not been described for *B. napus* before. They are classified as stressins (13 compounds) and MICAs (7 compounds). Both groups are structurally related and were detected in *B. napus* but not in *A. thaliana* or *C. sativa* after infection with *V. longisporum*.

3.3.3.2 Phytoalexins

The core structure of the newly described infection markers strongly resembled the structure of cyclobrassinin, a well characterized indole-derived phytoalexin in *B. napus* (Fig. 23 A) (reviewed in Pedras and Yaya 2010). Cyclobrassinin itself ($[M+H]^+$ 235.0364, $C_{11}H_{11}N_2S_2$, retention time 6.33 min) was extracted within the non-polar phase and shows an infection related intensity pattern. The comparison with the MS/MS fragmentation pattern of the authentic standard provided by Prof. Kutschy (J.P. Safárik University, Košice, Slovak Republic) confirmed the identification of cyclobrassinin as infection marker. The fragmentation pattern of the phytoalexin showed high similarities to the stressins and MICAs and indicates therefore a close relation of the new infection markers to cyclobrassinin. The MS data of cyclobrassinin fragmentation is summarised in the supplemental data (chapter 7.2, page 141)

In addition to cyclobrassinin a second infection marker ($[M+H]^+$ 249.0156, $C_{11}H_9N_2OS_2$, retention time 4.84 min) was extracted in the non-polar extraction phase (Fig. 32 A). MS/MS fragmentation analysis showed the same characteristic fragment as was found for the oxidized core structure of the stressins (b, $[C_9H_6NOS]^+$, 176.0170 Da). Until now the described oxidized forms of cyclobrassinin are

cyclobrassinin sulfoxide (Devys et al. 1990), cyclobrassinon (Gross et al. 1994) and rutalexin (Pedras et al. 2004) which could be excluded to be the detected infection marker by their molecular weight. The obtained fragmentation data clearly hinted to a new, undescribed derivative of cyclobrassinin as depicted in Fig. 32 B. It was named cyclobrassininon. The obtained MS/MS data can be found on page 141 in the supplemental data. If it possesses antifungal activity like cyclobrassinin (described e.g. for *Botrytis cinerea* by Pedras et al. 2011b) and can therefore be regarded as a phytoalexin still has to be elucidated.

The accumulation of cyclobrassinin started already at early time points during fungal infection with a significant increase in roots from 5 dpi and in shoot tissue from 7 dpi on (data not shown). The highest intensities of cyclobrassinin and cyclobrassininon were detected in the hypocotyl at late time points (Fig. 32 C + D), as it was found for the stressins. Cyclobrassininon was detected in lower amounts in infected plant tissues than cyclobrassinin. That might explain why it was not discovered until now. It is probably below detection limits in stem and leaf tissue as well as in samples at early time points. Cyclobrassinin and cyclobrassininon were not detected in the extracted apoplastic fluids. The open ring analogue of cyclobrassinin known as brassinin was not found in metabolite fingerprinting of *V. longisporum* infected *B. napus* plants.

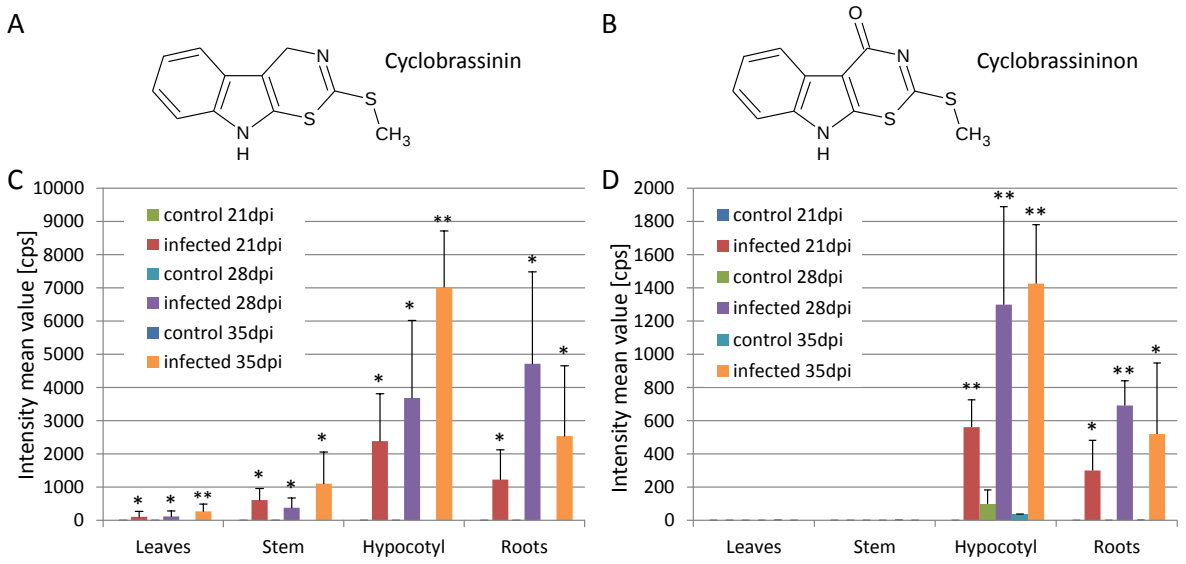

Fig. 32: Time course and tissue specific distribution of the phytoalexin cyclobrassinin and of cyclobrassininon in *B. napus* plants

Structural formulas of (A) the phytoalexin cyclobrassinin and (B) its derivative 2-methylthio-1,3-thiazino-5,6-indol-4-one named as cyclobrassininon. Accumulation of (C) cyclobrassinin and (D) cyclobrassininon in plant tissues at late infection time points. Data were determined from three technical replicates of three biological replicates. Asterisks indicate intensity values with significant differences compared to the corresponding control in an unpaired Students t-test (* = p-value < 0.05; ** = p-value < 0.001). Error bars represent the standard deviation.

It can be concluded that the biotic stress, triggered by the *V. longisporum* infection led to the accumulation of the phytoalexin cyclobrassinin and a closely related, newly discovered oxidized form

named cyclobrassininon. They show the highest intensities in fungal invaded tissues like the hypocotyl and are structurally related to the groups of newly described infection markers, stressins and MICAs. Those therefore can be regarded as phytoalexin related substances.

Phytoalexins are mostly species specific and therefore it was not surprising that neither cyclobrassinin nor any of the newly described metabolites was detected in the closely related species *A. thaliana* and *C. sativa* after infection with *V. longisporum* (data not shown).

3.3.3.3 Raphanusamic acid

A strong infection correlated marker ($[M+H]^+$ 163.9840, $C_4H_6NO_2S_2$, retention time 1.50 min) was extracted in the polar extraction phase from apoplastic fluids and tissues. Database searches provided a hit for 2-thioxothiazolidine-4-carboxylic acid (raphanusamic acid, RA), a metabolite so far described for *A. thaliana* by Bednarek et al. (2005). The identity of RA was confirmed by coelution with the authentic standard. The structural formula is displayed in Fig. S 8. RA was detected to accumulate in all organs and apoplastic fluids of *B. napus* plants (Fig. 33).

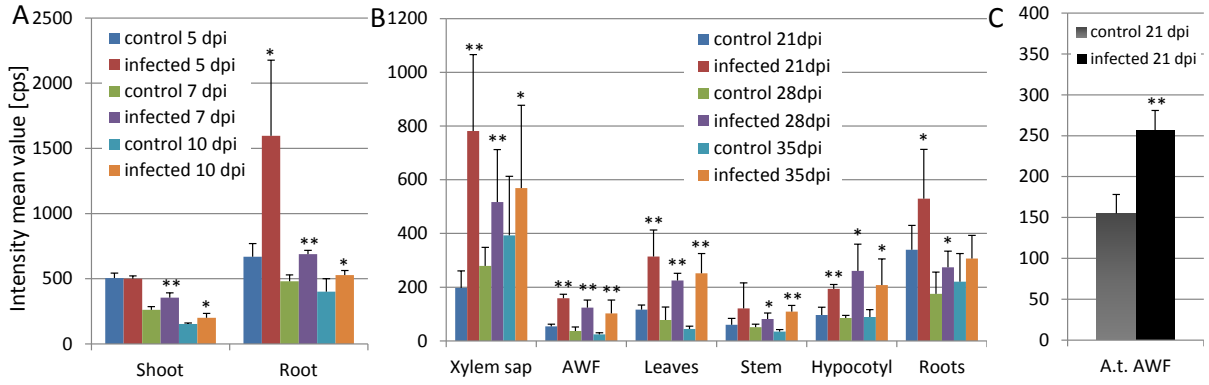

Fig. 33: Time course and tissue specific distribution of raphanusamic acid (RA) in *B. napus* and *A. thaliana* plants

Accumulation of RA in (A) roots and shoots at early time points of infection, in (B) apoplastic fluids and plant tissues at late infection time points in *B. napus* and in (C) AWF of *A. thaliana* at 21 dpi. Data were determined from two technical replicates of two (early time points B.n.) or three (late time points B.n. and A.t.) biological replicates. Asterisks indicate intensity values with significant differences compared to the corresponding control in an unpaired Students t-test (* = p-value < 0.05; ** = p-value < 0.001). Error bars represent the standard deviation.

The metabolite was detected in increased amounts in roots from 5 dpi in shoots from 7 dpi on and is therefore an early infection marker (Fig. 33 A). At later time points of the infection process a significant increase in intensity was measurable in all samples displaying the highest amounts in the xylem sap (Fig. 33 B). This suggests RA to be a mobile signal within the plant. RA was not only found in *B. napus* but also in *A. thaliana* where it was already described to occur in roots of pathogen challenged plants by Bednarek et al. (2005). In the metabolite fingerprinting analysis of AWF of *V. longisporum* infected *A. thaliana* plants a significant increase of RA was detected (Fig. 33 C). This

suggests a more general role for RA in the infection processes of Brassicaceae than for the phytoalexin related metabolites.

3.3.3.4 Salicylic acids and derivatives

Formation of salicylic acid (SA) and salicylic acid glucoside (SAG) has been described to be induced upon infection of *B. napus* with *V. longisporum* (Ratzinger et al. 2009). It was therefore a proof of concept that SA ($[M-H]^-$ 137.0236, $C_7H_5O_3$, retention time 4.17 min) and SAG ($[M-H]^-$ 299.0768, $C_{13}H_{15}O_8$, retention time 2.70 min) were detected as accumulated markers of infected *B. napus* plants. Their identity was confirmed by retention time comparison with authentic standards. When SAG was fragmented in an MS/MS experiment it dissociated to a mass matching SA. The corresponding glucose moiety was not detected (data not shown).

Two additional infection markers with an identical exact mass were detected in *B. napus* plants ($[M-H]^-$ 315.0716, $C_{13}H_{15}O_9$, retention time 2.15 min and 2.32 min, respectively). When tissue extracts were treated with *ß*-glucosidase, the markers vanished and led to new corresponding masses ($[M-H]^-$ 153.0188 , $C_7H_5O_4$, retention time 2.66 min and 2.98 min, respectively). These masses were assigned to be dihydroxybenzoic acids (DHBA). The deglycosylated compounds were confirmed to be 2,5-DHBA (retention time 2.66 min) and 2,3-DHBA (retention time 2.98 min) by comparison to the authentic standards. Since both substances were not detected in *ß*-glucosidase untreated infected plant tissue, the infection markers must be the glycosylated form of dihydroxybenzoic acids (DHBAG). It is assumed that 2,5-DHBAG corresponds to the marker with the early retention time of 2.15 min and 2,3-DHBAG elutes at 2.32 min. Additionally, MS/MS experiments were performed with 2,5-DHBAG (Fig. S 3). The structural formulas for SA and its derivatives are displayed in Fig. S 8.

Accumulation of SA was detected in high amounts in the xylem sap at late infection time points whereas only minor amounts accumulate upon *V. longisporum* in the AWF and in plant tissue of *B. napus* (Fig. 34 A). SAG in contrast was a strongly accumulating infection marker in xylem sap, AWF, stem, hypocotyl and roots. Interestingly, all SA related markers displayed in leaf tissue intensities below 100 cps and can therefore not be regarded as infection markers in this plant organ. In the upper plant tissue (stem and hypocotyl) 2,5-DHBAG was the most intensive marker (Fig. 34 C) where 2,3-DHBAG only occurs in minor amounts but it displayed a high intensity in belowground tissue (roots) (Fig. 34 D). 2,5-DHBAG was the only infection marker of the SA related marker group, which was detectable in tissue of control plants.

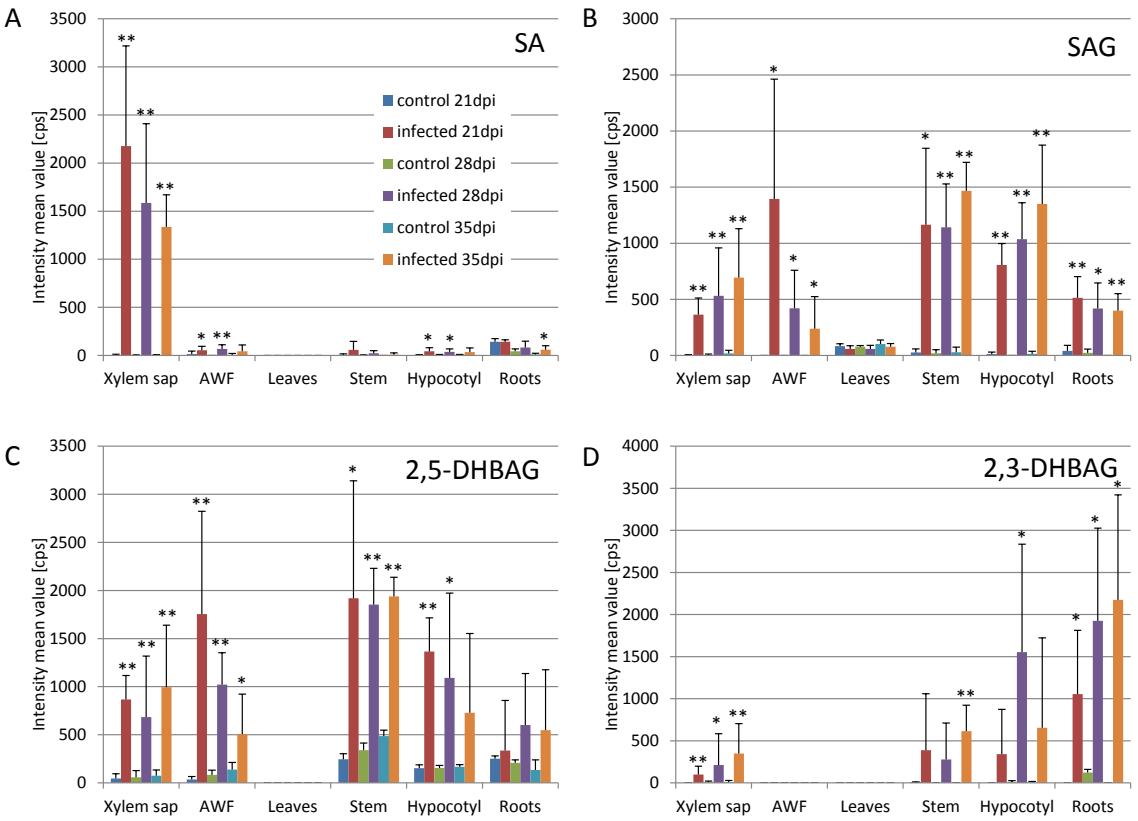

Fig. 34: Time course and tissue specific distribution of salicylic acid (SA) and salicylic acid derivatives in *B. napus* plants (late time points)

Accumulation of (A) salicylic acid (SA), (B) salicylic acid glucoside (SAG), (C) 2,5-dihydroxybenzoic acid glucoside (2,5-DHBAG) and (D) 2,3-dihydroxybenzoic acid glucoside (2,3-DHBAG) in apoplastic fluids and plant tissues at late infection time points. Data were determined from two technical replicates of three biological replicates. Asterisks indicate intensity values with significant differences compared to the corresponding control in an unpaired Students t-test (* = p-value < 0.05; ** = p-value < 0.001). Error bars represent the standard deviation.

SA was not accumulating in roots and shoots shortly after infection (5, 7 and 10 dpi) (Fig. 35 A). Interestingly, SA levels in roots were generally higher than the amounts detected in shoot extracts. In contrast the SAG content increased already at 5 dpi in root tissue and at 7 dpi in aboveground plant organs (Fig. 35 B).

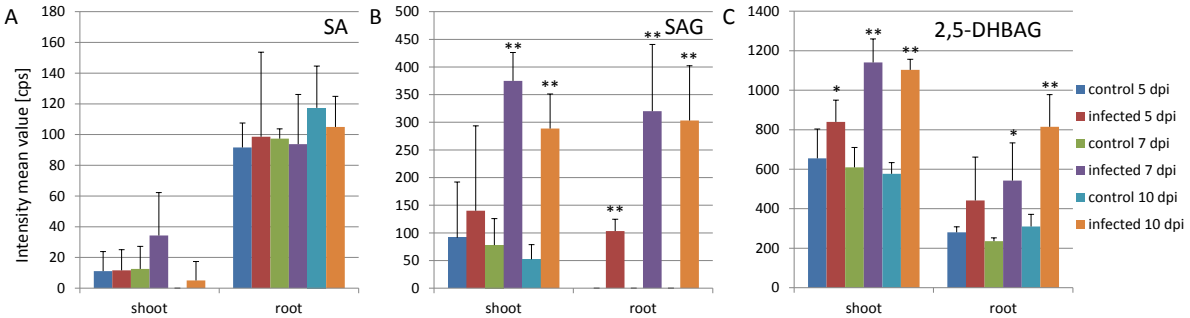

Fig. 35: Time course and tissue specific distribution of salicylic acid (SA) and salicylic acid derivatives in *B. napus* plants (early time points)

Accumulation of (A) salicylic acid (SA), (B) salicylic acid glucoside (SAG) and (C) 2,5-dihydroxybenzoic acid glucoside (2,5-DHBAG) in roots and shoots at early time points of infection. Data were determined from two technical replicates of two biological replicates. Asterisks indicate intensity values with significant differences compared to the corresponding control in an unpaired Students t-test (* = p-value < 0.05; ** = p-value < 0.001). Error bars represent the standard deviation.

Also the amount of 2,5-DHBAG accumulated significantly in shoots from 5 dpi on and from 7 dpi on in roots (Fig. 35 C) whereas the levels of 2,3-DHBAG are only significantly increased in roots from 10 dpi on (data not shown).

Due to the finding, that not only glycosylation but also malonylglycosylation occurs in the phytoalexin related metabolites, the datasets were searched for putative malonyl derivatives of SAG and DHBAG. No conclusive results were obtained since for putative candidates the intensities were too low for fragmentation analysis and/or the detected retention times were contradictory. Therefore the question if malonylglycosylation is a common feature in the response to fungal invasion still remains to be elucidated. Bartsch et al. (2010) found 2,3-DHBA 3-*O-ß*-xyloside to accumulate in *A. thaliana* in response to pathogens and in aging leaves, but this metabolite was not detected in *B. napus* tissue. Furthermore the non-glycosylated dihydroxybenzoic acids 2,5-DHBA (gentisic acid) and 2,3-DHBA were not detected in any analysed sample.

The results from *B. napus* were compared to AWF of *A. thaliana* at 21 dpi. SA was detected in low amounts with an unchanged level after *V. longisporum* infection but SAG was a strong and reliable infection marker for both Brassicaceae (Fig. 36). 2,5-DHBAG and 2,3-DHBAG are infection markers in *A. thaliana* as well. While 2,5-DHBAG seems to play only a minor role in *A. thaliana* compared to the high levels detected in the AWF of *B. napus,* 2,3-DHBAG is measurable in larger amounts in the AWF of *A. thaliana* than of *B. napus*.

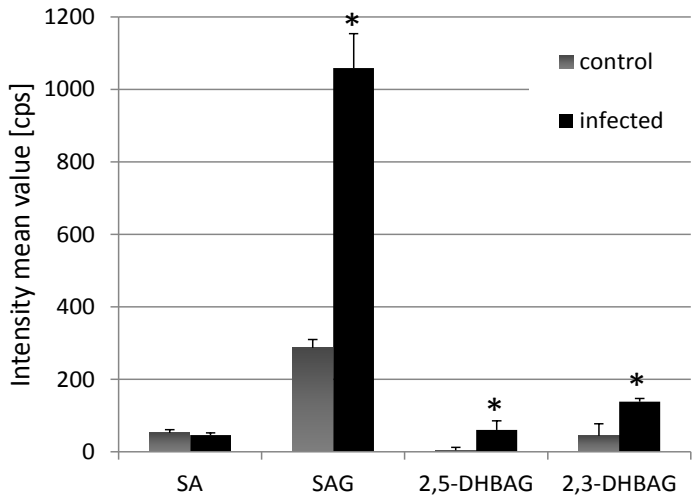

Fig. 36: Intensity of salicylic acid (SA) and its derivatives in AWF of infected *A. thaliana* plants
Accumulation of SA and SA derivatives (SAG, 2,5-DHBAG and 2,3-DHBAG) in AWF of mock treated and infected *A. thaliana* plants 21 dpi. Data were determined from two technical replicates of three biological replicates. Asterisks indicate intensity values with significant differences compared to the corresponding control in an unpaired Students t-test (* = p-value < 0.05; ** = p-value < 0.001). Error bars represent the standard deviation.

It can be concluded that SA accumulated only in the xylem sap of *B. napus* whereas SAG, 2,5-DHBAG and 2,3-DHBAG were detected in increased amounts upon *V. longisporum* infection in both *B. napus* and *A. thaliana* (Fig. 34, 35, 36). This indicates a common mechanism for their involvement in the pathogen response.

3.3.3.5 Pipecolic acid

A single infection marker ($[M+H]^+$ 130.0868, $C_6H_{12}NO_2$, retention time 0.61 min) was detected in the analysis of the polar extraction phase. The identity of pipecolic acid was confirmed by coelution with the authentic standard and MS/MS fragmentation experiments (Fig. S 4). The structural formula is displayed in Fig. S 8.

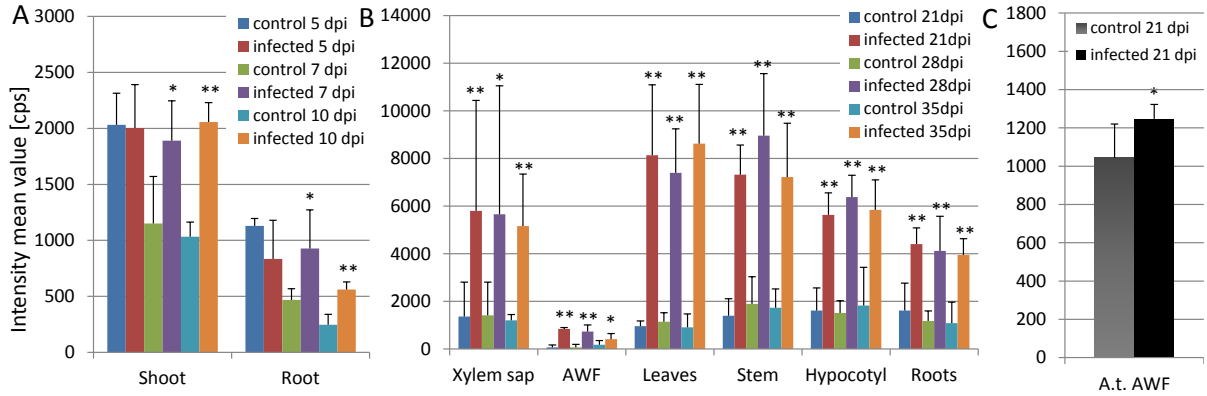

Fig. 37: Time course and tissue specific distribution of pipecolic acid in *B. napus* and *A. thaliana*
Accumulation of pipecolic acid in (A) roots and shoots at early time points of infection, (B) apoplastic fluids and plant tissues at late infection time points in *B. napus* and (C) AWF of *A. thaliana* at 21 dpi. Data were determined from two technical replicates of two (early time points B.n.) or three (late time points B.n. and A.t.) biological replicates. Asterisks indicate intensity values with significant differences compared to the corresponding control in an unpaired Students t-test (* = p-value < 0.05; ** = p-value < 0.001). Error bars represent the standard deviation.

Pipecolic acid was present in all analysed samples from *B. napus* and was significantly accumulated already from 7 dpi on in aboveground and belowground tissue (Fig. 37 A). At late time points pipecolic acid was measured ubiquitously in significantly increased amounts (Fig. 37 B). In the AWF of *A. thaliana* pipecolic acid was found to significantly accumulate as well (Fig. 37 C). This suggests a role for pipecolic acid in the biotic stress of both Brassicaceae species.

3.3.3.6 Oxylipins

Two closely related infection markers were found to accumulate specifically in the apoplastic fluids. The first marker ($[M-H]^-$ 327.2173 , $C_{18}H_{31}O_5$, retention time 5.05 min) differs from the second ($[M-H]^-$ 329.2327 , $C_{18}H_{33}O_5$, retention time 5.23 min) by the characteristic mass difference of 2.0157 Da being consistent to two hydrogen atoms. A database search by MarVis provided hits for trihydroxy-octadecenoic acid and trihydroxy-octadecadienoic acid. The compounds differ in one double bond, explaining the mass difference of 2.0157 Da and the corresponding retention time shift. Both compounds form a large number of adducts which could be attributed to these masses (Fig. 13). The position of the hydroxyl groups and the double bonds in the trihydroxy fatty acids were unequivocally attributed by MS/MS experiments. The first marker ($C_{18}H_{32}O_5$) was identified as

9,12,13-trihydroxy-10,15-octadecadienoic acid (TriHOD), the second marker ($C_{18}H_{34}O_5$) as 9,12,13-trihydroxy-10-octadecenoic acid (TriHOE) (Fig. S 5). The structural formulas are displayed in Fig. S 8.

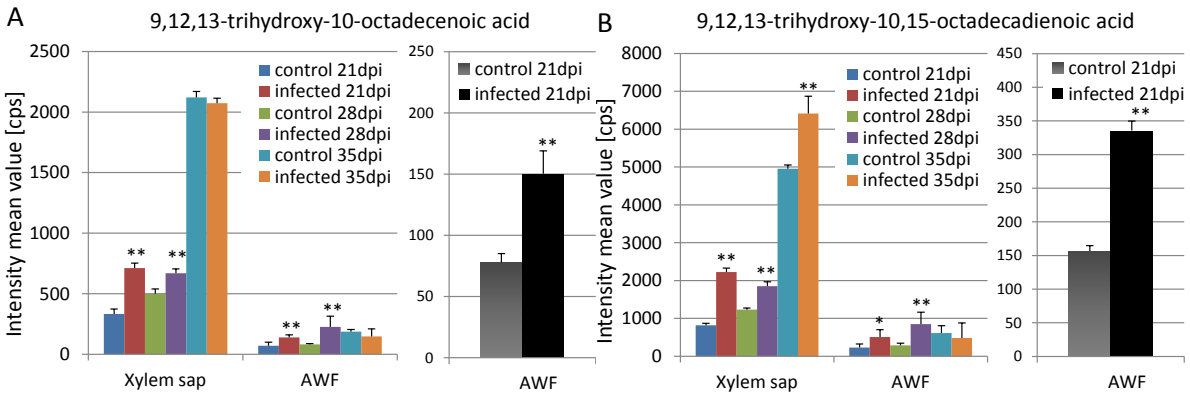

Fig. 38: Time course and specific distribution of oxylipins in apoplastic fluids of *B. napus* and *A. thaliana*
Accumulation of (A) 9,12,13-trihydroxy-10-octadecenoic acid (TriHOE) and (B) 9,12,13-trihydroxy-10,15-octadecadienoic acid (TriHOD) in apoplastic fluids at late infection time points in *B. napus* (left-hand side) and *A. thaliana* (right-hand side). Data were determined from three technical replicates of one representative experiment (xylem sap B.n.) or three biological replicates (AWF B.n. and A.t.). Asterisks indicate intensity values with significant differences compared to the corresponding control in an unpaired Students t-test (* = p-value < 0.05; ** = p-value < 0.001). Error bars represent the standard deviation.

Both trihydroxy fatty acids accumulate significantly in AWF and xylem sap of *B. napus* 21 and 28 dpi (Fig. 38 A + B, left panels). This increase is not significant anymore at the latest infection time point (35 dpi) since the detected amount in the control increases as well. In general a much higher intensity was measured in the xylem sap than in AWF. In the analysed tissues from *B. napus* the oxylipins could not be detected in substantial amounts at any time point. The levels of the oxylipins in early infection phases remain to be elucidated since no neither AWF nor xylem sap was obtained at early infection time points. A significant increase of both oxylipins was detected in the AWF of *A. thaliana* as well (Fig. 38 A + B, right panels).

3.3.3.7 Apoplastic wash fluid (AWF) specific marker groups in *B. napus* and *A. thaliana* plants

In the AWF of *B. napus* several marker groups were detected that accumulate only in AWF upon *V. longisporum* infection. They were visible as groups in a retention time / m/z plane (scatter plot) generated from the metabolite fingerprinting data in MarVis. Five groups of markers displayed characteristic mass differences of 14.0157 Da. In combination with a distinct retention time shift it indicated a substance class with a growing carbon chain ($+CH_2$) (Fig. 39).

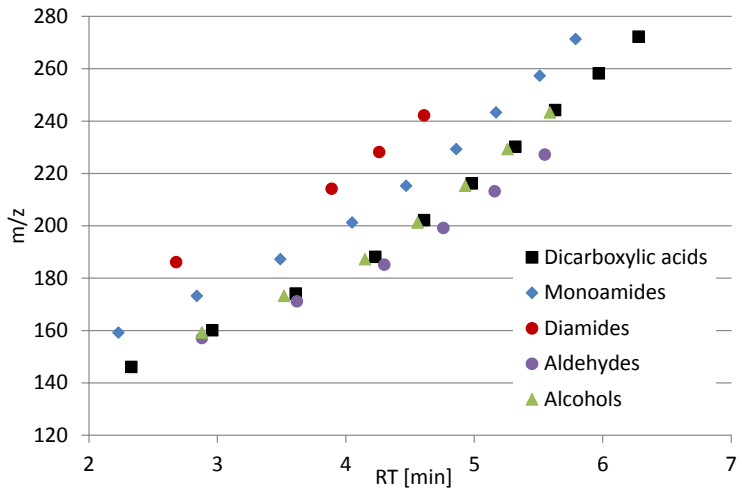

Fig. 39: Scatter plot of AWF infection markers in *B. napus* plants
AWF specific markers measured in metabolite fingerprinting displayed in a retention time / m/z plane.

3.3.3.7.1 Dicarboxylic acids

The compounds of one of the five marker groups could be assigned by database search as saturated dicarboxylic acids (Tab. 7). Their identity was confirmed by retention time comparison to the authentic standards. Azelaic acid ($[M+H]^+$ 189.1127, $C_9H_{17}O_4$, retention time 4.23 min) was additionally verified by MS/MS experiments (data not shown). The carbon chain length of the infection markers varied in *B. napus* from C6 to C15, in *A. thaliana* from C6 to C13. The structural formula for the dicarboxylic acids is displayed in Fig. S 8.

Tab. 7: Saturated dicarboxylic acids found as infection markers
The retention time (RT) was determined on the ACQUITY UPLC HSS T3 column running with the polar gradient.

Exact mass [Da]	RT [min]	Molecular formula	Name	Plant
146.0576	2.33	C6H10O4	Hexanedioic acid (Adipic acid)	*B. napus, A. thaliana*
160.0732	2.96	C7H12O4	Heptanedioic acid (Pimelic acid)	*B. napus, A. thaliana*
174.0888	3.61	C8H14O4	Octanedioic acid (Suberic acid)	*B. napus, A. thaliana*
188.1044	4.23	C9H16O4	Nonanedioic acid (Azelaic acid)	*B. napus, A. thaliana*
202.1200	4.61	C10H18O4	Decanedioic acid (Sebacic acid)	*B. napus, A. thaliana*
216.1356	4.98	C11H20O4	Undecanedioic acid	*B. napus, A. thaliana*
230.1512	5.32	C12H22O4	Dodecanedioic acid	*B. napus, A. thaliana*
244.1668	5.63	C13H24O4	Tridecanedioic acid	*B. napus, A. thaliana*
258.1824	5.97	C14H26O4	Tetradecanedioic acid	*B. napus*
272.1980	6.28	C15H28O4	Pentadecanedioic acid	*B. napus*

In *A. thaliana* as well as in *B. napus* a significant increase upon fungal infection for e.g. azelaic acid was measured in the AWF. In contrast, only low levels and no infection related accumulation was found for xylem sap and leaf tissue (Fig. 40). All identified dicarboxylic acids displayed a similar intensity distribution with C8 (suberic acid) and C9 (azelaic acid) being the most intensive ones. It can

be concluded that the increase of these markers is specific for the apoplastic space of infected leaves.

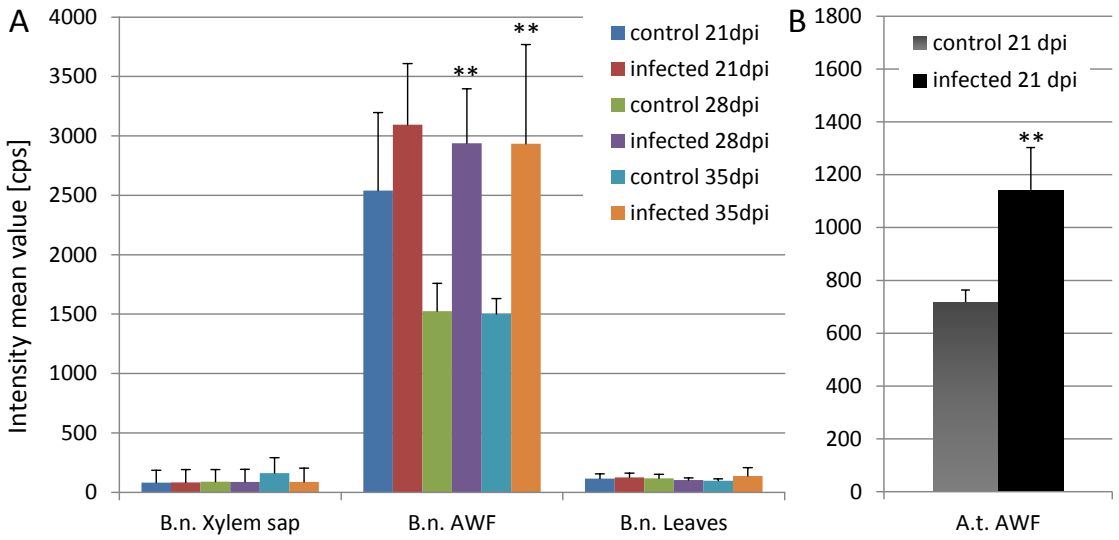

Fig. 40: Time course and tissue specific distribution of azelaic acid in *B. napus* and *A. thaliana* plants
Accumulation of azelaic acid in (A) AWF, xylem sap and leaf tissues at late infection time points in *B. napus* and (B) AWF of *A. thaliana* at 21 dpi. Data were determined from two technical replicates of three biological replicates. Asterisks indicate intensity values with significant differences compared to the corresponding control in an unpaired Students t-test (* = p-value < 0.05; ** = p-value < 0.001). Error bars represent the standard deviation.

Due to a high background level in all control samples it can be assumed that the dicarboxylic acids occur commonly in Brassicaceae. Azelaic acid was already described to occur in various plant families like Solanaceae, Convolvulaceae and Lamianceae (Sato et al. 2011).

3.3.3.7.2 Derivatives of dicarboxylic acids

Four other groups of AWF specific infection markers with the same characteristic mass difference could not be identified via database hits. Their molecular formulas were assigned by using the isotopic pattern information and their relation to the dicarboxylic acids. The marker groups can be described by molecular formulas as group I: $CH\text{-}(CH_2)_nNO_3$; group II: $(CH_2)_nN_2O_2$; group III: $CH\text{-}(CH_2)_nNO_2$ and group IV: $(CH_2)_nHNO_2$. Like the dicarboxylic acids they were accumulating in *B. napus* (group I-IV) and *A. thaliana* (group I) plants upon *V. longisporum* infection. Although a structural relation to the dicarboxylic acids reduces the number of putative structures a large variety remains. A few possibilities are displayed in Fig. 41.

Various commercially available substances were tested to be a member of an unidentified group but e.g. 12-amino-7-oxo-dodecanoic acid ($C_{12}H_{23}NO_3$) eluted at 3.03 min whereas the detected marker of group I (C12) had a retention time of 4.86 min and was therefore less polar. 2-amino-caprylic acid

eluted at 2.97 min instead of 2.88 min like the marker of group IV (C8), but 8-amino-caprylic acid had a retention time of 2.26 min and was too polar.

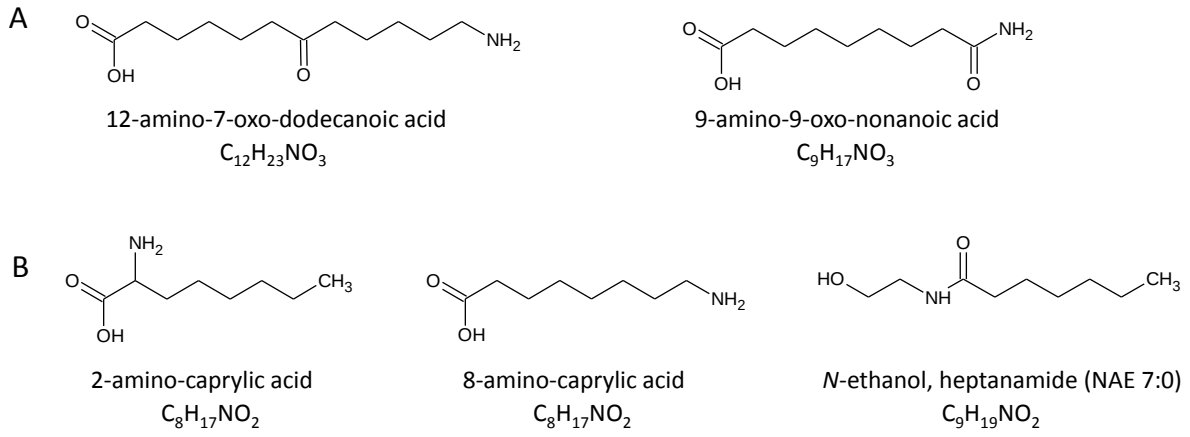

Fig. 41: Structural formulas of putative dicarboxylic acid derivatives
Examples for structures of tested compounds as putative infection markers fitting the molecular formula of (A) group I and (B) group IV

Group IV was suspected to correspond to *N*-acylethanolamines (NAEs) which are described to be lipid mediators, deriving from hydrolysis of a membrane phospholipid (Schmid et al. 1996) and can occur with different carbon chain lengths. Short chain NAEs were chemically synthesized in order to obtain standard compounds for comparison (as described under 2.2.12.1). UPLC-TOF-MS analysis indicated the successful chemical synthesis of NAE 7:0 ($[M+H]^+$ 174.1495, $C_9H_{20}NO_2$, retention time 4.31 min) and NAE 10:0 ($[M+H]^+$ 216.1965, $C_{12}H_{26}NO_2$, retention time 5.70 min). The retention times of the NAEs nevertheless did not match the retention times of the corresponding infection markers.

MS/MS experiments for members of the group I indicated a high degree of consistency with MS/MS pattern of the dicarboxylic acids. Hence only a hydroxyl group may have changed into an amino group leading to a monoamide derivative. Therefore 9-amino-9-oxo-nonanoic acid (azelaamic acid, C9) was chemically synthesized from mono-methyl-azelaic acid. The synthesis led not only to the C9 monoamide ($[M+H]^+$ 188.1287, $C_9H_{18}NO_3$, retention time 3.49 min) but also to monoamides with longer carbon chains (up to C13). However it could be shown by TOF MS analysis, that the starting material already contained impurities of other mono-methyl-dicarboxylic acids leading to a variety of monoamide products. Nevertheless the retention time and MS/MS comparison of the synthetic azelaamic acid with the infection marker identified azelaamic acid unequivocally as a member of the marker group I (Fig. S 6). The other members of group I were identified by retention time comparison to be the monoamides produced as by-products in the chemical synthesis. 7-amino-7-oxo-heptanoic acid and 8-amino-8-oxo-octanoic acid were assigned by their exact mass and the corresponding retention time shift to the other members of group I. This mode of identification applies also for the C14 and C15 monoamides.

Knowing group I to be the monoamide derivatives of the saturated dicarboxylic acids group II was suspected to be the corresponding diamides (group II). Since the abundance of these markers was too low for MS/MS experiments, dodecanediamide was synthesized chemically to obtain an authentic standard for identification. The synthesis was started from dodecanedioic acid. The end product of the chemical synthesis was successfully tested to contain dodecanediamide ($[M+H]^+$ 229.1916, $C_{12}H_{25}N_2O_2$, retention time 4.26 min). No other carbon chain lengths were detected but the dodecane monoamide was synthesized as a by-product (intensity about 15 % of the diamide). The monoamide was suspected to derive from a reaction of the activated carboxylic acid with water since aqueous ammonia was added slowly. To avoid this competitive reaction it would be preferable to provide the ammonia and add the activated intermediate product. The identity of the C12 infection marker of group II was nevertheless confirmed by retention time comparison as dodecanediamide suggesting the other markers to be the corresponding diamide derivatives of the saturated dicarboxylic acids (Tab. 8). The chemical synthesis of the mono- and diamide was planned and supervised by Dr. Farina Schill (Department of Plant Biochemistry, Georg-August-University, Göttingen, Germany).

Group III and IV of the AWF infection markers exhibited a lower intensity than the monoamides but a higher abundance than the diamides. Hence it was possible to fragment a representative compound of each group by MS/MS (Fig. S 7). When fragmenting a member of group III ($[M+H]^+$ 172.1338, $C_9H_{18}NO_2$, retention time 3.62 min) the loss of an amino group ($[M+H\text{-}NH_3]^+$ 155.1059) as well as an amino group and water ($[M+H\text{-}NH_3\text{-}H_2O]^+$ 137.0952) was observed. A fragment of 109.008 Da ($[C_8H_{13}]^+$) in positive ionization indicating the additional loss of carbon monoxoxide ($[M+H\text{-}NH_3\text{-}H_2O\text{-}CO]^+$). The fragments of the member of group IV ($[M+H]^+$ 174.1494 Da, $C_9H_{20}NO_2$, 3.52 min) also indicated the loss on a water molecule ($[M+H\text{-}H_2O]^+$ 156.1407) followed by cleavage of an amino group ($[M+H\text{-}H_2O\text{-}NH_3]^+$ 139.1139 Da). The loss of water preferred to the amino group indicated a hydroxyl as functional group for group IV whereas the fragmentation path of the group III points to an aldehyde indicated by the loss of CO_2. Those fragmentation patterns suggested the substances to be the corresponding aldehyde and alcohol derivatives of the monoamides (Tab. 8). The structural formulas of all amide derivatives are displayed in Fig. S 8.

The datasets were searched additionally for the diol and dialdehyde derivatives as well as for the hydroxyaldehydes and the hydroxycarboxylic acids but none of them was found.

Tab. 8: Amide derivatives identified as infection markers
The retention time (RT) was determined on the ACQUITY UPLC HSS T3 column running with the polar gradient. Intensity mean values and standard deviations (SD) of detected counts per second (cps) were calculated from supplemental dataset M1402. The values from 28 dpi (positive ionisation) were exemplarily chosen. n.d. = not detected as marker in this dataset

Exact mass [Da]	RT [min]	Molecular formula	Name	Plant	Intensity [cps]
			Monoamides (group I)		Mean + SD
159.0896	2.23	C7H13NO3	7-amino-7-oxo-heptanoic acid	*B. napus, A. thaliana*	1794 ± 746
173.1053	2.84	C8H15NO3	8-amino-8-oxo-octanoic acid	*B. napus, A. thaliana*	4804 ± 1274
187.1209	3.49	C9H17NO3	9-amino-9-oxo-nonanoic acid (Azelaamic acid)	*B. napus, A. thaliana*	51640 ± 18534
201.1366	4.05	C10H19NO3	10-amino-10-oxo-decanoic acid (Sebacamic acid)	*B. napus, A. thaliana*	4644 ± 1525
215.1524	4.47	C11H21NO3	11-amino-11-oxo-undecanoic acid	*B. napus, A. thaliana*	11938 ± 4155
229.1678	4.86	C12H23NO3	12-amino-12-oxo-dodecanoic acid	*B. napus, A. thaliana*	7627 ± 2710
243.1836	5.17	C13H25NO3	13-amino-13-oxo-tridecanoic acid	*B. napus, A. thaliana*	53990 ± 17681
257.1993	5.51	C14H27NO3	14-amino-14-oxo-tetradecanoic acid	*B. napus*	854 ± 451
271.2150	5.79	C15H29NO3	15-amino-15-oxo-pentadecanoic acid	*B. napus*	2132 ± 836
			Diamides (group II)		
186.1369	2.68	C9H18N2O2	Nonanediamide (Azelamide)	*B. napus*	532 ± 189
214.1683	3.89	C11H22N2O2	Undecanediamide	*B. napus*	106 ± 49
228.1839	4.26	C12H24N2O2	Dodecanediamide	*B. napus*	61 ± 24
242.1996	4.61	C13H26N2O2	Tridecanediamide	*B. napus*	403 ± 126
			Aldehydes (group III)		
157.1103	2.88	C8H15NO2	8-oxooctanamide	*B. napus*	315 ± 111
171.1259	3.62	C9H17NO2	9-oxononanamide	*B. napus*	2526 ± 877
185.1416	4.30	C10H19NO2	10-oxodecanamide	*B. napus*	n.d.
199.1572	4.76	C11H21NO2	11-oxoundecanamide	*B. napus*	609 ± 189
213.1729	5.16	C12H23NO2	12-oxododecanamide	*B. napus*	211 ± 127
227.1886	5.55	C13H25NO2	13-oxotridecanamide	*B. napus*	2362 ± 745
			Alcohols (group IV)		
159.1255	2.88	C8H17NO2	8-hydoxyoctanamide	*B. napus*	1003 ± 397
173.1417	3.52	C9H19NO2	9-hydoxynonanamide	*B. napus*	180 ± 30
187.1567	4.15	C10H21NO2	10-hydoxydecanamide	*B. napus*	n.d.
201.1723	4.56	C11H23NO2	11-hydoxyundecanamide	*B. napus*	180 ± 50
215.1887	4.93	C12H25NO2	12-hydoxydodecanamide	*B. napus*	1160 ± 408
229.2044	5.26	C13H27NO2	13-hydoxytridecanamide	*B. napus*	162 ± 74
243.2201	5.59	C14H29NO2	14-hydoxytetradecanamide	*B. napus*	n.d.

3.3.3.7.3 Intensities and distribution of AWF specific infection markers

The most intensive marker group was found to be the monoamide derivatives. In order to compare the intensity levels of the several groups of AWF markers, the intensity of azelaamic acid in *B. napus* was set to 100 %. This level was compared to the other C9 compound of all groups. The dicarboxylic acid (azelaic acid) showed an intensity level of 4 %, the diamide (azelamide) of only 0.5 %, the aldehyde (9-oxononanamide) of 11 % and the alcohol (9-hydroxynonanamide) of 0.5 %. The controls displayed the same ratios as the infected plants. This means that the ratio of the different groups did not change in the plant after *V. longisporum* infection but that only all levels increased.

As was already mentioned the carbon chain length of the dicarboxylic acids varied in *A. thaliana* from C6 to C13 and in *B. napus* even from C6 to C15. The monoamides were significant infection markers from C7 to C13 in *A. thaliana* and from C7 to C15 in *B. napus*. So the same gap of C14 and C15 as for the dicarboxylic acids is noticeable. In contrast representatives of group II to IV were only detected as

infection markers in oilseed rape. This might be due to low abundances in *A. thaliana* but even more pronounced markers do not display a clear tendency of accumulation in infected plants.

3.3.3.8 Glucosinolates

The substance class of glucosinolates are known to be involved in plant-pathogen interaction in Brassicaceae (Bednarek et al. 2009, Pfalz et al. 2011). Therefore it was investigated if they can be regarded as infection markers in *B. napus* after *V. longisporum* infection. For infected *B. napus* tissue at early time points many database hits for glucosinolates were given. Unfortunately, most of them could not be unequivocally assigned due to the existence of various structural isomers. The occurrence of a specific fragment ($[M-H]^-$ 259.0123 Da) described by Rochfort et al. (2008) identifies them nevertheless as glucosinolates. By retention time comparison to the authentic standards and / or by fragmentation pattern published by Velasco et al. (2011) three glucosinolates could unequivocally be identified. Indole-3-ylmethyl glucosinolate (I3G, glucobrassicin) was detected to accumulate ($[M-H]^-$ 447.0532, $C_{16}H_{19}N_2O_9S_2$, retention time 2.60 min) at 5 dpi in extracted shoot tissue. Furthermore 1- and 4-methoxyglucobrassicin ($[M-H]^-$ 477.0638, $C_{17}H_{21}N_2O_{10}S_2$, retention time 3.60 min and 3.13 min, respectively) were found to accumulate upon *V. longisporum* infection. A significant increase however was obtained in only one of two experiments and they could therefore not be regarded as reliable infection markers for *V. longisporum* infection in *B. napus*. In general high standard deviations were observed for the detected amounts of glucosinolates. From 7 to 10 dpi the induction faded away and suggested by this an early response in the plant-pathogen interaction. At late infection time points (21, 28 and 35 dpi) no infection related accumulation was detected in the extracted tissues of *B. napus*. In *A. thaliana* roots I3G, 4-hydroxy-I3G and three aliphatic glucosinolates (8-methylthiooctyl glucosinolate, 8-methylsulfinyloctyl glucosinolate, 8-methylsulfonyloctyl glucosinolate) were enhanced after *V. longisporum* infection (König 2011). They have been shown to increase early (5 to 7 dpi) with a subsequent decrease at 10 dpi as well. For a more detailed analysis and comparison to *A. thaliana* an extensive identification of the involved glucosinolate species is necessary but due to the high biological variability this identification was considered to be of minor importance.

3.4 Targeted analysis of polyamines in *B. napus* plants

Polyamines are known to accumulate in host plants upon fungal infection (Walters 2000). It has been observed that polyamines are not extracted by the MTBE-based extraction method and that they ionise weakly in ESI-MS measurements. Therefore a targeted analysis was performed in addition to the metabolite fingerprinting to record the levels of the diamine putrescine, the triamine spermidine and the tetraamine spermine (Fig. 42). For the measurement hypocotyl tissue was analysed due to its

high fungal DNA content. Plant material from the same homogenized pool as for metabolite fingerprinting was used for the measurements. The polyamine analysis was performed by Pia Meyer.

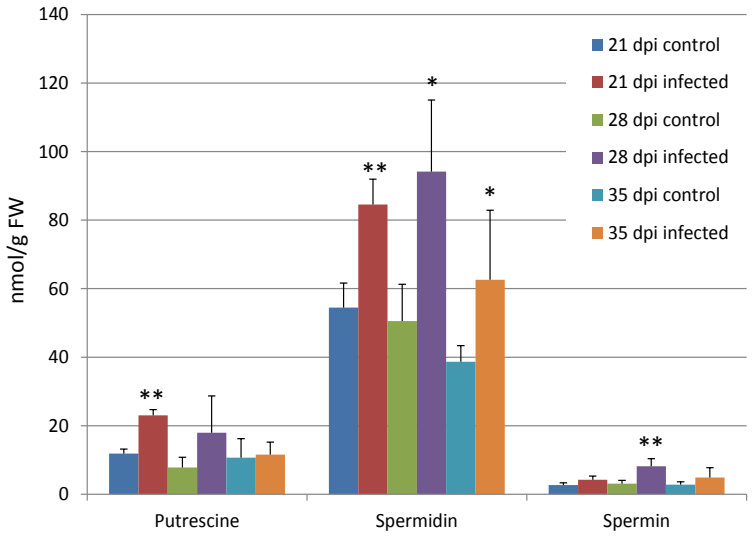

Fig. 42: Targeted analysis of polyamines in the hypocotyl of infected and control *B. napus* plants

The polyamines were extracted from hypocotyl tissue of *V. longisporum* infected and control plants, dansylated, separated by HPLC and analysed by a fluorescence detector. Data were determined from two technical replicates of three biological replicates. Asterisks indicate intensity values with significant differences compared to the corresponding control in an unpaired Students t-test (* = p-value < 0.05; ** = p-value < 0.001). Error bars represent the standard deviation.

For all analysed samples an accumulation of polyamines in the infected tissue was observed compared to the control plants, but this was only significant for putrescine at 21 dpi and for spermine at 28 dpi. For spermidine the detected levels were generally higher and the change due to fungal infection was significant for all analysed time points. The concentrations corresponded to the levels of polyamines measured in barley leaves when infected with powdery mildew (Walters 2000).

An analysis of the other plant organs including the apoplastic fluids will give a more detailed picture about the tissue specific distribution of polyamines within the infected plants. Additionally, the analysis of tissue from infected *A. thaliana* and *C. sativa* plants could provide more information of a general role of polyamines in the infection process of Brassicaceae.

From this chapter it can be concluded that the metabolic reaction in host plants can be divided into a species specific - mostly phytoalexin related - response and into the accumulation of metabolites that play a more general role in the pathogen response in Brassicaceae. More than 70 infection markers from both groups were structurally elucidated and unequivocally identified. They are summed up in Tab. S 1. All identified infection markers seem to be plant derived substances.

3.5 Identification of markers for *V. longisporum* infection in *C. sativa* plants

3.5.1 Infection monitoring

With the aim to get a deeper insight into similarities and differences in the processes of *V. longisporum* infection of different Brassicaceae another crop plant species *C. sativa* was infected with VL 43 fungal spores. Infection symptoms and metabolic changes were monitored and analysed analogously to *B. napus*. This was the first attempt to infect this oilseed crop with *V. longisporum*.

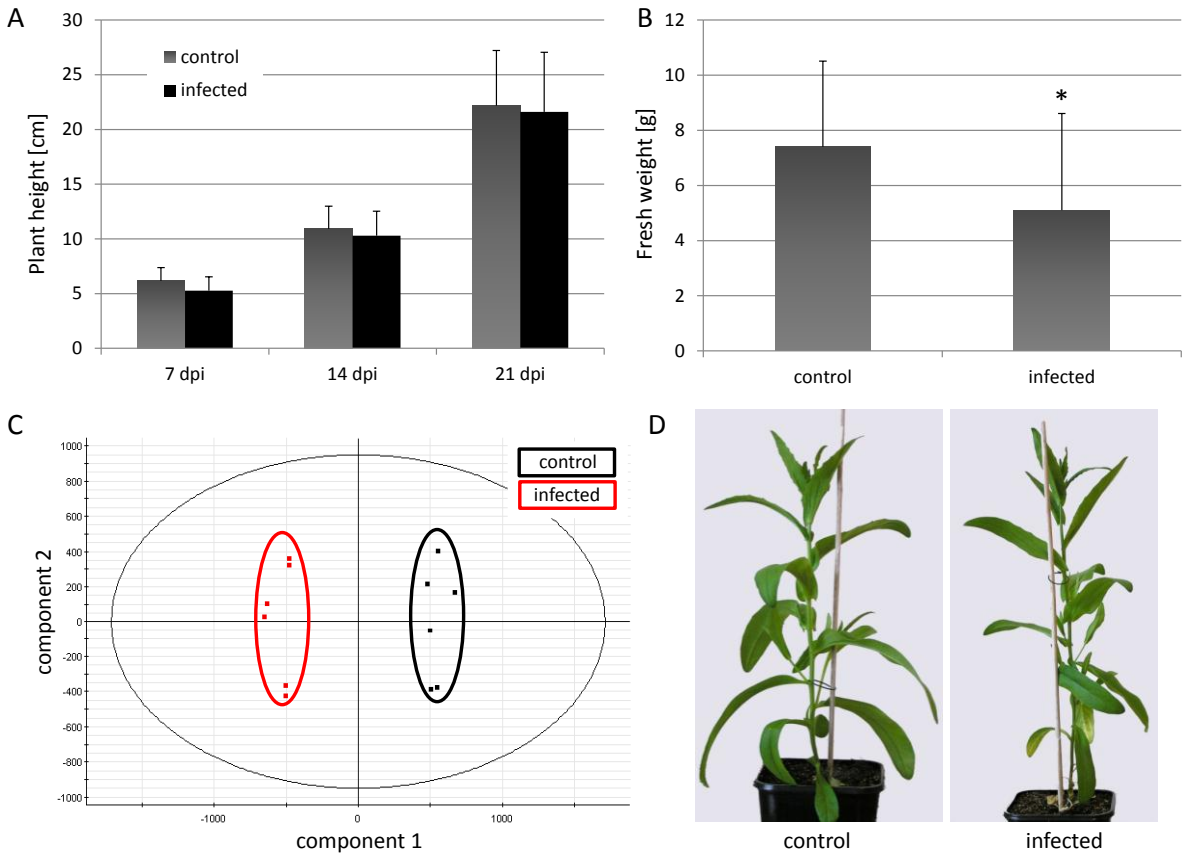

Fig. 43: Monitoring of the infection of *C. sativa* plants with *V. longisporum*
(A) Height of control and infected plants during the infection time course up to 21 days past infection (dpi). (B) Fresh weight of aboveground tissue per plant measured 21 dpi. A and B include three biological pools. Asterisks indicate intensity values with significant differences compared to the corresponding control in an unpaired Students t-test (* = p-value < 0.05). Error bars represent the standard deviation. (C) Sample-based PCA plot of positively ionized samples from extracted hypocotyl tissue 21 dpi. Samples from mock treated plants are framed in black whereas samples from infected plants are framed in red. For metabolite fingerprinting analysis three biological and two technical replicates of 15 plants each were analysed. (D) Representative control and infected *C. sativa* plant prior to sample collection (21 dpi).

Since stunting is a reproducible infection symptom in *B. napus* the plant height was monitored over three weeks after infection but no significant differences to mock treated control plants occurred (Fig. 43 A). Most infected plants showed a similar phenotype like the mock controls (Fig. 43 D). The fresh weight per single plant was nevertheless significantly reduced in infected plants indicating a fungal infection resulting in a reduced biomass production (Fig. 43 B). Additionally, the PCA plot of

control and infected samples from metabolic fingerprinting of hypocotyl tissue shows a clear separation of both conditions (Fig. 43 C). This indicated that the fungal infection has successfully influenced the metabolic pattern. The xylem sap and AWF as well as hypocotyl tissue from 21 dpi were analysed by metabolite fingerprinting analysis.

3.5.2 Phytoalexins as infection markers

Camalexin is known to be the typical phytoalexin in *A. thaliana* (Tsuji et al. 1992). Accumulation of camalexin was also described in *C. sativa* by infection with *Alternaria brassicae* (Browne et al. 1991). Since cyclobrassinin and related metabolites were found to be strongly affected by fungal invasion in *B. napus,* it was assumed that the camalexin abundance in *C. sativa* was influenced as well. Indeed was camalexin identified as infection marker in the polar extraction phase ($[M+H]^+$ 201.0486, $C_{11}H_9N_2S$, retention time 5.05 min) by retention time and MS/MS pattern comparison with the authentic standard. Additionally, the identity of methoxycamalexin ($[M+H]^+$ 231.0592, $C_{12}H_{11}N_2OS$, retention time 5.08 min) was confirmed by MS/MS experiments. Both phytoalexins accumulate significantly after *V. longisporum* infection in xylem sap and hypocotyl tissue with about five times higher intensity levels in xylem sap (Fig. 44). They were not detected in AWF (data not shown).

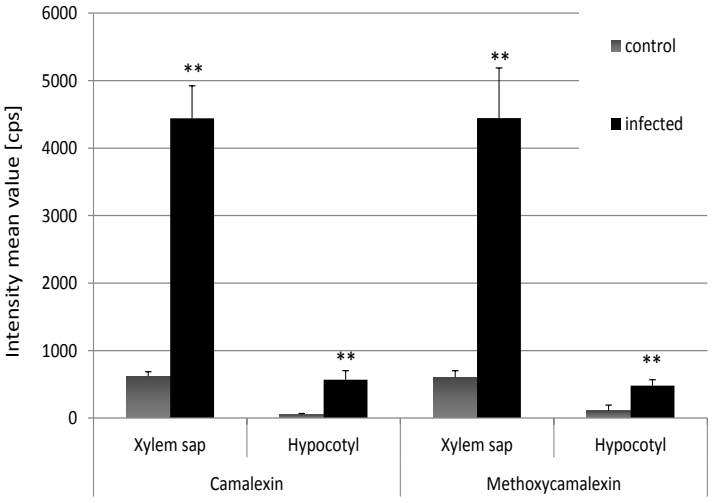

Fig. 44: Accumulation of camalexin and methoxycamalexin in *C. sativa* plants after infection with *V. longisporum*

Amount of camalexin and methoxycamalexin in *C. sativa* plants 21 dpi in xylem sap and hypocotyl tissue. Data were determined from three technical replicates of one representative experiment (xylem sap) or three biological replicates (hypocotyl). Asterisks indicate intensity values with significant differences compared to the corresponding control in an unpaired Students t-test (* = p-value < 0.05; ** = p-value < 0.001). Error bars represent the standard deviation.

Since cyclobrassinin is described to be specific for *Brassica* species (Pedras and Yaya. 2010) it was not surprising that neither the phytoalexin nor any of the new described cyclobrassinin related metabolites was found in *C. sativa*. Noticeable is that camalexin was found in high amounts in xylem sap whereas cyclobrassinin was only detectable in tissue samples but not in the apoplastic fluids of infected *B. napus*.

3.5.3 Comparison of the infection markers from *B. napus* and *A. thaliana* plants

A general comparison of the metabolic pattern of infected *C. sativa* plants with *B. napus* and *A. thaliana* should highlight if the reaction to *V. longisporum* was similar in the three Brassicaceae or if it was mostly species specific and significantly different. Therefore the data from the metabolite fingerprinting analysis of AWF of all species collected at 21 dpi was analysed. The datasets from positive ionisation were pre-processed together in MarkerLynx™ and analysed in MarVis. The resulting 1D-SOM indicated that although the three species belong to the same plant family their reaction to *V. longisporum* invasion differs significantly (Fig. 45 A). In the AWF no prototypes were detected that included accumulated markers for all three crucifers. Only one prototype (framed in black) suggested that there are common markers for *B. napus* and *A. thaliana*. This prototype included the already described infection markers dicarboxylic acids and its monoamide derivatives. In hypocotyl tissue from *B. napus* and *C. sativa* the differences were even more pronounced as indicated by the red framed species specific prototypes (Fig. 45 B).

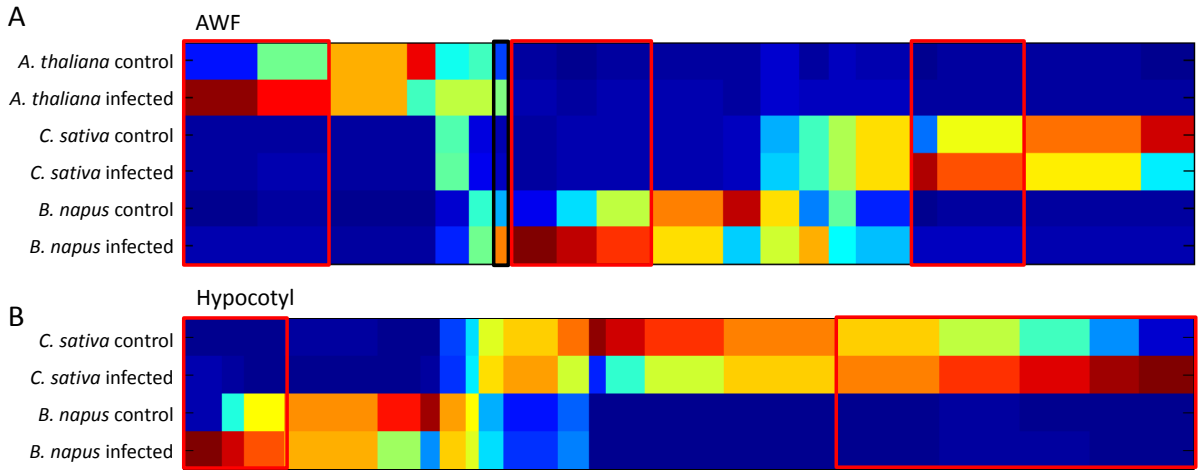

Fig. 45: Infection specific metabolite fingerprinting in tissue of different Brassicaceae after infection with *V. longisporum*
Measurements of the MTBE extracted polar phase of different Brassicaceae after fungal infection. Samples were harvested at 21 dpi. (A) 1D-SOM matrix after metabolite-based clustering of 6655 markers from AWF samples of *B. napus, A. thaliana* and *C. sativa.* Prototypes that include species specific infection markers are framed in red (A.t. 965 markers, C.s. 929 markers, B.n. 742 markers). Prototypes that include markers accumulated in infected *B. napus* and *A. thaliana* plants are framed in black (117 markers). (B) 1D-SOM matrix after metabolite-based clustering of 4500 markers from hypocotyl tissue of *B. napus* and *C. sativa*. Prototypes that include species specific infection markers are framed in red (C.s. 1594 markers, B.n. 451 markers). The displayed datasets include markers from positive ionisation mode with a p-value < 10^{-4} (Kruskal-Wallis test) (A) or a p-value < 0.001 (Kruskal-Wallis test) (B). The intensity was normalized and colour-coded. The 20 prototypes were scaled to the number of markers contained.

However, some common infection markers for all analysed Brassicaceae were found. RA is a reliably infection marker of *B. napus* and *A. thaliana* (Fig. 33). It accumulates also in xylem sap and hypocotyl of infected *C. sativa* plants but was not detectable in AWF (Fig. 46 A). SAG, 2,3-DHBAG and pipecolic

acid proved to accumulate in all three species upon fungal infection. These three markers were found significantly enhanced in high amounts (especially pipecolic acid) in infected hypocotyl tissue of *C. sativa* 21 dpi (Fig. 46 B). Interestingly 2,5-DHBAG was not detected. The amount of SA was not significantly enhanced in *C. sativa* in contrast to the results obtained from infected *A. thaliana.*

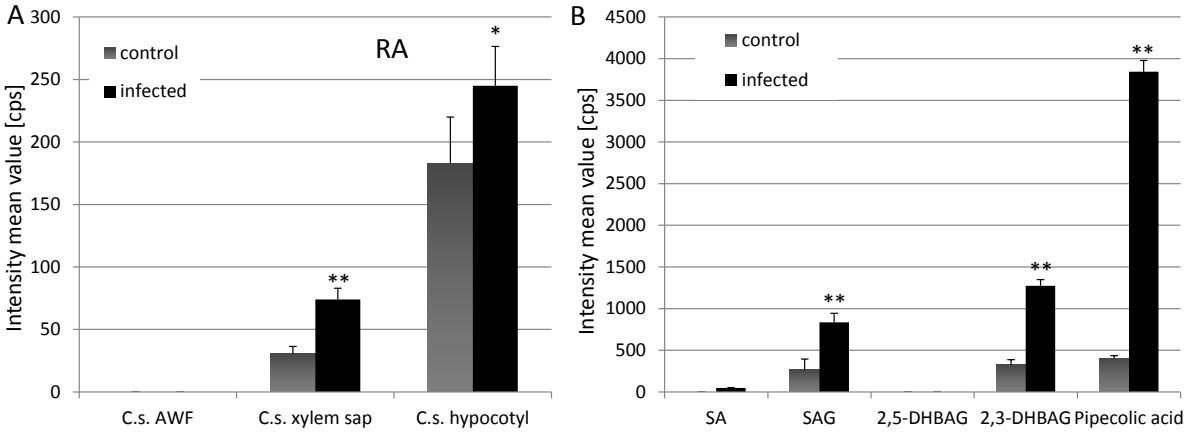

Fig. 46: Accumulation of raphanusamic acid, salicylic acid and derivatives in *C. sativa* plants after infection with *V. longisporum*

Amount at 21 dpi of (A) RA in AWF, xylem sap and hypocotyl tissue of *C. sativa* plants and (B) SA, SAG and pipecolic acid in hypocotyl tissue. Data were determined from two technical replicates of three biological replicates (AWF and hypocotyl) or three technical replicates of one representative biological sample (xylem sap). Asterisks indicate intensity values with significant differences compared to the corresponding control in an unpaired Students t-test (* = p-value < 0.05; ** = p-value < 0.001). Error bars represent the standard deviation.

Other identified infection markers like the oxylipins are either not detectable in apoplastic fluids (9,12,13-trihydroxy-10-octadecenoic acid) or do not accumulate after fungal invasion in *C. sativa* plants (9,12,13-trihydroxy-10,15-octadecadienoic acid). The AWF specific infection markers (dicarboxylic acids, monoamide and alcohol derivatives) were measured in the AWF of *C. sativa* as well but in contrast to *B. napus* or *A. thaliana* the levels were unchanged after infection. The diamides and aldehyde derivatives were not detectable.

It can be concluded that *C. sativa* was susceptible to infection with *V. longisporum* VL43 and can be colonized successfully. However, this does not lead to stunting symptoms like in *B. napus* but results in a reduced biomass and a significant change on metabolic level including a strong accumulation of the phytoalexins camalexin and methoxycamalexin. Neither the *Brassica* specific cyclobrassinin nor any related metabolite was found in *C. sativa* but RA proved to a general marker in Brassicaceae as well as SAG, 2,3-DHBAG and pipecolic acid.

3.6 Functional analyses

3.6.1 Luciferase assay in *A. thaliana* plants

A screening assay should be established with the aim to test the infection markers towards putative signalling function. Therefore *A. thaliana* mutants pip2.2::LUC provided by the work group of Prof. Gatz (Department of Molecular Biology and Plant Physiology, Georg-August-University, Göttingen, Germany) were used. The expression of the reporter gene can be monitored by the external application of firefly luciferin. The luciferase activity results in the release of a photon at 592 nm, which can be detected with sensitive camera equipment (de Ruijter et al. 2003). The promoter of pip2.2 was identified to be induced in *A. thaliana* after infection with *V. longisporum* (Tappe 2008). It was tested on soil cultivated plants whether a luciferase signal can guarantee a successful infection process. Therefore *A. thaliana* plants were infected with *V. longisporum* spore solution and the infection process was monitored by recording the luciferase activity.

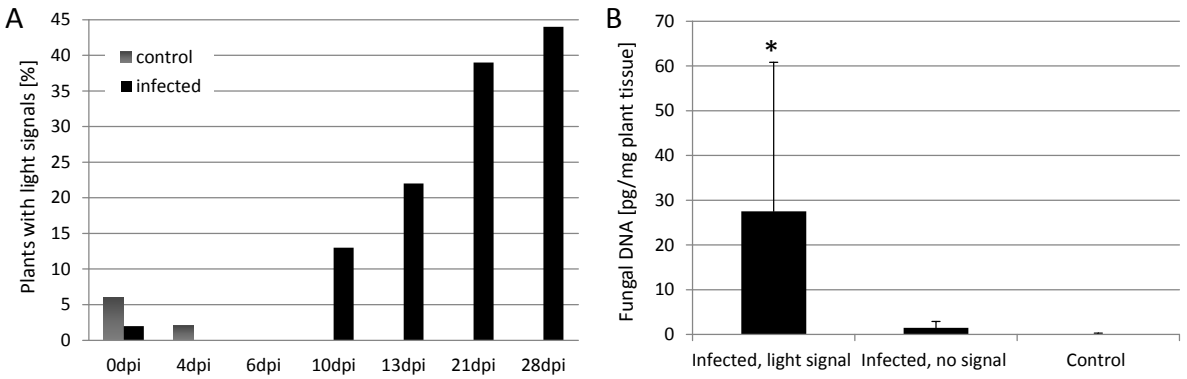

Fig. 47: Luciferase assays of pip2.2::LUC plants infected with *V. longisporum* VL 43 and grown on soil
(A) Ratio of control and infected plants that display detectable light signals after treatment with 1 mM firefly luciferin during the infection time course. Data included 54 plants per time point. (B) Fungal DNA content of mock-controls, infected plants with or without a luciferase signal. 15 plants were analysed per condition. Asterisks indicate fungal DNA values with significant differences compared to infected, no signal in an unpaired Students t-test (* = p-value < 0.05; ** = p-value < 0.001). Error bars represent the standard deviation.

However, the light signals of infected plants were too weak for quantification. Therefore all plants that exhibited a detectable spot were counted and the ratio of the total number of plants was calculated (Fig. 47 A). Up to 4 dpi a few signals from mock treated controls were recorded. From 10 dpi to 28 dpi the percentage of infected plants with detectable light signal increased from 12 % to nearly 45 %. This suggested that the activity of the pip2.2 promoter is indeed triggered by *V. longisporum* infection. In order to verify that a detectable light signal really indicated a successful infection, the fungal DNA content of 15 infected plants with and 15 infected plants without a measurable signal was analysed (Fig. 47 B). The DNA amount in plants with a detectable signal was indeed significantly higher compared to the plants without a signal. This led to the conclusion that

the pip2.2 promoter based luciferase activity reliably indicated a successful infection of the single plant. When the assay was transferred to a sterile, controllable surrounding for distinct application of pure substances unfortunately, the luciferase activity was not reliably connected to the infection procedure any more (Fig. 48).

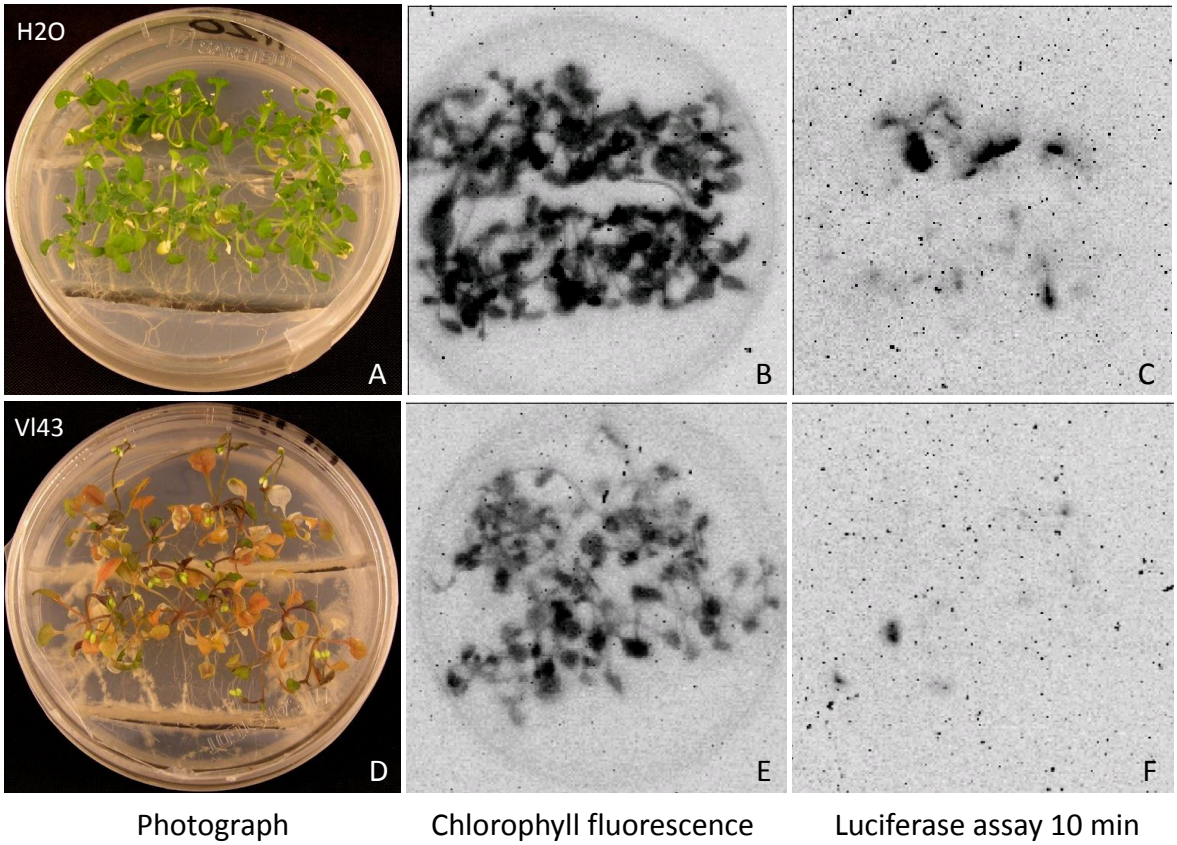

Fig. 48: Luciferase assays of pip2.2::LUC plants infected with *V. longisporum* VL 43 and grown on agar plates
Control plants depicted in the upper row (A-C), infected plants in the bottom row (D-F). For both conditions the photo (A+D), the chlorophyll fluorescence (B, E) and the luciferase activity (10 min exposure time, C, F) are shown. All photos were taken at 12 dpi. Plants were sprayed with 1 mM luciferin about 1 h prior to signal detection.

The chlorophyll fluorescence was recorded to document the health status of the plants and indicated that the fungus colonizes the plants and leads to reduced fluorescence (Fig. 48 E). The luciferase assay however contradicted the visible impression and the chlorophyll status. Mock treated plants often displayed even stronger luciferase activity than the infected plants (Fig. 48 C vs. F). Due to the high variation of the luciferase activity in the controls the assay could not be regarded as a reliable method. In order to obtain more stable results a pure substance was used as an alternative to the application of fungal spores. Knoth et al. (2009) identified 3,5-dichloroanthranilic acid (DCA) as a quick and strong inducer for a fungus specific promoter (CaBP22). Since different anthranilates were already detected to be produced by *V. longisporum,* 15 µM DCA was used for the pip2.2 luciferase assay. Although first experiments were promising they could not be repeated. The assay was tested

in various versions to optimize the luciferase reaction. Therefore approaches were conducted with single leafs, plants on large glass petri dishes or in PCR tubes. Additionally, another *A. thaliana* mutant was tested (CYP79B2/B3::LUC (Iven 2009)). But although the signals in VL 43 infected plants were stronger than in the infected pip2.2::LUC plants, the reaction was not reliable enough for monitoring infected plants on agar even less for a reliable screening of substances.

3.6.2 Flotation assay with *B. napus* leaves

As an alternative to the luciferase assay a flotation experiment as performed by Stenzel et al. (2003) was used. Several infection related metabolites were applied to *B. napus* leaves with the aim to test whether they could induce an infection related metabolite pattern. The experiments were carried out by Annette Weizbauer. 50 µM of the following substances were tested: SA, RA, pipecolic acid and various dicarboxylic acids (pimelic acid, suberic acid, azelaic acid, sebacic acid, undecanedioic acid, dodecanedioic acid, tridecanedioic acid and hexadecanedioic acid). All the metabolites (apart from hexadecanedioic acid) have been identified as infection markers in *B. napus*. As a positive control 250 mM NaCl was used. Water served as a negative control. A metabolite fingerprinting analysis was performed for the floated leaf material. When extracted leaf tissue was analysed after 6 h flotation time only weak changes could be monitored in the pattern of a 1D-SOM. Therefore the incubation time was extended to 24 h. The pH values were checked to remain stable during the incubation time. A successful infiltration was visible by brighter regions or spots in the leaf tissue. Additionally, e.g. pipecolic acid was measured in high amounts in the pipecolic acid treated samples indicating a successful uptake of the externally applied substance. Cyclobrassinin or related substances could not be detected in significant amounts in any sample. Only few markers with increased intensities in one or two conditions (particularly in dicarboxylic acid treated samples) were found (Fig. 49 A + C). None of them provided a reasonable database hit. 13 markers (Fig. S 49 B) were detected to accumulate when spores of the *V. longisporum* strains VL 43 and Bob instead of a substance were applied. All of them were very polar (retention time < 1 min) and were not increased in infected leaf material at late time points.

It must be stated that in the flotation assay no infection related metabolite fingerprint could be detected. The fungal spores induced markers might nevertheless be involved in very early infection processes that cannot be accessed by the established infection procedure. 24 h are putatively not long enough to induce the stress needed for the increase of e.g. phytoalexin related substances. Alternatively, the applied substances are not suitable to mimic a biotic stress situation in leaves. But nevertheless were some distinct metabolic changes detected so that in general a specific, substance related response can be monitored by this assay.

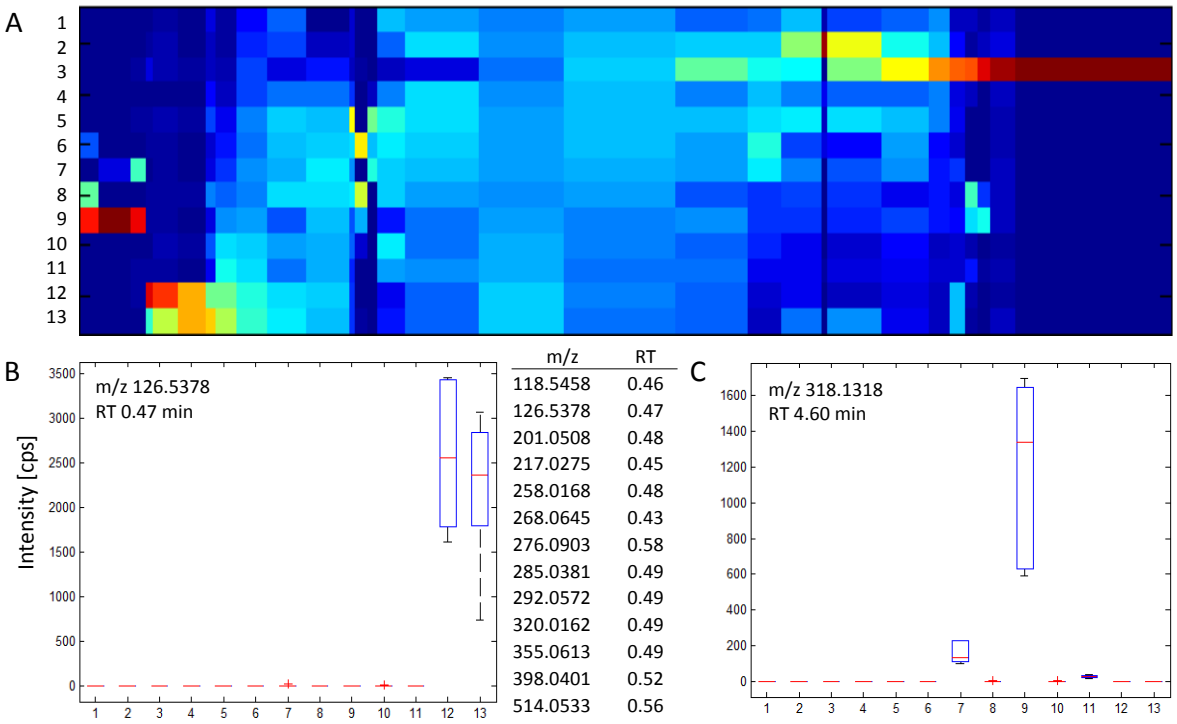

Fig. 49: Metabolite fingerprinting analysis of the flotation experiment
(A) 1D-SOM of extracted *B. napus* leaf material floated for 24 h on indicated substances (all 50 µM except NaCl 250 mM) or on fungal spore solution. The data included three biological replicates with two technical replicates each. 1575 markers from positive and negative ionization are displayed. (B) Box plot of a marker induced by VL spores and a table of other VL induced markers with their retention time. (C) Box plot of a marker induced by different dicarboxylic acids. 1 = H2O – control, 2 = SA, 3 = NaCl, 4 = RA, 5 = pipecolic acid, 6 = undecanedioic acid, 7 = dodecanedioic acid, 8 = tridecanedioic acid, 9 = suberic, sebacic and azelaic acid, 10 = pimelic acid, 11 = hexadecanedioic acid, 12 = VL 43 spores, 13 = VL Bob spores.

3.6.3 Abiotic stress by $CuCl_2$ in *B. napus* leaves

In the flotation assay the application of different substances, like the infection markers SA or RA could not induce an infection related metabolite pattern as obtained in the *in vivo* experiments in *B. napus* plants. In contrast to that, the accumulation of infection markers could be realized by the application of 10 mM $CuCl_2$ on *B. napus* leaves for 48 h. Phytoalexin related metabolites were significantly increased by this treatment although they were detected in lower amounts than during infection (Fig. 50). From the ten glycosylated stressins and stressinons only Mal-Glc-stressinon was not detected. The group of MICAs in contrast was absent with the exception of Mal-Glc-MICA. Cyclobrassinin and cyclobrassininon were detected in significantly increased amounts in the $CuCl_2$ treated tissue.

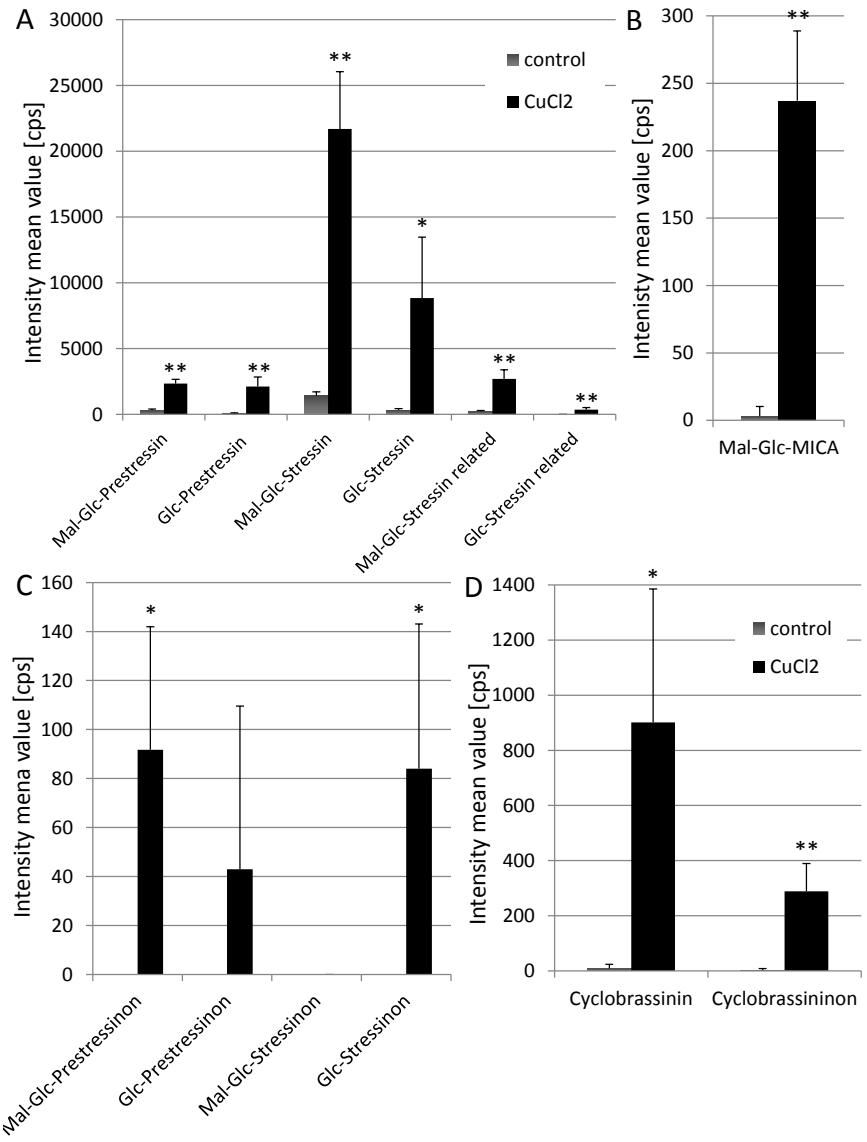

Fig. 50: Accumulation of cyclobrassinin related infection markers in *B. napus* leaves after abiotic stress treatment

Amount of (A) stressins and derivatives, (C) stressinons and derivatives, (B) Mal-Glc-MICA (the only detected MICA) as well as (D) cyclobrassinin and cyclobrassininon in mock or $CuCl_2$ treated leaves of *B. napus*. Samples were harvested 48 h after treatment. Data were determined from three biological replicates with two technical replicates each. Asterisks indicate intensity values with significant differences compared to the corresponding control in an unpaired Students t-test (* = p-value < 0.05; ** = p-value < 0.001). Error bars represent the standard deviation.

Besides these phytoalexin related markers also SAG, pipecolic acid and RA increased after abiotic stress treatment (Fig. 51). However SA, 2,3-DHBAG and 2,5-DHBAG were not detected in appreciable amounts. The levels of the dicarboxylic acids were unchanged in the leaf tissue after $CuCl_2$ treatment but since an infection related change was only detected in AWF this was expected. Therefore it might be worthwhile to investigate the level of the dicarboxylic acids and the amide derivatives in AWF of $CuCl_2$ elicited leaves. The same holds true for the identified oxylipin infection markers that were not detected in the extracted leaf tissue at all. When $CuCl_2$ was applied by watering the plant 7 days

before harvesting a comparable metabolic pattern was found. The substances like Mal-Glc-prestressin showed enhanced levels especially in the roots but the effect was less pronounced than in the sprayed leaf tissue (data not shown).

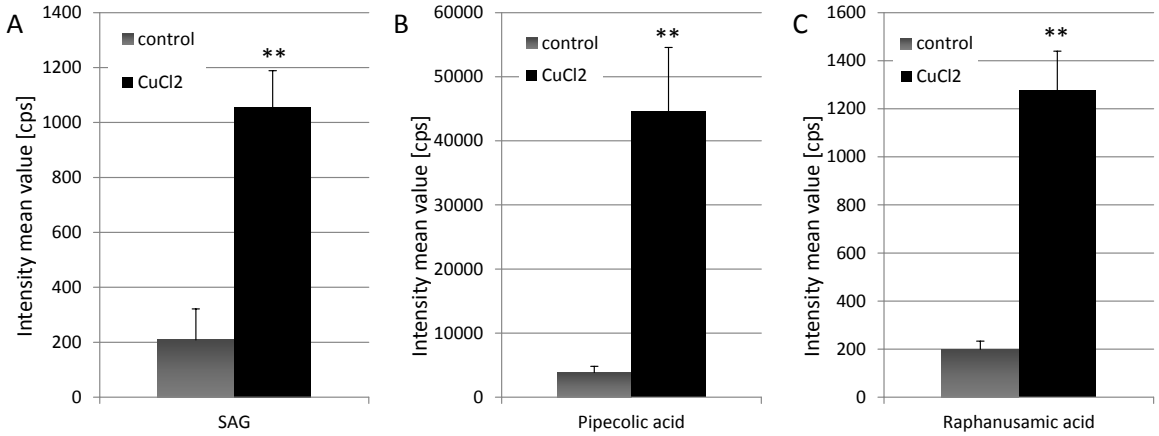

Fig. 51: Accumulation of the infection markers SAG, pipecolic acid and RA in *B. napus* leaves after abiotic stress treatment
Amount of (A) SAG, (B) Pipecolic acid and (C) RA in extracted samples of mock or $CuCl_2$ treated leaves of *B. napus*. Samples were harvested 48 h after treatment. Data were determined from three biological replicates with two technical replicates each. Asterisks indicate intensity values with significant differences compared to the corresponding control in an unpaired Students t-test (* = p-value < 0.05; ** = p-value < 0.001). Error bars represent the standard deviation.

From the obtained results it can be concluded that abiotic stress induced by $CuCl_2$ treatment of *B. napus* is leading to the accumulation of the same metabolic markers that can be monitored during the biotic stress of *V. longisporum* infection. Therefore most infection markers must be regarded as general stress markers for *B. napus*. This hints to a non-specific metabolic response of the host plant towards *V. longisporum* infection and it underlines the importance of the identified metabolites as stress markers. Furthermore no indication for a fungal metabolite circulating in the plant during infection was found.

3.6.4 Impact of plant derived substances on the fungal growth

All identified infection markers seemed to be plant derived substances. Their increase upon fungal infection might be connected to antifungal properties. To prove this hypothesis the substances were tested for their ability to inhibit the growth of *V. longisporum*. Neither the short chain dicarboxylic acids malonic acid and succinic acid nor the dicarboxylic acids with longer carbon chains (C8 to C16) happened to have an influence on the growth of *Verticillium*. Furthermore the chemically synthesized azelaamic acid, which still includes impurities of other monoamides of different carbon chain lengths, was tested and was not found to inhibit the fungal growth (Fig. 52 A). The fungal growth is exemplified for a control growing on PDA (control), and two colonies growing on PDA supplemented with 350 µM of the monoamide or 350 µM of 2,5-DHBA, respectively (Fig. 52 C). SA,

pipecolic acid and RA did not influence the mycelial growth of *V. longisporum* as well. Since the DHBA glucosides were not available the corresponding non-glycosylated 2,5-DHBA was tested. This substance was described to possess antifungal activity (Lattanzio et al. 1994). This also holds true for *V. longisporum* VL 43 (Fig. 52 B). The related 2,3-DHBA still remains to be tested. Oxylipins have been also shown to possess antifungal activity (Masui et al. 1989). Therefore an inhibition of *V. longisporum* growth by TriHOE and TriHOD seems likely. Unfortunately both substances were not available in sufficient amounts to perform a fungal growth inhibition test. The same was true for cyclobrassinin.

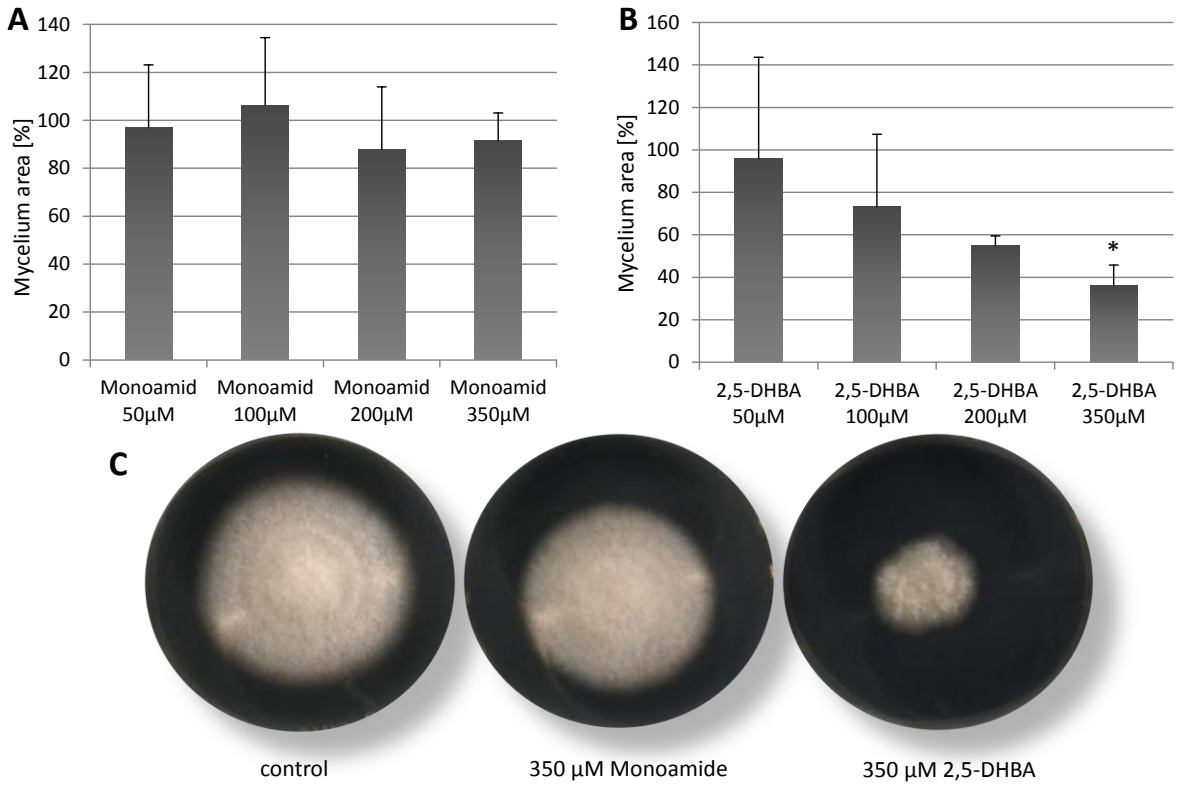

Fig. 52: Influence of monoamides and 2,5-DHBA on growth of *V. longisporum*
Fungal growth was analysed after exposure for 9 d to various concentrations of the following supplements (A) a monoamide mixture from chemical synthesis with azelaamic acid as main compound or (B) 2,5-DHBA. Area of VL 43 mycelium grown on PDA without supplements was set to 100 %. For each concentration three biological replicates were analysed. Asterisks indicate intensity values with significant differences compared to pure PDA in an unpaired Students t-test (* = p-value < 0.05). Error bars represent the standard deviation. (C) Fungal growth on PDA plates (control) and supplemented with 350 µM monoamide mixture or 350 µM 2,5-DHBA, respectively.

3.6.5 Metabolic conversion of phytoalexins by *V. longisporum*

In order to see if *V. longisporum* is able to metabolize and possibly detoxify cyclobrassinin and camalexin, the phytoalexins were incubated with fungal mycelium. For that sterile xylem sap was used as medium over an incubation time of 48 h. The intensity of cyclobrassinin and camalexin in the supernatants was determined before and after incubation with *V. longisporum* but no differences

were detected. Furthermore no glycosylated products or other phytoalexin derived substances were measured. The result suggested either that *V. longisporum* is completely inhibited by the supplied phytoalexins or that the fungus is not able to convert the substances within the incubation time of two days.

3.6.6 Preliminary results of priming *B. napus* plants with azelaic acid

In *A. thaliana* systemic acquired resistance (SAR) can be primed prior to bacterial infection by the application of azelaic acid (Jung et al. 2009). Since azelaic acid was identified as infection marker in *B. napus* it should be tested if azelaic acid was able to prime oilseed rape against infection with *V. longisporum* as well. One day prior infection *B. napus* plants were watered and sprayed with 250 µM azelaic acid (C9). Additionally, another plant pool was primed with a mix of each 250 µM suberic (C8) and sebacic acid (C10). In order to compare the priming effect to the infection process without priming, a standard infection was additionally performed including infected and mock treated plants. Those two conditions were treated in the priming procedure with buffer solution. The following results were obtained from only one experiment and must therefore be considered as preliminary. The stunting was monitored during the whole infection process but the primed plants did not differ significantly from non-primed, infected plants (Fig. 53 A). When xylem sap, AWF and hypocotyl tissue samples were extracted and analysed, significantly altered levels of some infection markers were observed in the plants primed with azelaic acid compared to the plants treated with the standard infection procedure. The levels of the cyclobrassinin related infection marker groups of stressins and MICAs were significantly reduced. In Fig. 53 (B + C) the representative intensity distribution of Mal-Glc-MICA and Mal-Glc-prestressin in hypocotyl tissue is displayed. The detected amounts of cyclobrassinin and cyclobrassininon were unchanged. The priming with a mixture of suberic and sebacic acid (C8 and C10) did not result in significantly decreased levels of stressins and MICAs. The levels of pipecolic acid, SAG, 2,5-DHBAG and RA in the hypocotyl were unaffected by the priming event. The level of SA in contrast was higher in xylem sap obtained from primed plants than in the samples from infected non-primed plants. For the xylem sap only one biological replicate was analysed so far. In the AWF no significant changes in the amount of AWF specific infection markers like the dicarboxylic acids were found. The levels of oxylipins in xylem sap were irregular and not infection related at all. Hence no effect of the priming event on the metabolite level was found apart from stressins, MICAs and SA. It must be kept in mind that the selection of severely affected plants for the infected controls (< 70 % than mean control value in height) complicates the sample generation. When the primed plants are selected as well (as has been done) a putatively enhanced resistance phenotype due to the priming might not be included in the analysis at all. If in contrast no selection is performed plants that were not infected efficiently are included and can distort the metabolic pattern as well. It might indicate a false positive success in priming.

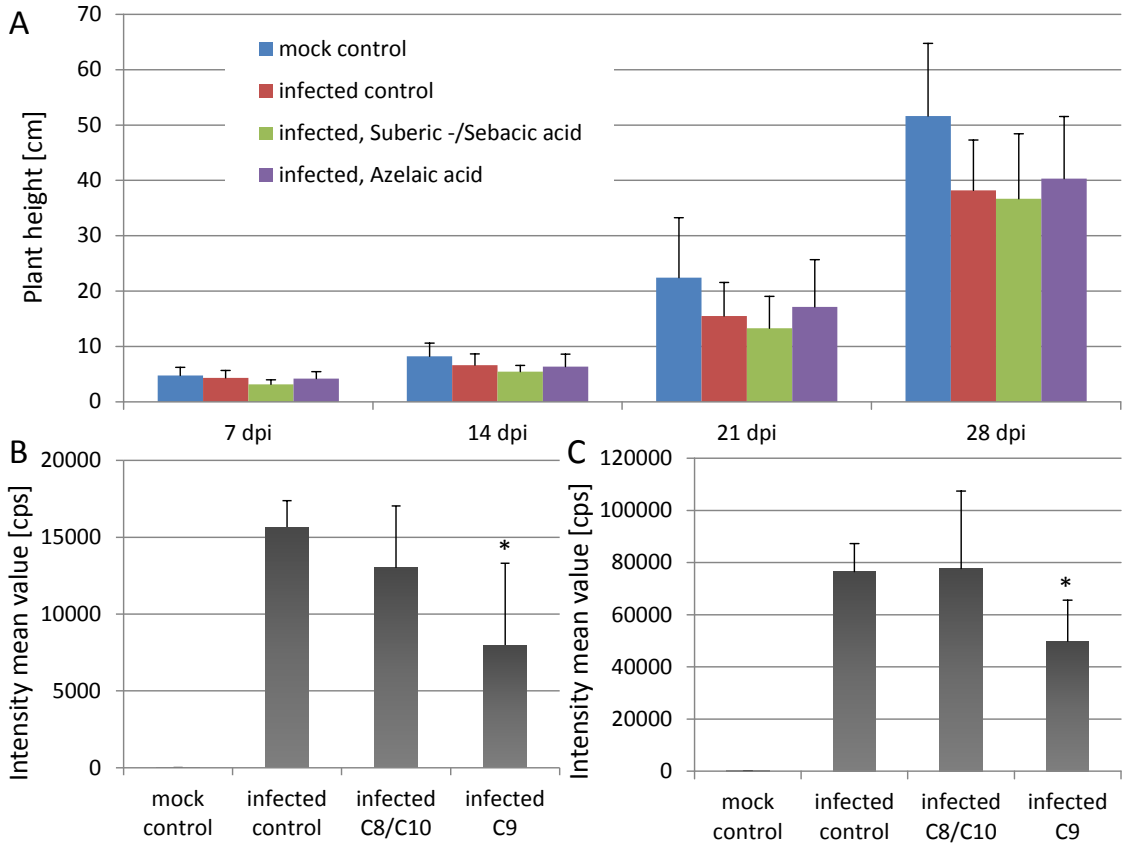

Fig. 53: Priming of *B. napus* plants with dicarboxylic acids prior to infection with *V. longisporum*
The plants were pretreated with a mixture of 250 mM suberic acid and sebacic acid each or 250 mM azelaic acid or buffer solution (infected control and mock control). (A) Plant height of control and unselected, infected plants during infection process 7, 14, 21 and 28 dpi. (B) Intensity of Mal-Glc-MICA 28 dpi in extracted hypocotyl tissue detected in metabolite fingerprinting. The samples include two biological replicates with three technical replicates each. Analysed, infected plants were smaller than 70 % of the control plant mean value. (C) Intensity of Mal-Glc-Prestressin 28 dpi in extracted hypocotyl tissue. Asterisks indicate intensity values with significant differences compared to the corresponding infected control in an unpaired Students t-test (* = p-value < 0.05). Error bars represent the standard deviation.

Due to these problems and the fact that the data were obtained only from a single experiment the results from the priming experiment are preliminary. The priming procedure might nevertheless be able to provide information about signalling functions of the identified infection markers.

4 Discussion

It was the aim of this thesis to identify metabolites that are crucial in the interaction of *V. longisporum* and its cruciferous host plants. For this a metabolite fingerprinting analysis was first optimized and then used. Identified substances should be tested in *in vitro* assays and should provide information about their role in the infection process. More than 70 metabolites were unequivocally identified within this work being either fungal substances or plant derived metabolites. They are summarized in supplemental tables (Tab. 4 + S 1). However functional assays provided only first evidence for a direct role in the plant-pathogen interaction of some of the substances.

4.1 Metabolites of the shikimate pathway detected in the culture supernatants of *V. longisporum* grown in a xylem like environment

In the attempt to identify putative mobile signals or toxins produced by *V. longisporum* in a xylem like environment, an *in vitro* assay was used. By means of metabolite fingerprinting analysis, metabolites from pathways like the shikimate pathway were detected to be altered. Metabolites from this pathway were not only altered when the fungus was grown in simulated xylem sap medium (SXM) but in provided xylem sap from healthy *B. napus* plants as well.

The biosynthesis of the three detected aromatic amino acids tryptophan, phenylalanine and tyrosine is based on the shikimate pathway, which provides branching points for various metabolic pathways and leads among others to the formation of the aromatic amino acids (Herrmann and Weaver 1999). From the branching point of chorismate tryptophan, phenylalanine and tyrosine are synthesized (Braus 1991). In organisms the feedback-controlled biosynthesis provides a balanced level of amino acids. In the provided media SXM and xylem sap the cultivation of *V. longisporum* seems to lead to an imbalanced amount of aromatic amino acids. This seems to activate the cross pathway control of *V. longisporum* and may be responsible for the degradation of the aromatic amino acids. This reaction could not be observed in the full medium PDB. Various organic acids especially the aromatic amino acids were found in decreased amounts in the culture supernatants of SXM and xylem sap (Fig. 20). Some might serve as carbon sources while other are converted into metabolites that can only be detected in *V. longisporum* culture supernatants. The acetylation of amino acids can be regarded as a frequently used conversion by *V. longisporum* leading to the formation of acetyltryptophan and acetylphenylalanine (Tab. 4). The acetylation of D-tryptophan has been described to be specific for fungi (Zenk and Schmitt 1964). Additionally, the hydroxylated derivative of tryptophan was detected (Tab. 4). Tryptophan was apparently also converted into different anthranilates. Anthranilate, acetylanthranilate and the most intensive derivative formylanthranilate (Fig. 21, Tab. 4) were detected in the culture supernatants from SXM and xylem sap. Furthermore

three indolic compounds (indole-3-carboxylic acid, indole-3-acetic acid and indole-3-lactic acid) were found to accumulate (Tab. 4). Indole-3-acetic acid is the well-known plant hormone auxin and is synthesized from tryptophan. Together with indole-3-lactic acid it was suggested to play a role in the microorganism-plant signalling (Schaepen et al. 2007). Indole-3-carboxylic acid was described to accumulate in *A. thaliana* roots upon infection with the fungus *Pythium sylvaticum* (Tan et al. 2004). Hence the indolic compounds were good candidates for extracellular, fungal metabolites produced in order to modify the hormone status of the host plants during infection.

Therefore it was suspected that the identified metabolites were not only found in provided xylem sap or xylem like medium but also in the xylem sap of infected *B. napus* plants. But neither the identified substances from the tryptophan metabolism nor any of the other accumulated markers in the *in vitro* cultivation experiment were detected in samples from infected plants. This either indicates that the metabolic situation *in vivo* differs too much from the situation in the *in vitro* assay due to the different environmental conditions like the constant supply of fresh xylem sap provided to the fungus by the transpiration stream in the xylem vessel. On the other hand the concentration of substances being specific for the fungus might be too low for detection *in planta.* Since relatively low levels of aromatic amino acids (e.g. 2 µM tryptophan) were measured by Singh et al. (2009) in the xylem sap of *B. napus,* derivatives like formylanthranilate might display considerably lower amounts than *in vitro* when they are produced and distributed within the plant. They might then be below the detection limits of the metabolite fingerprinting analysis or more likely they might be catabolized immediately by the plant. For fungi and bacteria formylanthranilate degradation was already described (Kamath and Vaidyanathan 1990, Max et al. 1999). Interestingly *Aspergillus niger* was found to convert the anthranilate derivative to catechol via 2,3-DHBA. If a similar process would have occurred in infected plants under our conditions it might additionally be an explanation for the increased levels of DHBAGs (Fig. 34 + 35). Therefore the detected metabolic situation *in vitro* might nevertheless reflect at least in part the situation *in vivo* although a different subset of metabolites was found in infected *B. napus* plants. This would explain the promising results from *B. napus* infection experiments with *V. longisporum* strains in which the mRNA of chorismate synthase was downregulated. These strains were shown to be less infective (Singh et al. 2009). The successful synthesis of tryptophan derived metabolites might therefore promote the infection process without being detectable in plant samples. By this the question if fungal compounds are transported within the plant especially in the early stages of infection is left open. As an alternative to small molecules also peptides or microRNA might be the transported molecules with signalling or toxic functions (Buhtz et al. 2010). These molecules would not have been detected by the chosen method.

The obtained results from the *in vitro* studies provide useful information about the metabolism of *V. longisporum* under different environmental conditions and they highlight how the fungus adapts its metabolism to the provided surrounding. This led to significantly different metabolite pattern in PDB, SXM and xylem sap. Nevertheless, some metabolic reactions were identified to occur in SXM and xylem sap environment. The identification of extracellular fungal substances offers the model of a putative metabolic response by the fungus in xylem sap environment which is based on a changed aromatic amino acid metabolism. If this metabolic consequences are valid for the situation *in planta* must be elucidated by even more sensitive methods. As for the differences to *V. dahliae* that were observed, further analysis might be able to pin down significant distinctions of the related strains that focus on different host plants. Preliminary results of the varying metabolite patterns indicate that this is likely to be related to the phytohormone metabolism.

4.2 *B. napus* specific infection markers point to a model for cyclobrassinin biosynthesis and degradation

The metabolic reaction in host plants can be divided into a species specific response and the accumulation of metabolites that seem to play a general role in the pathogen response in Brassicaceae. Moreover the response is found throughout the plant or only in specific areas. Members of all groups have been identified in this work. By depicting the accumulating infection markers of *B. napus* in Venn-Diagrams (Fig. 20, Fig. S2), general and matrix specific markers could be separated. Phytoalexins and phytoalexin related infection markers were detected ubiquitously but species specific, while matrix specific markers were identified in AWF (dicarboxylic acids and their derivatives). Oxylipins were found in the whole apoplast. In contrast, RA, pipecolic acid, SA and glycosylated SA derivatives were found in all analysed Brassicaceae. No metabolites of clear fungal origin have been detected in the analyses of infected plants.

The structure of the *B. napus* specific infection markers has been elucidated by fragmentation analysis. Specific fragments of the stressins (Tab. 5) and the MICAs (Tab. 6) are in accordance with fragments obtained from the phytoalexin cyclobrassinin. Therefore the obtained data strongly suggest that the infection markers represent cyclobrassinin related metabolites. The accumulation of these infection markers by application of $CuCl_2$ on *B. napus* plants demonstrated that the stressins are not only markers for biotic stress but also for abiotic stress (Fig. 50). This underlines the importance of the newly detected markers and highlights them as general stress related marker of *B. napus*. Moreover these findings indicate that these complex metabolites are synthesized by plant enzymes. That opens up the question about their relationship to each other and to cyclobrassinin.

A helpful concept for explaining their relations may be the camalexin biosynthesis pathway in *A. thaliana* recently published by Geu-Flores et al. (2011). The proposed pathway is depicted in Fig. 54 (left-hand side) in a simplified way.

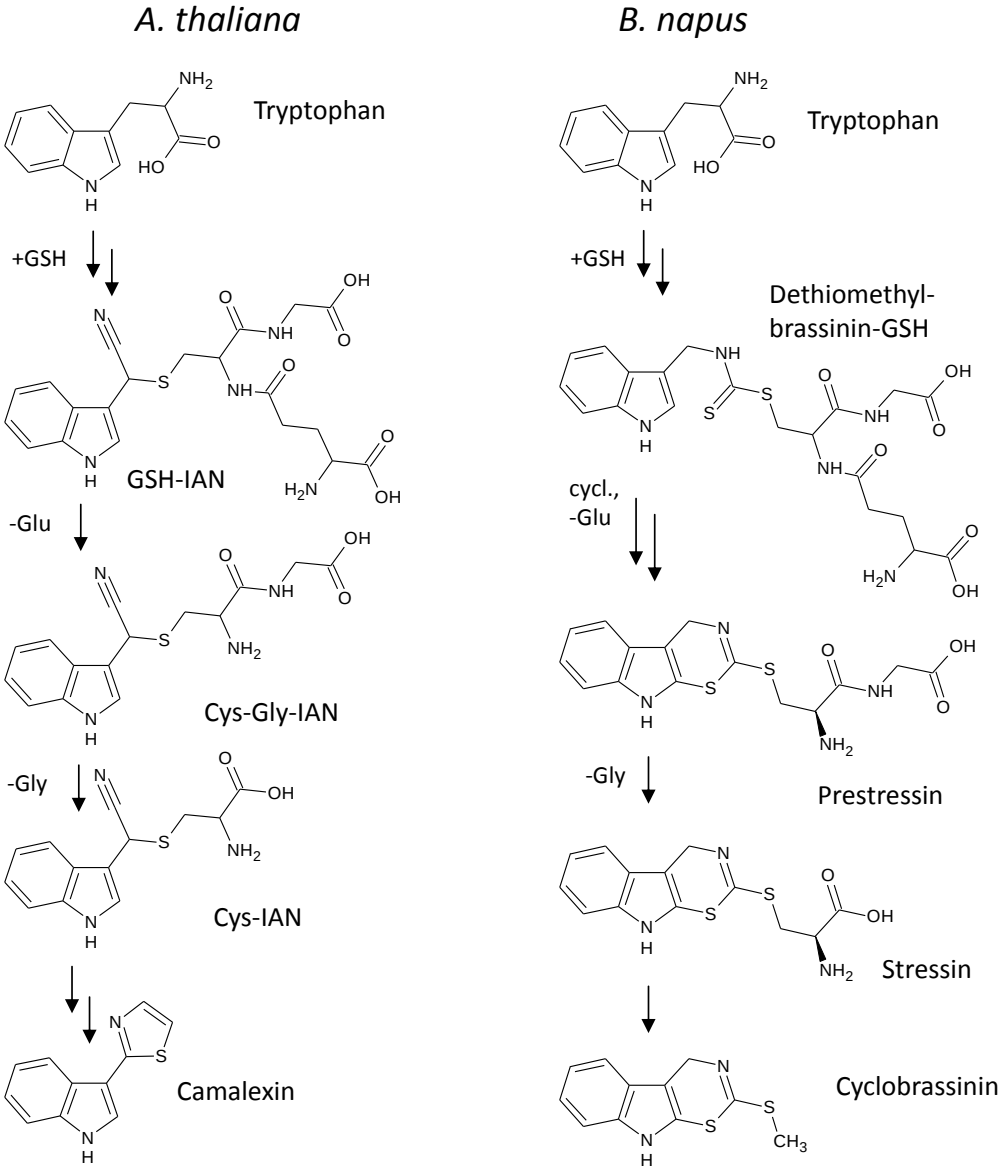

Fig. 54: Model of the phytoalexin biosynthesis in *A. thaliana* and *B. napus*
Scheme of the camalexin biosynthesis in *A. thaliana* as proposed by Geu-Flores et al. (2011) (left-hand side) and an analogue model for the putative biosynthesis of cyclobrassinin in *B. napus,* which involves the identified infection markers dethiomethyl-brassinin-GSH, prestressin and stressin (right-hand side). GSH = red. glutathione, IAN = indole-3-acetonitrile, cycl. = cyclisation.

It starts from the aromatic amino acid tryptophan, which is known to be converted via indole-3-acetaldoxime to indole-3-acetonitrile (IAN) by the enzymes CYP79B2/B3 and CYP71A13, respectively. The formation of the IAN glutathione conjugate (GSH-IAN) is postulated (Geu-Flores et al. 2011). GSH-IAN is subsequently processed by γ-glutamyl peptidases (GGP1/3) yielding Cys-Gly-IAN. In a next step glycine is proposed to be cleaved of by an until now unknown carboxypeptidase leading to the formation of Cys-IAN. Cys-IAN was detected as an intermediate in camalexin biosynthesis in *A. thaliana* (Böttcher et al. 2009). The enzyme CYP71B15 was shown to convert Cys-IAN in two subsequent reaction steps via dihydrocamalexic acid into the phytoalexin camalexin (Schuhegger et al. 2006).

It is known that the biosynthesis of cyclobrassinin in *B. napus* also starts from the precursor tryptophan (Pedras and Okinyo 2008). Bednarek et al. (2009) postulated a glutathione conjugate for the cyclobrassinin biosynthesis similar to the mechanism that was described by Geu-Flores et al. (2011). Cyclobrassinin itself seems to be a precursor for several other phytoalexins like brassilexin and rutalexin (Pedras and Yaya 2010) (Fig. 3). Astonishingly no other phytoalexins described for *B. napus* apart from cyclobrassinin were detected in the metabolite fingerprinting analysis (data not shown).

When the pathway for the camalexin biosynthesis of *A. thaliana* is transferred to *B. napus* a model for the biosynthesis of cyclobrassinin can be established (Fig. 54). This model takes the formation of a tricyclic compound as well as the infection markers prestressin and stressin into account. It also includes the formation of the glutathione conjugate, dethiomethyl-brassinin-GSH, from the precursor tryptophan as proposed by Bednarek et al. (2009). From this intermediate the infection markers prestressin, stressin and the phytoalexin cyclobrassinin can easily be formed. In subsequent steps a cyclization and the cleavage of the glutamate moiety are hypothesized leading to the detected infection marker prestressin. Analogue to *A. thaliana* the activity of a carboxypeptidase would lead to the formation of stressin by cleaving off glycine.

When the recorded datasets were searched for a marker that corresponds to the exact mass of the putative glutathione conjugate dethiomethyl-brassinin-GSH a significant infection marker with low intensity values ($[M+H]^+$ 496.1326, $C_{20}H_{26}N_5O_6S_2$, retention time 4.16 min) was detected. The infection related time course of dethiomethyl-brassinin-GSH as measured in extracted hypocotyl tissue of *B. napus* plants is displayed in Fig. 55 A.

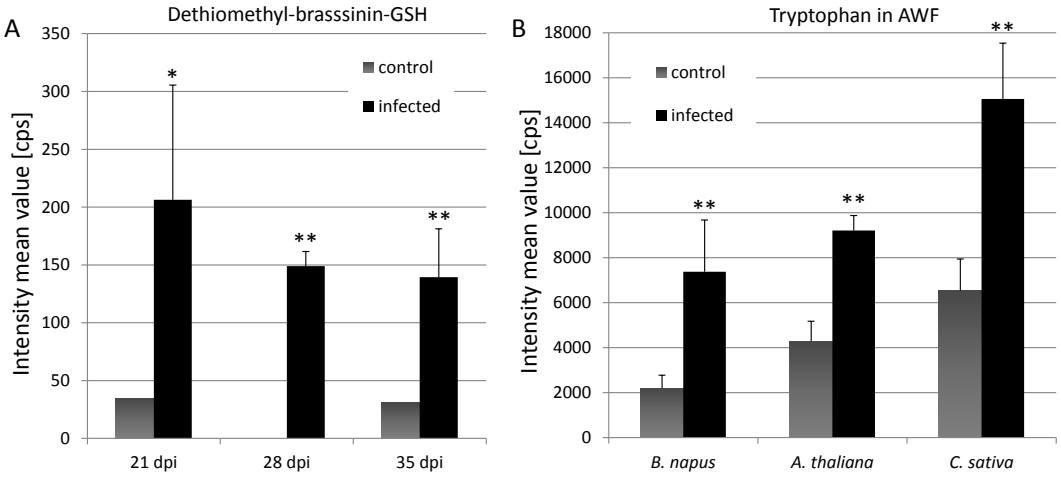

Fig. 55: Time course of an intermediate and a precursor of the phytoalexin biosynthesis in Brassicaceae
Accumulation of (A) dethiomethyl-brassinin-GSH in hypocotyl tissue from *B. napus* at late infection time points and of (B) tryptophan in AWF of *B. napus, A. thaliana* and *C. sativa* at 21 dpi. Data were determined from three biological replicates with two technical replicates each. Asterisks indicate intensity values with significant differences compared to the corresponding control in an unpaired Students t-test (* = p-value < 0.05; ** = p-value < 0.001). Error bars represent the standard deviation.

This finding strengthens the model for the cyclobrassinin biosynthesis as the three proposed intermediates and the end product could be detected to accumulate in an infection related manner. Furthermore tryptophan as the precursor of this pathway was detected. For *B. napus, A. thaliana* and *C. sativa* the intensity values for tryptophan measured from extracted AWF of all three species show a significant increase upon fungal infection (Fig. S 55 B). This indicates tryptophan as the common starting point in the phytoalexin biosynthesis of the three cruciferous species. The occurrence of glycosylated or malonylglycosylated forms of cyclobrassinin synthesized *in planta* has until now not been described. Glycosylated phytoalexins with and without malonic acid have only been described in *A. thaliana* so far. In this species the sugar moieties were attached for example to camalexin (Böttcher et al. 2009). These camalexin derivatives were detected in a non-targeted metabolic fingerprinting analysis to occur in the camalexin biosynthesis downstream of PAD3 enzyme activity. PAD 3 encodes an enzyme (CYP71B15) that can convert dihydrocamalexic acid into camalexin, the last step in the camalexin biosynthesis. Among others two hydroxycamalexin hexosides and *O*-malonyl-hydroxycamalexin hexoside were found to accumulate in *A. thaliana* upon biotic and abiotic stress treatment. The malonylglycosylated camalexin was described to be the most abundant camalexin derivative. This holds true for the detected cyclobrassinin related infection markers as well. The malonylglycosylated derivatives display the highest intensity levels among the stressins in the metabolite fingerprinting analysis (Fig. 56).

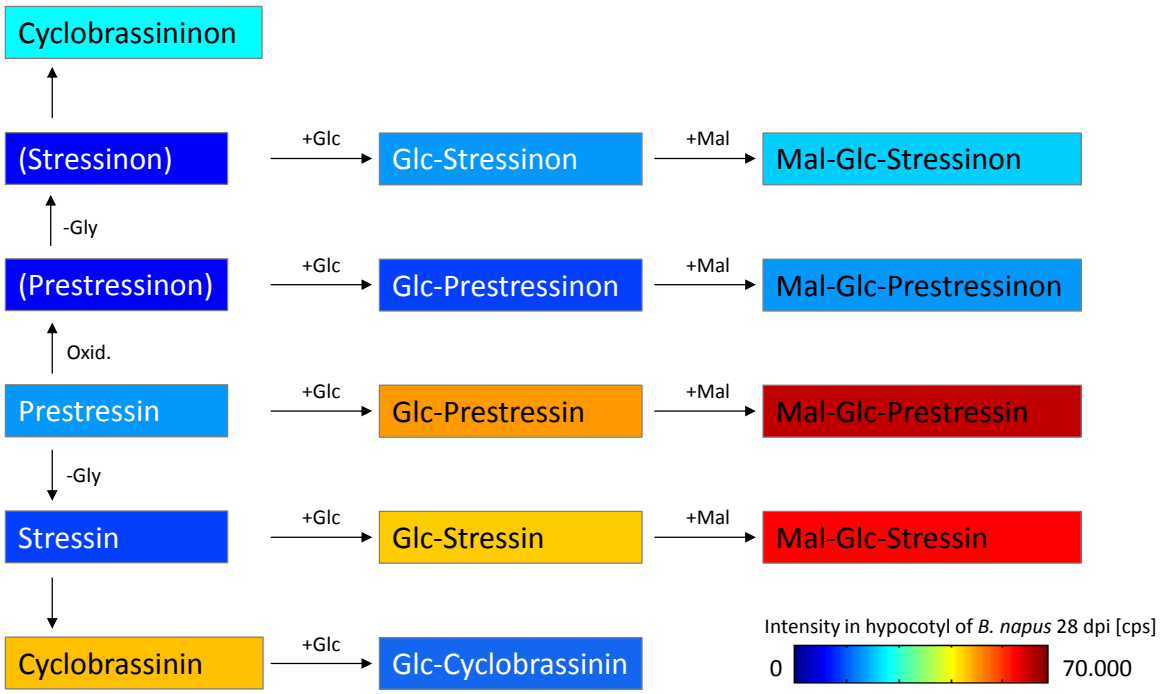

Fig. 56: Putative relationship of cyclobrassinin related metabolites
Oxidized metabolites are characterized by the ending –on. All metabolites are colour-coded by their intensity measured in the infected state 28 dpi in extracted hypocotyl of *B. napus* as indicated by the attached key code. The compounds in brackets stressinon and prestressinon has not been detected by metabolite fingerprinting.

In contrast to *A. thaliana* the glycosylated form of the phytoalexin was only detected in minor amounts and cyclobrassinin itself could not be detected as a malonylglycosylated derivative. In Fig. 56 the metabolites that may be involved in the biosynthesis are organized due to their proposed relationship to each other and are colour-coded by the detected intensity levels in the hypocotyl of infected plants 28 dpi.

The scheme in Fig. 56 couples the putative biosynthesis intermediates prestressin and stressin to their glycosylated derivatives indicating that malonylglycosylation might lead to end products that accumulate in the infected plant. This would explain the high levels of Mal-Glc-prestressin and Mal-Glc-stressin shown by the red colour code in Fig. 56. On the other hand an enhanced ionisation performance may explain the high intensity levels as well. This has to be considered for all presented data and checked by quantitative measurement of the corresponding standards if available. Alternatively, quantification for the infection markers could be based on UV-Vis detection if the absorption coefficient is available. A suitable method would have to be established.

Additionally, the oxidized metabolites indicated by the ending –on are included in Fig. 56. Assuming that the biosynthesis of cyclobrassininon is analogue to that of cyclobrassinin the proposed intermediates would be prestressinon and stressinon. These proposed metabolites could not be detected in the analysis. All oxidized forms that were detected (cyclobrassininon and the glycosylated

stressinons) showed a lower intensity level (less than 10 %) than the corresponding non-oxidized metabolites (e. g. Glc-prestressinon vs. Glc-prestressin) (Fig. 29, Fig. 30). Therefore the levels of the putative intermediates prestressinon and stressinon are supposed to be lower than for prestressin and stressin which were low intensity metabolites too (about 800 and 500 cps, respectively). It is therefore likely that prestressinon and stressinon are not recorded due to the detection limits in the metabolite fingerprinting analysis used since expected levels of less than 100 cps would not lead to a significant intensity profile. An alternative explanation could be a final oxidation step of all metabolites from the putative cyclobrassinin biosynthesis. This would supersede the model of a separate cyclobrassininon biosynthesis. On the other hand this scenario would not explain why the stressin related compound and its glycosylated forms do not occur in an oxidized state unless the closure of the third ring is needed for the oxidation step.

Whether the newly described metabolite cyclobrassininon can be regarded as a phytoalexin is still unclear since its antifungal activity has to be confirmed. This was difficult to show, because it was not possible to purify cyclobrassininon in sufficient amounts from plant material or to synthesize it. In *A. thaliana* no oxidized forms of camalexin and its precursors have been described (Böttcher et al. 2009, Geu-Flores et al. 2011).

The other cyclobrassinin related metabolites that could be identified by metabolite fingerprinting analysis in combination to fragmentation analysis are most likely not involved in the biosynthesis but may be part of the degradation of the phytoalexins. A new model based the degradation of on cyclobrassinin and cyclobrassininon, includes the structurally elucidated infection markers from the group of MICAs (Fig. 57).

It is suggested that the markers that were shown to include a carboxyl group (MICA (6), Glc-MICA (7), Mal-Glc-MICA (8), Glc-MICA-Glc (9) and Mal-Glc-MICA-Glc (10)) derive from cyclobrassininon whereas the decarboxylated derivatives (decarboxy-MICA (2), decarboxy-Glc-MICA (3), decarboxy-Mal-Glc-MICA (4)) might be cyclobrassinin degradation products. Similar to the metabolism of the stressins (Fig. 56) at first a glycosylation step can be observed followed by the addition of a malonic acid. The malonylglycosylated forms are again the most abundant markers detected (Fig. 31). For the infection markers Glc-Mica-Glc (9) and Mal-Glc-MICA-Glc (10) a second glycosylation can be observed. Both bisglycosidic metabolites were not detected in the abiotic stress treatment. It is unclear if this *O*-glycosylation is performed by *B. napus* or if the second glucose moiety is attached by *V. longisporum* enzymes in order to detoxify these substances. A fugal participation therefore cannot be excluded. It is tempting to suggest a detoxification by *V. longisporum.* A putative glucosyltransferase for this enzymatic step could be a homolog to the enzyme (VDAG_02071) identified to be responsible for pathogenicity in *V. dahliae* on *Nicotiana benthaminana* (Klosterman

et al. 2011). Alternatively 48 h of $CuCl_2$ treatment might have not been enough time to form these putative phytoalexin degradation products or the levels formed were below detection limits. Detoxification by glycosylation of phytoalexins as has been shown for several fungal species (Sexton et al. 2009).

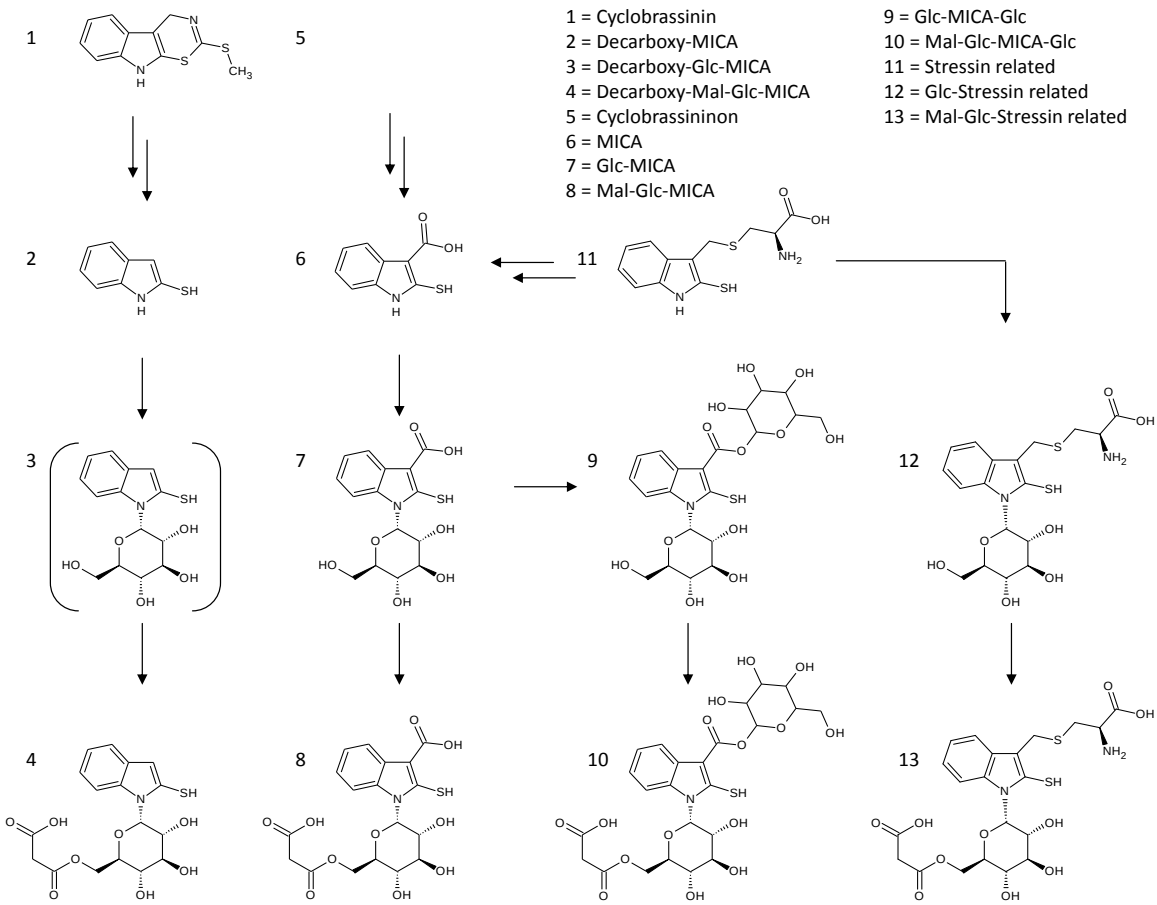

Fig. 57: Model of the degradation of cyclobrassinin and related metabolites in *B. napus*
Scheme of the putative degradation of cyclobrassinin, cyclobrassininon and the stressin related metabolite in *B. napus* involving a group of identified infection markers (MICAs). The markers including a carboxyl group (6-10) are supposed to derive from cyclobrassininon whereas the decarboxylated forms (2-4) seem to derive from cyclobrassinin. In contrast to all other metabolites the compound in brackets decarboxy-Glc-MICA (3) has not been detected by metabolite fingerprinting. Stressin related compounds and its glycosylated forms (11-13) are suspected to contribute to the formation of MICA (6).

Decarboxy-Glc-MICA (Fig. 57, (3)) could not be detected in the metabolite fingerprinting analysis in contrast to the infection markers decarboxy-MICA (2) and decarboxy-Mal-Glc-MICA (4). The MS/MS analysis of decarboxy-Mal-Glc-MICA offers an alternative structure that might carry an acetylation and the carboxyl group instead of the malonyl group (see supplemental data chapter 7.2, page 151). Since acetylation reactions have been shown to be involved in detoxification of e.g. deoxynivalenol (Karlovsky 2011) this could be an alternative to the addition of malonic acid. It would be the only

acetylation observed in this infection related context and it is not described for phytoalexin detoxification so far. The decarboxy-MICA would then be possibly a degradation product from MICA and would not be converted further. This alternative hypothesis would imply that the degradation of cyclobrassinin and cyclobrassininon would result only in the formation of MICA as a starting point of further conversions.

Included in Fig. 57 are also the stressin related metabolites (11-13). They also might either occur in the structural conformation depicted here or in an alternative structure since the binding position for the cysteine moiety could not be unequivocally elucidated (see supplemental data chapter 7.2, page 146). The precise relation between the stressin related substances and the degradation products of the phytoalexins is still unclear but assuming the cleavage of cysteine and a subsequent oxidation they might contribute to the formation of MICAs. In any case the data obtained from fragmentation analysis show a strong relation to the group of phytoalexin related infection markers. A NMR analysis of the newly described metabolites could confirm the tentative assignments obtained by fragmentation analysis. Currently the collection of material and the subsequent purification of the most complex member Mal-Glc-prestressin is performed in the group of Prof. Karlovsky (Department of Molecular Phytopathology, Georg-August-University, Göttingen, Germany).

Since biosynthesis and degradation of cyclobrassinin and the related compounds seems to occur simultaneously in the infected plant tissue there must be a reason why cyclobrassinin does not accumulate to higher levels. For camalexin in *A. thaliana* it has been demonstrated that this compound is phytotoxic above a certain level (Roger et al. 1996). This can explain the multiple metabolic transformations that were observed downstream of camalexin to be detoxification reactions (Böttcher et al. 2009). Many transformations performed by fungal enzymes to detoxify phytoalexins have been investigated by Pedras et al. (2011 b). It was shown that *Botrytis cinerea* is able to convert camalexin into indole-3-carboxylic acid yielding a less toxic substance structurally similar to MICA. Based on these results one may assume that also cyclobrassinin would be phytotoxic when accumulating in the plant tissue. Therefore *B. napus* may have to balance the level of cyclobrassinin and cyclobrassininon. The putative degradation products (Fig. 57) were mainly detected in the roots where the soil-borne fungus is present for the longest time (Fig. 31). In the short period of applying abiotic stress only minor amounts of the MICAs were detected (Fig. 50). These results could indicate that a longer time of stress exposure is needed for the synthesis of MICAs than for the stressins. To test this very late time points after infection e.g. eight weeks should be analysed. The formation of MICAs should then be strongly enhanced also in the upper tissues. Alternatively root specific formation of MICAs may occur.

With the structural elucidation of the *B. napus* specific biotic and abiotic stress markers a new model for the biosynthesis of cyclobrassinin analogue to camalexin in *A. thaliana* could be created. Also a model for the relationship of the MICAs as degradation products to the phytoalexin is proposed. Both pathways contain a high amount of glycosylated and malonylglycosylated derivatives, which indicate either detoxification steps or the attempt to increase the solubility of the involved substances. Various mechanisms of cyclobrassinin detoxification by fungal pathogens including glycosylation have been reviewed by Pedras et al. (2011) but until now no detoxification of its phytoalexins by *B. napus* was described indicating a balancing of the cyclobrassinin levels *in planta*.

4.3 Similarities and differences in the metabolic reaction to *V. longisporum* infection of different Brassicaceae

In addition to the species specific cyclobrassinins, infection markers were identified that accumulate upon fungal invasion in two or three of the analysed crucifer species. These markers and their relation to known pathogen response mechanisms are described in the following. It must be kept in mind that the analysis of *A. thaliana* is based only on the data from AWF in comparison to the comprehensive overview obtained for *B. napus* and *C. sativa*. However additional data are available from an accomplished PhD thesis (König 2011). Additionally, only the biotic stress by *V. longisporum* infection was applied to *A. thaliana* and *C. sativa* leaving the question open how an abiotic stress would act on the related metabolic pattern. Common markers can nevertheless hint to a similar response to biotic stresses in the plant family of Brassicaceae.

As was already mentioned above, tryptophan is an infection marker that accumulates in the AWF of all three analysed species at 21 dpi (Fig. 55 B). It nevertheless must be stated that the precursor of the phytoalexin biosynthesis cannot be regarded as an infection marker in *B. napus* in other samples and at later time points. In *B. napus* and *C. sativa* the biosynthetic products cyclobrassinin and camalexin, respectively, could be identified as infection markers (Fig. 32, Fig. 44) whereas in *A. thaliana* camalexin was not detected to accumulate upon fungal infection. This is in accordance with the data generated from infected *A. thaliana* root tissue (König 2011).

Another metabolite that might be connected to the phytoalexin biosynthesis is RA. Bednarek et al. (2009) postulated that a degradation of the glutathione conjugate from the phytoalexin biosynthesis would lead to the formation of RA and the corresponding amine. The amine (indole-3-methylamine for dethiomethyl-brassinin-GSH) however could not be detected in metabolite fingerprinting analysis whereas RA was detected in all analysed Brassicaceae species (Fig 33, Fig. 46). RA was first discovered in the crucifer *Raphanus sativus* var. *hortensis* (Hase et al. 1983). In human metabolism

RA is used as an indicator for the exposure with CS_2. An established monitoring is able to detect RA in urine samples (Amarnath et al. 2001). In plants RA was until now only described to accumulate in roots of *A. thaliana* after challenge with fungal pathogens (Bednarek et al. 2009, Bednarek et al. 2005). In the diploma thesis of Maren Bornemann (2010) an accumulation of RA in *A. thaliana* after wounding was demonstrated illustrating the more general role of RA in stress situations.

Accumulation of RA in *B. napus* and *C. sativa* is described to our knowledge for the first time in the work at hand. RA is the most general and ubiquitous infection marker detected in the metabolite fingerprinting analyses and it was found to accumulate in *B. napus* also in response to abiotic stress (Fig. 51). Therefore it can be concluded that RA is part of a common stress response in the Brassicaceae. It seems unlikely that RA is a degradation product from the glutathione conjugates in phytoalexin biosynthesis depicted in Fig. 54 since these intermediates differ in *A. thaliana* and *B. napus*. Additionally, RA is found predominantly in the xylem sap of *B. napus* whereas the postulated precursor dethiomethyl-brassinin-GSH mostly occurs in the hypocotyl tissue (Fig. 33, Fig. 55 A). A connection of RA to the biosynthesis of the phytoalexins or to the related glucosinolates is nevertheless very likely and it seems to include a modification and a biosynthetic step that is conserved in all three species and putatively even in all Brassicaceae. A direct role of RA in stress related responses it is not coupled to an antifungal activity against *V. longisporum* but might rather be a mobile signalling function indicated by the high amounts detected in the xylem sap of *B. napus*. In the flotation assay no effect caused by exogenous RA was detected (Fig. 49). Priming of plants with RA prior to infection might lead to more conclusive results. Alternatively, RA might be a degradation product without any function in the stress response.

The glucosinolates in *A. thaliana* as related substances are supposed to be synthesised in parallel to the phytoalexin camalexin as suggested by Geu-Flores et al. (2011). Therefore the cyclobrassinin biosynthesis seems not to be based on the degradation of glucosinolates as was proposed by Bednarek et al. (2009). The glucosinolate biosynthesis nevertheless was induced very early in the infection process. Several glucosinolates show an infection related, but not reliable accumulation at 5 dpi which faded away during the next days. Prominent glucosinolates in *A. thaliana* roots like 4-hydroxy-I3G and several aliphatic species (König 2011) were not found to accumulate in *B. napus*. The high biological variation in the detected intensities of glucosinolates makes it difficult to obtain significant results and find reliable infection markers in this substance class.

Similar to RA another ubiquitous infection marker was found to be pipecolic acid (2-piperidine carboxylic acid). It must be stated that the elucidated structure would also fit to the 3- or 4-piperidine carboxylic acid isomers since only the carboxyl group and the nitrogen containing ring piperidine were identified but only pipecolic acid is described for biological systems. No other related

metabolites have been found for the lysine derived compound. It does not seem to have any direct connection to the other identified infection markers apart from the incorporation of nitrogen which is shared to the amides identified in the AWF and the polyamines. In the AWF the lowest levels of pipecolic acids were detected (Fig. 37). It was suggested that it might be converted into other forms but at least the elucidated AWF infection markers, like the monoamide derivatives of the dicarboxylic acids are not congruent to an open form of pipecolic acid. Furthermore no derivatives were detected that would explain the different chain lengths found for the AWF specific markers. Possibly pipecolic acid may be a degradation product from the polyamines, which were also found to accumulate upon infection. It might be that pipecolic acid related but not annotated substances are still hidden in the recorded datasets that could solve the question of a putative connection to the other markers. Also the role of pipecolic acid remains unclear since it was never described to be related to plant-pathogen interactions. An inhibitory effect to *V. longisporum* could not be observed in the toxicity assay although it was shown to inhibit the growth of *Aspergillus sp*. (Brenner and Romeo 1986). Moreover pipecolic acid did not induce an infection related pattern in the flotation assay (Fig. 49). Priming of plants with pipecolic acid might give more information about a putative signalling function or if this metabolite is increased due to secondary effects. Pipecolic acid is nevertheless accumulated in AWF of *A. thaliana, B. napus* and *C. sativa* in significant amounts after the infection with *V. longisporum* (Fig. 37, Fig. 46) and in *B. napus* additionally after abiotic stress treatment (Fig. 51). Therefore a common regulation in Brassicaceae for the increase of pipecolic acid due to biotic and abiotic stress can be suggested.

Other identified infection markers are well-described in plant-pathogen interactions. The phytohormone SA has been shown to be involved in the defence against biotrophic pathogens (Glazebrook 2005) and is part of a cross-talk network that also involves the phytohormones jasmonic acid (JA) and ethylene as demonstrated in *A. thaliana* upon pathogen challenge (Leon-Reyes et al. 2010). In the reaction to *V. longisporum* an accumulation of JA was only observed in the AWF of *A. thaliana* (Floerl et al. submitted) whereas in *B. napus* and *C. sativa* only SA and SA derivatives were detected as infection markers (Fig. 34, Fig. 35, Fig. 46). No evidence of an involvement of JA, ethylene or ABA pathways in *B. napus* was detected, confirming the findings of Ratzinger et al. (2009). SA and the glycosylated form SAG were for the first time identified as markers for *V. longisporum* in *B. napus* by Ratzinger et al. (2009) but a more comprehensive analysis could show that SA itself accumulates in high amounts only in the xylem sap of *B. napus* while enhanced levels of SAG were detected ubiquitously in the plant with the exception of leaf tissue (Fig. 34). SAG was found to be enriched already at early time points after infection (Fig. 35) and is an infection marker also in *A. thaliana* and *C. sativa* (Fig. 36, Fig. 46). It also accumulated in the response to abiotic stress in *B. napus* (Fig. 51) indicating that elevated SAG levels are not specific for *V. longisporum* infection as assumed by

Ratzinger et al. (2009) but hints to general stress situations. Unchanged SAG levels in *B. napus* after infection with *V. dahliae* (Ratzinger et al. 2009) suggest that the infection was at least incomplete. This is supported by the lack of disease symptoms as reported by Eynck et al. (2007). Additionally, two SA derivatives, the dihydroxybenzoic acid glucosides (DHBAG) were identified as infection markers in the three crucifer species. 2,5-DHBAG was found to accumulate more in the aboveground plant tissue whereas 2,3-DHBAG was predominantly found upon infection in the root tissue (Fig. 34). For the biosynthesis of SAG two glucosyltransferases have been identified in *A. thaliana* which can either lead to the formation of SAG or SA glucose ester (Dean and Delaney 2008). In this work SA glucose ester was not detected in any sample. Whether the DHBAGs are formed from the corresponding DHBAs by glucosyltransferases as suggested by Bartsch et al. (2010) is unclear. Since the free DHBAs have not been detected in the metabolite fingerprinting analysis a hydroxylation of SAG as proposed by Dean and Delaney (2008) seems more likely. While the role of SAG is defined as a detoxification and vascular storage form of SA, the function of the DHBAGs is not known (Dean and Delaney 2008). The non-glycosylated 2,5-DHBA has been described to be involved in the defence signalling of tomato plants (Bellés et al. 1999) and an antifungal activity was reported (Lattanzio et al. 1994). In a toxicity test 2,5-DHBA shows an inhibitory effect also on *V. longisporum* (Fig. 52) whereas SA did not influence the mycelial growth.

The accumulation of the SA derivatives is part of the common metabolite pattern observed in the Brassicaceae although differences in the distribution indicate variable levels in the different species. For example no 2,5-DHBAG could be detected in the hypocotyl of *C. sativa* (Fig. 46) whereas it was the most intensive SA related marker there in *B. napus* (Fig. 34). This is supported by the absence of 2,3-DHBA-xyloside in the metabolite fingerprinting analysis of *B. napus* and *C. sativa*. 2,3-DHBA-xyloside is also a SA derivative that was identified to accumulate in *A. thaliana* after being challenged with pathogens (Bartsch et al. 2010) and that might be species specific. A common feature is the SA based pathogen response although the exact distribution within the plants and within the plant species must be elucidated further. Interestingly, high levels of SA were reported to induce the synthesis of glutathione and vice versa (Mateo et al. 2006). This might imply a connection of the SA related substances to the phytoalexin biosynthesis which is based on the formation of a glutathione conjugated intermediate.

9,12,13-trihydroxy-10-octadecenoic acid (TriHOE) and 9,12,13-trihydroxy-10,15-octadecadienoic acid (TriHOD), two infection markers of the apoplastic fluids of *A. thaliana* and *B. napus* (Fig. 38) belong to the substance class of oxylipins (Feussner and Wasternack 2002). They are most likely synthesized from linoleic acid and α-linolenic acid (Stumpe et al. 2006). This includes a first enzymatic step by a lipoxygenase followed by either a peroxygenase or an epoxy alcohol synthase. Subsequently an

epoxide hydrolase converts the epoxide into the trihydroxy fatty acid (Hamberg and Hamberg 1996, Hamberg 1999). An alternative biosynthetic pathway could include the degradation of cutin monomers as described for *threo*-9,10,18-trihydroxystearic acid (Schweizer et al. 1996). TriHOD was first discovered in the cyanobacterium *Lyngbya majuscule* and was therefore named malyngic acid (Cardellina and Moore 1980). Both identified oxylipins have been found to accumulate in rice after infection with *Pyricularia oryzae* (Kato et al. 1983). TriHOE showed antifungal activity against the black rot fungus (Masui et al. 1989) and an organic extract from *Pseudomonas aeruginosa* cultures containing TriHOE inhibited mycelial growth amongst others of *V. dahliae* (Martin-Arjol et al. 2010). Therefore an inhibition of *V. longisporum* growth by the oxylipins TriHOE and TriHOD seems to be likely but must be tested nevertheless since the antifungal activity of oxylipins differs significantly due to the number and position of hydroxyl groups (Hou and Forman 2000, Prost et al. 2005). The inhibitory effect is suspected to act more on physiochemical properties of the oxylipins than on interaction with a specific target (Prost et al. 2005). In barley priming with TriHOE and TriHOD led to a reduced infection with *Blumeria graminis* either by a systemic effect or due to a direct inhibition (Cowley and Walters 2005).

It is supposed that pathogenic fungi might hijack parts of the host oxylipin pathway to facilitate the infection process by increasing their mycotoxin synthesis and enhance the spore production (Gao and Kolomiets 2009), but this effect seems to be more related to the psi (precocious sexual inducers) factors than to trihydroxy fatty acids. However, the precursors in the biosynthesis of TriHOE and TriHOD can compete for the function of psi-factors (Brodhagen et al. 2008). It must be stated that these fungal oxylipins were not detected in this plant-pathogen interaction so far. The two identified oxylipins are most likely plant derived species since relevant amounts were detected as basal levels in the control plants (Fig. 38). Due to their accumulation only found in the apoplast of *B. napus* and *A. thaliana* an either direct or indirect mobile function against the fungal invader can be assumed. In *C. sativa* no infection related changes in the oxylipin levels could be detected (data not shown).

A small group of infection related metabolites – the polyamines – could only be detected by a targeted measurement. Polyamines have been shown to accumulate in response to fungal pathogens e.g. in barley after infection with powdery mildew (Walters 2000). This also holds true for the infection of *B. napus* with *V. longisporum* where they accumulate in the hypocotyl (Fig. 42). Their changed levels in barley are related to the systemic protection what might connect them to the systemic effect observed for the oxylipins (Cowley and Walters 2005). The polyamines contain nitrogen atoms, a feature that can be found also in the infection marker pipecolic acid and the amide derivatives of the AWF infection markers (Fig. S 8). A connection of these compound groups still has to be demonstrated. Until now no targeted analysis of the polyamine levels in *A. thaliana* and

C. sativa plant material infected with *V. longisporum* was performed but a general effect can be assumed due to the polyamine accumulation even in the distant relative barley. Therefore an increase in polyamine levels in infected *A. thaliana* and *C. sativa* can be expected.

4.3.1 The leaf apoplast includes a specific substance class of infection markers

When metabolite fingerprinting analysis was performed for the various samples taken from different parts of *V. longisporum* infected plants it became obvious that the fluid obtained from the apoplastic space in leaves (AWF) differed significantly not only from the tissues but also from the apoplastic xylem sap. The accumulation of different proteins in both fluids (Floerl at al. 2008, Floerl et al. submitted) as well as the accumulation of special infection markers indicates that the AWF represents a specific zone within the apoplastic space. The saturated dicarboxylic acids accumulate after *V. longisporum* infection in the AWF of *A. thaliana* and *B. napus* (Fig. 40) but show constant levels in *C. sativa* (data not shown). They have not been described to be enhanced in a homologous series before. Only azelaic acid was found in increased levels in leaves of *Pisum sativum* after infection with the phytopathogenic *Pectobacterium atrosepticum* (Mukhtarova et al. 2011). It also can be induced in sweet pepper by the application of cellulases (Sato et al. 2011). It is still unclear where the dicarboxylic acids derive from. For the pimeloyl moiety needed for biotin biosynthesis two pathways depending on the fatty acid biosynthesis have been described. Isotopic labelling showed nevertheless that free pimelic acid is not an intermediate in the biotin biosynthesis (Cronan and Lin 2011). Furthermore the proposed pathways could not explain the formation of the various chain lengths that were detected in the AWF. Alternatively a degradation of suberin which includes ω-hydroxy fatty acids and dicarboxylic acids might lead to the formation of the infection markers but due to the incorporated chain lengths (>20 carbon atoms) this seems unlikely. Azelaic acid seems nevertheless to be a ubiquitously distributed compound detected in various plant families like Lamiaceae, Convolvulaceae and Solanaceae (Sato et al. 2011), a finding expanded in this work to different Brassicaceae species. Azelaic acid was shown to have no antifungal effect (Jung et al. 2009). This result was confirmed for *V. longisporum* and *V. dahliae* not only for azelaic acid but also for the other members of the homologous series identified as infection markers as well (data not shown). Therefore a direct inhibitory effect can be excluded. Moreover Jung et al. (2009) reported a successful priming of *A. thaliana* with azelaic acid prior to *Pseudomonas syringae* infection. The priming of *A. thaliana* was found to result in an accumulation of SA and to lead to systemic acquired resistance (SAR) against the virulent bacterial strain. Priming prepares the plant to the pathogen attack but on a lower energetic level than is required for the resistance induction (Yi et al. 2009). When the priming procedure was transferred to *B. napus* preliminary results indicate no significantly enhanced resistance (Fig. 53 A). This was neither observed on physiological level (like reduced stunting) nor on metabolical level. The reduced amount of the stressins and MICAs in plants primed

with azelaic acid (Fig. 53 B + C) might indicate a shift in the cyclobrassinin metabolism but it did not result in an accumulation of the phytoalexin (data not shown). In contrast the treatment of *C. sativa* with the SA analogue benzothiadiazole (BTH) led to an increase in the camalexin levels (Henneken 2001). This indicates that the application of BTH - an inducer of systemic acquired resistance - is comparable to a treatment with the fungicide $CuCl_2$ and that both substances serve as factors for phytoalexin elicitation. The role of azelaic acid therefore seems inconsistent since the detected increase of SA levels in the xylem sap hints to a successful priming whereas the unchanged level of cyclobrassinin contradicts this. Nevertheless the biosynthesis and degradation of cyclobrassinin seems to be influenced by priming with azelaic acid. In order to obtain reliable results the experiment must be repeated and possibly the experimental design including sample selection must be varied. From the preliminary results, obtained in this work not enough evidence is found to claim a successful priming of *B. napus* by azelaic acid.

Additional to the group of the dicarboxylic acids four other groups of infection markers were identified in the AWF. While the dicarboxylic acids and the monoamide derivatives were infection regulated in *B. napus* and *A. thaliana*, the diamides, alcohol and aldehyde derivatives showed only in *B. napus* plants an infection related intensity pattern. This links the dicarboxylic acids directly to the monoamides and suggests the other groups to be subsequent modifications. This would be the insertion of a second amino group or two successive reduction steps. Alternatively, the dicarboxylic acids may be derived from the alcohol and aldehyde derivatives. A putative model for the relationship of the AWF marker groups is displayed in Fig. 58. The corresponding carboxylic acids were not detected.

The amide derivatives are poorly described in literature. Only the C12 and C13 monoamides were detected and tentatively assigned in a metabolic profiling approach of different tomato cultivars (Gómez-Romero et al. 2010) but no connection to plant-pathogen interactions was described before. Therefore this work demonstrates for the first time not only the involvement of azelaic acid but also of other dicarboxylic acids and various amide derivatives in the biotic response to fungal invasion. If the AWF markers are specific for *V. longisporum* infection or are part of the general stress response in *B. napus* is still to be elucidated. The detection of increased levels of azelaic acid and SA in *Capsicum annuum* after cellulose treatment points to a general role of the AWF infection markers (Sato et al. 2011). The AWF of $CuCl_2$ elicitated leaves should be able to provide more information about biotic and abiotic stress specificity of the newly described infection marker groups.

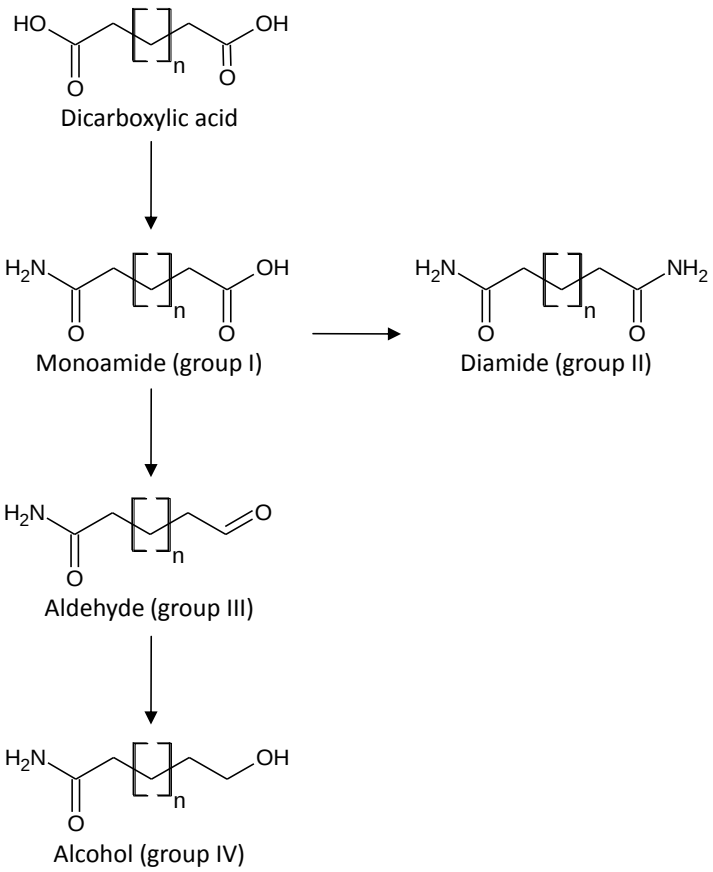

Fig. 58: Model of putative pathway for dicarboxylic acids and their amide derivatives
Dicarboxylic acids and their amide derivatives accumulate in AWF in *B. napus* and *A. thaliana* after fungal infection. The monoamides (group I) might be connected to the dicarboxylic acids and may then be the starting point for either insertion of a second amino group (group II) or subsequent reduction steps (group III and IV).

It can be concluded that the three analysed Brassicaceae species share a common subset of infection related metabolites (e.g. RA, pipecolic acid, SAG). Other metabolic pathways like the phytoalexin biosynthesis lead to different end products and intermediates (cyclobrassinin vs. camalexin). In the apoplastic space the relationship of *B. napus* and *A. thaliana* appears to be closer than to *C. sativa* (Fig. 45) as two groups of AWF infection markers and the accumulated oxylipins are common features in the two species after infection with *V. longisporum.* Many of the identified infection markers found by the metabolite fingerprinting analysis have already been described in plant-pathogen interactions (e.g. phytoalexins, SA and polyamines) whereas the infection related accumulation was described for the first time for the amide derivatives and for pipecolic acid. For most markers in *B. napus* a role in biotic as well as in abiotic stress could be demonstrated, which highlights the general importance of the identified substances.

4.3.2 *A. thaliana* can only partly substitute *B. napus* in the study of *V. longisporum* infection processes

In order to understand the interaction of *V. longisporum* with its host plants several analyses have been performed by using the model plant *A. thaliana* as a substitute for the natural host *B. napus*. The transcriptome analysis in roots, the identification of *V. longisporum* induced genes as well as the analysis of metabolic pathways influenced by the fungal infection have been performed in *A. thaliana* (Tappe 2008, Iven 2009, König 2011). Due to the availability of mutants, the option of selective genetic manipulation and its affiliation to the same plant family this is without any doubt the first choice. The results of this work nevertheless show that the obtained information not always can be transferred to *B. napus*. The metabolic markers that were found to accumulate in *A. thaliana* upon *V. longisporum* infection like sinapoyl glucose, coniferin and various lignans from the phenylpropanoid pathway (König 2011) were not detected in increased amounts in *B. napus*. For the AWF a different subset of up-regulated proteins was found in both species (Floerl et al. 2008, Floerl et al. submitted). This suggests to result in a differential metabolome in this compartment as was indeed found e.g. in respect to three of the five AWF specific marker groups (Fig. 58). Even the xylem sap that was analysed from healthy plants of both species revealed significant differences (Fig. 22). This means that different environmental conditions are provided to the entering fungus. How these changes in its environment have consequences on the fungal metabolism was shown for various provided media (PDB, SXM, xylem sap) in *in vitro* experiments. There the provided surrounding influenced significantly the subset of metabolites produced by the fungus. Therefore the different conditions in the xylem vessels of both species might lead to variable fungal reactions which on their part influence the plant defence response. Since *A. thaliana* is not the natural host of *V. longisporum* the increase of phenylpropanoids which are known to be part of the non-host resistance (Dixon and Paiva 1995) is to be expected. In contrast the accumulation of phenylpropanoids in *B. napus* is missing, which points to a more specialized plant-pathogen interaction. On the other hand most identified infection markers in *B. napus* were general stress markers and seem not to be coupled to a specific response to *V. longisporum*. It cannot be excluded that specifically enhanced metabolites were still not identified in the recorded data sets since they might be e.g. markers without a database hit or a low intensity. Alternatively, they might not be detected by the used method of metabolite fingerprinting (e.g. MTBE-extraction and ESI ionisation). The analysis of AWF from *A. thaliana* and various samples from *B. napus* however showed that there are similar metabolic pathways involved. They result in both plant species in the accumulation of e.g. SAG, RA, pipecolic acid and dicarboxylic acids. The increase of species specific but nevertheless related phytoalexins was demonstrated in *B. napus* but the corresponding camalexin was not found in *A. thaliana* although its

biosynthetic pathway was shown to be up-regulated on transcription level upon *V. longisporum* infection (Iven 2009).

Taken together it can be concluded that many similar, stress induced pathways seem to be commonly enhanced in *A. thaliana* and *B. napus* and that no *V. longisporum* specific response on metabolite level was detected so far in any of the species. On the other hand the environmental conditions provided from both species to the fungus differ significantly. This may result in certain characteristic but different metabolic responses and does not recommend the use of only the model plant *A. thaliana* for studying the interaction of *V. longisporum* and its host. An additional comparison to the infection process in *B. napus* seems to be necessary in any case.

4.4 Metabolite fingerprinting as successful method for biomarker identification

The term metabolite fingerprinting includes a complex workflow of sample preparation, measurement and data processing. Here all steps of the non-targeted approach were optimized and applied to select and to identify markers in plant-pathogen interactions. The established workflow using UPLC-TOF-MS measurements and a data analysis by the MarVis software toolbox (Kaever et al. 2009, Kaever et al. submitted) allowed testing of different analytical parameters in complex and undescribed samples. With the cluster analysis a method can be optimized without the necessity of identification of the recorded markers. This is a valuable tool for the analysis of complex and unknown metabolic blends. Based on the analysis of the distribution of markers (including their information of retention time and m/z) the usage of a higher desolvation temperature proved to be more effective (Fig. 17). The optimization led to the establishment of an extraction method for aqueous samples as well as to an enhanced LC and MS performance. Furthermore significant progress has been made in the data processing. The possibility to discard low quality data as provided with the MarVis Filter tool enables detection of reliable infection markers (Kaever et al. submitted). It also allows combining data sets from positive and negative ionisation as well as from independent experiments. In combination with an automated adduct detection it leads to a strong reduction in the numbers of markers promoting the faster detection of reliable, reproducible and important markers. The selection of a cluster of interest in the appropriate experimental context by MarVis Cluster additionally reduces the number of markers significantly and helps to find distinct marker groups. The discovery of marker groups of related structure and similar intensity pattern has become a valuable tool in this work. A group can be characterized by specific mass differences and retention time shifts as were detected for the AWF specific infection markers (Fig. 39) or by similar fragments as was found in the cyclobrassinin related substances (Fig. 28). Further improvements of the data analysis routine should focus more on the automated detection of marker groups. Therefore

a tool searching for typical or frequently occurring m/z differences might accelerate the workflow. In the step of identification, the existence of related markers often proved to be helpful in this work. The identity of the amide derivatives was for example only elucidated due to the previous identification of the structurally related dicarboxylic acids. Detection of a group of markers furthermore allows fragmentation experiments with its most abundant group member. This proved to be useful for the identification of the aldehyde and alcohol derivatives of the AWF specific markers where only the C9 metabolites were abundant enough for a MS/MS analysis (Fig. S 7). Due to the analogy to the dicarboxylic acids, mono- and diamides two groups with 13 markers could thereby be identified (Tab. 8).

On the other hand a search for marker groups leads to the possibility that important, unidentified single markers might still be included in the recorded datasets. This is even more likely when the single markers are not included in a database. The single markers pipecolic acid and RA were only found and identified due to their database annotation. The verification of the identity still is a bottleneck in the metabolite fingerprinting analysis workflow. An unequivocal identification should be based on more than the exact mass because for a single mass more than 100 database hits can be found (e.g. 234.1572 Da ± 0.005 Da provides 127 hits only in the Knapsack database). In general, the number of putative molecular formulas that can be calculated increases with the mass of the molecule. Therefore the availability of MS/MS databases becomes more and more important due to the limitation of availability of authentic standard substances. Although some attempts have been made to collect data from GC- and LC-MS analyses from different laboratories and to combine them into a common file format a multitude of different mass spectral databases has evolved (e.g. MassBank (Horai et al. 2010) or Golm-Metabolome-Database (Kopka et al. 2005)). An alternative for the unequivocal identification of metabolites is either the NMR analysis which can only be performed for bulky substances e.g. isolated from fungal cultures (Shams et al. 2011) or the chemical synthesis of the putative metabolite. The synthesis is only applicable if a putative structure is already assigned and cannot be performed offhand in a biological laboratory. Another approach for metabolite identification can be the fragmentation analysis. Mostly this technique is used to elucidate structures of certain substance class e.g. iridoid glycosides (Wu et al. 2009) or fulvic acids (These 2005) but it also allows to elucidate the structure of new so far undescribed compounds. The advantages of the fragmentation analysis are that only minor amounts are sufficient for LC-MS/MS experiments and that the metabolites do not have to be purified prior to measurement. For a fragmentation analysis it is necessary to obtain exact masses for the fragments in order to assign a molecular formula to the building block. Therefore only mass analysers with a high mass resolution as Q-TOF instruments can be used. Information acquired on e.g. a Q-TRAP MS can nevertheless support the fragmentation analysis although only nominal masses are measured.

The more information about related metabolites is available the easier is the construction of a hypothetical molecular structure as has been found for the identification of the amide derivatives occurring in the AWF. There the verified identity of the mono- and diamides and the very similar MS/MS pattern led to the identification of the aldehyde and alcohol derivatives (Fig. 58). A disadvantage in the analytical procedure is that a chromatography is necessary for the creation of meaningful fragments. This prevents a direct infusion with its possibility of quick changes in the analytical parameters but especially for Q-TRAP analyses too many masses are otherwise co-fragmented in a complex matrix sample. Additionally, it must be mentioned that the position of elucidated fragments to each other is not unequivocal. In order to propose a structural formula of the molecule the fragmentation data should be compared to information of related molecules from the literature. Furthermore the fragmentation data from a group of metabolites is necessary for significant results. Most information derives from the differences and similarities obtained from the different markers like the common cyclobrassinin related core fragment and its oxidized version which could be detected in various infection markers (Fig. 28). In this work the identification of markers by fragmentation analysis was successful for complex marker groups and led to the models of new metabolic pathways. The LC-MS based method of metabolite fingerprinting offers the advantage of recording all markers within a certain mass range in a complex sample in contrast to e.g. fluorescence detectors that are limited to specific wavelengths. Therefore MS datasets allow a subsequent search for additional markers that either fit to the already identified substances or are proposed to exist by a specific marker group pattern or metabolic pathway. This can be regarded as metabolite prediction. By this additional infection markers with low intensities or higher p-values can be identified that were hidden in the datasets like it was done in this study for e.g. dethiomethyl-brassinin-GSH and the non-glycosylated stressins. Complex connections to metabolic pathways can with this be elucidated long time after the measurement. This can for example take into account information from new, recently published literature. The datasets can furthermore be searched again anytime under another biological question. Additionally, metabolite fingerprinting analysis enables the finding of differences and similarities in very complex metabolic processes. This can be used in the comparison of different plant species or plant organs as was used for this work resulting in the finding of a common involvement of RA but a species specific formation of phytoalexins in reaction to the infection with *V. longisporum*. A disadvantage of metabolite fingerprinting is that due to the untargeted aspect of the method it cannot be guaranteed that the markers that are essential for the analysed experimental setup are really included. Biomarkers like signalling molecules or toxins might not be extracted with the chosen method or are not detectable in MS measurements due to e.g. low ionisation efficiency as could be observed for the polyamines. Therefore method optimization should lead to better metabolite coverage and a more comprehensive acquisition but might leave out

important biomarkers due to their chemical properties. Furthermore it must be taken into account that relevant signals might be also e.g. peptides like the *A. thaliana* defensin PDF1.1 involved in the interaction with various biotic stresses (De Coninck et al. 2010). Signals like that cannot be detected by metabolite fingerprinting. A further disadvantage is that for the identification the access to databases and the availability of standards must be guaranteed which can be very expensive. The identification via chemical synthesis or fragmentation analysis requires profound chemical knowledge or even chemical equipment and makes collaboration with chemists necessary.

For this work it can be concluded that metabolite fingerprinting analysis was a successful method for the identification of infection markers in the interaction of *V. longisporum* with different Brassicaceae species. For those samples the method was optimized, the data processing tools were improved and various techniques for metabolite identification had been used. The most valuable tool proved to be the finding of marker groups which was the key for subsequent identification and pathway description.

With this established workflow for metabolite fingerprinting it has in further studies to be investigated, how closely related the metabolic reaction to abiotic stress is in the Brassicaceae. Therefore stress treatments with *A. thaliana* and *C. sativa* plants have to be performed. Additionally, the targeted analysis of polyamines from sample of both plant species will give more information about the role of these infection markers. Furthermore the preliminary results from the priming experiment should be verified. The priming procedure may in addition be used for the analysis of other infection markers. The obtained results in this work nevertheless indicate that a profound change in the metabolome occurs after *V. longisporum* infection in the host plant. The increasing knowledge about the involved mechanisms can help to find methods to cope with this fungal pathogen since eventually the reduction of fungal infestation in the field is requested.

5 Summary

The soil-borne, hemibiotrophic pathogen *Verticillium longisporum* is a severe threat for oilseed rape (*Brassica napus*) cultivation. In order to develop effective, defensive treatments for infected plants a thorough understanding of the plant-pathogen interaction is necessary. Therefore this work was conducted to find and identify metabolic changes and involved metabolite pathways in the pathogenic fungus or in the invaded host plant. For that a metabolite fingerprinting approach was optimized by adjusting the analytical parameters and adapting extraction methods to the analysed types of samples. In order to identify extracellular metabolites that are produced by *V. longisporum* in the xylem vessel, an *in vitro* assay was established resulting in the identification of seven metabolites from the tryptophan metabolism that accumulates in a provided xylem like environment. Nevertheless none of the identified substances produced by the fungus *in vitro* was detectable *in planta* after *V. longisporum* infection. Hence all accumulating metabolites *in planta* were analysed. A comprehensive analysis of apoplastic fluids and different plant organs in a time course from 5 to 35 days past infection in *B. napus* revealed a strong change in the metabolite pattern caused by *V. longisporum* infection. The identification of ubiquitously accumulating infection markers resulted in the detection of the phytoalexin cyclobrassinin and 22 related newly described substances. Structure elucidation was performed by MS/MS and pseudo-MS/MS/MS fragmentation analysis. The distribution of the cyclobrassinin related compounds within the plant correlated with the amount of fungal DNA detected in the plant organs pointing to a high contamination and a strong metabolic response in the hypocotyl tissue. By combining the obtained structural information and a proposed pathway for the phytoalexin camalexin in *A. thaliana* an analogue model for the biosynthetic pathway of cyclobrassinin is proposed. A subgroup of the identified infection markers hints to a degradation of cyclobrassinin resulting in 2-mercapto-indole-3-carboxylic acid (MICA) derivatives. When samples from *Camelina sativa* – whose infection process with *V. longisporum* was accessed for the first time in this work - and *Arabidopsis thaliana* were included in the comprehensive analysis of Brassicaceae it was found, that other groups of infection markers are more general than the species specific cyclobrassinin related markers. Raphanusamic acid (RA), a substance putatively related to phytoalexin or glucosinolate metabolism, pipecolic acid and three glycosylated salicylic acid (SA) derivatives proved to accumulate in the three Brassicaceae. Two trihydroxy fatty acids were identified infection markers from apoplastic fluids of *B. napus* and *A. thaliana*. Furthermore five groups of infection markers were identified exclusively in the apoplastic wash fluid (AWF). The saturated dicarboxylic acids and their monoamide derivatives are infection markers in *B. napus* as well as in *A. thaliana*. Furthermore diamides, aldehydes and alcohol derivatives were found to accumulate in *B. napus* plants. The mono- and diamide derivatives were

unequivocally identified by chemically synthesized authentic standards. Three polyamine infection markers were additionally measured in a targeted analysis whereas the glucosinolates often involved in plant-pathogen interactions were not found to be reliable infection markers in *B. napus*. Preliminary results from a priming experiment of *B. napus* with the C9 dicarboxylic acid, azelaic acid, indicated only a shift in cyclobrassinin biosynthesis but no enhanced resistance to *V. longisporum* infection. An infection resembling metabolite pattern could not be achieved by flotation on several identified infection markers like SA or RA. The elicitation of *B. napus* leaves with $CuCl_2$ demonstrated that the cyclobrassinin related substances were plant derived substances. They as well as markers like RA, SAG and pipecolic acid accumulate upon biotic and abiotic stress in *B. napus*.

In summary more than 70 metabolites were unequivocally identified either as fungal substances that accumulate in *in vitro* assays or as plant-derived metabolites in Brassicaceae upon *V. longisporum* infection.

6 Literature

Allwood JW, Goodacre R (2010) An introduction to liquid chromatography - mass spectrometry instrumentation applied in plant metabolomic analyses. Phytochemical Analysis 21: 33-47

Allwood WJ, Clarke A, Goodacre R, Mur LAJ (2010) Dual metabolomics: A novel approach to understanding plant–pathogen interactions. Phytochemistry 71: 590-597

Amarnath V, Amarnath K, Graham DG, Qi Q, Valentine H, Zhang J, Valentine WM (2001) Identification of a new urinary metabolite of carbon disulfide using an improved method for the determination of 2-thioxothiazolidine-4-carboxylic acid. Chemical Research in Toxicology 14: 1277-1283

Annesley TM (2003) Ion suppression in mass spectrometry. Clinical Chemistry 49: 1041-1044

Arabidopsis Genome Initiative (2000) Analysis of the genome sequence of the flowering plant Arabidopsis thaliana. Nature 408: 796-815

Ayer W, Craw P, Ma Y, Miao S (1992) Synthesis of camalexin and related phytoalexins. Tetrahedron 48: 2919-2924

Bartsch M, Bednarek P, Vivancos PD, Schneider B, von Roepenack-Lahaye E, Foyer CH, Kombrink E, Scheel D, Parker JE (2010) Accumulation of isochorismate-derived 2,3-dihydroxybenzoic 3-O-beta-D-xyloside in arabidopsis resistance to pathogens and ageing of leaves. The Journal of Biological Chemistry 285: 25654-25665

Baumgartner C, Osl M, Netzer M, Baumgartner D (2011) Bioinformatic-driven search for metabolic biomarkers in disease. Journal of Clinical Bioinformatics 1: 2-2

Bednarek P, Pislewska-Bednarek M, Svatos A, Schneider B, Doubsky J, Mansurova M, Humphry M, Consonni C, Panstruga R, Sanchez-Vallet A, Molina A, Schulze-Lefert P (2009) A glucosinolate metabolism pathway in living plant cells mediates broad-spectrum antifungal defense. Science 323: 101-106

Bednarek P, Schneider B, Svatos A, Oldham NJ, Hahlbrock K (2005) Structural Complexity, Differential Response to Infection, and Tissue Specificity of Indolic and Phenylpropanoid Secondary Metabolism in Arabidopsis Roots. Plant Physiology 138: 1058-1070

Bell AA, Wheeler MH (1986) Biosynthesis and Functions of Fungal Melanins. Annual Review of Phytopathology 24: 411-451

Bellés JM, Garro R, Fayos J, Navarro P, Primo J, Conejero V (1999) Gentisic Acid As a Pathogen-Inducible Signal, Additional to Salicylic Acid for Activation of Plant Defenses in Tomato. Molecular Plant-Microbe Interactions 12: 227-235

Berlanger I, Powelson ML (2000) Verticillium wilt. The Plant Health Instructor

Bishop WS (1945) Chemical synthesis of methyl sebacamic acid. Organic Syntheses: 71-71

Blancaflor EB, Hou G, Chapman KD (2003) Elevated levels of N-lauroylethanolamine, an endogenous constituent of desiccated seeds, disrupt normal root development in Arabidopsis thaliana seedlings. Planta 217: 206-217

Bornemann M (2010) Biosynthesis of raphanusamic acid in Brassicaceae. Diplomarbeit, Georg-August-University, Göttingen.

Böttcher C, Westphal L, Schmotz C, Prade E, Scheel D, Glawischnig E (2009) The Multifunctional Enzyme CYP71B15 (PHYTOALEXIN DEFICIENT3) Converts Cysteine-Indole-3-Acetonitrile to Camalexin in the Indole-3-Acetonitrile Metabolic Network of Arabidopsis thaliana. The Plant Cell 21: 1830-1845

Braus GH (1991) Aromatic amino acid biosynthesis in the yeast Saccharomyces cerevisiae: a model system for the regulation of a eukaryotic biosynthetic pathway. Microbiological Reviews 55: 349-370

Brenner SA, Romeo JT (1986) Fungitoxic effects of nonprotein imino acids on growth of saprophytic fungi isolated from the leaf surface of Calliandra haematocephala. Applied and Environmental Microbiology 51: 690-693

Brodhagen M, Tsitsigiannis DI, Hornung E, Goebel C, Feussner I, Keller NP (2008) Reciprocal oxylipin-mediated cross-talk in the Aspergillus-seed pathosystem. Molecular Microbiology 67: 378-391

Broeckling CD, Broz AK, Bergelson J, Manter DK, Vivanco JM (2008) Root exudates regulate soil fungal community composition and diversity. Applied and Environmental Microbiology 74: 738-744

Brown M, Dunn WB, Dobson P, Patel Y, Winder CL, Francis-McIntyre S, Begley P, Carroll K, Broadhurst D, Tseng A, Swainston N, Spasic I, Goodacre R, Kell DB (2009) Mass spectrometry tools and metabolite-specific databases for molecular identification in metabolomics. The Analyst 134: 1322-1332

Browne L (1991) The camalexins: New phytoalexins produced in the leaves of camelina sativa (cruciferae). Tetrahedron 47: 3909-3914

Buhtz A, Pieritz J, Springer F, Kehr J (2010) Phloem small RNAs, nutrient stress responses, and systemic mobility. BMC Plant Biology 10: 64-64

Cappiello A, Famiglini G, Palma P, Pierini E, Termopoli V, Trufelli H (2008) Overcoming Matrix Effects in Liquid Chromatography−Mass Spectrometry. Analytical Chemistry 80: 9343-9348

Cardellina J, Moore R (1980) Malyngic acid, a new fatty acid from Lyngbya majuscula. Tetrahedron 36: 993-996

Castillo JA, Infante MR, Manresa À, Vinardell MP, Mitjans M, Clapés P (2006) Chemoenzymatic Synthesis and Antimicrobial and Haemolytic Activities of Amphiphilic Bis(phenylacetylarginine) Derivatives. ChemMedChem 1: 1091-1098

Catchpole GS, Beckmann M, Enot DP, Mondhe M, Zywicki B, Taylor J, Hardy N, Smith A, King RD, Kell DB, Fiehn O, Draper J (2005) Hierarchical metabolomics demonstrates substantial compositional similarity between genetically modified and conventional potato crops. Proceedings of the National Academy of Sciences of the United States of America 102: 14458-14462

Chapple CC, Vogt T, Ellis BE, Somerville CR (1992) An Arabidopsis mutant defective in the general phenylpropanoid pathway. The Plant Cell 4: 1413-1424

Clay NK, Adio AM, Denoux C, Jander G, Ausubel FM (2009) Glucosinolate metabolites required for an Arabidopsis innate immune response. Science 323: 95-101

Cowgill UM, Milazzo DP (1989) The culturing and testing of two species of duckweed. Aquatic Toxicology and Hazard Assessment: 379-391

Cowley T, Walters D (2005) Local and systemic effects of oxylipins on powdery mildew infection in barley. Pest Management Science 61: 572-576

Cronan JE, Lin S (2011) Synthesis of the α,ω-dicarboxylic acid precursor of biotin by the canonical fatty acid biosynthetic pathway. Current Opinion in Chemical Biology 15: 407-413

Dalby A (2003) Food in the ancient world, A-Z. Routledge, London; New York

De Coninck BMA, Sels J, Venmans E, Thys W, Goderis IJWM, Carron D, Delauré SL, Cammue BPA, De Bolle MFC, Mathys J (2010) Arabidopsis thaliana plant defensin AtPDF1.1 is involved in the plant response to biotic stress. The New Phytologist 187: 1075-1088

De Ruijter NCA, Verhees J, Leeuwen W, Krol AR (2003) Evaluation and Comparison of the GUS, LUC and GFP Reporter System for Gene Expression Studies in Plants. Plant Biology 5: 103-115

De Vos RCH, Moco S, Lommen A, Keurentjes JJB, Bino RJ, Hall RD (2007) Untargeted large-scale plant metabolomics using liquid chromatography coupled to mass spectrometry. Nature Protocols 2: 778-791

Dean JV, Delaney SP (2008) Metabolism of salicylic acid in wild-type, ugt74f1 and ugt74f2 glucosyltransferase mutants of Arabidopsis thaliana. Physiologia Plantarum 132: 417-425

Dettmer K, Aronov PA, Hammock BD (2007) Mass spectrometry-based metabolomics. Mass Spectrometry Reviews 26: 51-78

Devane WA, Hanus L, Breuer A, Pertwee RG, Stevenson LA, Griffin G, Gibson D, Mandelbaum A, Etinger A, Mechoulam R (1992) Isolation and structure of a brain constituent that binds to the cannabinoid receptor. Science 258: 1946-1949

Devys M, Barbier M, Kollmann A, Rouxel T, Bousquet J-F (1990) Cyclobrassinin sulphoxide, a sulphur-containing phytoalexin from Brassica juncea. Phytochemistry 29: 1087-1088

Dixon RA, Paiva NL (1995) Stress-induced phenylpropanoid metabolism. The Plant Cell 7: 1085-1097

Djamei A, Schipper K, Rabe F, Ghosh A, Vincon V, Kahnt J, Osorio S, Tohge T, Fernie AR, Feussner I, Feussner K, Meinicke P, Stierhof Y-D, Schwarz H, Macek B, Mann M, Kahmann R (2011) Metabolic priming by a secreted fungal effector. Nature 478: 395-398

Dunker S, Keunecke H, Steinbach P, von Tiedemann A (2008) Impact of Verticillium longisporum on Yield and Morphology of Winter Oilseed Rape (Brassica napus) in Relation to Systemic Spread in the Plant. Journal of Phytopathology 156: 698-707

Evans AM, DeHaven CD, Barrett T, Mitchell M, Milgram E (2009) Integrated, Nontargeted Ultrahigh Performance Liquid Chromatography/Electrospray Ionization Tandem Mass Spectrometry Platform for the Identification and Relative Quantification of the Small-Molecule Complement of Biological Systems. Analytical Chemistry 81: 6656-6667

Eynck C, Koopmann B, Grunewaldt-Stoecker G, Karlovsky P, Tiedemann A (2007) Differential interactions of Verticillium longisporum and V. dahliae with Brassica napus detected with molecular and histological techniques. European Journal of Plant Pathology 118: 259-274

Eynck C, Koopmann B, Karlovsky P, von Tiedemann A (2009) Internal resistance in winter oilseed rape inhibits systemic spread of the vascular pathogen Verticillium longisporum. Phytopathology 99: 802-811

Eynck C, Koopmann B, von Tiedemann A (2009) Identification of Brassica accessions with enhanced resistance to Verticillium longisporum under controlled and field conditions. Journal of plant diseases and protection 116: 63-72

Fahey JW, Zalcmann AT, Talalay P (2001) The chemical diversity and distribution of glucosinolates and isothiocyanates among plants. Phytochemistry 56: 5-51

Feussner I, Wasternack C (2002) The lipoxygenase pathway. Annual Review of Plant Biology 53: 275-297

Fiehn O (2002) Metabolomics--the link between genotypes and phenotypes. Plant Molecular Biology 48: 155-171

Fiehn O, Kopka J, Trethewey RN, Willmitzer L (2000) Identification of uncommon plant metabolites based on calculation of elemental compositions using gas chromatography and quadrupole mass spectrometry. Analytical Chemistry 72: 3573-3580

Flannery ML, Mitchell FJG, Coyne S, Kavanagh TA, Burke JI, Salamin N, Dowding P, Hodkinson TR (2006) Plastid genome characterisation in Brassica and Brassicaceae using a new set of nine SSRs. Theoretical and Applied Genetics 113: 1221-1231

Floerl S, Druebert C, Aroud H, Karlovsky P, Polle A (2010) Disease symptoms and mineral nutrition in Arabidopsis thaliana in response to Verticillium longisporum VL43 infection. Journal of Plant Pathology 92: 693-700

Floerl S, Druebert C, Majcherczyk A, Karlovsky P, Kües U, Polle A (2008) Defence reactions in the apoplastic proteome of oilseed rape (Brassica napus var. napus) attenuate Verticillium longisporum growth but not disease symptoms. BMC Plant Biology 8: 129-129

Floerl S, Majcherczyk A, Possienke M, Feussner K, Feussner I, Kües U, Polle A Verticillium longisporum infection affects the leaf apoplastic proteome, metabolome, and cell wall properties in Arabidopsis thaliana. submitted

Fradin EF, Thomma BPHJ (2006) Physiology and molecular aspects of Verticillium wilt diseases caused by V. dahliae and V. albo-atrum. Molecular Plant Pathology 7: 71-86

Frases S, Salazar A, Dadachova E, Casadevall A (2007) Cryptococcus neoformans can utilize the bacterial melanin precursor homogentisic acid for fungal melanogenesis. Applied and Environmental Microbiology 73: 615-621

Gao X, Kolomiets MV (2009) Host-derived lipids and oxylipins are crucial signals in modulating mycotoxin production by fungi. Toxin Reviews 28: 79-88

Gaskell SJ (1997) Electrospray: Principles and Practice. Journal of Mass Spectrometry 32: 677-688

Geu-Flores F, Moldrup ME, Bottcher C, Olsen CE, Scheel D, Halkier BA (2011) Cytosolic -Glutamyl Peptidases Process Glutathione Conjugates in the Biosynthesis of Glucosinolates and Camalexin in Arabidopsis. The Plant Cell 23: 2456-2469

Glazebrook J (2005) Contrasting mechanisms of defense against biotrophic and necrotrophic pathogens. Annual Review of Phytopathology 43: 205-227

Göbel C, Feussner I (2009) Methods for the analysis of oxylipins in plants. Phytochemistry 70: 1485-1503

Gómez-Romero M, Segura-Carretero A, Fernández-Gutiérrez A (2010) Metabolite profiling and quantification of phenolic compounds in methanol extracts of tomato fruit. Phytochemistry 71: 1848-1864

Gross D, Porzel A, Schmidt J (1994) Indole phytoalexins from the Kohlrabi (Brassica oleracea var. gongyloes). Zeitschrift für Naturforschung 49: 281-285

Haas BJ, Kamoun S, Zody MC, Jiang RHY, Handsaker RE, Cano LM, Grabherr M, Kodira CD, Raffaele S, Torto-Alalibo T, Bozkurt TO, Ah-Fong AMV, Alvarado L, Anderson VL, Armstrong MR, Avrova A, Baxter L, Beynon J, Boevink PC, Bollmann SR, Bos JIB, Bulone V, Cai G, Cakir C, Carrington JC, Chawner M, Conti L, Costanzo S, Ewan R, Fahlgren N, Fischbach MA, Fugelstad J, Gilroy EM, Gnerre S, Green PJ, Grenville-Briggs LJ, Griffith J, Grünwald NJ, Horn K, Horner NR, Hu C-H, Huitema E, Jeong D-H, Jones AME, Jones JDG, Jones RW, Karlsson EK, Kunjeti SG, Lamour K, Liu Z, Ma L, MacLean D, Chibucos MC, McDonald H, McWalters J, Meijer HJG, Morgan W, Morris PF, Munro CA, O'Neill K, Ospina-Giraldo M, Pinzón A, Pritchard L, Ramsahoye B, Ren Q, Restrepo S, Roy S, Sadanandom A, Savidor A, Schornack S, Schwartz DC, Schumann UD, Schwessinger B, Seyer L, Sharpe T, Silvar C, Song J, Studholme DJ, Sykes S, Thines M, van de Vondervoort PJI, Phuntumart V, Wawra S, Weide R, Win J, Young C, Zhou S, Fry W, Meyers BC, van West P, Ristaino J, Govers F, Birch PRJ, Whisson SC, Judelson HS, Nusbaum C (2009) Genome sequence and analysis of the Irish potato famine pathogen Phytophthora infestans. Nature 461: 393-398

Häffner E, Karlovsky P, Diederichsen E (2010) Genetic and environmental control of the Verticillium syndrome in Arabidopsis thaliana. BMC Plant Biology 10: 235-235

Hamberg M (1999) An epoxy alcohol synthase pathway in higher plants: biosynthesis of antifungal trihydroxy oxylipins in leaves of potato. Lipids 34: 1131-1142

Hamberg M, Hamberg G (1996) Peroxygenase-Catalyzed Fatty Acid Epoxidation in Cereal Seeds (Sequential Oxidation of Linoleic Acid into 9(S),12(S),13(S)-Trihydroxy-10(E)-Octadecenoic Acid). Plant Physiology 110: 807-815

Harper FR, Berkenkamp B (1975) Revised growth-stage key for Brassica campestris and B. napus. Canadian Journal of Plant Science 55: 657-658

Hase T, Koreeda M, Hasegawa K (1983) A growth inhibitor, 2-thiooxothiazolidine-4-carboxylic acid from Sakurajima radish seedlings. Phytochemistry 22: 1275-1276

Heale JB, Karapapa VK (1999) The verticillium threat to Canada's major oilseed crop: canola. Canadian Journal of Plant Pathology 21: 1-7

Henneken M (2001) HPLC-Analyse von Phytoalexinen zur Differenzierung von Camelina sativa (L.) Crtz.- Sorten. Dissertation, Universität-Gesamthochschule Paderborn.

Herrmann KM, Weaver LM (1999) The shikimate pathway. Annual Review of Plant Physiology and Plant Molecular Biology 50: 473-503

Horai H, Arita M, Kanaya S, Nihei Y, Ikeda T, Suwa K, Ojima Y, Tanaka K, Tanaka S, Aoshima K, Oda Y, Kakazu Y, Kusano M, Tohge T, Matsuda F, Sawada Y, Hirai MY, Nakanishi H, Ikeda K, Akimoto N, Maoka T, Takahashi H, Ara T, Sakurai N, Suzuki H, Shibata D, Neumann S, Iida T, Tanaka K, Funatsu K, Matsuura F, Soga T, Taguchi R, Saito K, Nishioka T (2010) MassBank: a public repository for sharing mass spectral data for life sciences. Journal of Mass Spectrometry: JMS 45: 703-714

Horie T (2006) Calcium Regulation of Sodium Hypersensitivities of sos3 and athkt1 Mutants. Plant and Cell Physiology 47: 622-633

Hou CT, Forman RJ (2000) Growth inhibition of plant pathogenic fungi by hydroxy fatty acids. Journal of Industrial Microbiology and Biotechnology 24: 275-276

Hrastar R, Petrisic MG, Ogrinc N, Kosir IJ (2009) Fatty acid and stable carbon isotope characterization of Camelina sativa oil: implications for authentication. Journal of Agricultural and Food Chemistry 57: 579-585

Inderbitzin P, Davis RM, Bostock RM, Subbarao KV (2011) The Ascomycete Verticillium longisporum Is a Hybrid and a Plant Pathogen with an Expanded Host Range. PLoS ONE 6: e18260-e18260

Iven T (2009) Transkriptomanalyse der Arabidopsis-Wurzel nach Infektion mit dem pilzlichen Pathogen Verticillium longisporum und Identifizierung von transkriptionellen Regulatoren der Pathogenantwort. Dissertation, Georg-August-University, Göttingen.

Johansson A, Staal J, Dixelius C (2006) Early responses in the Arabidopsis-Verticillium longisporum pathosystem are dependent on NDR1, JA- and ET-associated signals via cytosolic NPR1 and RFO1. Molecular Plant-Microbe Interactions: MPMI 19: 958-969

Jolliffe I (2002) Principal component analysis. Springer, New York

Jung HW, Tschaplinski TJ, Wang L, Glazebrook J, Greenberg JT (2009) Priming in Systemic Plant Immunity. Science 324: 89-91

Kaever A, Landesfeind M, Possienke M, Feussner K, Feussner I, Meinicke P MarVis-Filter: Ranking, filtering, adduct and isotope correction of mass spectrometry data. submitted

Kaever A, Lingner T, Feussner K, Göbel C, Feussner I, Meinicke P (2009) MarVis: a tool for clustering and visualization of metabolic biomarkers. BMC Bioinformatics 10: 92-92

Kamath AV, Vaidyanathan CS (1990) New pathway for the biodegradation of indole in Aspergillus niger. Applied and Environmental Microbiology 56: 275-280

Kanehisa M, Goto S, Furumichi M, Tanabe M, Hirakawa M (2009) KEGG for representation and analysis of molecular networks involving diseases and drugs. Nucleic Acids Research 38: D355-D360-D355-D360

Karapapa V, Bainbridge B, Heale J (1997) Morphological and molecular characterization of Verticillium longisporum comb, nov., pathogenic to oilseed rape. Mycological Research 101: 1281-1294

Karlovsky P (2011) Biological detoxification of the mycotoxin deoxynivalenol and its use in genetically engineered crops and feed additives. Applied Microbiology and Biotechnology 91: 491-504

Katajamaa M, Miettinen J, Oresic M (2006) MZmine: toolbox for processing and visualization of mass spectrometry based molecular profile data. Bioinformatics 22: 634-636

Kato T, Yamaguchi Y, Uyehara T, Yokoyama T, Namai T, Yamanaka S (1983) Self defensive substances in rice plant against rice blast disease. Tetrahedron Letters 24: 4715-4718

Kliebenstein D, Pedersen D, Barker B, Mitchell-Olds T (2002) Comparative analysis of quantitative trait loci controlling glucosinolates, myrosinase and insect resistance in Arabidopsis thaliana. Genetics 161: 325-332

Kliebenstein DJ (2001) Genetic Control of Natural Variation in Arabidopsis Glucosinolate Accumulation. Plant Physiology 126: 811-825

Klosterman SJ, Subbarao KV, Kang S, Veronese P, Gold SE, Thomma BPHJ, Chen Z, Henrissat B, Lee Y-H, Park J, Garcia-Pedrajas MD, Barbara DJ, Anchieta A, de Jonge R, Santhanam P, Maruthachalam K, Atallah Z, Amyotte SG, Paz Z, Inderbitzin P, Hayes RJ, Heiman DI, Young S, Zeng Q, Engels R, Galagan J, Cuomo CA, Dobinson KF, Ma L-J (2011) Comparative Genomics Yields Insights into Niche Adaptation of Plant Vascular Wilt Pathogens. PLoS Pathogens 7: e1002137-e1002137

Knoth C, Salus MS, Girke T, Eulgem T (2009) The Synthetic Elicitor 3,5-Dichloroanthranilic Acid Induces NPR1-Dependent and NPR1-Independent Mechanisms of Disease Resistance in Arabidopsis. Plant Physiology 150: 333-347

König S (2011) Phenylpropanoids and long chain fatty acid derivatives in the interaction of Arabidopsis thaliana and Verticillium longisporum. Dissertation, Georg-August-University, Göttingen.

Kopka J, Schauer N, Krueger S, Birkemeyer C, Usadel B, Bergmuller E, Dormann P, Weckwerth W, Gibon Y, Stitt M, Willmitzer L, Fernie AR, Steinhauser D (2004) GMD@CSB.DB: the Golm Metabolome Database. Bioinformatics 21: 1635-1638

Kutschy P, Mezencev R (2008) Indole phytoalexins from Brassicaceae: Synthesis and anticancer activity. Targets in Heterocyclic Systems: 120-148

Lattanzio V, De Cicco D, Di Venere D, Lima G, Salerno M (1994) Antifungal activity of phenolics against fungi commonly encountered during storage. Italian Journal of Food Science 6: 23-30

Lemière F (2001) Mass analysers for LC-MS. Guide to LC-MS. LC-GC Europe, pp 22-28

Leon-Reyes A, Du Y, Koornneef A, Proietti S, Körbes AP, Memelink J, Pieterse CMJ, Ritsema T (2010) Ethylene signaling renders the jasmonate response of Arabidopsis insensitive to future suppression by salicylic acid. Molecular Plant-Microbe Interactions: MPMI 23: 187-197

Lucio M, Fekete A, Weigert C, Wägele B, Zhao X, Chen J, Fritsche A, Häring H-U, Schleicher ED, Xu G, Schmitt-Kopplin P, Lehmann R (2010) Insulin Sensitivity Is Reflected by Characteristic Metabolic Fingerprints - A Fourier Transform Mass Spectrometric Non-Targeted Metabolomics Approach. PLoS ONE 5: e13317-e13317

Martin-Arjol I, Bassas-Galia M, Bermudo E, Garcia F, Manresa A (2010) Identification of oxylipins with antifungal activity by LC-MS/MS from the supernatant of Pseudomonas 42A2. Chemistry and Physics of Lipids 163: 341-346

Masui H, Kondo T, Kojima M (1989) An antifungal compound, 9,12,13-trihydroxy-(E)-10-octadecenoic acid, from Colocasia antiquorum inoculated with Ceratocystis fimbriata. Phytochemistry 28: 2613-2615

Mateo A, Funck D, Mühlenbock P, Kular B, Mullineaux P, Karpinski S (2006) Controlled levels of salicylic acid are required for optimal photosynthesis and redox homeostasis. Journal of Experimental Botany 57: 1795-1807

Matyash V, Liebisch G, Kurzchalia TV, Shevchenko A, Schwudke D (2008) Lipid extraction by methyl-tert-butyl ether for high-throughput lipidomics. Journal of Lipid Research 49: 1137-1146

Max N, Betz A, Facey S, Lingens F, Hauer B, Fetzner S (1999) Cloning, sequence analysis, and expression of the Pseudomonas putida 33/1 1H-3-hydroxy-4-oxoquinoline 2,4-dioxygenase gene, encoding a carbon monoxide forming dioxygenase. Biochimica Et Biophysica Acta 1431: 547-552

Meinicke P, Lingner T, Kaever A, Feussner K, Gobel C, Feussner I, Karlovsky P, Morgenstern B (2008) Metabolite-based clustering and visualization of mass spectrometry data using one-dimensional self-organizing maps. Algorithms for Molecular Biology 3: 9-9

Melotto M, Underwood W, Koczan J, Nomura K, He SY (2006) Plant Stomata Function in Innate Immunity against Bacterial Invasion. Cell 126: 969-980

Mintz-Oron S, Mandel T, Rogachev I, Feldberg L, Lotan O, Yativ M, Wang Z, Jetter R, Venger I, Adato A, Aharoni A (2008) Gene expression and metabolism in tomato fruit surface tissues. Plant Physiology 147: 823-851

Mol L, van Riessen HW (1995) Effect of plant roots on the germination of microsclerotia of Verticillum dahliae. European Journal of Plant Pathology 101: 673-678

Mukhtarova LS, Mukhitova FK, Gogolev YV, Grechkin AN (2011) Hydroperoxide lyase cascade in pea seedlings: Non-volatile oxylipins and their age and stress dependent alterations. Phytochemistry 72: 356-364

Nagaharu U (1935) Genome analysis in Brassica with special reference to the experimental formation of B. napus and peculiar mode of fertilisation. Japanese Journal of Botany 7: 389-452

Nahlik K, Dumkow M, Bayram O, Helmstaedt K, Busch S, Valerius O, Gerke J, Hoppert M, Schwier E, Opitz L, Westermann M, Grond S, Feussner K, Goebel C, Kaever A, Meinicke P, Feussner I, Braus GH (2010) The COP9 signalosome mediates transcriptional and metabolic response to hormones, oxidative stress protection and cell wall rearrangement during fungal development. Molecular Microbiology 78: 964-979

Neumann MJ, Dobinson KF (2003) Sequence tag analysis of gene expression during pathogenic growth and microsclerotia development in the vascular wilt pathogen Verticillium dahliae. Fungal Genetics and Biology: FG & B 38: 54-62

Parker D, Beckmann M, Zubair H, Enot DP, Caracuel-Rios Z, Overy DP, Snowdon S, Talbot NJ, Draper J (2009) Metabolomic analysis reveals a common pattern of metabolic re-programming during invasion of three host plant species by Magnaporthe grisea. The Plant Journal 59: 723-737

Pate JS, Atkins CA, White ST, Rainbird RM, Woo KC (1980) Nitrogen Nutrition and Xylem Transport of Nitrogen in Ureide-producing Grain Legumes. Plant Physiology 65: 961-965

Pedras MSC, Hossain S (2011) Interaction of cruciferous phytoanticipins with plant fungal pathogens: indole glucosinolates are not metabolized but the corresponding desulfo-derivatives and nitriles are. Phytochemistry 72: 2308-2316

Pedras MSC, Hossain S, Snitynsky RB (2011) Detoxification of cruciferous phytoalexins in Botrytis cinerea: spontaneous dimerization of a camalexin metabolite. Phytochemistry 72: 199-206

Pedras MSC, Montaut S, Suchy M (2004) Phytoalexins from the crucifer rutabaga: structures, syntheses, biosyntheses, and antifungal activity. The Journal of Organic Chemistry 69: 4471-4476

Pedras MSC, Okinyo DPO (2008) Remarkable incorporation of the first sulfur containing indole derivative: another piece in the biosynthetic puzzle of crucifer phytoalexins. Organic & Biomolecular Chemistry 6: 51-54

Pedras MSC, Yaya EE (2010) Phytoalexins from Brassicaceae: news from the front. Phytochemistry 71: 1191-1197

Pedras MSC, Yaya EE, Glawischnig E (2011) The phytoalexins from cultivated and wild crucifers: chemistry and biology. Natural Product Reports 28: 1381-1405

Pedras MSC, Zheng Q-A, Gadagi RS, Rimmer SR (2008) Phytoalexins and polar metabolites from the oilseeds canola and rapeseed: differential metabolic responses to the biotroph Albugo candida and to abiotic stress. Phytochemistry 69: 894-910

Pfalz M, Mikkelsen MD, Bednarek P, Olsen CE, Halkier BA, Kroymann J (2011) Metabolic Engineering in Nicotiana benthamiana Reveals Key Enzyme Functions in Arabidopsis Indole Glucosinolate Modification. The Plant Cell 23: 716-729

Pommerrenig B, Feussner K, Zierer W, Rabinovych V, Klebl F, Feussner I, Sauer N (2011) Phloem-Specific Expression of Yang Cycle Genes and Identification of Novel Yang Cycle Enzymes in Plantago and Arabidopsis. The Plant Cell 23: 1904-1919

Prost I (2005) Evaluation of the Antimicrobial Activities of Plant Oxylipins Supports Their Involvement in Defense against Pathogens. Plant Physiology 139: 1902-1913

Qiu F, Luo J, Yao S, Ma L, Kong L (2009) Preparative isolation and purification of anthocyanins from purple sweet potato by high-speed counter-current chromatography. Journal of Separation Science 32: 2146-2151

Ratzinger A, Riediger N, von Tiedemann A, Karlovsky P (2009) Salicylic acid and salicylic acid glucoside in xylem sap of Brassica napus infected with Verticillium longisporum. Journal of Plant Research 122: 571-579

Ravi S, Padmanabhan D, Mamdapur VR (2001) Macrocyclic musk compounds: Synthetic approaches to key intermediates for exaltolide, exaltone and dilactones. Journal of the Indian Institute of Sciences 81: 299-312

Rochfort SJ, Trenerry VC, Imsic M, Panozzo J, Jones R (2008) Class targeted metabolomics: ESI ion trap screening methods for glucosinolates based on MSn fragmentation. Phytochemistry 69: 1671-1679

Rogers EE, Glazebrook J, Ausubel FM (1996) Mode of action of the Arabidopsis thaliana phytoalexin camalexin and its role in Arabidopsis-pathogen interactions. Molecular Plant-Microbe Interactions: MPMI 9: 748-757

Rouxel T, Renard M, Kollmann A, Bousquet J-F (1990) Brassilexin accumulation and resistance to Leptosphaeria maculans in Brassica spp. and progeny of an interspecific cross B. juncea x B. napus. Euphytica 46: 175-181

Sato C, Oka N, Nabeta K, Matsuura H (2011) Cellulase applied to the leaves of sweet pepper (Capsicum annuum L. var. grossum) upregulates the production of salicylic and azelaic acids. Bioscience, Biotechnology, and Biochemistry 75: 761-763

Schmid H, Schmid P, Natarajan V (1996) The N-acylation-phosphodiesterase pathway and cell signalling. Chemistry and Physics of Lipids 80: 133-142

Schripsema J (2010) Application of NMR in plant metabolomics: techniques, problems and prospects. Phytochemical Analysis: PCA 21: 14-21

Schuhegger R, Nafisi M, Mansourova M, Petersen BL, Olsen CE, Svatos A, Halkier BA, Glawischnig E (2006) CYP71B15 (PAD3) catalyzes the final step in camalexin biosynthesis. Plant Physiology 141: 1248-1254

Schweizer P, Felix G, Buchala A, Muller C, Metraux J-P (1996) Perception of free cutin monomers by plant cells. The Plant Journal 10: 331-341

Sellick CA, Knight D, Croxford AS, Maqsood AR, Stephens GM, Goodacre R, Dickson AJ (2010) Evaluation of extraction processes for intracellular metabolite profiling of mammalian cells: matching extraction approaches to cell type and metabolite targets. Metabolomics 6: 427-438

Sexton AC, Minic Z, Cozijnsen AJ, Pedras MSC, Howlett BJ (2009) Cloning, purification and characterisation of brassinin glucosyltransferase, a phytoalexin-detoxifying enzyme from the plant pathogen Sclerotinia sclerotiorum. Fungal Genetics and Biology 46: 201-209

Shams M, Mitterbauer R, Corradini R, Wiesenberger G, Dall'asta C, Schuhmacher R, Krska R, Adam G, Berthiller F (2011) Isolation and characterization of a new less-toxic derivative of the fusarium mycotoxin diacetoxyscirpenol after thermal treatment. Journal of Agricultural and Food Chemistry 59: 9709-9714

Singh S, Braus-Stromeyer S, Timpner C, Tran V, Lohaus G, Reusche M, Knüfer J, Teichmann T, von Tiedemann A, Braus G (2009) Silencing of Vlaro2 for chorismate synthase revealed that the phytopathogen Verticillium longisporum induces the cross-pathway control in the xylem. Applied Microbiology and Biotechnology 85: 1961-1976

Singh S, Braus-Stromeyer SA, Timpner C, Valerius O, von Tiedemann A, Karlovsky P, Druebert C, Polle A, Braus GH (2011) The plant host Brassica napus induces in the pathogen Verticillium longisporum the expression of functional catalase peroxidase which is required for the late phase of disease. Molecular Plant-Microbe Interactions, accepted

Sjoblad RD, Bollag JM (1977) Oxidative coupling of aromatic pesticide intermediates by a fungal phenol oxidase. Applied and Environmental Microbiology 33: 906-910

Smith G (1960) An introduction to industrial mycology. Arnold LR, London

Spaepen S, Vanderleyden J, Remans R (2007) Indole-3-acetic acid in microbial and microorganism-plant signaling. FEMS Microbiology Reviews 31: 425-448

Stark C (1961) Das Auftreten der Verticillium-Tracheomykosen in Hamburger Gartenbaukulturen. Gartenbauwissenschaft 26: 493-528

Stenzel I, Hause B, Miersch O, Kurz T, Maucher H, Weichert H, Ziegler J, Feussner I, Wasternack C (2003) Jasmonate biosynthesis and the allene oxide cyclase family of Arabidopsis thaliana. Plant Molecular Biology 51: 895-911

Stumpe M, Feussner I (2006) Formation of oxylipins by CYP74 enzymes. Phytochemistry Reviews 5: 347-357

Su T, Xu J, Li Y, Lei L, Zhao L, Yang H, Feng J, Liu G, Ren D (2011) Glutathione-indole-3-acetonitrile is required for camalexin biosynthesis in Arabidopsis thaliana. The Plant Cell 23: 364-380

Sud M, Fahy E, Cotter D, Brown A, Dennis EA, Glass CK, Merrill AH, Jr., Murphy RC, Raetz CRH, Russell DW, Subramaniam S (2007) LMSD: LIPID MAPS structure database. Nucleic Acids Research 35: D527-532-D527-532

Takasugi M, Katsui N, Shirata A (1986) Isolation of three novel sulphur-containing phytoalexins from the chinese cabbage Brassica campestris L. ssp. pekinensis(cruciferae). Journal of the Chemical Society, Chemical Communications: 1077-1077

Tan J, Bednarek P, Liu J, Schneider B, Svatos A, Hahlbrock K (2004) Universally occurring phenylpropanoid and species-specific indolic metabolites in infected and uninfected Arabidopsis thaliana roots and leaves. Phytochemistry 65: 691-699

Tappe H (2008) Verticillium longisporum induced gene expression in Arabidopsis thaliana. Dissertation, Georg-August-University, Göttingen.

These A (2005) Strukturelle Charakterisierung von Fulvinsäure-Molekülen mittels LC-MS/MS: Hinweise zu Quellen, Bildung und Reaktivität. Dissertation, Technische Universität, Berlin.

Tiziani S, Emwas A, Lodi A, Ludwig C, Bunce C, Viant M, Gunther U (2008) Optimized metabolite extraction from blood serum for 1H nuclear magnetic resonance spectroscopy. Analytical Biochemistry 377: 16-23

Tsuji J, Jackson EP, Gage DA, Hammerschmidt R, Somerville SC (1992) Phytoalexin Accumulation in Arabidopsis thaliana during the Hypersensitive Reaction to Pseudomonas syringae pv syringae. Plant Physiology 98: 1304-1309

VanEtten HD, Mansfield JW, Bailey JA, Farmer EE (1994) Two Classes of Plant Antibiotics: Phytoalexins versus "Phytoanticipins". The Plant Cell 6: 1191-1192

Velasco P, Francisco M, Moreno DA, Ferreres F, García-Viguera C, Cartea ME (2011) Phytochemical fingerprinting of vegetable Brassica oleracea and Brassica napus by simultaneous identification of glucosinolates and phenolics. Phytochemical Analysis 22: 144-152

Vinayavekhin N, Homan EA, Saghatelian A (2010) Exploring disease through metabolomics. ACS Chemical Biology 5: 91-103

Walters D (2000) Polyamines in plant–microbe interactions. Physiological and Molecular Plant Pathology 57: 137-146

Weiberg A, Karlovsky P (2009) Components of variance in transcriptomics based on electrophoretic separation of cDNA fragments (cDNA-AFLP). Electrophoresis 30: 2549-2557

Weizbauer A (2011) Metabolical consequences in Brassica napus in reaction to flowering and fungal infection. B.Sc.-Thesis, Georg-August-University, Göttingen.

Williams B, Kabbage M, Kim H-J, Britt R, Dickman MB (2011) Tipping the Balance: Sclerotinia sclerotiorum Secreted Oxalic Acid Suppresses Host Defenses by Manipulating the Host Redox Environment. PLoS Pathogens 7: e1002107-e1002107

Williams PH, Hill CB (1986) Rapid-cycling populations of brassica. Science (New York, N.Y.) 232: 1385-1389

Wittkop B, Snowdon RJ, Friedt W (2009) Status and perspectives of breeding for enhanced yield and quality of oilseed crops for Europe. Euphytica 170: 131-140

Wittmann C, Krömer JO, Kiefer P, Binz T, Heinzle E (2004) Impact of the cold shock phenomenon on quantification of intracellular metabolites in bacteria. Analytical Biochemistry 327: 135-139

Wu Q, Yuan Q, Liu EH, Qi L-W, Bi Z-M, Li P (2009) Fragmentation study of iridoid glycosides and phenylpropanoid glycosides in Radix Scrophulariae by rapid resolution liquid chromatography with diode-array detection and electrospray ionization time-of-flight mass spectrometry. Biomedical Chromatography: 808-819

Yalpani N, Balke NE, Schulz M (1992) Induction of UDP-Glucose:Salicylic Acid Glucosyltransferase in Oat Roots. Plant Physiology 100: 1114-1119

Yi H-S, Heil M, Adame-Alvarez RM, Ballhorn DJ, Ryu C-M (2009) Airborne induction and priming of plant defenses against a bacterial pathogen. Plant Physiology 151: 2152-2161

Zeise K, von Tiedemann A (2001) Morphological and Physiological Differentiation among Vegetative Compatibility Groups of Verticillium dahliae in Relation to V. longisporum. Journal of Phytopathology 149: 469-475

Zeise K, von Tiedemann A (2002) Host Specialization among Vegetative Compatibility Groups of Verticillium dahliae in Relation to Verticillium longisporum. Journal of Phytopathology 150: 112-119

Zenk MH, Schmitt J (1964) Enzymatische Acetylierung von D-Tryptophan. Die Naturwissenschaften 51: 510-511

Zhang P, Foerster H, Tissier CP, Mueller L, Paley S, Karp PD, Rhee SY (2005) MetaCyc and AraCyc. Metabolic Pathway Databases for Plant Research. Plant Physiology 138: 27-37

Zhou L, Hu Q, Johansson A, Dixelius C (2006) Verticillium longisporum and V. dahliae: infection and disease in Brassica napus. Plant Pathology 55: 137-144

Zubr J (1997) Oil-seed crop: Camelina sativa. Industrial Crops and Products 6: 113-119

7 Supplemental data

7.1 Figures and tables

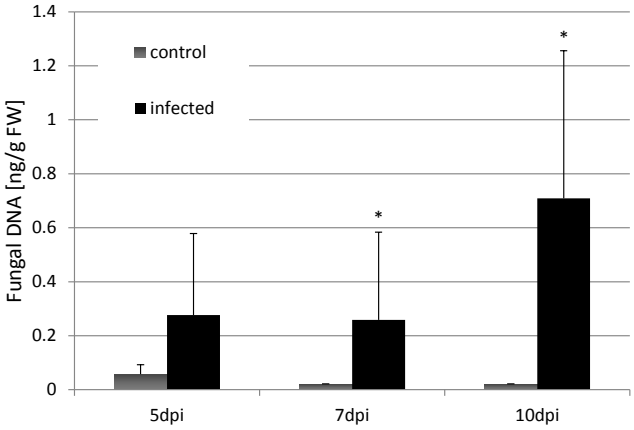

Fig. S 1: Analysis of fungal DNA in roots of *B. napus* at early time points
Abundance of *V. longisporum* in control and infected plant tissue was analysed by real-time PCR with the *Verticillium* spp. specific primers OLG70 and OLG71. Plant material was harvested 5, 7 and 10 dpi. Root samples from one representative experiment (two biological replicates) were extracted and measured twice. Asterisks indicate intensity values with significant differences compared to the corresponding control in an unpaired Students t-test (* = p-value < 0.05). Error bars represent the standard deviation.

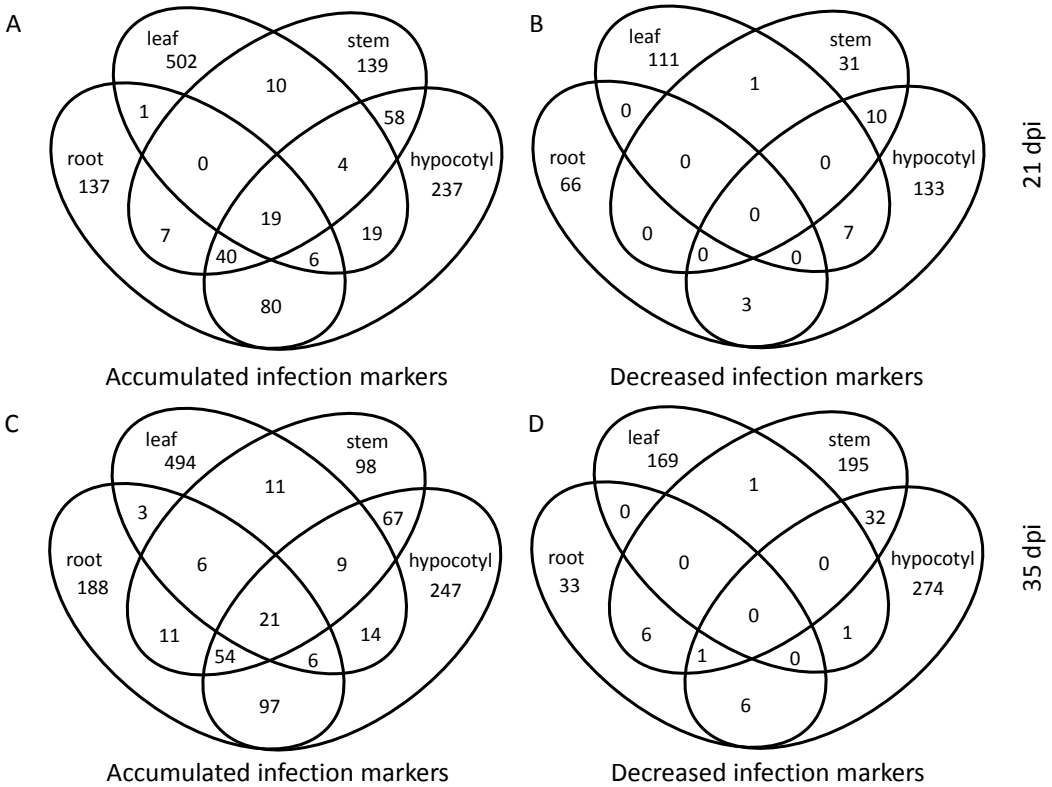

Fig. S 2: Tissue specific and ubiquitous infection markers in *B. napus* plants
Venn-Diagram of (A) infection specific accumulated markers at 21 dpi in four different plant tissues and (B) of infection specific decreased markers at 21 dpi from the same datasets. Venn-Diagram of (C) infection specific accumulated markers at 35 dpi in four different plant tissues and (D) of infection specific decreased markers at 35 dpi from the same datasets. Overlap of markers was calculated with MarVis Filter as described under 2.2.6.2. The data sets include analysis of three independent experiments, two technical replicates each, two ionization modes and four plant organs.

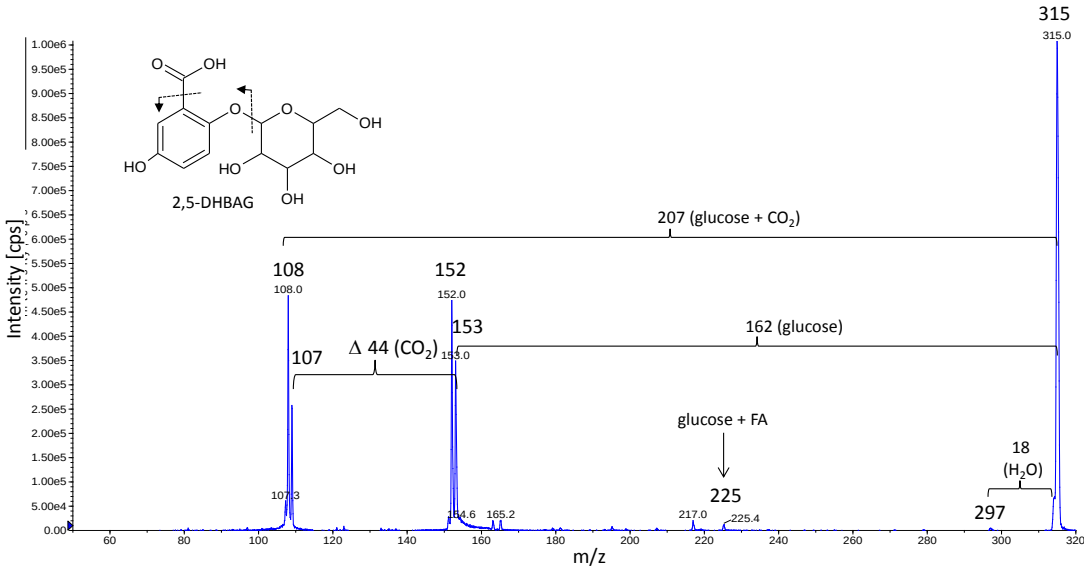

Fig. S 3: MS/MS spectrum of the infection marker 2,5-dihydroxybenzoic acid glucoside (2,5-DHBAG)
The substance was fragmented on the UPLC-Q-TRAP. A sample of extracted hypocotyl tissue of infected *B. napus* plants was used. The spectrum is a summed overlay of three measurements with different CEs (5, 20, 40 eV). Assigned neutral losses are indicated. The assumed fragmentation within the structure is displayed. FA = formic acid

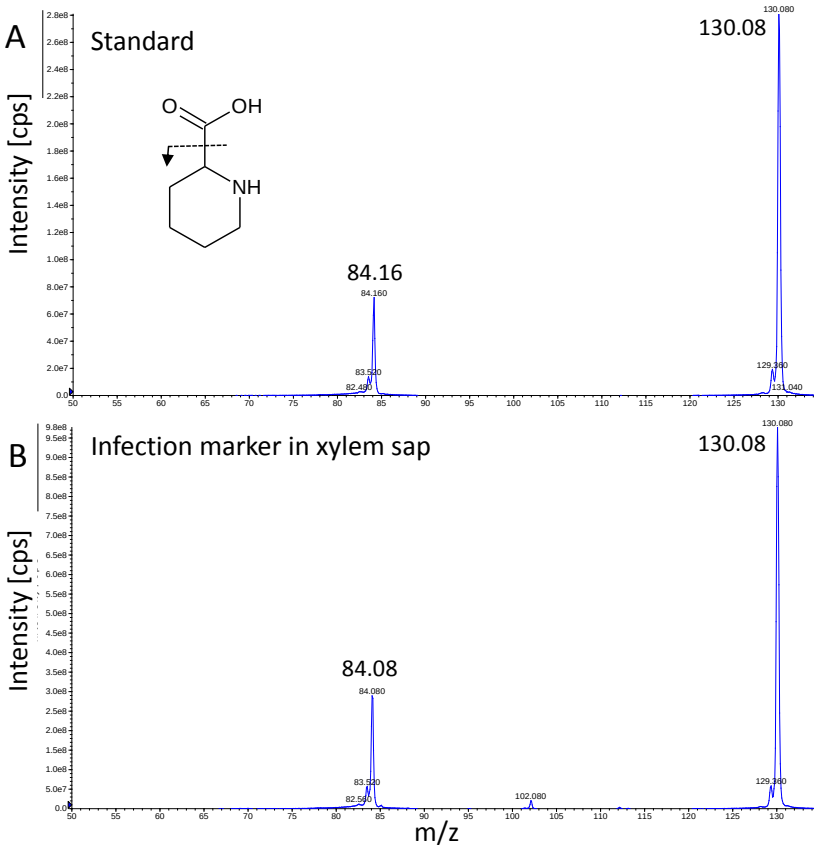

Fig. S 4: MS/MS spectra of the authentic standard and the infection marker pipecolic acid
The substance was fragmented on the Q-TRAP by direct infusion from (A) the authentic standard and (B) from xylem sap of infected *B. napus* plants. The spectrum was recorded applying a CE of 5 eV. The assumed fragmentation within the structure is displayed.

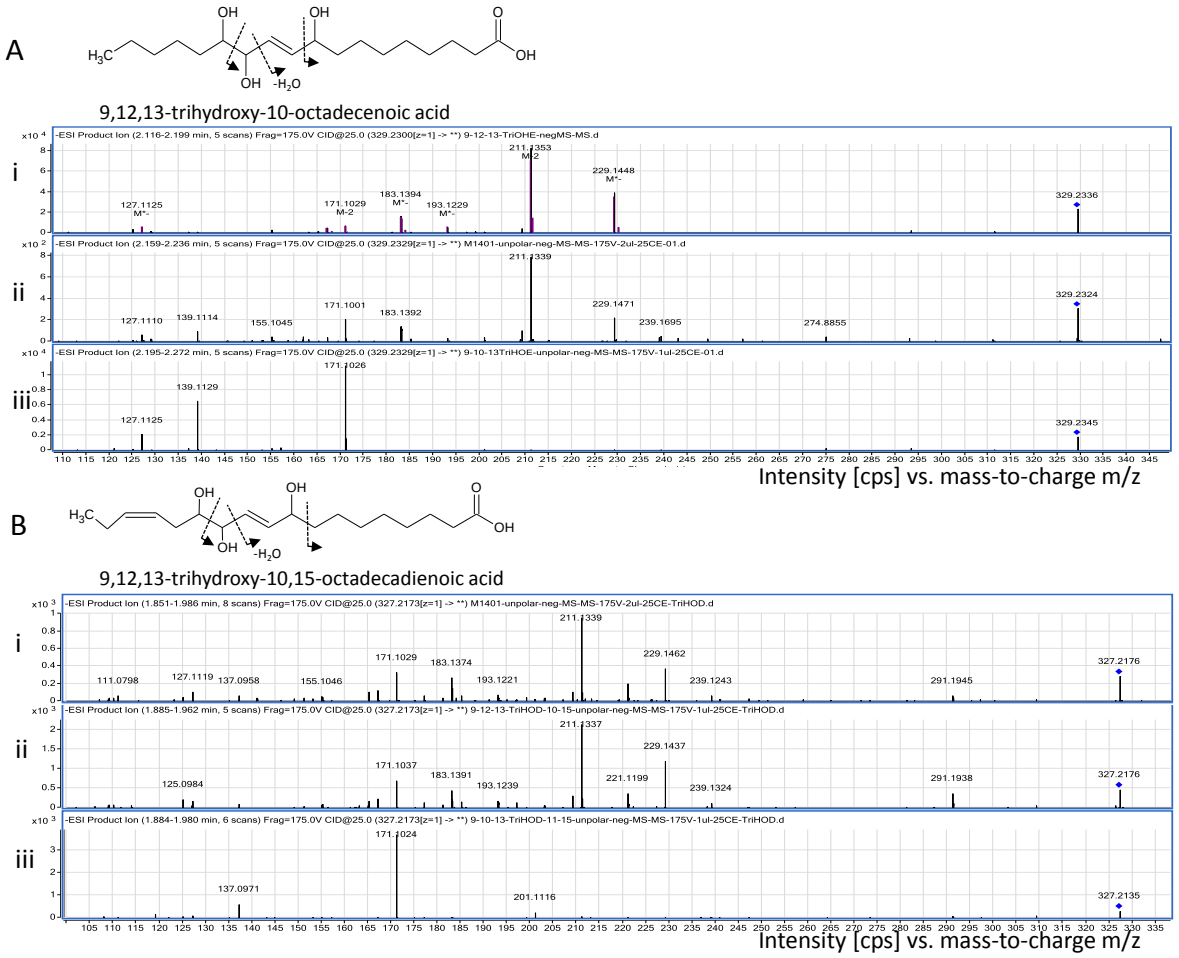

Fig. S 5: Structural formula and MS/MS spectra of oxylipins identified as infection marker

MS/MS spectra of trihydroxy fatty acid infection markers and authentic standards eluting at the same retention time. (A) 9,12,13-trihydroxy-10-octadecenoic acid: Comparison of oxylipin infection marker (i) with the standard compounds 9,12,13-trihydroxy-10-octadecenoic acid (ii) and 9,10,13-trihydroxy-11-octadecenoic acid (iii) eluting at retention time 2.2 min. (B) 9,12,13-trihydroxy-10,15-octadecadienoic acid: Comparison of oxylipin infection marker (i) with the standard compounds 9,12,13-trihydroxy-10,15-octadecadienoic acid (ii) and 9,10,13-trihydroxy-11,15-octadecadienoic acid (iii) eluting at retention time 1.9 min. The spectra were obtained on an UPLC-Q-TRAP applying a fragmentor voltage of 175 V and a CE of 25 eV. Putative fragmentation is indicated by dotted arrows in the structure.

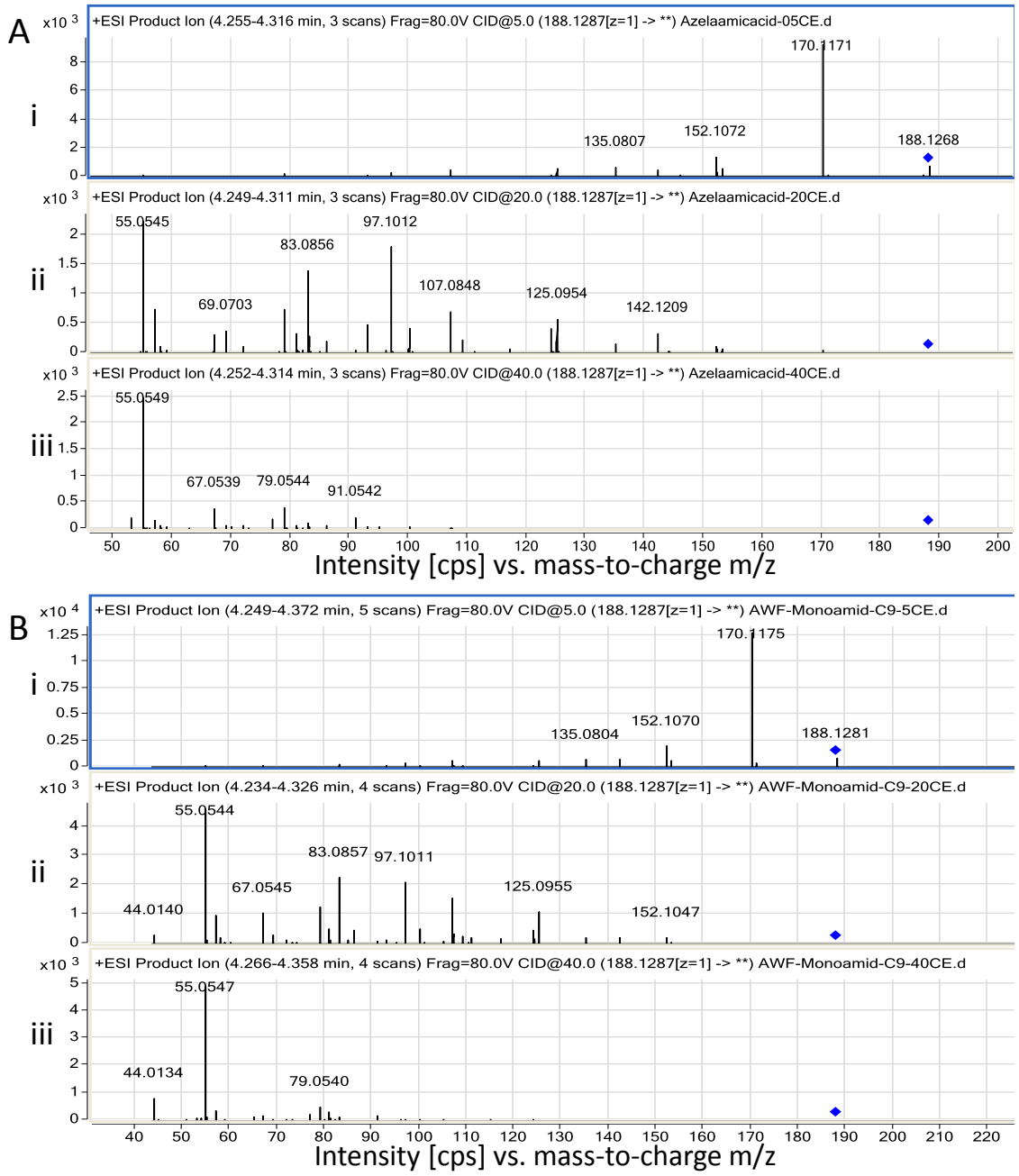

Fig. S 6: MS/MS spectra of azelaamic acid (9-amino-9-oxo-nonanoic acid) identified as infection marker
MS/MS spectra of (A) chemically synthesized azelaamic acid and (B) the infection marker in AWF from *V. longisporum* infected Brassicaceae (here: *B. napus*). The spectra were obtained on an UHPLC-Q-TOF as ESI product ions applying a fragmentor voltage of 80 V and a CE of 5 (i), 20 (ii) and 40 (iii) eV.

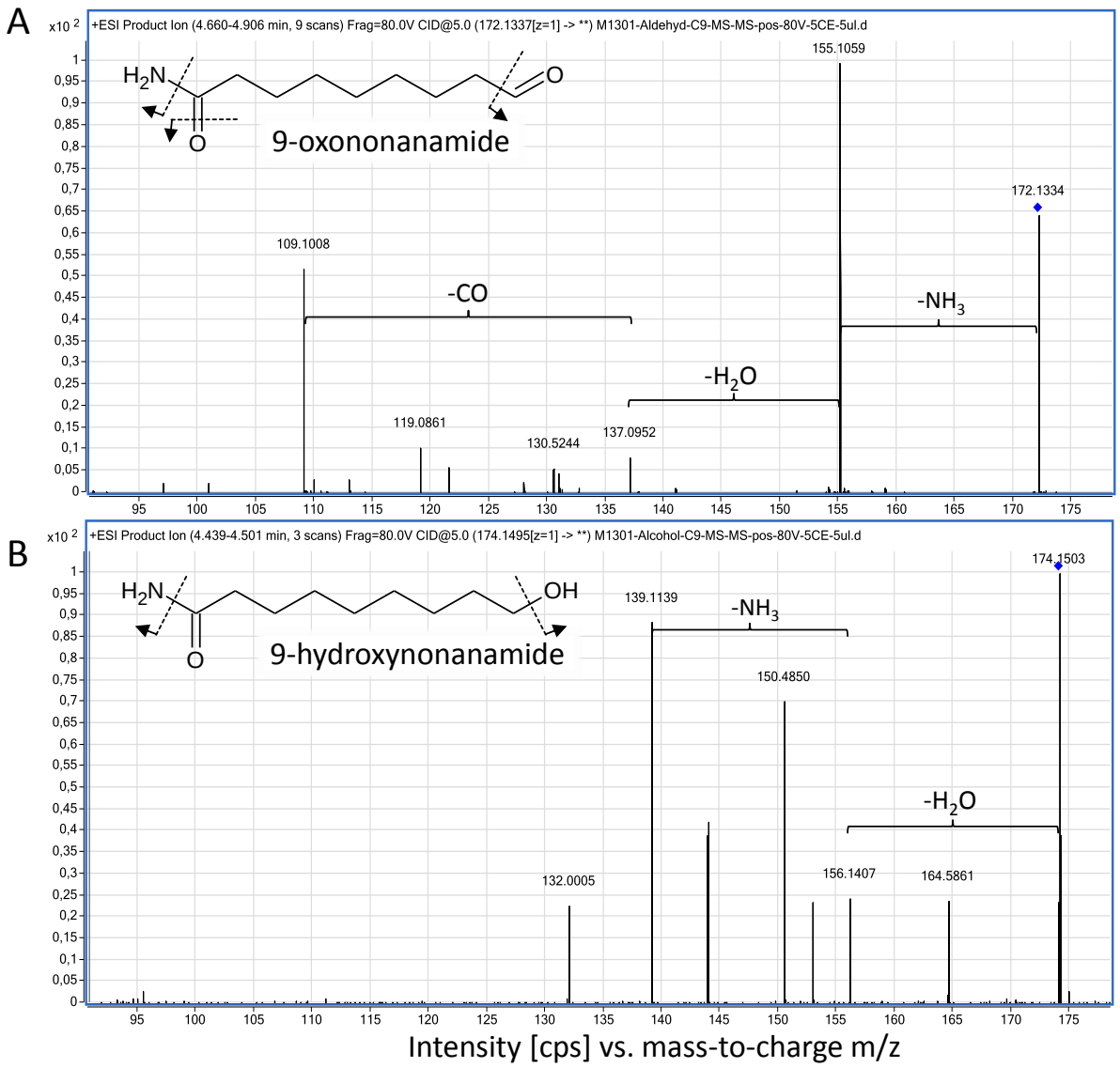

Fig. S 7: Structural formula and MS/MS spectra of 9-oxononanamide and 9-hydroxynonanamide identified as infection marker

MS/MS spectra of (A) 9-oxononanamide ($[M+H]^+$ 172.1338) and (B) 9-hydroxynonanamide ($[M+H]^+$ 174.1495) in AWF from *V. longisporum* infected Brassicaceae (here: *A. thaliana*). The spectra were obtained on an UHPLC-Q-TOF as ESI product ions applying a fragmentor voltage of 80 V and a CE of 5 eV. Assigned neutral losses are indicated. The assumed fragmentation within the structure is displayed.

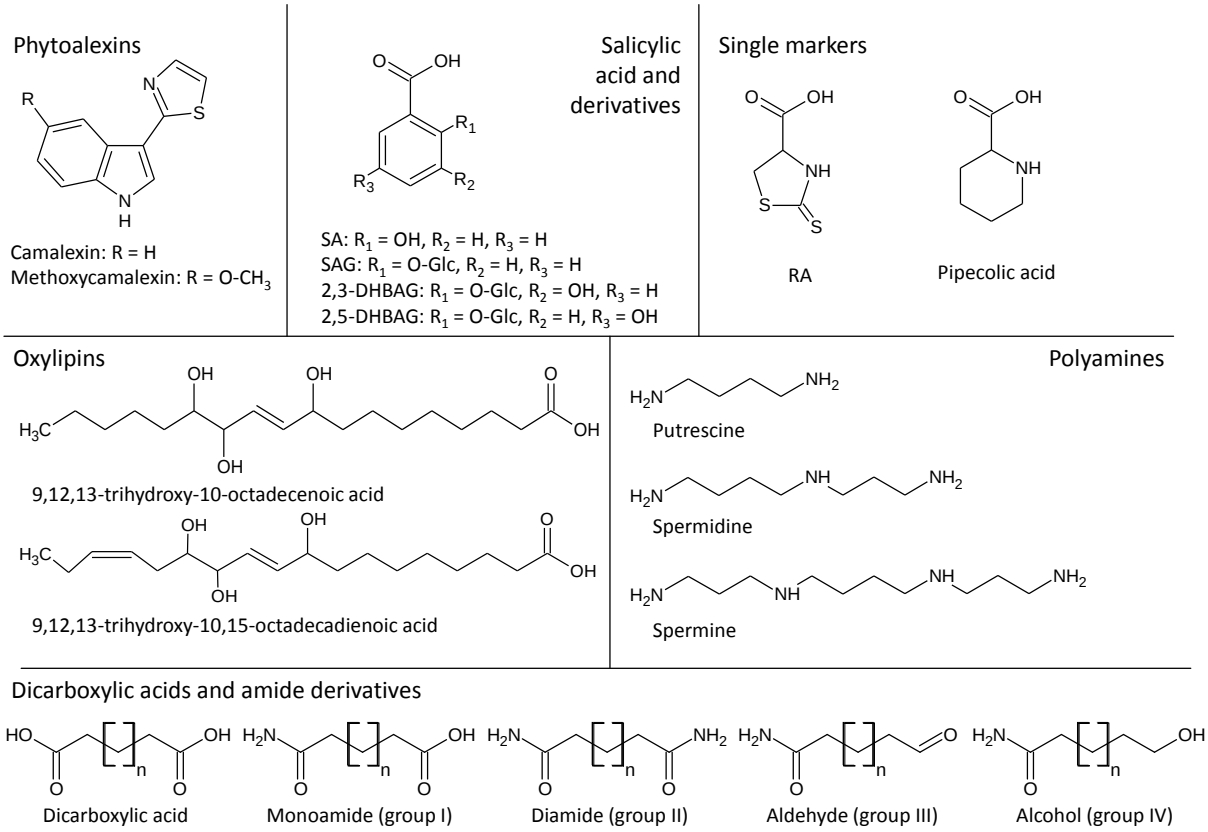

Fig. S 8: Structural formulas of identified markers for *V. longisporum* infection in different Brassicaceae
Structural formulas of two phytoalexins, SA and three derivatives, RA, pipecolic acid, two oxylipins, three polyamines and five groups of AWF specific infection markers (dicarboxylic acids and their amide derivatives).

Tab. S 1: Identified infection markers for *V. longisporum* infection in Brassicaceae

Exact mass [Da]	RT [min]	Molecular formula	Name	Plant	*B. napus* infection marker in	Mode of Identification
234.0285	6.33	C11H10N2S2	Cyclobrassinin	*B. napus*	all tissues	A, B
248.0078	4.84	C11H8N2OS2	Cyclobrassininon	*B. napus*	all tissues	D
200.0409	5.05	C11H8N2S	Camalexin	*C. sativa*	-	A, B
230.0514	5.08	C12H10N2OS	Methoxycamalexin	*C. sativa*	-	D
612.1197	3.40	C24H28N4O11S2	Mal-Glc-Prestressin	*B. napus*	ubiquitous	E
526.1194	3.22	C21H26N4O8S2	Glc-Prestressin	*B. napus*	ubiquitous	E
364.0664	3.40	C15H16N4O3S2	Prestressin	*B. napus*	ubiquitous	E
626.0976	4.20	C24H26N4O12S2	Mal-Glc-Prestressinon	*B. napus*	ubiquitous	E
540.0985	4.14	C21H24N4O9S2	Glc-Prestressinon	*B. napus*	ubiquitous	E
555.0983	3.45	C22H25N3O10S2	Mal-Glc-Stressin	*B. napus*	ubiquitous	E
469.0979	3.28	C19H23N3O7S2	Glc-Stressin	*B. napus*	ubiquitous	E
307.0449	3.48	C13H13N3O2S2	Stressin	*B. napus*	ubiquitous	E
569.0774	4.04	C22H23N3O11S2	Mal-Glc-Stressinon	*B. napus*	ubiquitous	E
483.0772	3.99	C19H21N3O8S2	Glc-Stressinon	*B. napus*	ubiquitous	E
530.1030	3.60	C21H26N2O10S2	Mal-Glc-Stressin related	*B. napus*	ubiquitous	E
444.1026	3.20	C18H24N2O7S2	Glc-Stressin related	*B. napus*	ubiquitous	E
282.0497	3.75	C12H14N2O2S2	Stressin related	*B. napus*	ubiquitous	E
495.1246	4.16	C20H25N5O6S2	Dethiomethyl-brassinin-GSH	*B. napus*	ubiquitous	G
441.0730	4.10	C18H19NO10S	Mal-Glc-MICA	*B. napus*	ubiquitous	E
355.0741	3.75	C16H13N5O3S	Glc-MICA	*B. napus*	ubiquitous	E
193.0198	4.12	C9H7NO2S	MICA	*B. napus*	ubiquitous	E
603.1250	3.41	C24H29NO15S	Mal-Glc-MICA-Glc	*B. napus*	ubiquitous	E
517.1254	3.11	C21H27NO12S	Glc-MICA-Glc	*B. napus*	ubiquitous	E
397.0732	4.41	C17H19NO8S	Decarboxy-Mal-Glc-MICA	*B. napus*	ubiquitous	E
149.0299	4.41	C8H7NS	Decarboxy-MICA	*B. napus*	ubiquitous	E
138.0317	4.17	C7H6O3	Salicylic acid	*B. napus*	xylem sap	A
300.0845	2.76	C13H16O8	Salicylic acid glucoside	*B. napus, A. thaliana, C. sativa*	ubiquitous	A, B
316.0794	2.15	C13H16O9	2,5-dihydoxybenzoic acid glucoside	*B. napus, A. thaliana*	ubiquitous	E; deglycosylated: A, B, C
316.0794	2.32	C13H16O9	2,3-dihydoxybenzoic acid glucoside	*B. napus, A. thaliana, C. sativa*	roots	E; deglycosylated: A, B, C
162.9763	1.50	C4H5NO2S2	Raphanusamic acid	*B. napus, A. thaliana, C. sativa*	ubiquitous	A
129.0790	0.61	C6H11NO2	Pipecolic acid	*B. napus, A. thaliana, C. sativa*	ubiquitous	A, B, C
328.2251	5.05	C18H32O5	9,12,13-Trihydroxy-10,15-octadecadienoic acid	*B. napus, A. thaliana*	xylem sap, AWF	A, B
330.2407	5.23	C18H34O5	9,12,13-Trihydroxy-10-octadecenoic acid	*B. napus, A. thaliana*	xylem sap, AWF	A, B
88.1000	n.d.	C4H12N2	Putrescine	*B. napus*	analysed: hypocotyl	A
145.1579	n.d.	C7H19N3	Spermidine	*B. napus*	analysed: hypocotyl	A
202.2157	n.d.	C10H26N4	Spermine	*B. napus*	analysed: hypocotyl	A
			Dicarboxylic acids			
146.0576	2.33	C6H10O4	Hexanedioic acid (Adipic acid)	*B. napus, A. thaliana*	AWF	F
160.0732	2.96	C7H12O4	Heptanedioic acid (Pimelic acid)	*B. napus, A. thaliana*	AWF	A
174.0888	3.61	C8H14O4	Octanedioic acid (Suberic acid)	*B. napus, A. thaliana*	AWF	A
188.1044	4.23	C9H16O4	Nonanedioic acid (Azelaic acid)	*B. napus, A. thaliana*	AWF	A, B
202.1200	4.61	C10H18O4	Decanedioic acid (Sebacic acid)	*B. napus, A. thaliana*	AWF	A
216.1356	4.98	C11H20O4	Undecanedioic acid	*B. napus, A. thaliana*	AWF	A
230.1512	5.32	C12H22O4	Dodecanedioic acid	*B. napus, A. thaliana*	AWF	A
244.1668	5.63	C13H24O4	Tridecanedioic acid	*B. napus, A. thaliana*	AWF	A
258.1824	5.97	C14H26O4	Tetradecanedioic acid	*B. napus*	AWF	A
272.1980	6.28	C15H28O4	Pentadecanedioic acid	*B. napus*	AWF	F
			Monoamides (group I)			
159.0896	2.23	C7H13NO3	7-amino-7-oxo-heptanoic acid	*B. napus, A. thaliana*	AWF	F
173.1053	2.84	C8H15NO3	8-amino-8-oxo-octanoic acid	*B. napus, A. thaliana*	AWF	F
187.1209	3.49	C9H17NO3	9-amino-9-oxo-nonanoic acid (Azelaamic acid)	*B. napus, A. thaliana*	AWF	A, B
201.1366	4.05	C10H19NO3	10-amino-10-oxo-decanoic acid (Sebacamic acid)	*B. napus, A. thaliana*	AWF	A, B
215.1524	4.47	C11H21NO3	11-amino-11-oxo-undecanoic acid	*B. napus, A. thaliana*	AWF	A, B
229.1678	4.86	C12H23NO3	12-amino-12-oxo-dodecanoic acid	*B. napus, A. thaliana*	AWF	A, B
243.1836	5.17	C13H25NO3	13-amino-13-oxo-tridecanoic acid	*B. napus, A. thaliana*	AWF	A, B
257.1993	5.51	C14H27NO3	14-amino-14-oxo-tetradecanoic acid	*B. napus*	AWF	F
271.2150	5.79	C15H29NO3	15-amino-15-oxo-pentadecanoic acid	*B. napus*	AWF	F
			Diamides (group II)			
186.1369	2.68	C9H18N2O2	Nonanediamide (Azelamide)	*B. napus*	AWF	F
214.1683	3.89	C11H22N2O2	Undecanediamide	*B. napus*	AWF	F
228.1839	4.26	C12H24N2O2	Dodecanediamide	*B. napus*	AWF	A, B
242.1996	4.61	C13H26N2O2	Tridecanediamide	*B. napus*	AWF	F
			Aldehydes (group III)			
157.1103	2.88	C8H15NO2	8-oxooctanamide	*B. napus*	AWF	F
171.1259	3.62	C9H17NO2	9-oxononanamide	*B. napus*	AWF	D
185.1416	4.30	C10H19NO2	10-oxodecanamide	*B. napus*	AWF	F
199.1572	4.76	C11H21NO2	11-oxoundecanamide	*B. napus*	AWF	F
213.1729	5.16	C12H23NO2	12-oxododecanamide	*B. napus*	AWF	F
227.1886	5.55	C13H25NO2	13-oxotridecanamide	*B. napus*	AWF	F
			Alcohols (group IV)			
159.1255	2.88	C8H17NO2	8-hydoxyoctanamide	*B. napus*	AWF	F
173.1417	3.52	C9H19NO2	9-hydoxynonanamide	*B. napus*	AWF	D
187.1567	4.15	C10H21NO2	10-hydoxydecanamide	*B. napus*	AWF	F
201.1723	4.56	C11H23NO2	11-hydoxyundecanamide	*B. napus*	AWF	F
215.1887	4.93	C12H25NO2	12-hydoxydodecanamide	*B. napus*	AWF	F
229.2044	5.26	C13H27NO2	13-hydoxytridecanamide	*B. napus*	AWF	F
243.2201	5.59	C14H29NO2	14-hydoxytetradecanamide	*B. napus*	AWF	F

A) RT comparison / coelution with authentic standard
B) MS/MS spectra comparison with authentic standard
C) MS/MS spectra comparison with massbank.jp
D) Fragmentational comparison to related substance
E) Fragmentation studies
F) Comparison of RT to related substance
G) Only exact mass measurement

7.2 MS data for structural elucidation of cyclobrassinin related compounds

Peaks with an absolute abundance of < 100 cps or a relative abundance of < 5 % were not taken into account unless otherwise stated. All structures are annotated based on the data obtained by MS analysis and comparison of the fragmentation pattern with literature data unless otherwise stated. Fragmentation data was assigned and listed by Dr. Farina Schill (Department of Plant Biochemistry, Georg-August-University, Göttingen, Germany).

Pseudo-MS/MS/MS fragmentation data of building blocks

3-Methylene-1,3-dihydro-2*H*-indol-2-thione (a):

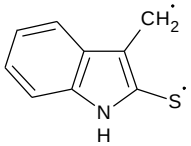

Exact mass, calcd. for C_9H_7NS: 161.0299 [M_f].

MS (Q-TOF): Positive mode; CE = 25 V, *m/z* (%) = 162.0376 (21) [M_f + H, $C_9H_8NS]^+$, 130.0653 (27) [M_f – S + H, $C_9H_8N]^+$, 128.0496 (97) $[C_9H_6N]^+$, 118.0648 (100) [M_f – CS + H, indole + H, $C_8H_8N]^+$, 117.0575 (62) [indole, $C_8H_7N]^+$, 101.0387 (31) $[C_8H_5]^+$, 91.0547 (22) $[C_7H_7]^+$, 77.0388 (39) $[C_6H_5]^+$.

(2-Thioxo-1,2-dihydro-3*H*-indol-3-ylidene)methanone (b):

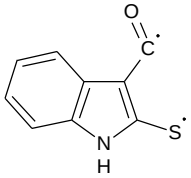

Exact mass, calcd. for C_9H_5NOS: 175.0092 [M_f].

MS (Q-TOF): Positive mode; CE = 15 CE, *m/z* (%) = 176.0163 (100) [M_f + H, $C_9H_6NOS]^+$, 148.0214 (77) [M_f – CO + H, $C_8H_6NS]^+$; CE = 25 V, 176.0163 (8) [M_f + H, $C_9H_6NOS]^+$, 160.0636 (8), 148.0213 (100) [M_f – CO + H, $C_8H_6NS]^+$, 143.0337 (6) [M_f – S, $C_9H_5NO]^+$, 121.0119 (49) $[C_7H_5S]^+$, 104.0497 (26) $[C_7H_6N]^+$, 77.0395 (12) $[C_6H_5]^+$.

***S*-Cyanocysteinylglycine, NC-Cys-Gly (c):**

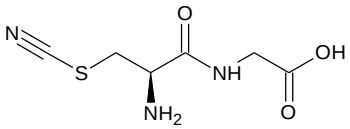

Exact mass, calcd. for $C_6H_9N_3O_3S$: 203.0365 [M_f].

MS (Q-TOF): Positive mode; CE = 5 V, *m/z* (%) = 204.0337 (100) [M_f + H, $C_6H_{10}N_3O_3S]^+$, 101.0101 (20) $[C_3H_3NO_3]^+$. Negative mode; CE = 5 V, *m/z* (%) = 202.0299 (100) [M_f – H, $C_6H_8N_3O_3S]^-$, 168.0405 (32) [M_f – H_2S – H, $C_6H_6N_3O_3]^-$, 158.0383 (13) [M_f – CO_2 – H, $C_5H_8N_3OS]^-$, 156.0389 (22) $[C_5H_6N_3O_3]^-$, 124.0508 (23) [M_f – H_2S – CO_2 – H, $C_5H_6N_3O]^-$.

_S_-Cyanocysteine, NC-Cys (d):

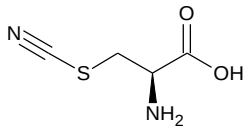

Exact mass, calcd. for $C_4H_6N_2O_2S$: 146.0150 [M_f].

MS (Q-TOF): Positive mode; no reasonable data obtained. Negative mode; *m/z* (%) = 145.0057 (19) [M_f – H, $C_4H_5N_2O_2S]^-$, 144.0455 (49) [M_f – 2 × H, $C_4H_4N_2O_2S]^-$, 101.0171 (9) [M_f – CO_2 – H, $C_3H_5N_2S]^-$, 67.0314 (100) [M_f – CO_2 – H_2S – H, $C_3H_3N_2]^-$.

Cysteine, Cys (e):

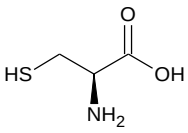

Exact mass, calcd. for $C_3H_7NO_2S$: 121.0198 [M_f].

Detectable as a fragment only in Mal-Glc-stressin related**.** MS/MS fragmentation failed.

ß-D-Glucose – H_2O, Glc, (f):

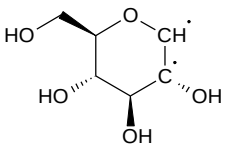

Exact mass, calcd. for $C_6H_{10}O_5$: 162.0528 [M_f].

Not detectable as a fragment itself, identified by its characteristic neutral loss.

6-*O*-Malonyl-ß-D-glucose – H_2O, Mal-Glc (g):

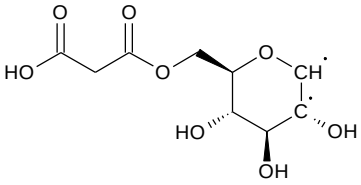

Exact mass, calcd. for $C_9H_{12}O_8$: 248.0532 [M_f].

Not detectable as a fragment itself, calculated from Mal-Glc-prestressin, Mal-Glc-prestressinon, Mal-Glc-prestressin and Mal-Glc-prestressinon, respectively. MS data of **g** were obtained by MS/MS fragmentation of Mal-Glc-prestressin into fragment **c** and a fragment consisting of **a** and **g**, followed by further fragmentation of **a**-**g**. MS (Q-TOF): Positive mode; CE = 5 V, *m/z* (%) = 162.0369 (100) [**a** + H, $C_9H_8NS]^+$, 159.0277 (14) $[C_6H_7O_5]^+$, 145.0492 (11) [M_f – HO_2C-CH_2-CO_2, $C_6H_9O_4]^+$, 127.0389 (11) $[C_6H_7O_3]^+$, 109.0287 (12) $[C_6H_5O_2]^+$, 105.0182 (9) [HO_2C-CH_2-CO_2H + H, $C_3H_5O_4]^+$, 87.0074 (5) [**g** – **f** + H, HO_2C-CH_2-CO, $C_3H_3O_3]^+$, 85.0285 (23) $[C_4H_5O_2]^+$, 81.0337 (8) $[C_5H_5O]^+$.

MS data of cyclobrassinin and cyclobrassininon:

The assigned retention times were measured on the ACQUITY UPLC HSS T3 column.

2-(Methylthio)-4,9-dihydro[1,3]thiazino[6,5-*b*]indole, cyclobrassinin:

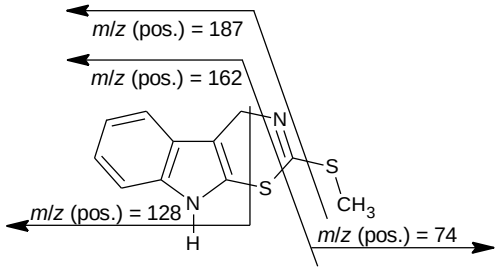

t_r = 6.33 min.

Exact mass, calcd. for $C_{11}H_{10}N_2S_2$: 234.0285 [M].

MS (Q-TOF): Positive mode; CE = 5 V, *m/z* (%) = 235.0362 (44) [M + H, $C_{11}H_{11}N_2S_2]^+$, 234.0239 (16) [M, $C_{11}H_{10}N_2S_2]^+$, 187.0330 (7) [M – SCH_3, $C_{10}H_7N_2S]^+$, 162.0376 (100) [M – N≡C-S-CH_3 + H, **a** + H, $C_9H_8NS]^+$; CE = 20 V, *m/z* (%) = 234.0234 (6) [M, $C_{11}H_{10}N_2S_2]^+$, 187.0325 (5) [M – SCH_3, $C_{10}H_7N_2S]^+$, 162.0374 (100) [M – N≡C-S-CH_3 + H, **a** + H, $C_9H_8NS]^+$, 128.0492 (9) [M – N≡C-S-CH_3 – SH, **a** – SH, $C_9H_6N]^+$, 118.0650 (11) [indole + H, $C_8H_8N]^+$, 74.0061 (14) [N≡C-S-CH_3 + H, $C_2H_4NS]^+$.

2-(Methylthio)[1,3]thiazino[6,5-*b*]indol-4(9*H*)-one, cyclobrassininon:

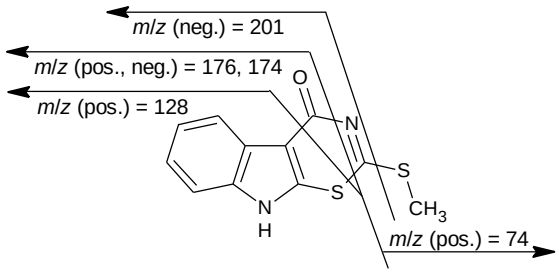

t_r = 4.84 min.

Exact mass, calcd. for $C_{11}H_8N_2OS_2$: 248.0078 [M].

MS (Q-TOF): Positive mode; CE = 5 V, *m/z* (%) = 249.0142 (100) [M + H, $C_{11}H_9N_2OS_2]^+$, 176.0166 (17) [M – N≡C-S-CH_3 + H, **b** + H, $C_9H_6NOS]^+$; CE = 20 V, *m/z* (%) = 176.0165 (100) [M – N≡C-S-CH_3 + H, **b** + H, $C_9H_6NOS]^+$, 148.0216 (10) [M – CO-N≡C-S-CH_3 + H, **b** – CO + H, $C_8H_6NS]^+$, 74.0060 (15) [N≡C-S-CH_3 + H, $C_2H_4NS]^+$; CE = 40 V, *m/z* (%) = 176.0167 (28) [M – N≡C-S-CH_3 + H, $C_9H_6NOS]^+$, 148.0209 (100) [M – CO-N≡C-S-CH_3 + H, **b** – CO + H, $C_8H_6NS]^+$, 121.0100 (34) $[C_7H_5S]^+$, 74.0057 (82) [N≡C-S-CH_3 + H, $C_2H_4NS]^+$. Negative mode; CE = 5 V, *m/z* (%) = 247.0014 (100) [M – H, $C_{11}H_7N_2OS_2]^-$, 201.0111 (11) [M – SCH_3, $C_{10}H_5N_2OS]^-$, 174.0015 (46) [M – N≡C-S-CH_3 – H, **b** – H, $C_9H_4NOS]^-$.

MS data of cyclobrassinin related compounds identified by fragmentation analysis

The assigned retention times were measured on the ACQUITY UPLC HSS T3 column.

[9-(6-*O*-Malonyl-ß-D-glucopyranosyl)-4,9-dihydro[1,3]thiazino[6,5-*b*]indol-2-yl]cysteinylglycine, Mal-Glc-Prestressin:

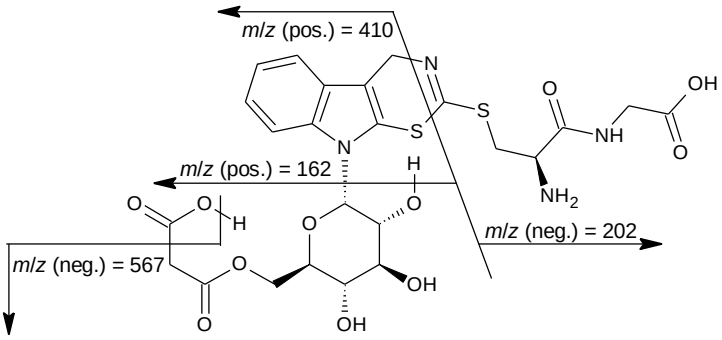

t_r = 3.40 min.

Exact mass, calcd. for $C_{24}H_{28}N_4O_{11}S_2$: 612.1196 [M].

MS (Q-TOF): Positive mode; CE = 5 V, *m/z* (%) = 613.1275 (86) [M + H, $C_{24}H_{29}N_4O_{11}S_2]^+$, 410.0910 (100) [M – **c** + H, $C_{18}H_{20}NO_8S]^+$, 162.0372 (21) [M – **c** – **g** + H, **a** + H, $C_9H_8NS]^+$; CE = 20 V, *m/z* (%) = 410.0901 (47) [M – **c** + H, $C_{18}H_{20}NO_8S]^+$, 162.0373 (100) [M – **c** – **g** + H, **a** + H, $C_9H_8NS]^+$, 127.0387 (8) $[C_6H_7O_3]^+$, 85.0284 (6) $[C_4H_5O_2]^+$; CE = 40 V, *m/z* (%) = 162.0374 (100) [M – **c** – **g** + H, **a** + H, $C_9H_8NS]^+$, 159.0286 (8) $[C_6H_7O_5]^+$, 127.0388 (9) $[C_6H_7O_3]^+$, 109.0279 (8) $[C_6H_5O_2]^+$, 97.0281 (6) $[C_5H_5O_2]^+$, 85.0284 (17) $[C_4H_5O_2]^+$, 81.0342 (5) $[C_5H_5O]^+$. Negative mode; CE = 5 V, *m/z* (%) = 611.1135 (100) [M – H, $C_{24}H_{27}N_4O_{11}S_2]^-$, 567.1242 (96) [M – CO_2 – H, $C_{23}H_{27}N_4O_9S_2]^-$, 202.0317 (19) [M – **a** – **g** – H, **c** – H, $C_6H_8N_3O_3S]^-$.

MS (Q-TRAP): Positive mode; CE = 20 V, *m/z* (%) = 613.0 (77) [M + H, $C_{24}H_{29}N_4O_{11}S_2]^+$, 410.0 (100) [M – **c** + H, $C_{18}H_{20}NO_8S]^+$, 162.1 (67) [M – **c** – **g** + H, **a** + H, $C_9H_8NS]^+$. Additionally, a peak at 231.0 (1) was detected which presumably corresponds to [M – **c** – **a** – H_2O + H, **g** – H_2O + H, $C_9H_{11}O_7]^+$. Negative mode; CE = 20 V, *m/z* (%) = 611.2 (56) [M – H, $C_{24}H_{27}N_4O_{11}S_2]^-$, 567.2 (100) [M – CO_2 – H, $C_{23}H_{27}N_4O_9S_2]^-$, 363.1 (6), 202.1 (17) [M – **a** –**g** – H, **c** – H, $C_6H_8N_3O_3S]^-$.

Exact mass, calcd. for $C_{24}H_{28}N_4O_{11}S^{34}S$: 614.1154 [M].

MS (Q-TRAP): Positive mode; CE = 20 V, *m/z* (%) = 615.1 (75) [M(^{34}S) + H, $C_{24}H_{29}N_4O_{11}S^{34}S]^+$, 412.0 (100) [M(^{34}S) – **c** + H, $C_{18}H_{20}NO_8{}^{34}S]^+$, 411.0 (26), 410.0 (76) [M(^{32}S) – **c** + H, $C_{18}H_{20}NO_8S]^+$, 164.1 (23) [M(^{34}S) – **c** – **g** + H, **a** + H, $C_9H_8N^{34}S]^+$, 163.0 (14), 162.1 (37) [M(^{32}S) – **c** – **g** + H, **a** + H, $C_9H_8NS]^+$. Additionally, a peak at 231.0 (1) was detected which presumably corresponds to [M – **c** – **a** + H, **g** – H_2O + H, $C_9H_{11}O_7]^+$.

[9-(ß-D-Glucopyranosyl)-4,9-dihydro[1,3]thiazino[6,5-*b*]indol-2-yl]cysteinylglycine, Glc-Prestressin:

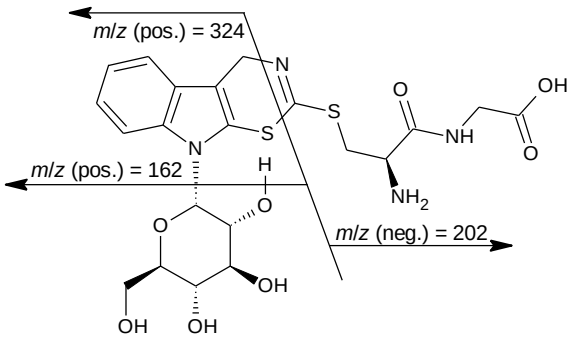

t_r = 3.22 min.

Exact mass, calcd. for $C_{21}H_{26}N_4O_8S_2$: 526.1192 [M].

MS (Q-TOF): Positive mode; CE = 5 V, *m/z* (%) = 527.1273 (47) [M + H, $C_{21}H_{27}N_4O_8S_2]^+$, 324.0909 (100) [M – **c** + H, $C_{15}H_{18}NO_5S]^+$, 162.0376 (47) [M – **c** – **f** + H, **a** + H, $C_9H_8NS]^+$; CE = 20 V, *m/z* (%) = 324.0904 (8) [M – **c** + H, $C_{15}H_{18}NO_5S]^+$, 162.0375 (100) [M – **c** – **f** + H, **a** + H, $C_9H_8NS]^+$; CE = 40 V, *m/z* (%) = 324.0908 (8) [M – **c** + H, $C_{15}H_{18}NO_5S]^+$, 162.0374 (100) [M – **c** – **f** + H, **a** + H, $C_9H_8NS]^+$. Negative mode; CE = 5 V, *m/z* (%) = 525.1111 (100) [M – H, $C_{21}H_{25}N_4O_8S_2]^-$, 202.0297 (27) [M – **a** – **f** – H, **c** – H, $C_6H_8N_3O_3S]^-$.

[9-(6-*O*-Malonyl-ß-D-glucopyranosyl)-4-oxo-4,9-dihydro[1,3]thiazino[6,5-*b*]indol-2-yl]-cysteinylglycine, Mal-Glc-Prestressinon:

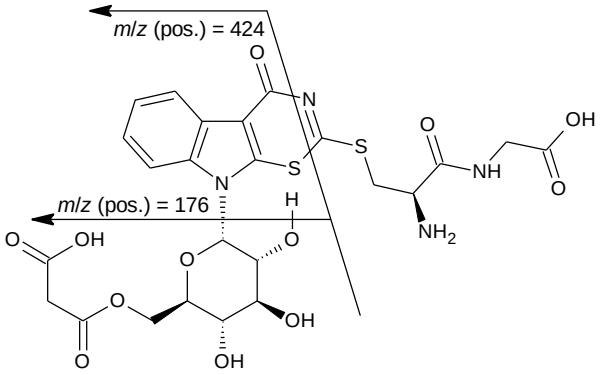

t_r = 4.20 min.

Exact mass, calcd. for $C_{24}H_{26}N_4O_{12}S_2$: 626.0989 [M].

MS (Q-TOF): Positive mode; CE = 5 V, *m/z* (%) = 424.0689 (100) [M – **c** + H, $C_{18}H_{18}NO_9S]^+$; CE = 20 V, *m/z* (%) = 176.0156 (100) [M – **c** – **g** + H, **b** + H, $C_9H_6NOS]^+$; CE = 40 V, *m/z* (%) = 206.0503 (42), 205.0478 (100). 176.0173 (70) [M – **c** – **g** + H, **b** + H, $C_9H_6NOS]^+$. Negative mode; no reasonable data obtained.

[9-(ß-D-Glucopyranosyl)-4-oxo-4,9-dihydro[1,3]thiazino[6,5-*b*]indol-2-yl]cysteinylglycine, Glc-Prestressinon:

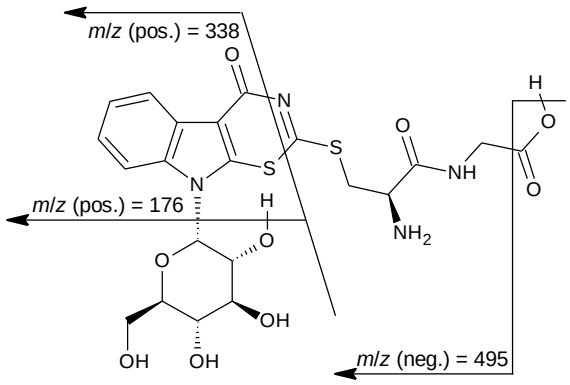

t_r = 4.14 min.

Exact mass, calcd. for $C_{21}H_{24}N_4O_9S_2$: 540.0985 [M].

MS (Q-TOF): Positive mode; CE = 5 V, *m/z* (%) = 541.1034 (100) [M + H, $C_{21}H_{25}N_4O_9S_2]^+$, 338.0735 (32) [M – **c** + H, $C_{15}H_{16}NO_6S]^+$,[16] 176.0169 (32) [M – **c** – **f** + H, **b** + H, $C_9H_6NOS]^+$;[16] CE = 20 V, *m/z* (%) = 176.0173 (100) [M – **c** – **f** + H, **b** + H, $C_9H_6NOS]^+$; CE = 40 V, no reasonable data obtained. Negative mode; CE = 5 V, *m/z* (%) = 539.0817 (24) [M – H, $C_{21}H_{23}N_4O_9S_2]^-$,[16] 495.0556 (100) [M – CO_2 – H, $C_{20}H_{23}N_4O_7S_2]^-$, 453.0503 (35) $[C_{18}H_{21}N_4O_6S_2]^-$.

[9-(6-*O*-Malonyl-ß-D-glucopyranosyl)-4,9-dihydro[1,3]thiazino[6,5-*b*]indol-2-yl]cysteine, Mal-Glc-Stressin:

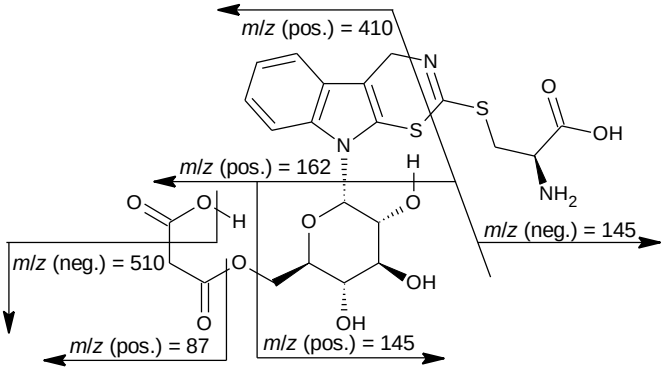

t_r = 3.45 min.

Exact mass, calcd. for $C_{22}H_{25}N_3O_{10}S_2$: 555.0981 [M].

MS (Q-TOF): Positive mode; CE = 5 V, *m/z* (%) = 556.1045 (47) [M + H, $C_{22}H_{26}N_3O_{10}S_2]^+$, 410.0907 (100) [M – **d** + H, $C_{18}H_{20}NO_8S]^+$, 162.0374 (22) [M – **d** – **g** + H, **a** + H, $C_9H_8NS]^+$; CE = 20 V, *m/z* (%) = 410.0901 (25) [M – **d** + H, $C_{18}H_{20}NO_8S]^+$, 162.0374 (100) [M – **d** – **g** + H, **a** + H, $C_9H_8NS]^+$, 145.0495 (6) [**g** – HO_2C-CH_2-CO_2, $C_6H_9O_4]^+$, 127.0386 (12) $[C_6H_7O_3]^+$, 85.0290 (6) $[C_4H_5O_2]^+$; CE = 40 V, *m/z* (%) = 162.0372 (100) [M – **d** – **g** + H, **a** + H, $C_9H_8NS]^+$, 159.0282 (8) $[C_6H_7O_5]^+$, 127.0385 (12) $[C_6H_7O_3]^+$, 109.0282 (11) $[C_6H_5O_2]^+$, 97.0283 (6) $[C_5H_5O_2]^+$, 87.0075 (6) [**g** – **f** + H, HO_2C-CH_2-CO, $C_3H_3O_3]^+$, 85.0287 (16) $[C_4H_5O_2]^+$, 81.0339 (10) $[C_5H_5O]^+$. Negative mode; CE = 5 V, *m/z* (%) = 554.0906 (42) [M – H, $C_{22}H_{24}N_3O_{10}S_2]^-$, 510.1019 (100) [M – CO_2 – H, $C_{21}H_{24}N_3O_8S_2]^-$, 145.0069 (72) [M – **a** – **g** – H, **d** – H, $C_4H_5N_2O_2S]^-$, 67.0304 (6) [**d** – CO_2 –H_2S, – H, $C_3H_3N_2]^-$.

[9-(ß-D-Glucopyranosyl)-4,9-dihydro[1,3]thiazino[6,5-*b*]indol-2-yl]cysteine, Glc-Stressin:

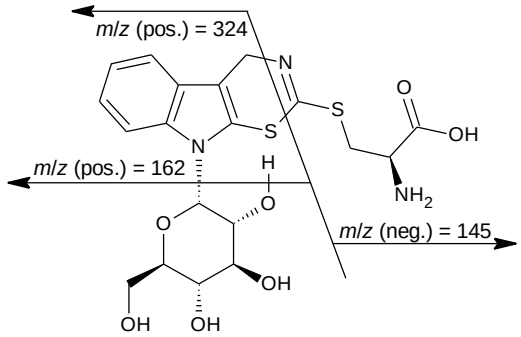

t_r = 3.28 min.

Exact mass, calcd. for $C_{19}H_{23}N_3O_7S_2$: 469.0977 [M].

MS (Q-TOF): Positive mode; CE = 5 V, *m/z* (%) = 470.1050 (26) [M + H, $C_{19}H_{24}N_3O_7S_2]^+$, 324.0905 (100) [M – **d** + H, $C_{15}H_{18}NO_5S]^+$, 162.0374 (51) [M – **d** – **f** + H, **a** + H, $C_9H_8NS]^+$; CE = 20 V, *m/z* (%) = 324.0899 (6) [M – **d** + H, $C_{15}H_{18}NO_5S]^+$, 162.0371 (100) [M – **d** – **f** + H, **a** + H, $C_9H_8NS]^+$, CE = 40 V, *m/z* (%) = 162.0377 (100) [M – **d** – **f** + H, **a** + H, $C_9H_8NS]^+$. Negative mode; CE = 5 V, *m/z* (%) = 468.0897 (100) [M – H, $C_{19}H_{22}N_3O_7S_2]^-$, 145.0066 (99) [M – **a** – **f** – H, **d** – H, $C_4H_5N_2O_2S]^-$.

[9-(6-*O*-Malonyl-ß-D-glucopyranosyl)-4-oxo-4,9-dihydro[1,3]thiazino[6,5-*b*]indol-2-yl]cysteine, Mal-Glc-Stressinon:

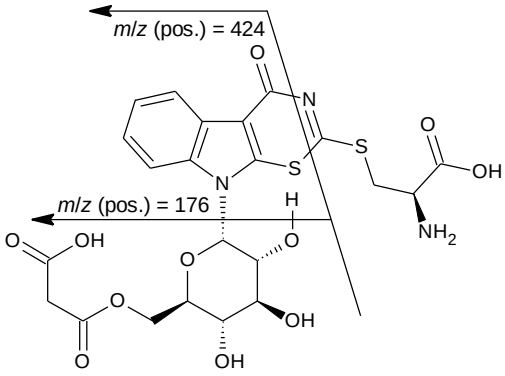

t_r = 4.04 min.

Exact mass, calcd. for $C_{22}H_{23}N_3O_{11}S_2$: 569.0774 [M].

MS (Q-TOF): Positive mode; CE = 5 V, *m/z* (%) = 570.0817 (100) [M + H, $C_{22}H_{24}N_3O_{11}S_2]^+$, 424.0677 (62) [M – **d** + H, $C_{18}H_{18}NO_9S]^+$; CE = 20 V, *m/z* (%) = 424.0655 (100) [M – **d** + H, $C_{18}H_{18}NO_9S]^+$, 176.0172 (100) [M – **d** – **g** + H, **b** + H, $C_9H_6NOS]^+$, CE = 40 V, *m/z* (%) = 176.0160 (100) [M – **d** – **g** + H, **b** + H, $C_9H_6NOS]^+$. Negative mode; no reasonable data obtained.

[9-(ß-D-Glucopyranosyl)-4-oxo-4,9-dihydro[1,3]thiazino[6,5-*b*]indol-2-yl]cysteine, Glc-Stressinon:

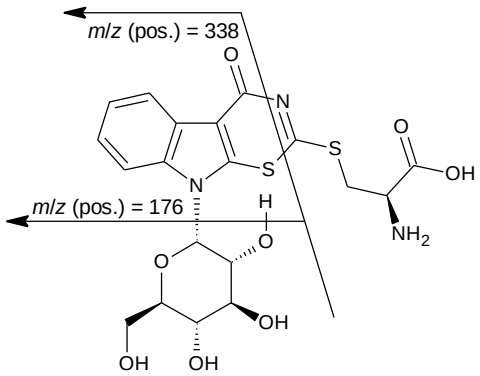

t_r = 3.99 min.

Exact mass, calcd. for $C_{19}H_{21}N_3O_8S_2$: 483.0770 [M].

MS (Q-TOF): Positive mode; CE = 5 V, *m/z* (%) = 484.0832 (91) [M + H, $C_{19}H_{22}N_3O_8S_2]^+$, 338.0713 (22) [M – **d** + H, $C_{15}H_{16}NO_6S]^+$, 176.0166 (100) [M – **d** – **f** + H, **b** + H, $C_9H_6NOS]^+$; CE = 20 V, *m/z* (%) = 320.0584 (14) [M – **d** – H_2O + H, $C_{15}H_{14}NO_5S]^+$, 176.0163 (100) [M – **d** – **f** + H, **b** + H, $C_9H_6NOS]^+$; CE = 40 V, *m/z* (%) = 176.0179 (100) [M – **d** – **f** + H, **b** + H, $C_9H_6NOS]^+$. Negative mode; no reasonable data obtained.

3-{[1-(6-*O*-Malonyl-ß-D-glucopyranosyl)-3-methyl-1*H*-indol-2-yl]dithio}alanine or

***S*-{[1-(6-*O*-Malonyl-ß-D-glucopyranosyl)-2-mercapto-1*H*-indol-3-yl]methyl}cysteine**

Mal-Glc Stressin related:

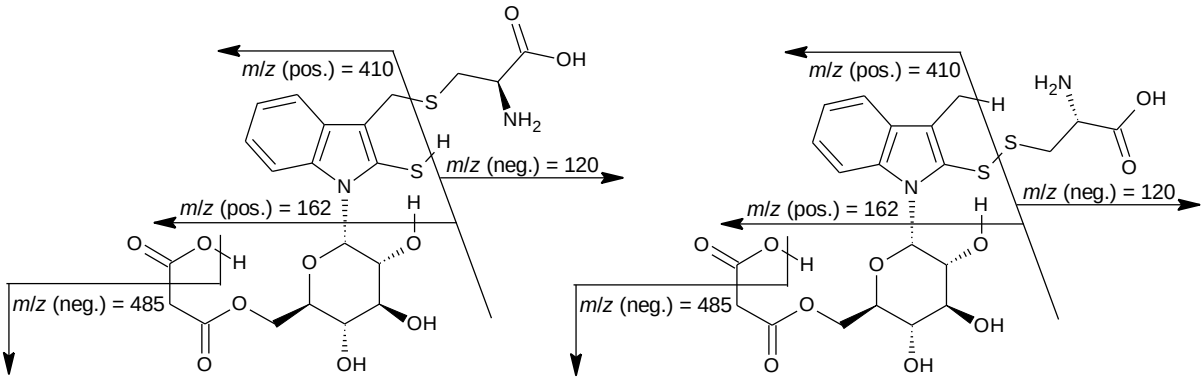

t_r = 3.60 min.

Exact mass, calcd. for $C_{21}H_{26}N_2O_{10}S_2$: 530.1029 [M].

MS (Q-TOF): Positive mode; CE = 5 V, *m/z* (%) = 531.1058 (15) [M + H, $C_{21}H_{27}N_2O_{10}S_2]^+$, 410.0889 (100) [M – **e** + H, $C_{18}H_{20}NO_8S]^+$, 162.0365 (21) [M – **e** – **g** + H, **a** + H, $C_9H_8NS]^+$; CE = 20 V, *m/z* (%) = 410.0935 (17) [M – **e** + H, $C_{18}H_{20}NO_8S]^+$, 213.0404 (6) $[C_9H_9O_6]^+$, 162.0384 (100) [M – **e** – **g** + H, **a** + H, $C_9H_8NS]^+$, 159.0291 (12) $[C_6H_7O_5]^+$, 145.0482 (6) [**g** – HO_2C-CH_2-CO_2, $C_6H_9O_4]^+$, 127.0391 (15) $[C_6H_7O_3]^+$, 97.0296 (7) $[C_5H_5O_2]^+$, 85.0290 (14) $[C_4H_5O_2]^+$; CE = 40 V, *m/z* (%) = 162.0371 (100) [M – **e** – **g** + H, **a** + H, $C_9H_8NS]^+$ 159.0281 (13) $[C_6H_7O_5]^+$, 127.0386 (20) $[C_6H_7O_3]^+$, 109.0269 (12) $[C_6H_5O_2]^+$, 97.0284 (15) $[C_5H_5O_2]^+$, 87.0079 (7) [**g** – **f** + H, HO_2C-CH_2-CO, $C_3H_3O_3]^+$, 85.0283 (14) $[C_4H_5O_2]^+$, 81.0344 (7) $[C_5H_5O]^+$, 68.9966 (6), 57.0345 (6) $[C_3H_5O]^+$. Negative mode *m/z* (%) = 529.0902 (54) [M – H, $C_{21}H_{25}N_2O_{10}S_2]^-$, 485.1057 (100) [M – CO_2 – H, $C_{20}H_{25}N_2O_8S_2]^-$, 120.0117 (94) [**e** – H, $C_3H_6NO_2S]^-$.

3-{[1-(ß-D-Glucopyranosyl)-3-methyl-1*H*-indol-2-yl]dithio}alanine or

***S*-{[1-(ß-D-glucopyranosyl)-2-mercapto-1*H*-indol-3-yl]methyl}cysteine**

Glc-Stressin related:

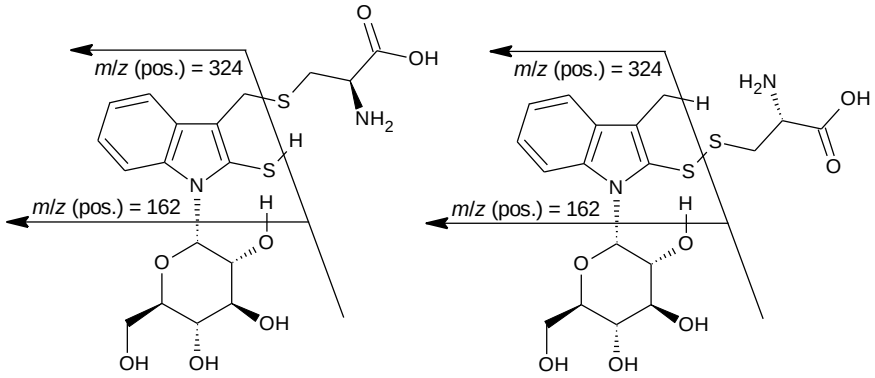

t_r = 3.20 min.

Exact mass, calcd. for $C_{18}H_{24}N_2O_7S_2$: 444.1025 [M].

MS (Q-TOF): Positive mode; CE = 5 V, *m/z* (%) = 445.1085 (6) [M + H, $C_{18}H_{25}N_2O_7S_2]^+$,[16] 324.0900 (100) [M – **e** + H, $C_{15}H_{18}NO_5S]^+$, 162.0370 (65) [M – **e** – **f** + H, **a** + H, $C_9H_8NS]^+$; CE = 20 V, *m/z* (%) = 162.0370 (100) [M – **e** – **f** + H, **a** + H, $C_9H_8NS]^+$; CE = 40 V, *m/z* (%) = 162.0384 (100) [M – **e** – **f** + H, **a** + H, $C_9H_8NS]^+$. Negative mode; no reasonable data obtained.

1-(6-*O*-Malonyl-ß-D-glucopyranosyl)-2-mercapto-1*H*-indole-3-carboxylic acid, Mal-Glc-MICA:

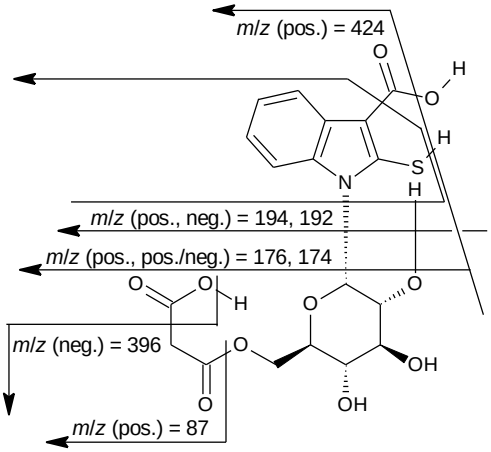

t_r = 4.10 min.

Exact mass, calcd. for $C_{18}H_{19}NO_{10}S$: 441.0730 [M].

MS (Q-TOF): Positive mode; CE = 5 V, *m/z* (%) = 424.0697 (100) [M – H_2O + H, $C_{18}H_{18}NO_9S]^+$, 194.0247 (14) [M – **g** + H, **b** + H_2O + H, $C_9H_8NO_2S]^+$, 176.0164 (36) [M – **g** – H_2O + H, **b** + H, $C_9H_6NOS]^+$, 127.0390 (28) $[C_6H_7O_3]^+$; CE = 20 V, *m/z* (%) = 194.0276 (33) [M – **g** + H, **b** + H_2O + H, $C_9H_8NO_2S]^+$, 176.0162 (100) [M – **g** – H_2O + H, **b** + H, $C_9H_6NOS]^+$, 159.0295 (19) $[C_6H_7O_5]^+$, 85.0274 (22) $[C_4H_5O_2]^+$; CE = 40 V, *m/z* (%) = 176.0158 (100) [M – **g** – H_2O + H, **b** + H, $C_9H_6NOS]^+$, 148.0213 (29) [M – **g** – H_2O – CO + H, **b** – CO + H, $C_8H_6NS]^+$, 117.0557 (18) [indole, $C_8H_7N]^+$, 109.0283 (18) $[C_6H_5O_2]^+$, 97.0280 (20) $[C_5H_5O_2]^+$, 87.0077 (28) [**g** – **f** + H, $HO_2C\text{-}CH_2\text{-}CO$, $C_3H_3O_3]^+$, 85.0287 (39) $[C_4H_5O_2]^+$, 81.0336 (26) $[C_5H_5O]^+$, 69.0333 (40) $[C_4H_5O]^+$, 53.0388 (15) $[C_4H_5]^+$.

MS (Q-TRAP): Positive mode; CE = 5 V, *m/z* (%) = 442.0 (11) [M + H, $C_{18}H_{20}NO_{10}S]^+$, 424.0 (100) [M – H_2O + H, $C_{18}H_{18}NO_9S]^+$, 382.2 (6); CE = 20 V, *m/z* (%) = 424.0 (100) [M – H_2O + H, $C_{18}H_{18}NO_9S]^+$, 406.0 (22) [M – 2 × H_2O + H, $C_{18}H_{16}NO_8S]^+$, 388.0 (14), 362.0 (5), 284.0 (10), 258.0 (5), 240.1 (8), 236.0 (7), 218.0 (19), 213.0 (12) $[C_9H_9O_6]^+$, 194.0 (11) [M – **g** + H, **b** + H_2O + H, $C_9H_8NO_2S]^+$, 190.0 (5), 176.1 (36) [M – **g** – H_2O + H, **b** + H, $C_9H_6NOS]^+$, 148.1 (5) [M – **g** – H_2O – CO + H, **b** – CO + H, $C_8H_6NS]^+$; CE = 40 V, *m/z* (%) = 194.0 (10) [M – **g** + H, **b** + H_2O + H, $C_9H_8NO_2S]^+$, 190.0 (5), 176.0 (100) [M – **g** – H_2O + H, **b** +

H, $C_9H_6NOS]^+$, 174.0 (5) [M – **g** – H_2O – H, **b** – H, $C_9H_4NOS]^+$, 148.1 (23) [M – **g** – H_2O – CO + H, **b** – CO + H, $C_8H_6NS]^+$. Negative mode; CE = 5 V, *m/z* (%) = 440.0 (8) [M – H, $C_{18}H_{18}NO_{10}S]^-$, 396.1 (100) [M – CO_2 – H, $C_{17}H_{18}NO_8S]^-$, 352.1 (21) [M – 2 × CO_2 – H, $C_{16}H_{18}NO_6S]^-$, 192.0 (29) [M – **g** – H, **b** + H_2O – H, $C_9H_6NO_2S]^-$, 148.0 (7) [M – **g** – CO_2 – H, **b** – CO + H, $C_8H_6NS]^+$; CE = 20 V, *m/z* (%) = 396.1 (21) [M – CO_2 – H]$^-$, 192.0 (100) [M – **g** – H, **b** + H_2O – H, $C_9H_6NO_2S]^-$, 174.0 (7) [M – **g** – H_2O – H, **b** – H, $C_9H_4NOS]^-$, 148.0 (19) [M – **g** – CO_2 – H, **b** – CO + H, $C_8H_6NS]^-$; CE = 40 V, *m/z* (%) = 192.0 (100) [M – **g** – H, **b** + H_2O – H, $C_9H_6NO_2S]^-$, 174.0 (53) [M – **g** – H_2O – H, **b** – H, $C_9H_4NOS]^-$, 148.0 (26) [M – **g** – CO_2 – H, **b** – CO + H, $C_8H_6NS]^-$.

1-(ß-D-Glucopyranosyl)-2-mercapto-1*H*-indole-3-carboxylic acid, Glc-MICA:

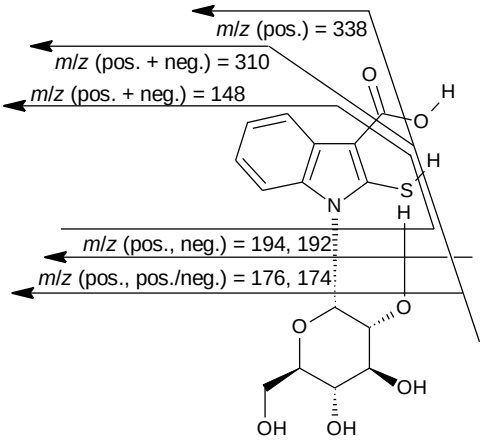

t_r = 3.75 min.

Exact mass, calcd. for $C_{15}H_{17}NO_7S$: 355.0726 [M].

MS (Q-TOF): Positive mode; CE = 5 V, *m/z* (%) = 355.1736 (51) [M, $C_{15}H_{17}NO_7S]^+$, 194.0270 (100) [M – **f** + H, **b** + H_2O + H, $C_9H_8NO_2S]^+$, 176.0138 (41) [M – **f** – H_2O + H, **b** + H, $C_9H_6NOS]^+$; CE = 20 V, *m/z* (%) = 194.0275 (70) [M – **f** + H, **b** + H_2O + H, $C_9H_8NO_2S]^+$, 176.0176 (100) [M – **f** – H_2O + H, **b** + H, $C_9H_6NOS]^+$; CE = 40 V, *m/z* (%) = 176.0156 (100) [M – **f** – H_2O + H, **b** + H, $C_9H_6NOS]^+$. Negative mode; no reasonable data obtained.

MS (Q-TRAP): Positive mode; CE = 5 V, *m/z* (%) = 356.1 (21) [M + H, $C_{15}H_{18}NO_7S]^+$, 338.0 (100) [M – H_2O + H, $C_{15}H_{16}NO_6S]^+$, 320.0 (17) [M – 2 × H_2O + H, $C_{15}H_{14}NO_5S]^+$, 315.0 (11), 310.0 (15) [M – H_2O –CO + H, **b** + **f** – CO + H, $C_{14}H_{16}NO_5S]^+$, 296.1 (43), 258.0 (5), 255.0 (14), 214.1 (9), 198.0 (17), 194.1 (60) [M – **f** + H, **b** + H_2O + H, $C_9H_8NO_2S]^+$, 176.0 (59) [M – **f** – H_2O + H, **b** + H, $C_9H_6NOS]^+$, 148.1 (5) [M – **f** – H_2O – CO_2 + H, **b** – CO + H, $C_8H_6NS]^+$; CE = 20 V, *m/z* (%) = 337.9 (12) [M – H_2O + H, $C_{15}H_{16}NO_6S]^+$, 320.0 (20) [M – 2 × H_2O + H, $C_{15}H_{14}NO_5S]^+$, 296.1 (17), 255.0 (24), 236.0 (6), 198.0 (40), 197.0 (5), 194.0 (100) [M – **f** + H, **b** + H_2O + H, $C_9H_8NO_2S]^+$, 184.0 (8), 176.1 (92) [M – **f** – H_2O + H, **b** + H, $C_9H_6NOS]^+$, 150.1 (5) [M – **f** – CO_2 + H, **b** + H_2O – CO_2 + H, $C_8H_8NS]^+$, 148.1 (34) [M – **f** – H_2O – CO_2 + H, **b** – CO + H, $C_8H_6NS]^+$; CE = 40 V, *m/z* (%) = 198.1 (25), 197.1 (5), 194.0 (7) [M – **f** + H, **b** + H_2O + H, $C_9H_8NO_2S]^+$, 184.1 (11), 182.1 (9), 176.0 (86) [M – **f** – H_2O + H, **b** + H, $C_9H_6NOS]^+$, 150.0 (5) [M – **f** – CO_2 + H, **b** + H_2O – CO_2 + H, $C_8H_8NS]^+$, 148.1 (100) [M – **f** – H_2O – CO_2 + H, **b** – CO + H, $C_8H_6NS]^+$, 117.0 (5) [indole, $C_8H_7N]^+$, 100.1 (5), 99.0 (10). Negative mode; CE = 5 V, *m/z* (%) = 354.1 (100) [M – H, $C_{15}H_{16}NO_7S]^-$, 310.2 (15) [M – CO_2 – H, $C_{14}H_{16}NO_5S]^-$, 192.1 (31) [M – **f** – H, **b** + H_2O – H, $C_9H_6NO_2S]^-$, 148.1 (8) [M – **f** – CO_2 – H, **b** – CO + H, $C_8H_6NS]^-$; CE = 20 V, *m/z* (%) = 354.1 (19) [M – H, $C_{15}H_{16}NO_7S]^-$, 310.1 (5) [M – CO_2 – H, $C_{14}H_{16}NO_5S]^-$, 192.0 (100) [M – **f** – H, **b** + H_2O – H, $C_9H_6NO_2S]^-$, 174.1 (6) [M – **f** – H_2O – H, **b** –

H, $C_9H_4NOS]^-$, 148.1 (23) [M – **f** – CO_2 – H, **b** – CO + H, $C_8H_6NS]^-$; CE = 40 V, *m/z* (%) = 192.0 (99) [M – **f** – H, **b** + H_2O – H, $C_9H_6NO_2S]^-$, 174.0 (100) [M – **f** – H_2O – H, **b** – H, $C_9H_4NOS]^-$, 148.1 (38) [M – **f** – CO_2 – H, **b** – CO + H, $C_8H_6NS]^-$.

ß-D-Glucopyranose 1-(6-*O*-Malonyl-ß-D-glucopyranosyl)-2-mercapto-1*H*-indole-3-carboxylate, Mal-Glc-MICA-Glc:

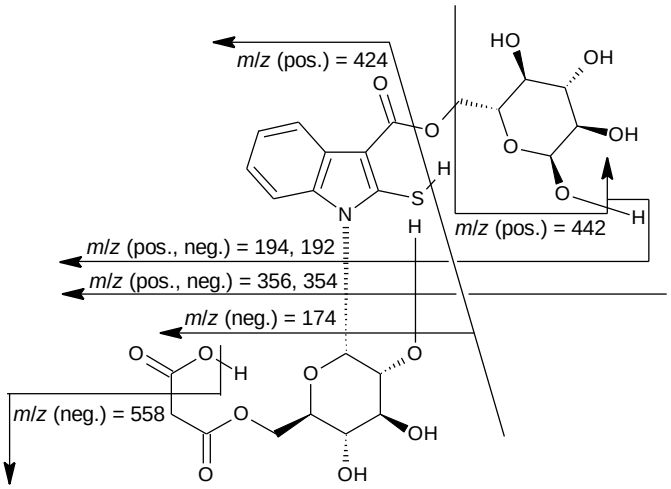

t_r = 3.41 min.

Exact mass, calcd. for $C_{24}H_{29}NO_{15}S$: 603.1258 [M].

MS (Q-TOF): Positive mode;[17] CE = 5, 20 V, no reasonable data obtained; CE = 40 V, *m/z* (%) = 603.2057 (100) [M, $C_{24}H_{29}NO_{15}S]^+$. Negative mode; no reasonable data obtained.

MS (Q-TRAP): Positive mode; CE = 5 V, *m/z* (%) = 604.2 (30) [M + H, $C_{24}H_{30}NO_{15}S]^+$, 586.2 (31) [M – H_2O + H, $C_{24}H_{28}NO_{14}S]^+$, 442.1 (28) [M – **f** + H, $C_{18}H_{20}NO_{10}S]^+$, 424.1 (100) [M – **f** – H_2O + H, $C_{18}H_{18}NO_9S]^+$, 366.2 (14), additionally, a peak at 356.1 (7) was detected which presumably corresponds to [M – **g** + H, $C_{15}H_{18}NO_7S]^+$; CE = 20 V, *m/z* (%) = 424.1 (100) [M – **f** – H_2O + H, $C_{18}H_{18}NO_9S]^+$, 406.0 (14) [M – **f** – 2 × H_2O + H, $C_{18}H_{16}NO_8S]^+$, 218.0 (15); CE = 40 V, no reasonable data obtained.

Negative mode; CE = 5 V, *m/z* (%) = 602.2 (19) [M – H, $C_{24}H_{28}NO_{15}S]^-$, 558.2 (100) [M – CO_2 – H, $C_{23}H_{28}NO_{13}S]^-$; CE = 20 V, *m/z* (%) = 558.2 (100) [M – CO_2 – H, $C_{23}H_{28}NO_{13}S]^-$, 354.1 (25) [M – **g** – H, $C_{15}H_{16}NO_7S]^-$; CE = 40 V, *m/z* (%) = 558.2 (5) [M – CO_2 – H, $C_{23}H_{28}NO_{13}S]^-$, 378.0 (5) [M – **f** – H_2O – CO_2 – H, **b** + **g** – CO_2 – H, $C_{17}H_{16}NO_7S]^-$, 354.1 (100) [M – **g** – H, $C_{15}H_{16}NO_7S]^-$, 192.0 (17) [M – **g** – **f** – H, **b** + H_2O – H, $C_9H_6NO_2S]^-$, 174.0 (74) [M – **g** – **f** – H_2O – H, **b** – H, $C_9H_4NOS]^-$.

ß-D-Glucopyranose 1-(ß-D-glucopyranosyl)-2-mercapto-1*H*-indole-3-carboxylate, Glc-MICA-Glc:

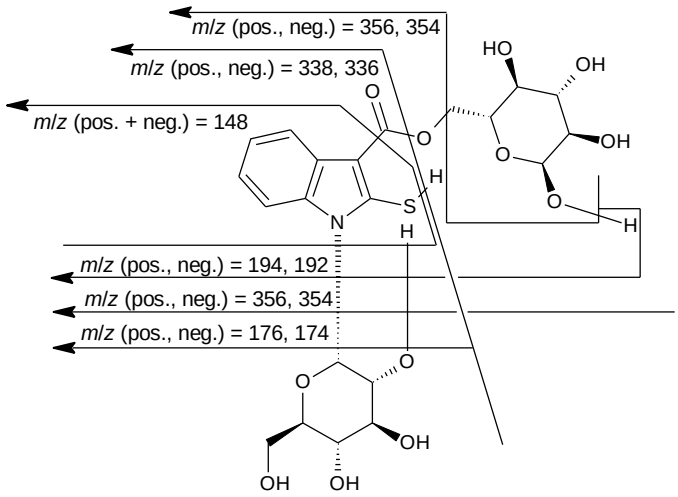

t_r = 3.11 min.

Exact mass, calcd. for $C_{21}H_{27}NO_{12}S$: 517.1254 [M].

MS (Q-TOF): Positive and negative mode; no reasonable data obtained.

MS (Q-TRAP): Positive mode;[17] CE = 5 V, *m/z* (%) = 518.3 (42) [M + H, $C_{21}H_{28}NO_{12}S]^+$, 501.3 (12) [M – OH + H, $C_{21}H_{27}NO_{11}S]^+$, 500.2 (28) [M – H_2O + H, $C_{21}H_{26}NO_{11}S]^+$, 458.2 (12), 398.2 (14), 390.2 (14), 356.1 (42) [M – **f** + H, $C_{15}H_{18}NO_7S]^+$, 338.1 (100) [M – **f** – H_2O + H, $C_{15}H_{16}NO_6S]^+$, 193.9 (24) [M – 2 × **f** + H, **b** + H_2O + H, $C_9H_8NO_2S]^+$, 175.9 (32) [M – 2 × **f** – H_2O + H, **b** + H, $C_9H_6NOS]^+$; CE = 20 V, *m/z* (%) = 518.4 (50) [M + H, $C_{21}H_{28}NO_{12}S]^+$, 518.1 (24) [M + H, $C_{21}H_{28}NO_{12}S]^+$, 390.2 (14), 338.2 (44) [M – **f** – H_2O + H, $C_{15}H_{16}NO_6S]^+$, 320.1 (26) [M – **f** – 2 × H_2O + H, $C_{15}H_{14}NO_5S]^+$, 241.0 (14), 194.0 (98) [M – 2 × **f** + H, **b** + H_2O + H, $C_9H_8NO_2S]^+$, 176.0 (100) [M – 2 × **f** – H_2O + H, **b** + H, $C_9H_6NOS]^+$, 148.0 (18) [M – 2 × **f** – H_2O – CO + H, **b** – CO + H, $C_8H_6NS]^+$; CE = 40 V, *m/z* (%) = 320.0 (16) [M – **f** – 2 × H_2O + H, $C_{15}H_{14}NO_5S]^+$, 194.0 (49) [M – 2 × **f** + H, **b** + H_2O + H, $C_9H_8NO_2S]^+$, 176.0 (100) [M – 2 × **f** – H_2O + H, **b** + H, $C_9H_6NOS]^+$, 148.1 (30) [M – 2 × **f** – H_2O – CO + H, **b** – CO + H, $C_8H_6NS]^+$. Negative mode; CE = 5 V, *m/z* (%) = 516.2 (100) [M – H, $C_{21}H_{26}NO_{12}S]^-$, 354.2 (10) [M – **f** – H, $C_{15}H_{16}NO_7S]^-$; CE = 20 V, *m/z* (%) = 516.2 (100) [M – H, $C_{21}H_{26}NO_{12}S]^-$, 354.1 (61) [M – **f** – H, $C_{15}H_{16}NO_7S]^-$, 336.1 (6) [M – **f** – H_2O – H, $C_{15}H_{14}NO_6S]^-$; CE = 40 V, *m/z* (%) = 354.1 (65) [M – **f** – H, $C_{15}H_{16}NO_7S]^-$, 336.1 (38) [M – **f** – H_2O – H, $C_{15}H_{14}NO_6S]^-$, 192.0 (17) [M – 2 × **f** – H, **b** + H_2O – H, $C_9H_6NO_2S]^-$, 174.0 (100) [M – 2 × **f** – H_2O – H, **b** – H, $C_9H_4NOS]^-$.

Acetylated 1-(ß-D-Glucopyranosyl)-2-mercapto-1*H*-indole-3-carboxylic acid or decarboxylated 1-(6-*O*-Malonyl-ß-D-glucopyranosyl)-2-mercapto-1*H*-indole-3-carboxylic acid

Decarboxy-Mal-Glc-MICA:

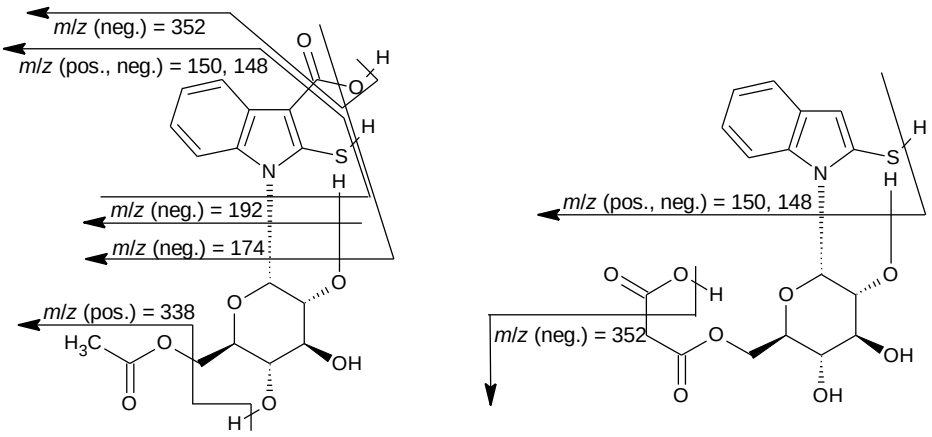

t_r = 4.41 min.

Exact mass, calcd. for $C_{17}H_{19}NO_8S$: 397.0831 [$M_{1,2}$]. Ac = M_1; (–CO_2) = M_2

MS (Q-TOF): Positive and negative mode; no reasonable data obtained.

MS (Q-TRAP): Positive mode; CE = 5 V, *m/z* (%) = 397.9 (100) [$M_{1,2}$ + H, $C_{17}H_{20}NO_8S]^+$, 338.0 (9) [M_1 – H_3C-CO_2H + H, **b** + **f** + H, $C_{15}H_{16}NO_6S]^+$, 150.1 (33) [**b** + H_2O – CO_2 + H or M_2 – **g** + H, $C_8H_8NS]^+$; CE = 20 V, *m/z* (%) = 398.0 (40) [$M_{1,2}$ + H, $C_{17}H_{20}NO_8S]^+$, 338.0 (5) [M – H_3C-CO_2H, **b** + **f** + H, $C_{15}H_{16}NO_6S]^+$, 231.0 (5) [**g** – H_2O + H, $C_9H_{11}O_7]^+$, 198.0 (7), 150.1 (100) [**b** + H_2O – CO_2 + H or M_2 – **g** + H, $C_8H_8NS]^+$; CE = 40 V, *m/z* (%) = 198.0 (9), 150.1 (100) [**b** + H_2O – CO_2 + H or M_2 – **g** + H, $C_8H_8NS]^+$, 117.1 (17) [indole, $C_8H_7N]^+$, 109.0 (5) [$C_6H_5O_2]^+$, 99.1 (6), 97.1 (5) [$C_5H_5O_2]^+$, 81.1 (5) [$C_5H_5O]^+$. Negative mode; CE = 5 V, *m/z* (%) = 396.1 (100) [$M_{1,2}$ – H, $C_{17}H_{18}NO_8S]^-$, 352.2 (14) [$M_{1,2}$ – CO_2 – H, $C_{16}H_{18}NO_6S]^-$, 192.1 (52) [M_1 – **f** – H_3C-CO, **b** + H_2O – H, $C_9H_6NO_2S]^-$, 148.1 (9) [M_1 – **f** – H_3C-CO – CO_2, **b** – CO + H, $C_8H_6NS]^-$; CE = 20 V, *m/z* (%) = 396.1 (25) [$M_{1,2}$ – H, $C_{17}H_{18}NO_8S]^-$, 352.1 (5) [$M_{1,2}$ – CO_2 – H, $C_{16}H_{18}NO_6S]^-$, 192.0 (100) [M_1 – **f** – H_3C-CO, **b** + H_2O – H, $C_9H_6NO_2S]^-$, 174.1 (9) [**b** – H, $C_9H_4NOS]^-$, 148.1 (27) [M_1 – **f** – H_3C-CO – CO_2, **b** – CO + H, $C_8H_6NS]^-$; CE = 40 V, *m/z* (%) = 192.0 (100) [M_1 – **f** – H_3C-CO, **b** + H_2O – H, $C_9H_6NO_2S]^-$, 174.1 (80) [**b** – H, $C_9H_4NOS]^-$, 148.1 (40) [M_1 – **f** – H_3C-CO – CO_2, **b** – CO + H, $C_8H_6NS]^-$.

Putative structural formulas of cyclobrassinin related compounds identified by exact mass

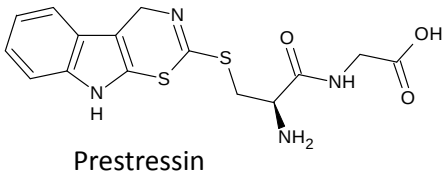

Prestressin

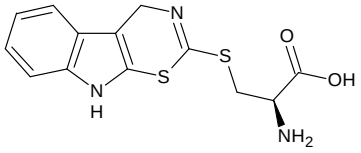

Stressin

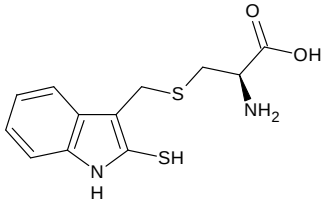

or

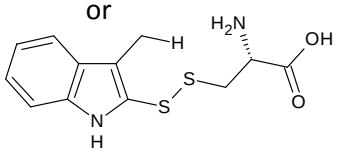

Stressin related

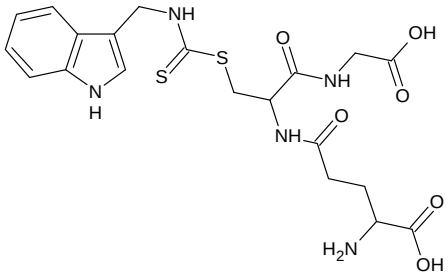

Dethiomethyl-brassinin-GSH

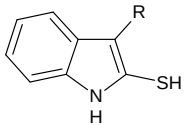

MICA: R = COOH
Decarboxy-MICA: R = H

7.3 Supplemental datasets

The supplemental datasets were generated from the datasets recorded in metabolite fingerprinting after the pre-processing performed in MarkerLynx (see material and methods 2.2.6.1). The unfiltered datasets from positive and negative ionization mode were combined. The ionization mode is indicated in the column dataset: 1 stands for negative and 2 for positive ionization. No adduct correction was performed. The column KWpValue gives the p-value calculated for the marker by the Kruskal-Wallis algorithm. Identified infection markers were assigned. The retention time is given in minutes. The resulting csv-files were combined in five xlsx-files where the tab labels provide information about the corresponding experiment. For tissue samples a polar and a nonpolar spreadsheet was created due to the differing retention times. Aqueous samples provide one spreadsheet.

Supplemental Dataset 1: Metabolite fingerprinting data from early time points of *V. longisporum* infection in *B. napus*

Data of shoots (M2501) and roots (M2502) at early time points of infection from one representative experiment including two biological replicates. *B. napus* plants were harvested 5 (highlighted in green), 7 (blue) or 10 dpi (red). Infection procedure was performed as described in chapter materials and methods.

Supplemental Dataset 2: Metabolite fingerprinting data from late time points of *V. longisporum* infection in *B. napus*

Data of AWF (M1402, from one representative experiment including three biological replicates), xylem sap (from three experiments (M1401 (highlighted in green), M1601 (blue) and M2001 (red) with one biological replicate each), leaves (from two experiments (M1403 (green) and M1603 (blue) with three biological replicates each)), stem (from three experiments (M1404 (green), M1604 (blue) and M2004 (red) with one biological replicate each)), hypocotyl (from three experiments (M1405 (green), M1605 (blue) and M2005 (red) with one biological replicate each)) and root (from three experiments (M1406 (green), M1606 (blue) and M2006 (red) with one biological replicate each)). *B. napus* plants were harvested 21, 28 or 35 dpi. Infection procedure was performed as described in chapter materials and methods.

Supplemental Dataset 3: Metabolite fingerprinting data from *V. longisporum* infected *A. thaliana* and *C. sativa*

Data of AWF from *V. longisporum* infection experiment with *A. thaliana* (M1301), of AWF from *C. sativa* (M1702, from one experiment including three biological replicates), xylem sap of *C. sativa* (from one experiment with one biological replicate) and hypocotyl of *C. sativa* (from one experiment

including three biological replicates). *A. thaliana* and *C. sativa* plants were harvested 21 dpi. The dataset M1301 from *A. thaliana* was submitted with the publication Floerl et al. (submitted).

Supplemental Dataset 4: Metabolite fingerprinting data from functional analyses

Data of abiotic stress: Data of *B. napus* plants after $CuCl_2$ abiotic stress treatment (M270X) includes data from sprayed leaves after 48 h (M2701, highlighted in green) as well as from whole plant assay after 7 d from shoot (M2703, blue) and root (M2706, red). The corresponding method is described under 3.6.3.

Data of flotation assay: Data of *B. napus* leaves floated 24 h on the following substances: water (control), SA, NaCl, RA, pipecolic acid, undecanedioic acid, dodecanedioic acid, triedecanedioic acid, suberic, sebacic and azelaic acid, pimelic acid, hexadecanedioic acid, VL 43 spores, VL Bob spores (from one experiment including three biological replicates). The corresponding method is described under 3.6.2.

Data of priming experiment: Data of *B. napus* plants after priming with dicarboxylic acids (M260X) includes data from AWF (M2602, from one experiment including two biological replicates), from xylem sap (M2601, from one experiment with one biological replicate) and hypocotyl (M2605, from one experiment including two biological replicates). The corresponding method is described under 2.2.3.7.

Supplemental Dataset 5: Metabolite fingerprinting data from *V. longisporum in vitro* experiments

Data of transfer experiment (SXM): Data of culture supernatants and pure media from *in vitro* experiments with *V. longisporum* from three independent experiments (M0601, M0606, M0608) including three biological replicates each. For culture supernatants: the first medium indicates medium used for 4d during spore germination, the second medium stands for the fresh medium supplied for the mycelium subsequently for another 4 d. The corresponding method is described under 2.2.1.1.

Data of transfer experiment (xylem sap): Data of culture supernatants and xylem sap from *in vitro* experiments with *V. longisporum, V. dahliae* and two chorismate synthase mutant strains (CS-6, CS12) from three independent experiments (M0613 (highlighted in green), M0614 (blue), M0615 (red)) with one biological replicate each. The corresponding method is described under 2.2.1.1.

Data of xylem sap comparison to SXM: Data of pure SXM and xylem sap of healthy *A. thaliana* and *B. napus* plants from one experiment including three technical replicates. Xylem sap was obtained as described under 2.2.3.6.

Danksagung

An erster Stelle möchte ich Herrn Prof. Ivo Feußner für die Möglichkeit an diesem spannenden Thema zu arbeiten danken, sowie ihm und Frau Prof. Andrea Polle für die gute Betreuung. Dr. Kirstin Feußner half mir bei dieser Arbeit mit inspirierenden Ideen und stand mir bei fachlichen und technischen Fragen immer zur Seite. Dr. Farina Schill war mir bei der Strukturaufklärung eine große Hilfe. Ohne sie wären eine Identifizierung vieler Infektionsmarker und die chemische Synthese der AWF spezifischen Substanzen nicht möglich gewesen. Dr. Cornelia Herrfurth, Susanne Mester, Gerd Mader und Christoph Mader danke ich für die Hilfe bei der Aufrechterhaltung des Arbeitsablaufs von der Pflanzenanzucht über die analytischen Messungen zur Datenauswertung.

Ein herzlicher Dank geht zudem an die Verticillium-Forscher der DFG-Forschergruppe FOR 546, vor allem an die AG Braus insbesondere an Clara Hoppenau und Christian Timpner, die mir in vielen Infektionsexperimenten zur Seite standen. Monika Franke-Klein (AG Polle) danke ich für die zahlreichen AWF-Ernten und der AG Gatz und der AG Dröge-Laser für das Saatgut der LUC-Reporterpflanzen. Ohne MarVis und die Unterstützung der Bioinformatiker (Alex Kaever, Manuel Landesfeind und Peter Meinicke der AG Morgenstern) wäre eine Analyse der umfangreichen Metabolite-Fingerprinting Datensätze sicher nicht möglich gewesen. Vielen Dank nochmal für eure oft schnelle und wichtige Hilfe! Ein Dank geht auch an die DFG, die dieses Projekt finanzierte.

Ich möchte mich zudem bei allen Kollegen – aktuellen oder ehemaligen – für die Unterstützung im Laboralltag und die nette Arbeitsatmosphäre bedanken vor allem bei all den fertigen Doktoren: Amina Ibrahim, Danuta Kaczmarzyk, Katharina Michels, Alexandra Andreou, Dirk Jessen und Michael Scharnewski. Ein herzliches Dankeschön gebührt auch Maren Bornemann und Annette Weizbauer, die während ihrer Praktika bzw. Bachelor-Arbeit wichtige Experimente für diese Arbeit durchgeführt haben.

Dr Hugo Ramos, Dr. Alexandra Andreou und Dr. Katharina Michels danke ich ebenso wie Dr. Kirstin Feußner für das Korrektur lesen dieser Arbeit.

Insbesondere möchte ich meinen Eltern danken, die mich immer ermutigt und bestärkt haben, sich Sorgen und Erfolge angehört haben und mein Leben lang hinter mir standen.

Mein herzlichster Dank geht an meinen Mann, der mir diese Arbeit ermöglicht hat durch seinen Zuspruch und seine Liebe und weil er immer an mich geglaubt hat.

Erklärung

Hiermit versichere ich, dass ich die vorliegende Arbeit „Signals and metabolic consequences during the interaction of Brassicaceae and *Verticillium longispo*rum“ selbständig verfasst und keine anderen als die angegebenen Hilfsmittel und Quellen verwendet habe.

Göttingen, Dezember 2011

Mareike Possienke